



**HAL**  
open science

# Novel Mesoporous Bioactive Glasses (MBGs) as fillers in dental adhesives “ Synthesis, Physico-chemical and biological evaluation ”

Jesu Delihtha Liyaa Fernando

## ► To cite this version:

Jesu Delihtha Liyaa Fernando. Novel Mesoporous Bioactive Glasses (MBGs) as fillers in dental adhesives “ Synthesis, Physico-chemical and biological evaluation ”. Biomaterials. Université de Lyon, 2018. English. NNT: 2018LYSE1072 . tel-01943600

**HAL Id: tel-01943600**

**<https://theses.hal.science/tel-01943600>**

Submitted on 4 Dec 2018

**HAL** is a multi-disciplinary open access archive for the deposit and dissemination of scientific research documents, whether they are published or not. The documents may come from teaching and research institutions in France or abroad, or from public or private research centers.

L'archive ouverte pluridisciplinaire **HAL**, est destinée au dépôt et à la diffusion de documents scientifiques de niveau recherche, publiés ou non, émanant des établissements d'enseignement et de recherche français ou étrangers, des laboratoires publics ou privés.



N°d'ordre NNT : xxx

**THESE de DOCTORAT DE L'UNIVERSITE DE LYON**  
opérée au sein de  
**l'Université Claude Bernard Lyon 1**  
**Ecole Doctorale N° accréditation**  
**(ECOLE DOCTORALE INTERDISCIPLINAIRE SCIENCES SANTE)**

**Spécialité de doctorat : Biomatériaux**  
**Discipline : (Eventuellement)**

Soutenue publiquement le 03/05/2018, par :  
**(Jesu Delihita Liyaa Fernando)**

---

**Novel Mesoporous Bioactive Glasses (MBGs)  
as fillers in dental adhesives « Synthesis,  
Physico-chemical and biological evaluation »**

---

Devant le jury composé de :

<b>Hill Robert</b>	<b>Pr</b>	<b>Queens Mary University</b>	<b>Rapporteur</b>
<b>Turkun Sebnem</b>	<b>Pr</b>	<b>Ege University</b>	<b>Rapporteuse</b>
<b>Berdal Ariane</b>	<b>PU-PH</b>	<b>Université Paris Diderot</b>	<b>Rapporteuse</b>
<b>Jackson Phil</b>	<b>Dr</b>	<b>LUCIDEON, Ltd</b>	<b>Examineur</b>
<b>Colon Pierre</b>	<b>PU-PH</b>	<b>Université Paris Diderot</b>	<b>Directeur de thèse</b>
<b>Attik Nina</b>	<b>Dr-MCA</b>	<b>Université Lyon 1</b>	<b>Co-directrice de thèse</b>
<b>Pradelle-Plasse Nelly</b>	<b>MCU-PH</b>	<b>Université Paris Diderot</b>	<b>Co-directrice de Thèse</b>
<b>Grosogoeat Brigitte</b>	<b>PU-PH</b>	<b>Université Lyon 1</b>	<b>Invitée</b>

# UNIVERSITE CLAUDE BERNARD - LYON 1

## Président de l'Université

Président du Conseil Académique

Vice-président du Conseil d'Administration

Vice-président du Conseil Formation et Vie Universitaire

Vice-président de la Commission Recherche

Directrice Générale des Services

**M. le Professeur Frédéric FLEURY**

M. le Professeur Hamda BEN HADID

M. le Professeur Didier REVEL

M. le Professeur Philippe CHEVALIER

M. Fabrice VALLÉE

Mme Dominique MARCHAND

## *COMPOSANTES SANTE*

Faculté de Médecine Lyon Est – Claude Bernard

Directeur : M. le Professeur G.RODE

Faculté de Médecine et de Maïeutique Lyon Sud – Charles Mérieux

Directeur : Mme la Professeure C. BURILLON

Faculté d'Odontologie

Directeur : M. le Professeur D. BOURGEOIS

Institut des Sciences Pharmaceutiques et Biologiques

Directeur : Mme la Professeure C. VINCIGUERRA

Institut des Sciences et Techniques de la Réadaptation

Directeur : M. X. PERROT

Département de formation et Centre de Recherche en Biologie Humaine

Directeur : Mme la Professeure A-M. SCHOTT

## *COMPOSANTES ET DEPARTEMENTS DE SCIENCES ET TECHNOLOGIE*

Faculté des Sciences et Technologies

Directeur : M. F. DE MARCHI

Département Biologie

Directeur : M. le Professeur F. THEVENARD

Département Chimie Biochimie

Directeur : Mme C. FELIX

Département GEP

Directeur : M. Hassan HAMMOURI

Département Informatique

Directeur : M. le Professeur S. AKKOUCHE

Département Mathématiques

Directeur : M. le Professeur G. TOMANOV

Département Mécanique

Directeur : M. le Professeur H. BEN HADID

Département Physique

Directeur : M. le Professeur J-C PLENET

UFR Sciences et Techniques des Activités Physiques et Sportives

Directeur : M. Y.VANPOULLE

Observatoire des Sciences de l'Univers de Lyon

Directeur : M. B. GUIDERDONI

Polytech Lyon

Directeur : M. le Professeur E.PERRIN

Ecole Supérieure de Chimie Physique Electronique

Directeur : M. G. PIGNAULT

Institut Universitaire de Technologie de Lyon 1

Directeur : M. le Professeur C. VITON

Ecole Supérieure du Professorat et de l'Education

Directeur : M. le Professeur A. MOUGNIOTTE

Institut de Science Financière et d'Assurances

Directeur : M. N. LEBOISNE

## Acknowledgements

First of all, I would like to extend my sincere gratitude to Prof. Pierre Colon for having been a very supportive and strong supervisor during my PhD journey. Thank you very much for your confidence, motivation and guidance that have kept me moving forward. I am really grateful to you for all the things you have done for me.

Next, I would like to thank Dr. Phil Jackson my industrial supervisor for having been equally supportive in these three years. Phil, I learned a lot from you. Your discipline, commitment to work and balanced approach to life has been a real inspiration. Thank you for that! Thanks a lot to Dr. Mark Cresswell for the technical guidance provided during my PhD research work.

My heartfelt thanks to Dr. Nina Attik for having been a pillar of strength during my PhD. Nina you were not just a mentor but also a good friend ☺. Thank you for being by my side during good and tough times and pushing me to get things done. If not for you, I wouldn't have had a smooth sail! Thank you very much.

My special thanks to my colleague and friend Vincenzo Farano. Henzo, you really made these three years memorable. You have helped me in so many ways and have been a true well-wisher all the while. I really cherish your company and thank you for being there for me every time I needed and for your support!

I would like to thank all my colleagues from Lyon and LUCIDEON- Federico, Hazem, Fatima, Alexi, Caroline, Hannen, Hayeri, Rodica, Franck, Françoise, Bruno, Fatiha, Cecile, Chris, Ian. Thank you all for helping me in my research work.

I'm also thankful to the other members of the BIODENSOL team- Prof. Brigitte, Prof. Christelle, Prof. Jean, Dr. Krestin and Dr. Cyril. Thanks for all your inputs and support.

My sincere thanks to my reviewers- Prof. Robert Hill, Prof. Turkun Sebnem and Prof. Ariane Berdal. Thank you very much for evaluating my work.

I would like to thank my friends Joaquin, Gopika, Divya, Lavi, Nandhu, Sandra and Andy. Thanks for your encouragement and love.

**Mom, dad, Akka, Annan and Venky- words are not enough to express my gratitude and love for you! You are the reason for my success and will always be. I dedicate this work to you!**

## Contents

<b>Abbreviations</b> .....	<b>9</b>
<b>1. Introduction</b> .....	<b>11</b>
1.1. Clinical Background.....	11
1.2. Composite restoration and the adhesive interface .....	12
1.3. Strategies to stabilize the interface .....	14
1.4. Bioactive glasses .....	15
1.5. Mesoporous bioactive glasses .....	18
1.6. Research concept.....	19
1.7. Research aim .....	20
<b>2. Bioactive glass for dentin remineralization-A systematic review.</b> .....	<b>22</b>
2.1. Introduction.....	22
<b>3. Elaboration of Mesoporous Bioactive Glasses (MBGs)</b> .....	<b>32</b>
3.1. Introduction.....	32
3.2. Materials and methods.....	34
3.2.1. Materials.....	34
3.2.2. Fabricating MBG and BG using nitrate precursors .....	34
3.2.3. Literature repeat.....	34
3.2.4. Fabrication of MBGs using acetate precursors.....	35
3.2.5. Differential scanning calorimetry (DSC) and Differential thermogravimetric (DTG) Analysis ..	35
3.2.6. X-ray diffraction (XRD).....	35
3.3. Results and discussion .....	37
3.3.1. Fabricating MBG using nitrate precursors.....	37
3.3.2. MBG vs BG comparison.....	38
3.3.3. Literature repetition.....	40
3.3.4. Acetate system:.....	42
3.4. Conclusion .....	46
<b>4. Influence of scale on the surface characteristics of MBGs</b> .....	<b>47</b>
4.1. Introduction.....	47
4.2. Materials and Methods .....	47
4.2.1. Materials and Sample preparation.....	47
4.2.2. X-ray diffraction .....	47
4.2.3. BET/BJH .....	48
4.3. Results and discussion .....	48

4.4. Conclusion.....	51
<b>5. Influence of network modifiers on the surface characteristics of MBGs .....</b>	<b>52</b>
5.1. Introduction.....	52
<b>6. The influence of precursor addition order on the porosity of sol-gel bioactive glasses .....</b>	<b>64</b>
6.1. Introduction.....	64
<b>7. The influence of increasing surfactant concentration on the microstructure of MBGs.....</b>	<b>77</b>
7.1. Introduction.....	77
7.2. Materials and Methods.....	77
7.2.1. Materials.....	77
7.2.2. Sample preparation .....	78
7.2.3. Sample characterization.....	78
7.2.3.1. XRD.....	78
7.3. Results and Discussion.....	79
7.4. Conclusion.....	91
<b>8. Evaluation of “apatite forming ability” and “cytocompatibility” of MBGs on Human Gingival Fibroblasts. ....</b>	<b>92</b>
<b>8.1. Introduction.....</b>	<b>92</b>
8.2. Materials and methods.....	93
8.2.1. Materials.....	93
8.2.2. Simulated Body Fluid (SBF) preparation .....	93
8.2.3. Apatite forming ability in vitro (SBF test).....	94
8.2.4. Cytocompatibility evaluation on Human gingival fibroblasts .....	95
8.3. Results and discussion .....	96
8.3.1. Apatite forming ability.....	96
8.3.2. Cytocompatibility.....	103
8.4. Conclusion.....	106
<b>9. MBGs in adhesives-Particle size reduction, viscosity and apatite forming ability .....</b>	<b>107</b>
9.1. Introduction.....	107
9.2. Materials and Methods.....	107
9.2.1. 0Na MBG preparation .....	107
9.2.2. Ball milling.....	107
9.2.3. Particle size measurement.....	108
9.2.4. BET/BJH. ....	108
9.2.5. Adhesive with MBG-Viscosity and pellet preparation.....	108
9.2.6. Apatite forming ability.....	109

9.2.7. SEM.....	109
9.3. Results and discussion .....	109
9.4. Conclusion .....	118
<b>10. Conclusion .....</b>	<b>119</b>
10.1. Future perspectives .....	123
<b>11. References .....</b>	<b>125</b>
<b>12. Abstract .....</b>	<b>148</b>

## List of Figures

<b>Figure 1</b> Development of non-cavitated enamel caries (From Axelsson [3]) .....	11
<b>Figure 2</b> Amalgam (Left) and composite (Right) restoration (Clinical case, Prof.Pierre colon).....	13
<b>Figure 3</b> Secondary caries at the in interface (Clinical case, Prof.Pierre colon) .....	14
<b>Figure 4</b> Mechanism of bioactivity of bioactive glasses [43] .....	16
<b>Figure 5</b> Templates synthesis of mesoporous silica [75].....	18
<b>Figure 6</b> Research outline .....	21
<b>Figure 7</b> 10Na MBG prepared using nitrate precursors after 700°C calcination for 4 hours .....	37
<b>Figure 8</b> 10Na MBG prepared using nitrate precursors after 850°C and 950°C calination in a gradient kiln.....	38
<b>Figure 9</b> XRD of 10Na MBG prepared using nitrate precursors after 950°C calcination.....	38
<b>Figure 11</b> XRD of 10Na BG prepared using nitrate precursors after 700°C calcination.....	39
<b>Figure 10</b> Large scale samples prepared using nitrate precursors after 700°C calcination for 5 hours .....	39
<b>Figure 12</b> (A)Literature replicate sample after 700°C calcination (B) 10Na MBG sample after 700°C calcination .....	40
<b>Figure 13</b> XRD of literature replicate sample after 700°C calcination .....	40
<b>Figure 14</b> DSC curves of small scale samples of various compositions prepared using acetate precursors .....	42
<b>Figure 15</b> DTG curves of small scale samples of various compositions prepared using acetate precursors .....	43
<b>Figure 16</b> Small scale samples prepared using acetate precursors calcined at 450°C for 5hours .....	44
<b>Figure 17</b> Small scale samples prepared using acetate precursors calcined at 480°C for 5hours; (A) 10Na MBG (B) 7.5Na MBG (C) 5Na MBG .....	44

<b>Figure 18</b> DSC curves of large scale samples of various compositions prepared using acetate precursors .....	45
<b>Figure 19</b> DTG curves of small scale samples of various compositions prepared using acetate precursors .....	45
<b>Figure 20</b> Large scale samples prepared using acetate precursors calcined at 380°C for 5hours; (A) 10Na MBG (B) 7.5Na MBG (C) 5Na MBG .....	45
<b>Figure 21</b> XRD of samples after thermal treatment (A) Small scale samples calcined at 480°C (SS) (B) Large scale sample calcined at 380°C (LS).....	48
<b>Figure 22</b> BET/BJH analysis of small scale samples (SS MBGs) and large scale samples (LS MBGs). (A) Surface area (B) Pore volume (C) Pore size .....	49
<b>Figure 23</b> Adsorption and desorption isotherms of small scale samples (SS MBGs, A) and large scale samples (LS MBGs, B).....	50
<b>Figure 24</b> Pore size distribution of small scale samples (SS MBGs, A) and large scale samples (LS MBGs, B) .....	50
<b>Figure 25</b> (A) 4wt% 0Na MBG, (B) 8wt% 0Na MBG and (C)16wt% 0Na MBG after direct calcination at 380°C .....	79
<b>Figure 26</b> (A) 4wt% 0Na MBG, (B) 8wt% 0Na MBG and (C)16wt% 0Na MBG after ethanol ultrasonication and calcination at 380°C .....	80
<b>Figure 27</b> (A) 4wt% 0Na MBG,(B) 8wt% 0Na MBG and (C)16wt% 0Na MBG after ethanol ultrasonication and calcination at 340°C .....	80
<b>Figure 28</b> Phase composition of 0Na BG, 1.8Wt%, 4wt%, 8wt% and 16wt% 0Na MBGs.....	81
<b>Figure 29</b> Phase composition of 10Na BG, 1.8Wt% and 4wt% 10Na MBGs.....	82
<b>Figure 30</b> Surface area, pore volume and pore size results of 0Na BG, 1.8Wt%, 4wt%, 8wt% and 16wt% 0Na MBGs.....	83
<b>Figure 31</b> Surface area, pore volume and pore size results of 10Na BG with 0 wt% (BG) 1.8Wt% and 4wt% (MBG) surfactant .....	84
<b>Figure 32</b> Hysteresis loops of (A) 0Na BG, (B)1.8wt% 0Na MBG, (C) 4wt% 0Na MBG,(D) 8wt% 0Na MBG and (E) 1.6wt% 0Na MBG.....	85
<b>Figure 33</b> Hysteresis loops of (A) 10Na BG, (B)1.8wt% 10Na MBG and (C) 4wt% 10Na MBG.....	85
<b>Figure 34</b> Pore size distributions of A) 0Na BG, (B)1.8wt% 0Na MBG, (C) 4wt% 0Na MBG,(D) 8wt% 0Na MBG and (E) 1.6wt% 0Na MBG.....	86
<b>Figure 35</b> Pore size distributions of (A) 10Na BG, (B)1.8wt% 10Na MBG and (C) 4wt% 10Na MBG .....	86

<b>Figure 36</b> pH of 0Na, 5Na and 10Na MBG thermal treated at 310°C; (A) in De-ionised water (B) in SBF .....	97
<b>Figure 37</b> XRD of MBGs before and after immersion in SBF; (A) 0Na MBG (B) 10Na MBG for up to a week (short time points) .....	97
<b>Figure 38</b> FTIR of 0Na and 10Na MBG before immersion in SBF .....	98
<b>Figure 39</b> FTIR of MBGs after immersion in SBF (A) 0Na MBG (B) 10Na MBG for up to a week (short time points).....	99
<b>Figure 40</b> XRD of MBGs before and after immersion in SBF; (A) 0Na MBG (B) 10Na MBG for up to 3 weeks (long time points) .....	100
<b>Figure 41</b> FTIR of MBGs after immersion in SBF (A) 0Na MBG (B) 10Na MBG for up to 3 weeks (long time points).....	100
<b>Figure 42</b> Morphology of 0Na MBG and 10Na MBG at day 0, day 3 and day 7 in SBF; Scale bar 5µm .....	102
<b>Figure 43</b> Optical microscopic images of MBGs interfaced with Human gingival fibroblasts at day 1 and day 3.....	104
<b>Figure 44</b> Live dead images of MBGs interfaced with human gingival fibroblasts at day 3.....	104
<b>Figure 45</b> Metabolic activity of human gingival fibroblasts interfaced with MBGs at day 2 and day 6 .....	105
<b>Figure 46</b> Particle size distribution of 0Na MBG thermally treated at 310°C; (A) unmilled, (B) dry ball milled and (C) wet ball milled.....	110
<b>Figure 47</b> Hysteresis loops of 0Na MBG thermal treated at 310°C; (A) unmilled, (B) dry ball milled and (C) wet ball milled.....	111
<b>Figure 48</b> Pore size distribution of 0Na MBG thermal treated at 310°C; (A) unmilled, (B) dry ball milled and (C) wet ball milled.....	112
<b>Figure 49</b> Impact of milling on loss of particle porosity, change of pore structure and size.....	113
<b>Figure 50</b> Viscosity of unfilled commercial resin with varying weight percent of 0Na MBG .....	114
<b>Figure 51</b> SEM images of 0%, 10% and 30% filled adhesive resin immersed in SBF upto 21 days..	117

## Abbreviations

**ATR-FTIR:** Attenuated total reflectance-Fourier transform infra red spectroscopy

**BG, BAG:** Bioactive glass

**Bis-GMA:** Bisphenol A diglycidyl ether dimethacrylate

**BET/BJH:** Brunauer-Emmett-Teller/Barret-Joyner-Halenda

**CTAB:** Cetrimonium bromide

**CLSM:** Confocal laser scanning microscopy

**DSC/TGA:** Differential scanning calorimetry/Thermogravimetric analysis

**DTG:** Differential thermogravimetric

**DMEM:** Dulbecco's modified Eagle's medium

**EISA:** Evaporation induced self assembly

**ER:** Etch and rinse

**EDTA:** Ethylenediamine tetra-acetic acid

**FTIR:** Fourier transform infra red spectroscopy

**FDA:** Food and drug Administration

**FBS:** Fetal bovine serum

**GIC:** Glass ionomer cement

**HCA:** Hydroxyapatite

**HEMA:** 2-Hydroxyethyl methacrylate

**HGF:** Human gingival fibroblasts

**ICP-OES:** Inductively coupled plasma-optical emission spectrometry

**ISO:** International standards organization

**MBG:** Mesoporous bioactive glass

**MMP:** Matrix metalloproteinases

**PCS:** Polycarboxylated calcium silicate

**PDP:** Polycarboxylated calcium silicate doped brushite microfillers.

**PRISMA:** Preferred reporting items for systematic reviews and meta-analyses

**PBS:** Phosphate buffered saline

**REACH:** Registration, evaluation, authorisation and restriction of chemicals

**RT:** Room temperature

**SE:** Self etch

**SEM:** Scanning electron microscopy

**SEM-EDX:** Scanning electron microscopy coupled with Energy dispersive X-ray spectroscopy

**SBF:** Simulated body fluid

**TEM:** Transmission electron microscopy

**TEM-SAED:** Transmission electron microscopy coupled with selected area electron diffraction

**TEGDMA:** Triethylene glycol dimethacrylate

**TEOS:** Tetraethyl orthosilicate

**TEP:** Triethyl phosphate

**UDMA:** Urethane dimethacrylate

**XRD:** X-ray diffraction

**XRF:** X-ray fluorescence

# 1. Introduction

## 1.1. Clinical Background

Caries or tooth decay is an infectious oral disease that leads to loss of the tooth tissue. To understand this disease one needs to be aware that the biofilm in the oral environment supports a complex 'micro-ecosystem' of bacteria whose homeostasis is crucial to prevent the occurrence of this disease [1] **Figure 1**. In simplified terms, the bacteria produce acid while breaking down the sugary food we ingest which consequently lowers the pH of the biofilm. It is important to note that the acidic pH rips the calcium phosphate mineral phase off the tooth tissue (demineralization) whilst neutral pH promotes gain of minerals (remineralization). This temporary reduction in pH and neutralization is a normal cyclic process involved in the homeostasis mechanism which occurs several times daily in the dental plaque.

However, the initial enamel lesion appears only when the **balance is lost**. Excessive sugar based diets or acidic food consumption without sufficient hygiene measures to promote neutralization creates a shift in dynamics towards acidic conditions and as a result demineralization dominates remineralization [2].

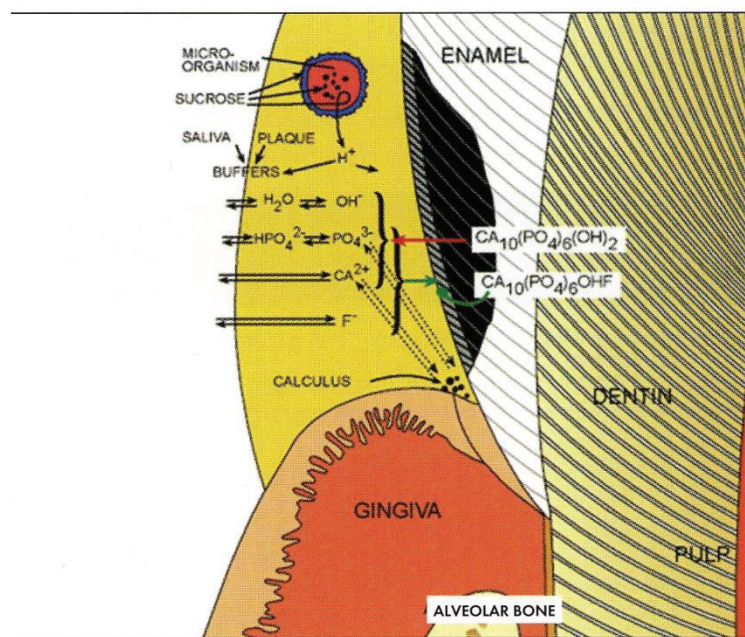


**Figure 1 Development of non-cavitated enamel caries (From Axelsson [3])**

In terms of clinical symptoms, early stages of caries manifests as a white spot lesion [4] in the enamel which when not treated progresses gradually into deeper tooth tissues such as the dentin and pulp. Pulp inflammation appears at early stages of initial caries and remains reversible. The development of deeper lesions leads to irreversible inflammation and irreversible pulpitis requiring evicton of pulp tissues and endodontic therapy.

Besides caries, the exposure of dentinal tubules through abrasion and/or erosion process or the gingival recession leads to dentin hypersensitivity [5,6] that causes pain and heightened sensitivity while eating warm or cold foods.

Tooth erosion [6] is the result of clinical condition which leads to loss of minerals and this is mainly due to over consumption of acidic drinks, food or gastrointestinal acid refluxes.

## **1.2. Composite restoration and the adhesive interface**

Composite restorations are one of the most widely used types of restoration to replace tissue lost by carious lesions. It is a resin based material which contains a blend of methacrylate monomers [7]. In order to perform a restoration with this material, the clinician first removes the caries infected part of the tooth. Let us consider that the caries has progressed up to the dentin as restoration in this part of the tissue is more complex compared to enamel. Once the infected part is removed the lesions are cleaned and subjected to acid etching with 30% phosphoric acid [8]. The aim of this acid etching is to demineralise the tissue in order to create microporosities for the resin based materials of the restoration to infiltrate. Once etching is performed the spot is rinsed with water, air dried and then the first restorative layer- “the adhesive” is applied.

The adhesive is an important component of the composite restoration and as the name implies it bonds the tooth tissue with the filling material (composite). The bond is created by infiltrating the microporosities created in the tissue (etching) with the adhesive components (primer and adhesive) to form resin tags in dentin. These resin tags create mechanical interlocking of the adhesive resin with dentin [9–11]. The mixture of the organic dentin matrix (collagen) with the seed crystallites in combination with the adhesive resin monomers and solvents is termed the hybrid layer [12,13]. In order to penetrate the complete depths of the demineralised dentin it is obvious that the adhesive resin should be of very low viscosity to flow through the dentin and cover the demineralised regions. Also, it should contain hydrophilic monomers to effectively wet the surface of the dentin [11]. Once the adhesive is applied and light cured (to polymerise the resin monomers) a thin bonding layer is created.

Dental adhesives have gone through a massive evolution since their introduction. The early stage adhesive was only applied on the smear layer. In 1990’s “etch and rinse” system (ER) for dentin was introduced and as explained above it involved etching, rinsing, application of primer (solvent and

hydrophilic resin monomers) followed by application of adhesive (more hydrophobic monomers). Then it was simplified into a 2 step ER system wherein the primer and adhesives were combined as a single adhesive component. Another approach is the “self etch” (SE) adhesive which no longer needs

the etching step. This was achieved by including acidic monomers into the adhesive resin which contains a mixture of hydrophilic monomers, hydrophobic monomers and solvent [12–14]. Even though these simplified adhesives are present in the market they have not completely replaced the early ER adhesives as each system has its own advantages and limitations.

After applying the adhesive, composite filling needs to be performed to complete the restoration. The composite filling is generally a highly viscous paste containing 70 percent silica glass particles powder filler in combination with barium and strontium to ensure good mechanical properties and radiopacity [14,15]. After the composite paste is applied over the adhesive layer and shaped (to mimic the crevices in the tooth) the material is light cured and the restoration is performed.

Composite restorations are aesthetically superior to other restorations (**Figure 2**). However, one of the main drawbacks is the short life time of these restorations as they last only about 7 years (half the average life time of amalgam restorations) [11,16]. However, some researchers have also claimed an improvement in the longevity of composite restorations [17]. Failure of restoration is a real problem not only due to the economical constraints for the patient but also mainly because the removal of failed restoration leads to loss of adjacent tooth tissue which means there is less mineralised tissue to anchor the next restoration.



**Figure 2 Amalgam (Left) and composite (Right) restoration (Clinical case, Prof.Pierre colon)**

Some of the main reasons for the failure of restorations are reported to be the problems occurring at the adhesive interface. To elaborate, once the mineral part of the dentin is removed by etching, the organic part (collagen) becomes exposed and simultaneously water enters and quickly fills the regions previously occupied by the mineral [18,19]. Removing the mineral part of the dentin activates the matrix metalloproteinases (MMPs) and cathepsins in that area. These proteases are hydrolases, which means they hydrolyze the peptide bond of the collagen by using free water molecules thus leading to its degradation [16–20].

The adhesive resin should ideally penetrate the entire demineralised dentin substrate to provide adequate retention as well as seal the exposed tissue. However, as this is not the case in reality, there are resin sparse regions in the substrate that are susceptible to water accumulation. Now, it is important to understand that over drying the dentin and complete dehydration can lead to the collapse of collagen fibrils as a certain amount of water is needed for their integrity. Therefore water cannot be completely eliminated from the procedure but its presence should be minimised.

Water not only leads to collagen degradation but its entry into the adhesive resin (water trees) leads to the hydrolysis of the resin polymers into monomers which jeopardises the integrity of the resin and weakens the bond strength [20–23]. Furthermore, remnant water molecules in the hybrid layer interfere with cross linking of resin monomers and reduce their degree of polymerisation [24]. Water uptake by resins also leads to a swelling of the polymer network and the monomers released upon their relaxation create new channels for water penetration into the hybrid layer [25,26]. Also, water trapped at the adhesive composite interface by the hydrophobic composite resin forms water blisters which play a detrimental role in affecting the bond strength between the composite and adhesive [13].

Another problem is the polymerisation shrinkage of the adhesive resin. The reduction in resin volume due to polymerisation shrinkage creates gaps at the adhesive-dentin interface. These gaps on one hand compromise the bonding efficiency and on the other act as attractive spots for the accumulation of bacteria to bring about secondary caries [27,28] **(Figure 3)**. Most composite restoration failures have been reported to occur due to recurrent caries.



**Figure 3 Secondary caries at the in interface (Clinical case, Prof.Pierre colon)**

### **1.3. Strategies to stabilize the interface**

To deal with the problems at the adhesive interface several strategies have been proposed which mainly focus on improving the resin impregnation into the mineralised and demineralised dentin substrates, improving the strength of the polymer in the adhesive system and reducing the enzymatic degradation of collagen fibrils. Some of the strategies are summarised below.

- Vigorous rubbing of the adhesive to enhance its penetration into the dentin substrate.
- Multiple coats of adhesive application for simplified adhesive system [29–31].
- Hydrophobic coating after simplified adhesive application to limit water penetration [32].
- Extended light curing to increase the degree of polymerization and reduce permeability.
- Use of MMP inhibitors such as Chlorhexidine [33,34], ethylenediamine tetra-acetic acid (EDTA) [35], tetracyclines [36,37], galardin [38].
- Use of collagen cross-linkers such as glutaraldehyde and proanthocyanidins [39] to improve the mechanical properties and decrease the degradation of collagen.

Remineralization on the other hand is an emerging concept that is being explored to extend the longevity of the interface. The concept is that remineralization of collagen fibrils by ion releasing materials such as amorphous calcium phosphate [40], and bioactive glasses can replace water, recreate apatite crystals and inactivate the MMPs in the dentin [41].

#### 1.4. Bioactive glasses

Bioactive glass was introduced by Prof. Larry Hench in 1970 and it was the first material deemed to be bioactive [42]. Before the advent of bioactive glass the standard for biomaterials was to be bioinert, i.e. to avoid triggering any host inflammatory response. However, bioinert materials develop a fibrous encapsulation after implantation which deters a stable bond with the tissue. Implant loosening over time and tissue break down was reported as the most common mode of failure for bioinert materials. Furthermore the stress shielding effect due to varying elastic modulus between the tissue and implant material leads to bone resorption and failure [43].

Prof. Hench tried to overcome this problem and after years of research he invented Bioactive glass<sup>®</sup> of the composition 45SiO<sub>2</sub>-24.5CaO-24.5Na<sub>2</sub>O-6P<sub>2</sub>O<sub>5</sub> (45S5) in weight percent in which silica and phosphate are the glass network formers and sodium and calcium are the network modifiers. 45S5<sup>®</sup> demonstrated a direct and an inseparable bonding with bone which revolutionised the field of biomaterials and elevated their standard to be bioactive.

The discovery of bioactive glass consequently initiated the evaluation of other potentially bioactive ceramic materials such as hydroxyapatite and calcium phosphates [44–48]. Following the invention of bioactive glass Hench also explored the mechanism behind its bioactivity (**Figure 4**). Briefly, in the initial stages there is a rapid exchange of ions such as Na<sup>+</sup> and Ca<sup>2+</sup> with the H<sup>+</sup> ions in the surrounding environment. Simultaneously, water also hydrolyses the silica network and as a result surface silanols (Si-OH groups) are formed. The depolymerisation of the network leads to the release of PO<sub>4</sub><sup>3-</sup> ions and silica in the form of silicic acid (Si(OH)<sub>4</sub>). The surface silanols then condense to form

a silica rich layer. Once the calcium and phosphate ions have supersaturated the surrounding media they deposit on the Si-O-Si layer that acts as nucleation sites for the growth of crystals. At first the deposited calcium and phosphate remain as an amorphous calcium phosphate layer which eventually crystallises into hydroxyapatite. The formed hydroxyapatite adsorbs growth factors which attracts stem cell attachment and enhances their differentiation into osteoblasts. The osteoblasts then secrete the bone matrix which explains the strong bond between bioactive glass 45S5 and bone tissue. It should be noted that the heightened apatite forming ability of bioactive glass is key to its enhanced bioactivity [43,49].

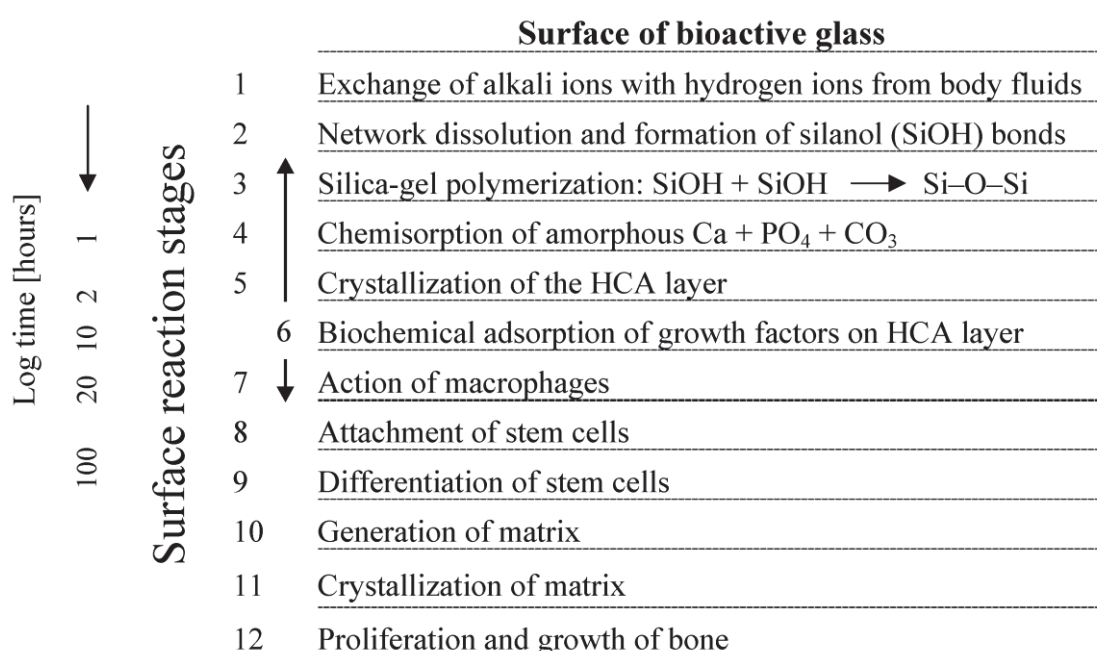


**Figure 4 Mechanism of bioactivity of bioactive glasses [43]**

The most commonly used methods to prepare bioactive glasses are melt quench and sol-gel techniques [50,51]. Melt quench is a conventional method and is still the most widely used technique to prepare these glasses. In this technique the precursors (oxides or materials like carbonates that can degrade to oxides) are added to a crucible, melted at very high temperatures in a furnace and then rapidly quenched (in water or a cooled metal) to avoid crystallization. Melt quenched glasses have high density and are non-porous. They have the advantage of being prepared at relatively low cost on an industrial scale. However some of the disadvantages of this processing method are the possibility of contamination, cost (temperature and crucibles), volatilisation of some components at high temperatures and compositional limitation as very high silica content glasses are difficult to melt [52].

Sol-gel is a “bottom up” low temperature processing route which enables bioactive glass preparation even at room temperatures. It is based on the hydrolysis and condensation reaction of glass monomer precursors in addition to a low temperature thermal treatment for their stabilization [53]. Sol-gel glasses contain innate porosity and as a result they have higher specific surface area than melt quenched glasses. The improved surface area of sol-gel bioactive glasses leads to enhanced ion release resulting in improved bioactivity in vitro [54]. Moreover, the sol-gel technique offer numerous process variables such as catalyst type, pH, solvent quantity, precursor type, ageing temperature and stabilization temperature which can be modulated to tailor the microstructure of the end product [50]. It should be noted that melt quenched glasses lose their bioactivity when the mole percentage of silica is above 60. However, the bioactivity of sol-gel glasses even with 90 percent silica has been demonstrated. This emphasises that the bioactivity of melt quenched glasses is mostly composition driven whereas in sol-gel glasses the textural properties and surface area properties of the materials play a vital role.

Lately, the compositions of bioactive glasses are also being modified by adding “dopants” to enhance biological/mechanical properties including the delivery of target specific bioactivity, bioresorbability and biodegradability. A well-known dopant in bioactive glasses is silver oxide (AgO) as it imparts antibacterial properties to the material. Besides silver, copper and zinc are also researched for their antibacterial properties and potential to enhance cell response [55–59]. Fluoride is favoured for dental applications as the formation of fluorapatite is more resistant to acid attack and supports remineralization of dental tissues [60,61]. Strontium promotes osteoblast differentiation [62–65] and is also being researched for its potential to stimulate odontoblast differentiation of pulp stem cells.

Bioactive glasses have thus found their application as bone grafts, orthopaedic and dental implant coatings and scaffold for tissue regeneration. Due to its enhanced apatite forming ability bioactive glass Novamin® is also used in dentifrice to treat dentin hypersensitivity by occluding the exposed dentinal tubules with newly formed apatite crystals [52]. Furthermore bioactive glasses are also considered as materials with heightened potential to remineralize dental tissues [66–68]. BiominF® is a further example of a recently developed toothpaste containing bioactive glass for enamel remineralization. Research is also focused on using bioactive glasses in air polishing [69,70] and in air abrasion techniques to stimulate mineralization of the tissue through apatite formation. Studies are also exploring the use of bioactive glasses as fillers in dental adhesive[71] and composites [72] to enhance the longevity of the restoration through remineralization and enhanced antibacterial effects.

## 1.5. Mesoporous bioactive glasses

Mesoporous Bioactive Glasses (MBGs) are an evolution of sol-gel bioactive glasses. MBGs are similar to mesoporous silicas [73] (SBA-15, MCM-41) in textural properties and superior to sol-gel bioactive glasses in their bioactivity [74]. They are obtained by introducing surfactants (structure directing agents) during the sol-gel synthesis of bioactive glasses.

There are different types of surfactants such as non-ionic, cationic, anionic, zwitterionic etc. The most commonly used surfactants in bioactive glass literature are Pluronic P123 and F127 which are non-ionic block copolymers. Ionic surfactants such as cetyltrimonium bromide (CTAB) are also used in some studies. The non-ionic organic block copolymers are amphiphilic in nature. They contain a hydrophobic tail (hydrophobic block) and hydrophilic head (hydrophilic block). When added to an aqueous or polar solvent the hydrophilic heads of the surfactant molecules have a strong interaction with the solvent whereas the hydrophobic tail positions themselves such that the interaction with the solvent is minimized. Once the surfactant molecules (unimers) in the system reach the critical micelle concentration they start to aggregate to form micelles. The unimers aggregate in such a fashion that the hydrophobic tails point inward and the hydrophilic heads freely contact the solvent (**Figure 5**).

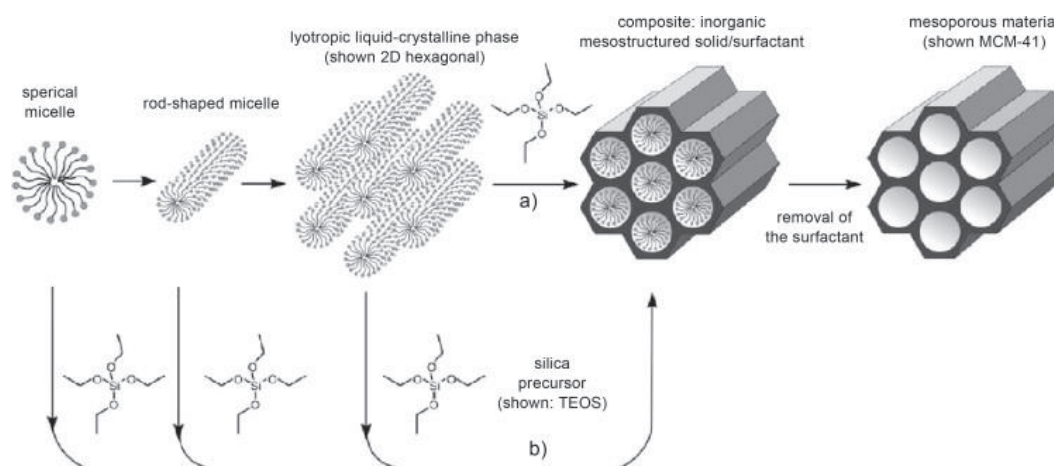


**Figure 5** Templates synthesis of mesoporous silica [75]

The glass precursors added during the sol-gel synthesis are attracted to the surface of the micelles after which further condensation results in the formation of the glass network around these micelles. After evaporation induced self-assembly and ageing the material is subjected to thermal treatment. Thermal treatment burns away the micelles and thus pores are induced in the places previously occupied by the pore forming agents. As a result MBGs have advanced textural characteristics such as high surface area, increased pore volume, pore size and hierarchical organization of pores. This in turn enhances their apatite forming ability which is much more rapid compared to normal sol-gel bioactive glasses. Besides increasing the porosity and surface area, studies have also shown that the particle morphology and size can be controlled by varying the surfactant concentration during MBG

preparation. In addition, MBG scaffolds are also shown to have much higher compressive strength than sol-gel bioactive glass scaffolds [76]. The ordered pore structure of MBGs has also attracted possibilities to use them as vehicles for drug delivery. Studies have reported that the uniform porosity in MBGs supports sustained drug release [74,77,78].

The potential of MBGs has been intensively explored in the bone tissue regeneration field over the past decade. Several findings have been reported proving a rapid apatite formation and crystallization of MBGs compared to sol-gel bioactive glasses [76,79–81]. Similar to normal bioactive glasses, MBGs can also be doped with various elements to increase their functionality. Studies have doped MBGs with silver, copper, zinc, cerium and gallium to study their antibacterial and in some cases angiogenic properties [82]. MBGs doped with strontium have also been explored for their ability to promote the osteogenic, odontogenic and cementogenic differentiation of cells.

The published work on MBGs in the dental literature is scarce yet motivating. Chen *et al.*, reported the potential of MBGs to occlude dentinal tubules [83][84]. The authors have also compared and demonstrated the enhanced apatite forming ability of MBGs versus sol-gel bioactive glasses. Lee *et al.*, developed MBG nanoparticles and showed the cell uptake and internalization of these particles. Their results also showed that the odontogenic related genes and markers for biomineralization were significantly up regulated in pulp stem cells treated with MBGs [85]. Kim *et al.*, prepared nanofibre composite scaffolds of MBG and polycaprolactone-gelatin [86] and demonstrated the material's ability to differentiate dental pulp stem cells into odontoblasts through integrin, BMP, and mitogen-activated protein kinases signalling pathway. Dong *et al.*, reported the potential of MBGs to remineralize enamel as the MBG treatment led to the formation of a 100 nm thick mineral layer which was similar to apatite and generated improvements in the mechanical properties of the mineralized tissue. Recently Lee *et al.*, published an in vivo study on the regeneration of dentinal hard tissue in rats using strontium-doped MBG loaded with a therapeutic drug Phenamil. The combined release of strontium ion and the drug facilitated the regeneration of the dentinal tissue through stimulation of both adult stem cell differentiation into odontoblasts and the BMP signaling pathway [87]. To the best of our knowledge and search, we haven't found any research paper using MBGs as fillers in dental adhesives [88].

## **1.6. Research concept**

After learning about the existing approaches to improve the longevity of the adhesive-dentin interface and use of ion releasing materials to aid remineralisation, using MBGs as fillers in dental adhesives appeared to be a novel and interesting approach to explore. The reasons are mentioned below.

First, the introduction of MBGs as fillers in adhesive resin could replace the trapped water molecules in the resin, improve their cross linking ability and reduce the polymerization shrinkage.

Next, as the fillers are porous they allow us to functionalise their pores with antibacterial drugs whose release could combat secondary caries. Certain antibacterial drugs, such as chlorhexidine, are also MMP inhibitors therefore the protection of underlying collagen could also be ensured. They could also be functionalised with growth factors whose release can stimulate odontoblasts to secrete mineralised dentin.

Most importantly, the reaction of MBGs with water, subsequent release of ions and the resultant formation of hydroxyapatite or calcium phosphate precipitate could protect the resin as well as the underlying collagen from hydrolytic and enzymatic degradation.

These tailored characteristics of MBGs make them a highly attractive candidate to be used as fillers in adhesives to improve the longevity of the interface.

### **1.7. Research aim**

The aim of the project is to study the potential of Mesoporous Bioactive glasses (MBGs) as fillers in adhesives to improve the longevity of the adhesive resin interface. The content of this research is about the formulation of novel MBGs and then an evaluation / optimization of their characteristics to be used as fillers in dental adhesives (**Figure 6**).

The broad aims of this research are:

1. Synthesis and characterization of novel compositions of MBGs suitable as fillers in adhesive resin.
2. Evaluate the effect of MBG fillers on the viscosity and apatite forming ability of adhesive resin.

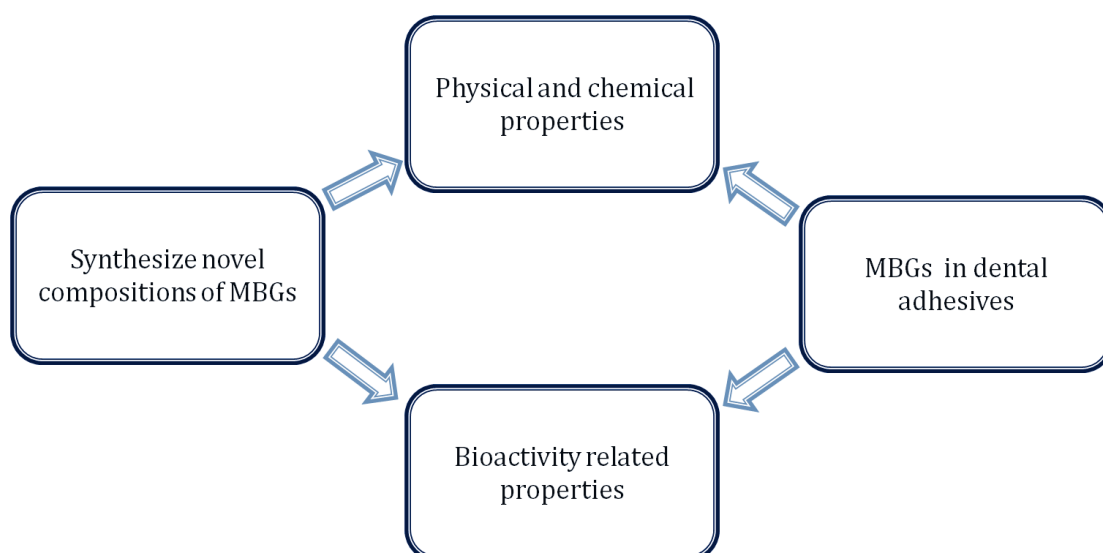


**Figure 6 Research outline**

Specifically, we aimed at synthesising MBGs with high surface area and porosity as improved surface area should facilitate enhanced ion release for remineralization. Also, porosity is needed to functionalize the pores with drugs. High calcium oxide in the composition was desired to improve their bioactivity. Furthermore, MBG fillers with enhanced apatite forming ability (remineralizing potential) and cytocompatibility were important for this application. The particle size of MBGs should also be optimal in order to be used as fillers in adhesive resins without negatively affecting the viscosity. Finally, MBG filled adhesive resin with flowable viscosity as well as apatite forming capability within the adhesive when immersed in remineralizing media were deemed important to evaluate their potential for the targeted application.

## **2. Bioactive glass for dentin remineralization-A systematic review.**

### **2.1. Introduction**

A systematic review was performed following PRISMA guidelines to evaluate if bioactive glasses can rematerialize dentin in a functional manner. By functional remineralization we mean the restoration of biomechanical properties of dentin after the gain of new minerals. Therefore, the emphasis was not only placed on the evaluation of new mineral content as a result of bioactive glass treatment but also on the changes in the mechanical properties of dentin.

This review has been published in the *Journal Material Science and Engineering C*.



Contents lists available at ScienceDirect

## Materials Science and Engineering C

journal homepage: [www.elsevier.com/locate/msec](http://www.elsevier.com/locate/msec)

## Review

## Bioactive glass for dentin remineralization: A systematic review



Delihtha Fernando <sup>a</sup>, Nina Attik <sup>a,b</sup>, Nelly Pradelle-Plasse <sup>a,c,f</sup>, Phil Jackson <sup>d</sup>,  
Brigitte Grosgeat <sup>a,b,c</sup>, Pierre Colon <sup>a,e,f</sup>

<sup>a</sup> Laboratoire des Multimateriaux et Interface, Université Claude Bernard Lyon 1, Lyon, France

<sup>b</sup> Faculté d'Odontologie, Université Claude Bernard Lyon 1, Lyon, France

<sup>c</sup> Service d'Odontologie, Hospices Civils de Lyon, Lyon, France

<sup>d</sup> Lucideon Inc., Penkhull, Stoke-On-Trent ST4 7LQ, UK

<sup>e</sup> Faculté d'Odontologie, Université Paris Diderot, Paris, France

<sup>f</sup> APHP, Hôpital Rothschild, Service d'Odontologie, Paris, France

## article info

## Article history:

Received 14 December 2016

Received in revised form 6 March 2017

Accepted 12 March 2017 Available online

14 March 2017

## Keywords:

Bioactive glass

Remineralization

Dentin

## Abstract

**Background and objectives:** Strategies to achieve dentin remineralization is at present an important target of restorative dentistry. Remineralization of dentin by a bioactive material is complete only when the tissue regains its functionality. This is achieved when there is adequate apatite formation which most importantly translates into improved mechanical properties of dentin as a result of intrafibrillar mineralization. Bioactive glass (BAG) is a well-known implant material for bone regeneration and is proven to have excellent ability of apatite formation. Hence, recent studies have proposed BAGs as one of the most desired materials for remineralization of dentin. Therefore the aim of this systematic review was to scope the evidence of bioactive glass to remineralize dentin.

**Methods:** The following research question was formulated: “Is there strong evidence for bioactive glass to remineralize dentin?” Three databases (Web of science, PubMed and Science direct) were scanned independent-ly following PRISMA guidelines. Inclusion and exclusion criteria were set to identify relevant articles based on title and abstract screening. Finally, potentially relevant articles were downloaded and the full text was scrutinized to select the articles included in this review.

**Results:** The first phase of search returned 303 articles. A total of 19 papers with full text were scrutinized for inclusion, of which 3 papers were chosen for the final synthesis. All three studies confirm that BAG treatment leads to enhanced apatite formation in dentin. Only 1 of the 3 studies has reported the mechanical properties of dentin after BAG treatment and it revealed that the Young's modulus and flexural bend strength of BAG treated dentin were much lower than natural dentin even though they had similar apatite content.

**Conclusions:** This review highlights the importance of assessing the mechanical properties of dentin alongside to the newly formed apatite content in order to prove BAGs efficiency to remineralize this tissue. Though studies have confirmed that BAGs stimulate excellent apatite formation in dentin, it should be concluded that there isn't sufficient evidence for bioactive glass to effectively remineralize this tissue as the mechanical properties of the BAG treated dentin haven't been well explored.

© 2017 Elsevier B.V. All rights reserved.

## Contents

1. Introduction . . . . .	1370
2. Methods . . . . .	1371
2.1. Research question . . . . .	1371
2.2. Search strategy . . . . .	1371
2.3. Keywords selection . . . . .	1371
2.4. Inclusion and exclusion criteria . . . . .	1371
2.5. Paper selection and data extraction . . . . .	1371

Corresponding author at: Faculté d'Odontologie, 11, Rue Guillaume Paradin, 69372 Lyon Cedex 08, France. E-mail address: [nina.attik@univ-lyon1.fr](mailto:nina.attik@univ-lyon1.fr) (N. Attik).

<http://dx.doi.org/10.1016/j.msec.2017.03.083>

0928-4931/© 2017 Elsevier B.V. All rights reserved.

3.	Results . . . . .	1371
3.1.	Study characteristics . . . . .	1372
3.1.1.	BAG characteristics . . . . .	1372
3.1.2.	Protocol . . . . .	1372
3.1.3.	Classification of included studies . . . . .	1372
3.2.	BAG indirect contact . . . . .	1372
3.3.	BAG direct contact . . . . .	1373
4.	Discussion . . . . .	1373
	Suggestions . . . . .	1375
5.	Conclusion . . . . .	1376
	Acknowledgements . . . . .	1376
	References . . . . .	1376

## 1. Introduction

Materials for tissue replacement have progressively evolved over-time. The discovery of bioactive glass (BAG) has played a key role in this evolution. The 1<sup>st</sup> generation of materials for tissue replacement had the requirement to be bio-inert without triggering any host inflammatory response [1]. In 1969 there was a revolution in tissue engineering when Professor Larry Hench introduced bioactive glass (a sodium calcium phosphor-silicate glass) which was the first material that exhibited bone bonding ability with an excellent bonding capacity [2,3]. Ever since, there was a shift in the paradigm of materials for tissue re-placement from being bio-inert to bioactive. A material that could inter-act beneficially with the host tissue to drive its repair and regeneration became the prime need. From this point there was a growth of bioactive materials (glass, ceramics) including modified bioactive glass, calcium phosphate [4,5], hydroxyapatite [6–8] and calcium silicates [9–11]. In the years following its invention, bioactive glass has been extensively researched and the mechanism behind its high bioactivity has been re-ported. The two main reasons for its bonding ability are as follows; 1. The ions leached from the glass form carbonated calcium deficient hydroxyl apatite (HCA) that binds with the collagen of the tissue 2. The ions also up regulate genes that encode growth factors and stimulate osteogenic cells to secrete bone matrix [2]. Bioactive glass has therefore been used in many applications such as a putty for bone repair [12, 13], coating on implants (bone and dental) [14,15], scaffolds for bone regeneration [16–18] and also for cartilage repair [19].

Next to bone regeneration, bioactive glass has found its niche in dentistry. The loss of mineral structures of the tooth enamel and dentin due to caries or erosion is a well-known clinical problem in dentistry [20,21]. The leaching of ions from bioactive glass and subsequent HCA formation eventually makes it a valuable candidate to be used for remineralization of these dental tissues. Hence, bioactive glasses are now used in tooth pastes [22,6,23], air polishing procedures [24] and their ability to treat tooth sensitivity and remineralize enamel has been proven [25–27]. Dentin remineralization is more demanding than enamel remineralization due to the difference in their composition. As 96% (weight %) of enamel is composed of mineral apatite, the mechanical properties of this tissue is mainly determined by its mineral content. However, the mineral in dentin accounts to only 70% and the remaining 30% is contributed by organic collagen, non-collagenous proteins and water. Furthermore, the design of dentin is such that it is supported by fibril scaffold-form of the collagen in which the mineral apatite is embedded in an extrafibrillar and intrafibrillar manner (Fig. 1). Therefore, the mechanical properties of this tissue not only depend on the overall mineral content but mainly on the intrafibrillar orientation of minerals in the collagen scaffold [28].

Hence, increased mineral content at the tissue after bioactive glass treatment is not enough to remineralize dentin as it is for enamel remineralization. The review of Bertassoni et al. [28] underlines that the improvement in mechanical properties of dentin through intrafibrillar mineralization is crucial to retain the functionality of this tissue.

This emphasizes the need to understand the phenomena of remineralization in the context of the tissue it is interfaced with and sufficient characterizations (physico-chemical and mechanical) are of utmost importance to prove the effective remineralization of dentin. Furthermore, remineralization of dentin by bioactive glass can also be complemented by stimulating the odontoblasts or odontoblast-like cells present in the pulp that can secrete reactionary or reparative den-tin. However, the new dentin that could be formed is limited only to the pulp dentin interface and the research in this field is at a very evolutionary stage. Therefore, at present, remineralization of dentin in a non-cellular manner through apatite formation by bioactive glass has gained the spotlight. Thus, there is active ongoing research to use bioactive glass as fillers in tooth restorative materials such as tooth pastes, Glass ionomer cements (GICs) [29] and dental composites [30–32] with the aim to occlude exposed dentinal tubules, improve the bonding at the dentin interface and most importantly to repair the underlying mineral depleted dentin through remineralization and such studies are reporting the efficiency of bioactive glasses for dentin remineralization.

Furthermore, it is well known that the excellent bioactivity of the first developed bioactive glass 45S5 was mainly due to its finely tuned composition. However, in recent years the glass production methods have become more varied with methods such as sol-gel [33] [34,35], flame spray [36] and spray pyrolysis [37] on offer in addition to the traditional melt-quench route. These methods give additional textural features such as porosity and fine particle size which increases the surface area of these particles. Recent studies suggest that, besides composition, surface textural properties also play a vital role in the bio-activity of these glasses [38–40].

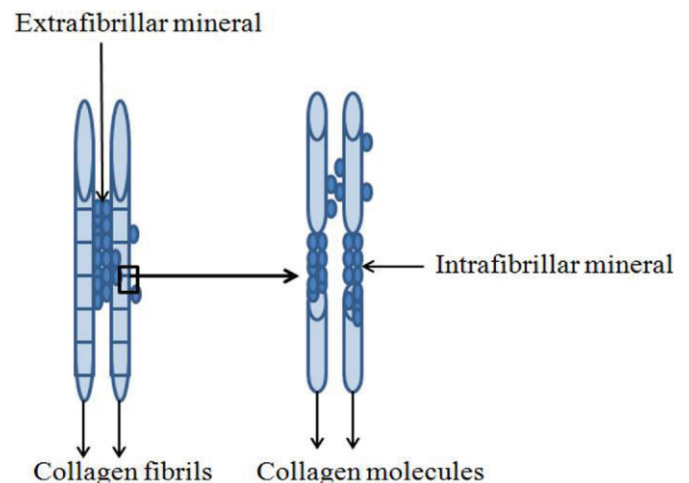


Fig. 1. Representation of extrafibrillar and intrafibrillar mineralization in the collagen structure of dentin. Adapted from [28].

Therefore, the aim of this systematic review was to assess if there is a real evidence for bioactive glass to effectively remineralize dentin. We equated effective remineralization of dentin using BAG treatment to improved mechanical properties of this tissue through intrafibrillar mineralization. In addition, we delved into analysing the characteristics of bioactive glass (a consequence of various preparation methods and modifications of material composition) that could highly influence the remineralization of dentin as a part of this review.

## 2. Methods

### 2.1. Research question

Prior to the initiation of this comprehensive systematic review, a re-search question was formulated: "Is there strong evidence for bioactive glass to remineralize dentin?"

### 2.2. Search strategy

Three individual electronic databases were searched accurately and independently by two reviewers (Delilha Fernando and Nina Attik) following Preferred Reporting Items for Systematic Reviews and Meta-Analyses (PRISMA) statements for assessing the methodological quality of systematic reviews [41]. The electronic databases searched for identifying the relevant studies included Web of Science, PubMed and Science Direct. The published scientific articles from January 2000 to July 2016 were systematically assessed for this review. The last search was conducted on 20th July 2016 in the Faculté d'Odontologie, Université Claude Bernard Lyon 1, Lyon, France.

### 2.3. Keywords selection

Three combinations of keywords were independently applied by the 2 investigators on Web of science, PubMed and Science direct. The key-word combination that returned the maximum papers was taken forward for the detailed systematic search.

### 2.4. Inclusion and exclusion criteria

In order to identify relevant studies, the following inclusion and exclusion criteria were set.

We only included the studies that:

- (1) Evaluated BAG effect on demineralized dentin tissue.
- (2) Interfaced BAGs on demineralized dentin through indirect (bonding resins, Glass ionomer cements, etc.) or through direct contact.
- (3) Have confirmed apatite formation by proper characterizations. Specifically, at least one of these characterizations such as X-ray diffraction (XRD), Raman spectroscopy and Fourier transform infrared spectroscopy (FTIR) and attenuated total reflectance-Fourier transform infrared spectroscopy (ATR-FTIR) should have been used along with qualitative analysis techniques such as scanning electron microscopy (SEM) either employed alone or coupled with energy dispersive X-ray spectroscopy (SEM-EDX), and confocal laser scanning microscopy (CLSM) to confirm the presence of apatite.
- (4) Studies that have reported data on the mechanical properties of the BAG treated dentin in addition to apatite formation were considered beneficial.

We therefore excluded the studies that:

- (1) Evaluated BAG effect on demineralized enamel or root cementum.
- (2) Used toothpastes containing BAGs for dentin remineralization.

- (3) Reported apatite formation based only on SEM imaging or confocal microscopy.
- (4) Reported only the mechanical properties without apatite confirmation.
- (5) Failed to provide any information about BAG characteristics such as composition, particle size and surface area.

### 2.5. Paper selection and data extraction

In each database, after performing the initial search using the selected keyword combination, any duplicates were identified and excluded from the total list of articles. In the second phase of evaluation, the titles and abstracts of the remaining papers were carefully read to identify the relevant articles based on the inclusion criteria. The studies that evaluated BAG effects on enamel, root cementum, dental cells for toxicity, bacterial strains for antibacterial effects and review articles were excluded right away. BAGs in tooth pastes and studies that used BAGs in substrates such as resins or cements to evaluate apatite formation with-out any contact with dentin tissue were also excluded at this stage. The remaining final list of relevant papers were downloaded and the full texts have been thoroughly scrutinized for information provided about the BAGs used, the quality and quantity of characterizations performed to confirm remineralization of dentin. The references of these papers were also checked to include any interesting papers that were missed during the search. If relevant, these new papers were also downloaded and added to the list of papers with full text for similar scrutinization. At this stage, the papers that reported only qualitative evaluation of apatite by SEM or CLSM without any other supporting characterizations such as XRD, Raman spectroscopy, FTIR, ATR-FTIR and TGA were excluded. Furthermore, the papers that reported only an interaction layer instead of apatite formation were also excluded and the reasons for exclusion were specified. The potentially relevant papers that had passed all these selections stages were included in the final synthesis. Pre-specified data elements were identified from individual studies which included the BAG characteristics such as composition, particle size, surface area, filler wt%, demineralization solution, remineralization solution, time and entered into the tables. The studies were separated based on the bioactive glass mode of application (indirect contact or direct contact) on demineralized dentin.

## 3. Results

The keyword combination "(bioactive glass OR bio-active glass OR bioglass OR bioceramic) AND (remineralization OR remineralisation)"

Table 1  
Keyword selection.

Keywords	Database and number of papers
((bioactive glass OR bioglass OR bioceramic) AND (remineralisation OR remineralization) AND (Dental OR tooth OR teeth) AND (enamel OR dentin OR dentine OR root cementum))	<ul style="list-style-type: none"> <li>• Web of science=45</li> <li>• PubMed = 28</li> <li>• Science direct =28</li> </ul>
((bioactive glass OR bio-active glass OR bioglass OR bioceramic) AND (remineralisation OR remineralization) AND (Dental OR tooth OR teeth OR tooth paste OR resin OR composite OR filler OR tooth restoration) AND (enamel OR dentin OR dentine OR root cementum))	<ul style="list-style-type: none"> <li>• Web of science =57</li> <li>• PubMed = 30</li> <li>• Science direct =19</li> </ul>
((bioactive glass OR bioglass OR bioceramic) AND (remineralization OR remineralisation) AND (Dental OR tooth OR teeth))	<ul style="list-style-type: none"> <li>• Web of science =44</li> <li>• PubMed = 37</li> <li>• Science direct =222</li> </ul>

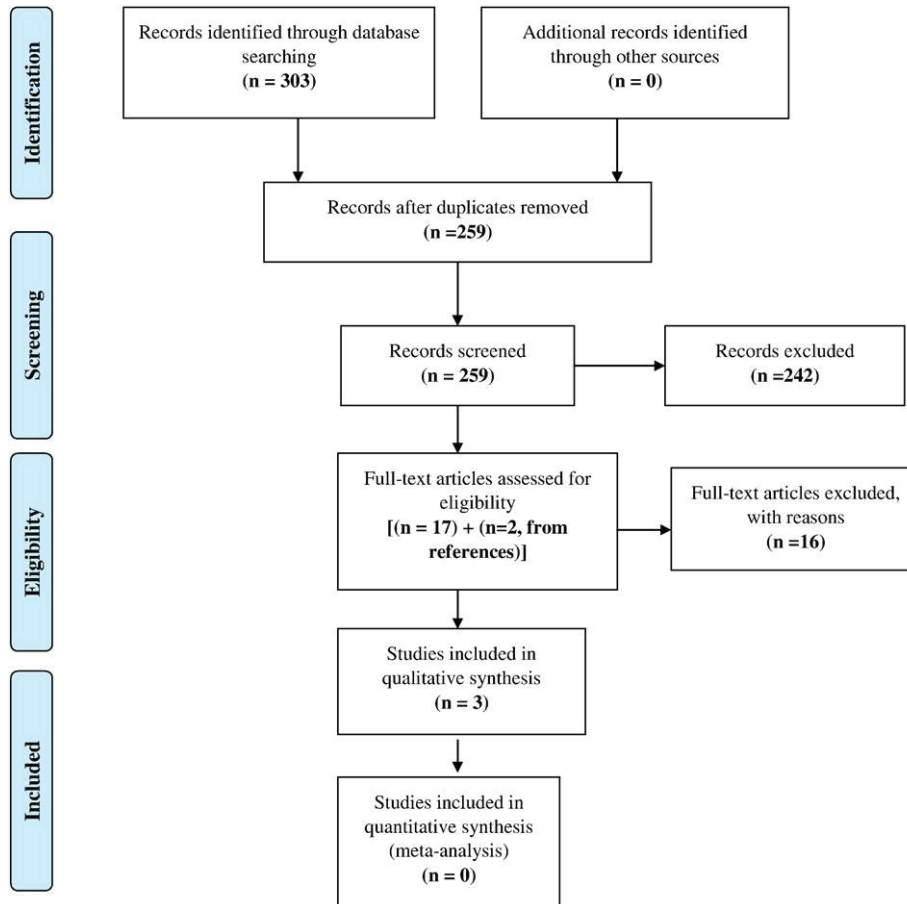


Fig. 2. Search strategy.

AND (Dental OR tooth OR teeth))” returned the maximum number of papers (Table 1) and hence was chosen for the review.

The initial electronic search using this keyword returned 303 articles. At the first phase of evaluation duplicate articles were excluded. The title and abstracts of the remaining 259 papers were screened and 242 papers were excluded as they were not relevant to the inclusion criteria. Finally, 17 relevant papers were scrutinized by downloading the papers and reading the full text. 2 papers were found from the references of the 17 selected papers and these were also assessed in a similar manner. A consensus between the two authors was reached to determine which studies fully met the selection criteria. 16 papers were excluded after reading the full text (Fig. 2). The reasons for exclusion are stated in Table 2. Finally, 3 key papers have been included in this review (Fig. 3).

### 3.1. Study characteristics

#### 3.1.1. BAG characteristics

All 3 papers have used 45S5 (45SiO<sub>2</sub>:24.5CaO: 24.5Na<sub>2</sub>O:6P<sub>2</sub>O<sub>5</sub>) as the chosen BAG composition. In the study of Wang et al. [55] BAG was modified with polyacrylic acid (PBAG) and in another study with soda lime glass (MBAG) [56]. Only one paper [36] has compared the effect of nano-sized BAG (nano BAG) with micro sized BAG (micro BAG) and the remaining 2 papers have used micro BAG (Tables 3 and 4).

#### 3.1.2. Protocol

Briefly, in all studies a caries-free human third molar has been used. The tooth has been cut to expose the dentin and was subjected to demineralization by acid or ethylene-diamine-tetra-acetic acid (EDTA) treatment. Wang et al. have used orthophosphoric acid [55], Vollenweider et al., and Wang et al. have used EDTA to cleave minerals

from the tooth [36,56]. After demineralization, the dentin was brought into contact with BAG followed by immersion in remineralization solution. 2 studies have used artificial saliva [55,56], 1 study immersed dentin in deionised water for remineralization [36]. At selected time points, the experimental samples were characterized for newly formed apatite (Tables 3 and 4, Fig. 3).

#### 3.1.3. Classification of included studies

Data were divided into 2 types based on the mode of BAG application for remineralization. Wang et al. [55] have used BAG in resins in order to assess the remineralization efficiency of BAG when used in resin based dental restorative materials (BAG indirect contact). The resin was a combination of urethane dimethacrylate (UDMA), bisphenol A diglycidyl ether dimethacrylate (Bis-GMA), triethylene glycol dimethacrylate (TEGDMA) and 2-hydroxyethyl methacrylate (HEMA) (Table 3).

BAGs without any substrate (resin or cement) were used in 2 studies (BAG direct contact). Vollenweider et al. [36] immersed demineralized dentin in a BAG water suspension and Wang et al. [56] rubbed BAG on the demineralized dentin prior to immersion in artificial saliva (Table 4).

### 3.2. BAG indirect contact

Wang et al. [55] compared the remineralization efficiency of resin containing (33% filler) polycarboxylated BAG (PBAG), polycarboxylated calcium silicate (PCS), and polycarboxylated calcium silicate doped brushite (PDP) microfillers. Unfilled resins contacted with dentin served as controls. The polymerized bioactive resin disks were held in close contact with acid etched dentin while immersed in artificial saliva for 14-days. The authors evaluated the mineral changes through ATR-FTIR,

**Table 2**  
Studies excluded with reasons.

Studies	Reasons for exclusion
Forsback et al., 2004 [42]	Characterization of apatite only by SEM
Schmidlin et al., 2007 [43]	Only mechanical properties characterized, apatite not confirmed
Xie et al., 2008 [44]	Characterization of apatite only by SEM
Curtis et al., 2010 [45]	Characterization of apatite only by SEM-EDX evaluation
Bakry et al., 2011 [46]	The mineral deposit in dentin was brushite, monetite and not apatite
Gandolfi et al., 2011 [47]	Analysis of tricalcium silicate, dicalcium silicate, tricalcium aluminate, calcium sulfate, barium sulfate and not a bioactive glass
Osorio et al., 2012 [48]	Characterization of apatite only by SEM-EDX evaluation
Sauro et al., 2012 [49]	Apatite forming ability of bioglass in resin disks was confirmed by XRD but only CLSM was used to show apatite in dentin
Sauro et al., 2012 [32]	Characterization of apatite only by CLSM
Lynch et al., 2012 [50]	Apatite forming ability of bioglass was confirmed by XRD but this was not confirmed in dentin
Bakry et al., 2013 [51]	The mineral deposit in dentin was brushite and not apatite
Chen et al., 2013 [40]	The mineral deposit in dentin was monocalcium phosphate monohydrate and not apatite
Khoroushi et al., 2013 [52]	Characterization of apatite only by SEM
Profeta et al., 2014 [53]	Characterization of apatite only by SEM and CLSM
Osorio et al., 2015 [29]	Only $\mu$ TBS and SEM image of debonding was characterized
Sauro et al., 2015 [54]	Analysis of beta-tricalcium phosphate and not a bioactive glass

Raman spectroscopy and CLSM. Furthermore, they also performed a micro tensile bond strength ( $\mu$ TBS) test to measure the bonding ability at resin-dentin interface. Overall, they found that both PBAG and PCS exhibited higher levels of apatite formation in dentin compared to PDP and the control. Furthermore, PBAG treated group exhibited the highest mineral matrix ratio after day 14, followed by the PCS group. They also reported that even though there was a significant drop in  $\mu$ TBS after 3 month's storage in artificial saliva the CLSM showed a strong reflection corresponding to the mineral deposit in the hybrid layer. This lead to a reduction in nano-leakage in the BAG treated group supporting the remineralization effects of this bioactive filler.

### 3.3. BAG direct contact

Vollenweider et al. [36] compared the remineralization effects of nano BAG (30–50 nm) and micro BAG on demineralized dentin. They immersed the EDTA treated dentin in BAG containing de-ionized water for 1, 10 up to 30 days. They used Raman spectroscopy combined with SEM-EDX to identify the newly formed apatite. Furthermore, they also implemented thermogravimetry to quantitatively assess the level of mineral formation. The nano BAG demonstrated substantially faster apatite development compared to the micro BAG due to their increased surface area. The ion release profile (from the BAG particles alone) explained the faster apatite formation induced by nano BAG. Those particles showed a rapid release of calcium and silica, which was 20 times higher than micro BAG at early time points, and also had 10 times higher basicity compared to the micro BAGs treated solution. At 24 h, Raman spectroscopy confirmed a phosphate peak corresponding to apatite in the dentin sample immersed in the suspension of nano BAG whereas no peak was observed in the dentin treated with micro BAG. However, both treatment groups demonstrated apatite development at day 10 which became even higher at day 30. The quantification of mineral content by thermogravimetric analysis showed that nano BAG treatment

had a markedly increased mineral content than micro BAG at day 10 and day 30. Further at day 30, the nano BAG treated dentin's mineral content was equivalent to natural dentin. Interestingly, they also found that nano BAG treatment lowered the mechanical properties of the mineralized dentin in comparison to micro BAG treatment group and both of them were much lower than natural dentin.

In 2011 Wang et al. [56], evaluated the dentin remineralization induced by bioactive glass (BAG) and bioactive glass modified with spherical soda lime particles (MBAG). They performed a partial and complete demineralization of dentin with EDTA treatment followed by application of BAG, MBAG for each treatment groups and immersion in artificial saliva for 1, 3 and 7 days. The controls were demineralized dentin without any treatment. They quantified the mineral variation on partially demineralized dentin using ATR-FTIR and on the completely demineralized dentin they performed ATR-FTIR, XRD and SEM-EDX to confirm the apatite formation. A gradual increase in phosphate peak was observed at different time points up to day 7 on both BAG treated groups compared to the control. The mineral matrix ratio also showed that both BAG treated groups resulted in increasing mineral concentration from day 1 to day 7 relative to the control. However, there was no significant difference in mineral content between the BAG and MBAG treatment groups. In addition, XRD confirmed apatite formation in the dentin treated with BAG and MBAG which was similar to the apatite peaks observed in the natural dentin whereas, on the control group, no apatite was detected. The SEM-EDX analysis revealed that apatite spherulites completely covered the dentine tubules in the BAG treated groups. In a similar fashion, MBAG treatment resulted in a homogeneous layer of needle like apatite covering the dentin tubules at day 7 of remineralization treatment. In conclusion, although MBAG has a lower concentration of bioactive glass and a uniform spherical shape compared to BAG both glass systems demonstrated similar potential in dentin remineralization through apatite formation.

## 4. Discussion

Dentin is one of the most highly mineralized tissues in the tooth after enamel. In the oral cavity, demineralization (loss of  $\text{Ca}^{2+}$ ,  $\text{PO}_4^{3-}$ ,  $\text{F}^-$  ions and subsequent apatite dissolution) and remineralization (gain of  $\text{Ca}^{2+}$ ,  $\text{PO}_4^{3-}$  and  $\text{F}^-$  ions and subsequent crystallization of apatite) are normal processes that are meant to be balanced. However, in-appropriate dietary habits and hygiene thwarts the balance and triggers demineralization to dominate remineralization. This results in initial enamel lesions that progress with time into the dentin. Remineralization process of such lesions in enamel or dentin using bio-active glass involves exchange of ions ( $\text{Na}^+$ ,  $\text{Ca}^{2+}$ ,  $\text{PO}_4^{3-}$ ,  $\text{F}^-$ ) from the silicate network of BAG with the surrounding oral fluid leading to supersaturating of ions in the fluid which later re-precipitate on the silicate network of BAG in the tissue. Following this, the precipitated amorphous calcium phosphate layer grows and crystallizes into apatite and forms a stable bond to the tissue.

The dentin is not only made of minerals (as in enamel) but also with organic collagen and water. Therefore it is important to note that the functional remineralization of dentin depends not only on increased apatite content in the extracellular collagen matrix but also on improving the mechanical properties of this tissue through intracellular mineralization (ie. apatite positioned in between the collagen fibrils, Fig. 1).

With a growing interest in using bioactive glass for dentin remineralization, this systematic review was performed to assess from the results in this field if there is evidence for bioactive glass stimulating dentin remineralization. We set high standards for inclusion criteria in order to avoid bias on the results. For instance, we excluded bioactive glasses in tooth pastes because the other components in dentifrices in addition to bioactive glass such as sodium fluoride, calcium fluoride are also involved in the process of remineralization. This way the sole effect of bioactive glass mediated remineralization cannot be distinguished. Likewise, we also did not include studies that didn't confirm

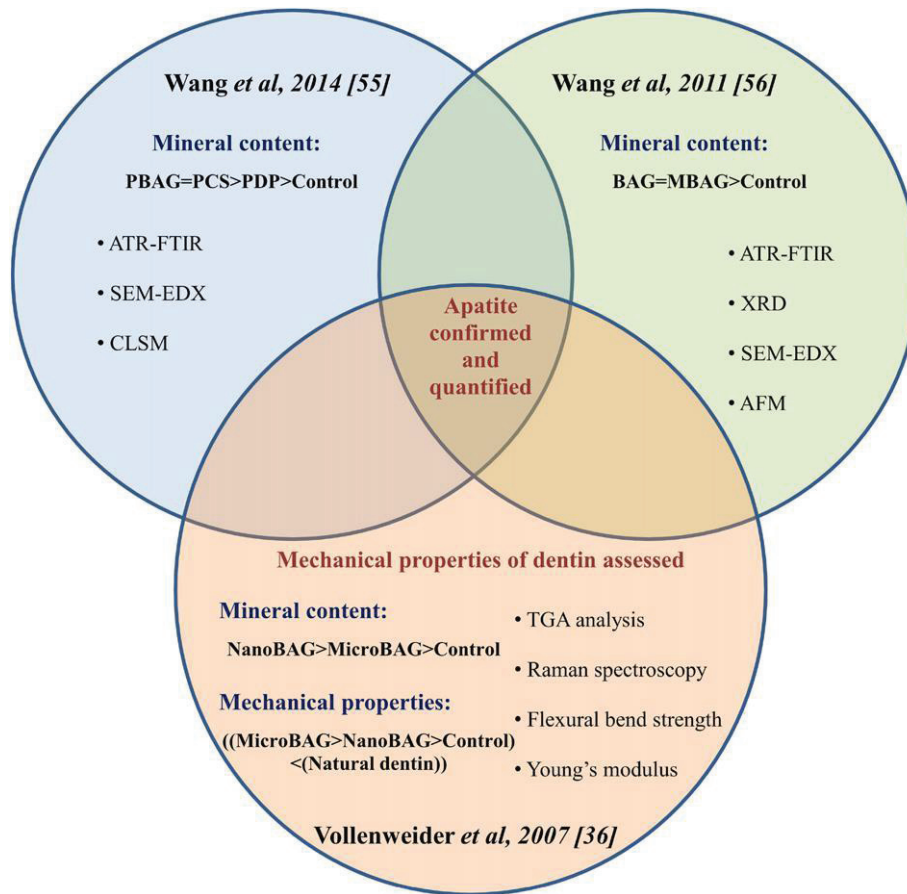


Fig. 3. Characterization methods and outcomes of included studies.

the apatite in dentin by suitable characterizations such as XRD or FTIR and Raman Spectroscopy. Curtis et al. [45] had interesting findings that showed nano BAGs are efficient in tubule occlusion as they form apatite rods plugged in the dentin tubules; this contrasts with micro BAG performance where an apatite layer covers the tubules. The study was not included in this survey as the apatite phase was not confirmed. Such exclusions were made because the authors wanted to be sure of apatite crystallization on dentin and not just precipitation of a calcium phosphate layer that could appear as mineral by qualitative analysis (SEM or CLSM). In the same way, studies that characterized and reported an interaction layer (brushite, calcium mono phosphate etc.) which are less stable phases that apatite were also excluded [46,51]. We found that there were some interesting studies [29,32] that have even characterized the mechanical properties of material-dentin interface after remineralization procedure; however due to the omission of robust characterization to confirm apatite these studies were once again omitted from this review. Sauro et al. studied the therapeutic effects of adhesives containing BAG and BAG doped with Zinc (BAG-Zn) at the

resin-dentin interface. They interfaced the demineralised dentin with resin containing BAG and BAG-Zn before immersing them in SBF for up to 3 months. The control was dentin interfaced with unfilled resin [49]. They showed the mineral content by CLSM on different regions of the dentin (e.g. the adhesive layer, hybrid layer and resin penetrated inside the tubules). Most importantly, they also performed mechanical characterizations (elastic modulus and hardness) after the treatment at different positions such as at the adhesive layer interface, on the hybrid, below the hybrid layer and in the intertubular dentin. They found that both the resin with BAG and with BAG-Zn had enhanced mineral formation after 3 months which was reflected as reduced nanoleakage in the hybrid layer. Furthermore the mechanical properties were different at different regions of the dentin and, in general there was a reduction in the elastic modulus at the adhesive layer for all groups after the treatment. However, there was improved elastic modulus in and below the hybrid layer for both BAG-treated resins. The reason why this study was not included in the final 3 papers selected (despite its interesting and well elaborated results) is that the data on

Table 3  
Study characteristics of BAG indirect contact.

Paper	Test material	Particle size (µm)	Weight percent	Resin type
[55]	(1) 10% PAA-45S5 BAG	b30	33	UDMA:Bis-GMA:TEGDMA:HEMA
	(2) 10% PAA-CS (Calcium silicate)	b30	33	UDMA:Bis-GMA:TEGDMA:HEMA
	(3) 10% PAA-PDP (CS doped brushite)	b30	33	UDMA:Bis-GMA:TEGDMA:HEMA
Paper	Tooth	Demineralization method	Remineralization method	Time
[55]	Human third molar	Solution: 10% orthophosphoric acid Time: 10 min	Application: polymerized resin disk in close contact with demineralized dentin. Solution: artificial saliva Refresh: every 72 h	14 days

**Table 4**  
Study characteristics of BAG direct contact.

Paper	Test material	Particle size ( $\mu\text{m}$ )	Fabrication method
[36]	(1) NBAG (45S5)	0.03–0.05	Flame spray
	(2) BAG (45S5)	90–710	Melt-quench
[56]	(1) BAG (45S5)	30–90	Not mentioned
	(2) MBAG (45S5+ 40% Sodalime glass)	4–80	Not mentioned
Tooth	Demineralization method	Remineralization method	Time
[36]	Solution: 17% EDTA pH: 8 Time: 2 h Partial:	Application: BAG in deionised water (172 mg/ml). Dentin stored in the above solution. Remin solution: BAG in water Refresh: no	1, 10 and 30 days
	Solution: 0.5 M EDTA pH: 7.4 Time: 5 min Complete:	Application: 20 mg BAG rubbed on dentin with cotton pellet. Time: 1 min Remin solution: artificial saliva Refresh: refreshed every day	
[56]	Solution: 0.5 M EDTA pH: 7.4 Time: 15 days		7 days

apatite confirmation by Raman spectroscopy is from the “resin + bioactive filler” disks immersed in SBF without any contact with the dentin (i.e. from the apatite forming ability of the biomaterial alone). The missing confirmation of the newly formed apatite on the demineralized dentin interfaced with these bioactive materials poses a risk of bias as to whether the changes in mechanical properties and mineral content observed by CLSM is a result of apatite or just an interaction layer in the dentin. Therefore, whilst studies such as these are encouraged, key characterizations must be afforded maximum importance to ensure we fully understand the process and so assess the true potential of bioactive glasses for the remineralization of dentin.

By following this rigorous methodology we arrived at 3 key papers that fulfilled our criteria to be included in this review.

All the three papers in this review have confirmed that bioactive glass results in enhanced apatite formation in dentin (Fig. 3) which is one important aspect for remineralization. Wang et al. have realized apatite formation using bioactive glass in completely demineralized dentin [56]. Apatite formation in completely demineralized dentin is strong evidence that this process was not influenced by seed crystallites in the dentin as in the other studies that employed a partial demineralization procedure. Furthermore, in 2014 Wang et al. demonstrated apatite formation in dentin by using bioactive glass as filler in dental resin [55]. This emphasizes that the apatite formation has also been possible via indirect contact to the dentin. Regarding the glass characteristics, Vollenweider et al. have shown that nano BAGs lead to faster apatite formation due to their improved surface area [36]. As previously stated, remineralization of dentin also demands mechanical recovery of the mineralized tissue to be similar to the natural dentin. The same study has characterized this aspect and they have found that treatments with both micro and nano BAGs could not match natural dentin in terms of the Young's modulus and flexural bend strength even though there was enhanced mineral content in the nano BAG treated group. This finding stresses the importance of defining remineralization of dentin not just from the overall apatite content but also from the mechanical properties of the remineralized tissue. Furthermore, from the 3 key papers in this review the data on the mechanical characterization of dentin after BAG treatment for remineralization was available from only one paper (Fig. 3). The lack of such important evaluations limits us from drawing firm conclusions. Kinney et al. tested if the hardness and modulus of dentin was proportional to its mineral concentration by comparing the values of normal dentin with dentin that lacked intrafibrillar mineralization [57]. They found that both hardness and Young's modulus decreased evidently in dentin without intrafibrillar mineralization. Based on these outcomes they pointed that mineral concentration alone may not be a sufficient end point for assessing the remineralization of dentin.

There are studies that have used other materials or cross linking agents such as poly amino amide dendrimer with nano amorphous calcium phosphate or glutaraldehyde for dentin remineralization [58,59] and have clearly evaluated dentin remineralization by confirming the development of apatite in dentin and further proving the improved mechanical properties of this tissue through intrafibrillar mineralization. Recently, Chen et al. used glutaraldehyde to improve the collagen cross linking of acid etched dentin and immersed them in remineralizing solution. In order to evaluate remineralization, they used transmission electron microscopy (TEM) to qualitatively show bands of intrafibrillar mineralization and the apatite was confirmed with corresponding selected area electron diffraction (SAED) patterns. Furthermore, they performed mechanical evaluation of treated dentin and confirmed that the glutaraldehyde treatment improved the Young's modulus and hardness of the dentin similar to natural dentin through intrafibrillar mineralization. We find that such clear evidence is lacking in studies that evaluate dentin remineralization using bioactive glass. The present systematic review highlights that bioactive glass treatment can increase apatite concentration in dentin; however, the potential of these particles to remineralize dentin in an intrafibrillar manner is unclear mainly due to lack of in-depth investigations to probe this aspect.

Bioactive glasses have been intensely researched over the decades and their potential for bone bonding through apatite formation and osteogenic cells stimulation is well known. In the dental field, bioactive glass use in tooth pastes for remineralisation of enamel by establishing new apatite in the tissue is also proven. Sensodyne<sup>®</sup> repair and protect is an example of a tooth paste that uses Novamin<sup>®</sup> (45S5 bioactive glass) for treating tooth sensitivity. All these are mainly due to the enhanced apatite forming capacity of bioactive glass. However, from this review it is clear that for dentin remineralization using bioactive glass research studies need to augment the established apatite structure by probing the mechanical aspects of the mineralized dentin so that the potential of bioactive glass for dentin remineralization can be truly realized.

### Suggestions

We recommend future studies on dentin remineralization using bio-active glass to give importance to the following key points as a means of ensuring a full comparison of results.

- Basic characteristics of the bioactive glass such as composition and particle size.
- Confirmation of apatite in dentin by using one of the following analytical techniques: XRD; FTIR; TEM combined with SAED pattern; Raman spectroscopy. A combination of 2 methods for confirmation,

as employed by Wang et al. [56], and quantification of the mineral content will strengthen the results.

- Most importantly mechanical properties of the dentin after remineralization treatment such as flexural strength, Young's modulus and hardness by techniques such as atomic force microscopy (AFM) or 3-point bending test are crucial.

## 5. Conclusion

This review confirms that bioactive glass treatment leads to enhanced apatite formation in dentin. Size of the bioactive glass powder particles influences the rate of apatite formation with nano bioactive glass powders having faster apatite forming kinetics. However, apatite formation is just one important aspect of dentin remineralization. There is only one study that has characterized the mechanical properties of the dentin after the new mineral phase formation. Further re-researches are necessary to study the mechanical properties of mineralized dentin in addition to new apatite development. Such work should be supported with appropriate characterization to assess if the bioactive glass can remineralize dentin. Therefore, it can be concluded that there isn't strong evidence to prove that bioactive glass can remineralize dentin.

## Acknowledgements

The research leading to this review has received funding from the European Union Seventh Framework Program (FP7/2007-2013) under grant agreement no. 608197.

## References

- [1] L.L. Hench, Chronology of bioactive glass development and clinical applications, *New J. Glass Ceram.* 03 (2013) 67–73, <http://dx.doi.org/10.4236/njgc.2013.32011>.
- [2] J.R. Jones, Review of bioactive glass: from Hench to hybrids, *Acta Biomater.* 9 (2013) 4457–4486, <http://dx.doi.org/10.1016/j.actbio.2012.08.023>.
- [3] V. Krishnan, T. Lakshmi, Bioglass: a novel biocompatible innovation, *J. Adv. Pharm. Technol. Res.* 4 (2013) 78–83, <http://dx.doi.org/10.4103/2231-4040.111523>.
- [4] J. Zhao, Y. Liu, W. Sun, H. Zhang, Amorphous calcium phosphate and its application in dentistry, *Chem. Cent. J.* 5 (2011) 40, <http://dx.doi.org/10.1186/1752-153X-5-40>.
- [5] C. Combes, C. Rey, Amorphous calcium phosphates: synthesis, properties and uses in biomaterials, *Acta Biomater.* 6 (2010) 3362–3378, <http://dx.doi.org/10.1016/j.actbio.2010.02.017>.
- [6] P. Tschoppe, D.L. Zandim, P. Martus, A.M. Kielbassa, Enamel and dentine remineralization by nano-hydroxyapatite toothpastes, *J. Dent.* 39 (2011) 430–437, <http://dx.doi.org/10.1016/j.jdent.2011.03.008>.
- [7] H. Yoshikawa, A. Myoui, Bone tissue engineering with porous hydroxyapatite ce-ramics, *J. Artif. Organs Off. J. Jpn. Soc. Artif. Organs* 8 (2005) 131–136, <http://dx.doi.org/10.1007/s10047-005-0292-1>.
- [8] J. Venkatesan, S.-K. Kim, Nano-hydroxyapatite composite biomaterials for bone tissue engineering—a review, *J. Biomed. Nanotechnol.* 10 (2014) 3124–3140.
- [9] L. Niu, W. Zhang, D.H. Pashley, L. Breschi, J. Mao, J. Chen, F.R. Tay, Biomimetic remineralization of dentin, *Dent. Mater.* 30 (2014), <http://dx.doi.org/10.1016/j.dental.2013.07.013>.
- [10] L. Niu, K. Jiao, T. Wang, W. Zhang, J. Camilleri, B.E. Bergeron, H. Feng, J. Mao, J. Chen, D.H. Pashley, F.R. Tay, A review of the bioactivity of hydraulic calcium silicate cements, *J. Dent.* 42 (2014) 517–533, <http://dx.doi.org/10.1016/j.jdent.2013.12.015>.
- [11] L. Han, T. Okiji, Bioactivity evaluation of three calcium silicate-based endodontic materials, *Int. Endod. J.* 46 (2013) 808–814, <http://dx.doi.org/10.1111/iej.12062>.
- [12] W. Jia, G.Y. Lau, W. Huang, C. Zhang, A.P. Tomsia, Q. Fu, Bioactive glass for large bone repair, *Adv. Healthc. Mater.* 4 (2015) 2842–2848, <http://dx.doi.org/10.1002/adhm.201500447>.
- [13] E. Schepers, M. de Clercq, P. Ducheyne, R. Kempeneers, Bioactive glass particulate material as a filler for bone lesions, *J. Oral Rehabil.* 18 (1991) 439–452.
- [14] A. Braem, T. Mattheys, B. Neirincq, M. Čeh, S. Novak, J. Schrooten, O. Van der Biest, J. Vleugels, Bioactive glass—ceramic coated titanium implants prepared by electrophoretic deposition, *Mater. Sci. Eng. C* 32 (2012) 2267–2273, <http://dx.doi.org/10.1016/j.msec.2012.06.013>.
- [15] B.A.J.A. van Oirschot, H.S. Alghamdi, T.O. Nārhi, S. Anil, A. Al Farraj Aldosari, J.J.J.P. van den Beucken, J.A. Jansen, In vivo evaluation of bioactive glass-based coatings on dental implants in a dog implantation model, *Clin. Oral Implants Res.* 25 (2014) 21–28, <http://dx.doi.org/10.1111/clr.12060>.
- [16] Y. Lin, W. Xiao, B.S. Bal, M.N. Rahaman, Effect of copper-doped silicate 13-93 bioactive glass scaffolds on the response of MC3T3-E1 cells in vitro and on bone regeneration and angiogenesis in rat calvarial defects in vivo, *Mater. Sci. Eng. C Mater. Biol. Appl.* 67 (2016) 440–452, <http://dx.doi.org/10.1016/j.msec.2016.05.073>.
- [17] S. Mooyen, N. Charoenphandhu, J. Teerapornpakit, J. Thongbunchoo, P. Suntonsaratoon, N. Krishnamra, I.-M. Tang, W. Pon-On, Physico-chemical and in vitro cellular properties of different calcium phosphate-bioactive glass composite chitosan-collagen (CaP@ChiCol) for bone scaffolds, *J. Biomed. Mater. Res. B Appl. Biomater* (2016), <http://dx.doi.org/10.1002/jbm.b.33652>.
- [18] F. Westhauser, C. Weis, M. Prokscha, L.A. Bittrich, W. Li, K. Xiao, U. Kneser, H.-U. Kauczor, G. Schmidmaier, A.R. Boccaccini, A. Moghaddam, Three-dimensional polymer coated 45S5-type bioactive glass scaffolds seeded with human mesenchymal stem cells show bone formation in vivo, *J. Mater. Sci. Mater. Med.* 27 (2016) 119, <http://dx.doi.org/10.1007/s10856-016-5732-3>.
- [19] A.J. Aho, T. Tirri, J. Kukkonen, N. Strandberg, J. Rich, J. Seppälä, A. Yli-Urpo, Injectable bioactive glass/biodegradable polymer composite for bone and cartilage reconstruction: Concept and experimental outcome with thermoplastic composites of poly( $\epsilon$ -caprolactone-co-D,L-lactide) and bioactive glass S53P4, *J. Mater. Sci. Mater. Med.* 15 (2004) 1165–1173, <http://dx.doi.org/10.1023/B:JMSM.0000046401.50406.9b>.
- [20] R. Cheng, H. Yang, M. Shao, T. Hu, X. Zhou, Dental erosion and severe tooth decay related to soft drinks: a case report and literature review\*, *J. Zhejiang Univ. Sci. B* 10 (2009) 395–399, <http://dx.doi.org/10.1631/jzus.B0820245>.
- [21] A. Davari, E. Ataei, H. Assarzadeh, Dentin hypersensitivity: etiology, diagnosis and treatment; a literature review, *J. Dent. Shīrāz Iran* 14 (2013) 136–145.
- [22] A.S. Bakry, H.Y. Marghalani, O.A. Amin, J. Tagami, The effect of a bioglass paste on enamel exposed to erosive challenge, *J. Dent.* 42 (2014) 1458–1463, <http://dx.doi.org/10.1016/j.jdent.2014.05.014>.
- [23] I. Farooq, I.A. Moheet, E. AlShwaimi, In vitro dentin tubule occlusion and remineralization competence of various toothpastes, *Arch. Oral Biol.* 60 (2015) 1246–1253, <http://dx.doi.org/10.1016/j.archoralbio.2015.05.012>.
- [24] I. Farooq, M. Tylkowski, S. Müller, T. Janicki, D.S. Brauer, R.G. Hill, Influence of sodium content on the properties of bioactive glasses for use in air abrasion, *Biomed. Mater. Bristol Engl.* 8 (2013) 065008, <http://dx.doi.org/10.1088/1748-6041/8/6/065008>.
- [25] B. Me, S. Mh, R. Bagheri, Bioactive Glasses in Dentistry: A Review, vol. 22, ResearchGate, 2015 [https://www.researchgate.net/publication/277608476\\_Bioactive\\_Glasses\\_in\\_Dentistry\\_A\\_Review](https://www.researchgate.net/publication/277608476_Bioactive_Glasses_in_Dentistry_A_Review) (accessed July 19, 2016).
- [26] H. Milly, F. Festy, T.F. Watson, I. Thompson, A. Banerjee, Enamel white spot lesions can remineralise using bio-active glass and polyacrylic acid-modified bio-active glass powders, *J. Dent.* 42 (2014) 158–166, <http://dx.doi.org/10.1016/j.jdent.2013.11.012>.
- [27] Z. Dong, J. Chang, Y. Zhou, K. Lin, In vitro remineralization of human dental enamel by bioactive glasses, *J. Mater. Sci.* 46 (2010) 1591–1596, <http://dx.doi.org/10.1007/s10853-010-4968-4>.
- [28] L.E. Bertassoni, S. Habelitz, J.H. Kinney, S.J. Marshall, G.W. Marshall, Biomechanical perspective on the remineralization of dentin, *Caries Res.* 43 (2009) 70–77, <http://dx.doi.org/10.1159/000201593>.
- [29] E. Osorio, T. Fagundes, M.F. Navarro, E.D. Zanotto, O. Peitl, R. Osorio, M. Toledano-Osorio, M. Toledano, A novel bioactive agent improves adhesion of resin-modified glass-ionomer to dentin, *J. Adhes. Sci. Technol.* 29 (2015) 1543–1552, <http://dx.doi.org/10.1080/01694243.2015.1030897>.
- [30] T.T. Tauböck, M. Zehnder, T. Schweizer, W.J. Stark, T. Attin, D. Mohn, Functionalizing a dentin bonding resin to become bioactive, *Dent. Mater.* 30 (2014) 868–875, <http://dx.doi.org/10.1016/j.dental.2014.05.029>.
- [31] X. Chatzistavrou, S. Velamakanni, K. DiRenzo, A. Lefkelidou, J.C. Fenno, T. Kasuga, A.R. Boccaccini, P. Papagerakis, Designing dental composites with bioactive and bactericidal properties, *Mater. Sci. Eng. C Mater. Biol. Appl.* 52 (2015) 267–272, <http://dx.doi.org/10.1016/j.msec.2015.03.062>.
- [32] S. Sauro, T.F. Watson, I. Thompson, A. Banerjee, One-bottle self-etching adhesives applied to dentine air-abraded using bioactive glasses containing polyacrylic acid: an in vitro microtensile bond strength and confocal microscopy study, *J. Dent.* 40 (2012) 896–905, <http://dx.doi.org/10.1016/j.jdent.2012.07.004>.
- [33] J. Zhong, D.C. Greenspan, Processing and properties of sol-gel bioactive glasses, *J. Biomed. Mater. Res.* 53 (2000) 694–701.
- [34] A. Balamurugan, G. Sockalingum, J. Michel, J. Fauré, V. Banchet, L. Wortham, S. Bouthors, D. Laurent-Maquin, G. Balossier, Synthesis and characterisation of sol gel derived bioactive glass for biomedical applications, *Mater. Lett.* 60 (2006) 3752–3757, <http://dx.doi.org/10.1016/j.matlet.2006.03.102>.
- [35] P. Sepulveda, J.R. Jones, L.L. Hench, Characterization of melt-derived 45S5 and sol-gel-derived 58S bioactive glasses, *J. Biomed. Mater. Res.* 58 (2001) 734–740.
- [36] M. Vollenweider, T.J. Brunner, S. Knecht, R.N. Grass, M. Zehnder, T. Imfeld, W.J. Stark, Remineralization of human dentin using ultrafine bioactive glass particles, *Acta Biomater.* 3 (2007) 936–943, <http://dx.doi.org/10.1016/j.actbio.2007.04.003>.
- [37] S.-J. Shih, Y.-J. Chou, I.-C. Chien, One-step synthesis of bioactive glass by spray pyrolysis, *J. Nanopart. Res.* 14 (2012) 1299, <http://dx.doi.org/10.1007/s11051-012-1299-1>.
- [38] J. Pérez-Pariante, F. Balas, J. Román, A.J. Salinas, M. Vallet-Regí, Influence of composition and surface characteristics on the in vitro bioactivity of SiO<sub>2</sub>-CaO-P<sub>2</sub>O<sub>5</sub>-MgO sol-gel glasses, *J. Biomed. Mater. Res.* 47 (1999) 170–175, [http://dx.doi.org/10.1002/\(SICI\)1097-4636\(199911\)47:2b170::AID-JBM6N3.0.CO;2-J](http://dx.doi.org/10.1002/(SICI)1097-4636(199911)47:2b170::AID-JBM6N3.0.CO;2-J).
- [39] S.-J. Shih, Y.-C. Lin, L. Valentino Posma Panjaitan, D. Rahayu Meyla Sari, The correlation of surfactant concentrations on the properties of mesoporous bioactive glass, *Materials* 9 (2016) 58, <http://dx.doi.org/10.3390/ma9010058>.
- [40] W.-C. Chen, J.-C. Kung, C.-H. Chen, Y.-C. Hsiao, C.-J. Shih, C.-S. Chien, Effects of bioactive glass with and without mesoporous structures on desensitization in dentinal tubule occlusion, *Appl. Surf. Sci.* 283 (2013) 833–842, <http://dx.doi.org/10.1016/j.apsusc.2013.07.027>.
- [41] D. Moher, L. Shamseer, M. Clarke, D. Ghersi, A. Liberati, M. Petticrew, P. Shekelle, L.A. Stewart, Preferred reporting items for systematic review and meta-analysis

- protocols (PRISMA-P) 2015 statement, *Syst. Rev.* 4 (2015) 1, <http://dx.doi.org/10.1186/2046-4053-4-1>.
- [42] A.-P. Forsback, S. Areva, J.I. Salonen, Mineralization of dentin induced by treatment with bioactive glass S53P4 in vitro, *Acta Odontol. Scand.* 62 (2004) 14–20.
- [43] P.R. Schmidlin, M. Zehnder, T. Imfeld, M.V. Swain, Comparative assessment of hard-ening of demineralized dentin under lining materials using an ultramicroindentation system, *J. Biomed. Mater. Res. B Appl. Biomater.* 83B (2007) 199–205, <http://dx.doi.org/10.1002/jbm.b.30784>.
- [44] D. Xie, J. Zhao, Y. Weng, J.-G. Park, H. Jiang, J.A. Platt, Bioactive glass-ionomer cement with potential therapeutic function to dentin capping mineralization, *Eur. J. Oral Sci.* 116 (2008) 479–487.
- [45] A.R. Curtis, N.X. West, B. Su, Synthesis of nanobioglass and formation of apatite rods to occlude exposed dentine tubules and eliminate hypersensitivity, *Acta Biomater.* 6 (2010) 3740–3746, <http://dx.doi.org/10.1016/j.actbio.2010.02.045>.
- [46] A.S. Bakry, H. Takahashi, M. Otsuki, A. Sadr, K. Yamashita, J. Tagami, CO2 laser improves 45S5 bioglass interaction with dentin, *J. Dent. Res.* 90 (2011) 246–250, <http://dx.doi.org/10.1177/0022034510387793>.
- [47] M.G. Gandolfi, P. Taddei, F. Siboni, E. Modena, E.D. De Stefano, C. Prati, Biomimetic remineralization of human dentin using promising innovative calcium-silicate hybrid “smart” materials, *Dent. Mater.* 27 (2011) 1055–1069, <http://dx.doi.org/10.1016/j.dental.2011.07.007>.
- [48] R. Osorio, M. Yamauti, S. Sauro, T.F. Watson, M. Toledano, Experimental resin cements containing bioactive fillers reduce matrix metalloproteinase-mediated dentin collagen degradation, *J. Endod.* 38 (2012) 1227–1232, <http://dx.doi.org/10.1016/j.joen.2012.05.011>.
- [49] S. Sauro, R. Osorio, T.F. Watson, M. Toledano, Therapeutic effects of novel resin bonding systems containing bioactive glasses on mineral-depleted areas within the bonded-dentine interface, *J. Mater. Sci. Mater. Med.* 23 (2012) 1521–1532, <http://dx.doi.org/10.1007/s10856-012-4606-6>.
- [50] E. Lynch, D.S. Brauer, N. Karpukhina, D.G. Gillam, R.G. Hill, Multi-component bioactive glasses of varying fluoride content for treating dentin hypersensitivity, *Dent. Mater.* 28 (2012) 168–178, <http://dx.doi.org/10.1016/j.dental.2011.11.021>.
- [51] A.S. Bakry, H. Takahashi, M. Otsuki, J. Tagami, The durability of phosphoric acid promoted bioglass-dentin interaction layer, *Dent. Mater.* 29 (2013) 357–364, <http://dx.doi.org/10.1016/j.dental.2012.12.002>.
- [52] M. Khoroushi, S.-M. Mousavinasab, F. Keshani, S. Hashemi, Effect of resin-modified glass ionomer containing bioactive glass on the flexural strength and morphology of demineralized dentin, *Oper. Dent.* 38 (2013) E1–10, <http://dx.doi.org/10.2341/11-325-L>.
- [53] A.C. Profeta, Preparation and properties of calcium-silicate filled resins for dental restoration. Part II: micro-mechanical behaviour to primed mineral-depleted dentine, *Acta Odontol. Scand.* 72 (2014) 607–617, <http://dx.doi.org/10.3109/00016357.2014.880188>.
- [54] S. Sauro, R. Osorio, T.F. Watson, M. Toledano, Influence of phosphoproteins' biomimetic analogs on remineralization of mineral-depleted resin-dentin interfaces created with ion-releasing resin-based systems, *Dent. Mater.* 31 (2015) 759–777, <http://dx.doi.org/10.1016/j.dental.2015.03.013>.
- [55] Z. Wang, Y. Shen, M. Haapasalo, J. Wang, T. Jiang, Y. Wang, T.F. Watson, S. Sauro, Polycarboxylated microfillers incorporated into light-curable resin-based dental adhesives evoke remineralization at the mineral-depleted dentin, *J. Biomater. Sci. Polym. Ed.* 25 (2014) 679–697, <http://dx.doi.org/10.1080/09205063.2014.891926>.
- [56] Z. Wang, T. Jiang, S. Sauro, Y. Wang, I. Thompson, T.F. Watson, Y. Sa, W. Xing, Y. Shen, M. Haapasalo, Dentine remineralization induced by two bioactive glasses developed for air abrasion purposes, *J. Dent.* 39 (2011) 746–756, <http://dx.doi.org/10.1016/j.jdent.2011.08.006>.
- [57] J.H. Kinney, S. Habelitz, S.J. Marshall, G.W. Marshall, The importance of intrafibrillar mineralization of collagen on the mechanical properties of dentin, *J. Dent. Res.* 82 (2003) 957–961.
- [58] C. Chen, C. Mao, J. Sun, Y. Chen, W. Wang, H. Pan, R. Tang, X. Gu, Glutaraldehyde-induced remineralization improves the mechanical properties and biostability of dentin collagen, *Mater. Sci. Eng. C* 67 (2016) 657–665, <http://dx.doi.org/10.1016/j.msec.2016.05.076>.
- [59] K. Liang, M.D. Weir, M.A. Reynolds, X. Zhou, J. Li, H.H.K. Xu, Poly (amido amine) and nano-calcium phosphate bonding agent to remineralize tooth dentin in cyclic artificial saliva/lactic acid, *Mater. Sci. Eng. C* 72 (2017) 7–17, <http://dx.doi.org/10.1016/j.msec.2016.11.020>.

## 3. Elaboration of Mesoporous Bioactive Glasses (MBGs)

### 3.1. Introduction

In this chapter we have outlined our initial attempts to fabricate MBG fillers, the challenges encountered during the preparation and the final outcome.

Before commencing the elaboration it was necessary to determine some of the main synthesis parameters such as the composition, type of surfactant and oxide precursors needed for the elaboration. The end target was to obtain MBGs that are amorphous with high surface area and porosity to facilitate accelerated ion release and offer potential for encapsulation and release of desirable actives.

The compositions stated in **Table 1** were derived based on a short literature review [89–97] of various MBG compositions and their influence on the resulting textural parameters and apatite forming abilities.

By analyzing data from the literature on MBG compositions, certain aspects were very clear:

- Surface area of the MBGs had a clear relation to the rate of apatite formation (Higher surface area ie, above  $300\text{m}^2\text{g}^{-1}$  favored rapid apatite formation).
- Since silica and phosphate are network formers, it seemed higher combined mole percentages of  $\text{SiO}_2$  and  $\text{P}_2\text{O}_5$  correlated to higher surface area. Moreover, it was also observed that increases in  $\text{P}_2\text{O}_5$  mole percent lead to further increases in surface area. But when increased above 30 percent the mesoporous structure collapsed leading to a reduction in pore volume and surface area [98]. Therefore, it seemed better to have a  $\text{P}_2\text{O}_5$  content less than 30 percent for improved textural properties.
- Similarly, increasing the mole percent of  $\text{CaO}$  was associated with a reduction in surface area because in these studies the increase in  $\text{CaO}$  was compensated by reducing the mole percent of  $\text{SiO}_2$  and  $\text{P}_2\text{O}_5$ . This lead to reduction in bioactivity (emphasizing the importance of surface area on bioactivity). It was also reported that when  $\text{CaO}$  content is above 30% the material turned in to glass-ceramic and surface apatite formation was not as rapid as for an amorphous bioactive glass [95].
- The findings of Vaid *et al.*, 2013 were interesting as they showed that quaternary glasses with  $\text{Na}_2\text{O}$  showed better apatite formation than ternary systems (only silica, calcium and

phosphate). Na<sub>2</sub>O not only improved the rate of apatite formation and crystallization but also lead to a thicker apatite layer (8µm) [94]. Na<sub>2</sub>O in the glass composition could also improve the mechanical properties of the glass which is required for filler application.

- The type of surfactant employed to create ordered porosity can highly determine the textural properties of MBG's [96,97]. The data from the review pointed that P123 is the most widely used surfactant and has been associated with increased surface area compared to F127 surfactant when tested in the same composition [97]. Therefore we decided to use P123 as surfactant for our studies as well.

Based on the above insights, our novel compositions were formulated. In all compositions the combined mole percent of SiO<sub>2</sub> and P<sub>2</sub>O<sub>5</sub> was maintained at 85 to achieve high surface area and the mole percent of CaO and Na<sub>2</sub>O were together maintained at 15 percent. Therefore, keeping the mole percent of the network formers (SiO<sub>2</sub> and P<sub>2</sub>O<sub>5</sub>) constant we varied systematically the network modifier ratio (CaO and Na<sub>2</sub>O) to study their influence on surface characteristics and bioactivity.

Sol-gel bioactive glasses are predominantly synthesised by using TEOS as oxide precursor for silica, TEP as oxide precursor for phosphate and nitrates for network modifying oxides including calcium, sodium, lithium, strontium. Therefore we also planned to start our elaborations using the same precursors.

**Table 1 Composition of MBGs chosen for formulation in mole percent**

<b>Composition</b>	<b>SiO<sub>2</sub></b>	<b>CaO</b>	<b>Na<sub>2</sub>O</b>	<b>P<sub>2</sub>O<sub>5</sub></b>
<b>10Na MBG</b>	<b>75</b>	<b>5</b>	<b>10</b>	<b>10</b>
<b>7.5Na MBG</b>	<b>75</b>	<b>7.5</b>	<b>7.5</b>	<b>10</b>
<b>5Na MBG</b>	<b>75</b>	<b>10</b>	<b>5</b>	<b>10</b>
<b>2.5Na MBG</b>	<b>75</b>	<b>12.5</b>	<b>2.5</b>	<b>10</b>
<b>0Na MBG</b>	<b>75</b>	<b>15</b>	<b>0</b>	<b>10</b>

## 3.2. Materials and methods

### 3.2.1. Materials

Tetraethyl orthosilicate (TEOS, 98%), triethyl phosphate (TEP, 99%), calcium nitrate tetra hydrate ( $\text{Ca}(\text{NO}_3)_2 \cdot 4\text{H}_2\text{O}$ , 99.0%), sodium nitrate ( $\text{NaNO}_3$ , 99.99%), calcium acetate monohydrate ( $\text{Ca}(\text{CH}_3\text{COO})_2 \cdot \text{H}_2\text{O}$ , 99%), sodium acetate anhydrous ( $\text{CH}_3\text{COONa}$ ), ethyl alcohol (EtOH, 99.7%), triblock copolymer  $\text{EO}_{20}\text{PO}_{70}\text{EO}_{20}$  (P123,  $M_w = 5650$ ) and glacial acetic acid ( $\text{CH}_3\text{COOH}$ ) were used as supplied from Sigma Aldrich.

### 3.2.2. Fabricating MBG and BG using nitrate precursors

To fabricate 10g of 10Na MBG, 4g of P123 surfactant were mixed in 50g ethanol, 42ml of 0.04M nitric acid and 5.36ml of water for an hour. Next, each precursor, 15.62g TEOS, 3.64g TEP, 1.18g Calcium nitrate tetra hydrate and 1.69g sodium nitrate was added in that order at 1 hour intervals. After 24hrs the sol was transferred into petri-dishes to undergo evaporation induced self-assembly (EISA). The next day the gelled plates were transferred into a 60°C oven and were dried for 3 days. After drying, the sample was milled and calcined at 600°C at a ramp rate of 2°C/min for 5 hours.

To fabricate 50g of 10Na MBG we mixed 8g of P123 surfactant in 100g ethanol, 212ml of 0.04M nitric acid and 26.86ml of water for an hour. Next, each precursor, 78.12g TEOS, 18.22g TEP, 15.90g calcium nitrate tetra hydrate and 8.50g sodium nitrate was added at 1 hour intervals. After 24 hours the sol was transferred into petri-dishes to undergo evaporation induced self-assembly (EISA). The next day the gelled plates were transferred into a 60°C oven and were dried for 3 days. After drying, the sample was milled and calcined at 700°C at a ramp rate of 1°C/min for 5 hours. To fabricate 50g of 10Na BG the same protocol was followed except for the addition of surfactant.

### 3.2.3. Literature repeat

To prepare 4g of 80SiO<sub>2</sub>-15CaO-5P<sub>2</sub>O<sub>5</sub>, 60ml of ethanol, 0.6ml of concentrated HNO<sub>3</sub> and 4g of P123 surfactant was added to a beaker and allowed to stir for an hour. 6.67g TEOS, 0.73g TEP, 1.42g calcium nitrate tetra hydrate was added at 1 hour intervals. After 24 hours the sol was transferred into petri-dishes to undergo evaporation induced self-assembly (EISA). This took 5 days. After drying the sample was milled and calcined at 700°C at a ramp rate of 1°C/min for 5 hours.

To prepare 4g of 10Na MBG, 60ml of ethanol, 0.6ml of concentrated HNO<sub>3</sub>, 4g of P123 surfactant and 30ml of de-ionised water were added to a beaker (to dissolve sodium nitrate) and allowed to stir for an hour. 6.25g TEOS, 1.46g TEP, 0.47g calcium nitrate tetra hydrate and 0.68g of sodium nitrate were

added at 1 hour intervals. After 24hrs the sol was transferred into petri-dishes to undergo evaporation induced self-assembly (EISA). This took 5 days. After drying, the sample was milled and calcined at 700°C at a ramp rate of 1°C/min for 5 hours.

#### 3.2.4. Fabrication of MBGs using acetate precursors

MBGs of increasing sodium oxide content (0Na MBG, 2.5Na MBG, 5Na MBG, 7.5Na MBG and 10Na MBG) were prepared in an acetic acid-assisted, acetate-based sol-gel system. This was performed at both, what we called a small scale (10g) and large scale (50g).

For both small scale and large scale preparations Step 1 involved dissolving 2g of P123 surfactant in 30g ethanol. In step 2, 37.5ml of de-ionised water and 214.5ml of glacial acetic acid were added to the ethanol surfactant mixture after one hour. Each glass precursor was added to the ongoing reaction in one hour intervals (step 3) in the order TEOS, TEP, calcium acetate monohydrate and sodium acetate. The quantities of precursors added are listed in **Table 2**. After 24 hours, small-scale samples were transferred in to Petri dishes to undergo EISA at room temperature (RT). However, for the large scale samples the solution gelled in about one hour after adding the last precursor and so was allowed to undergo EISA in the beaker at room temperature (RT). After undergoing EISA for 4 days, both small and large scale samples were dried at 60°C for 2 days. The samples were later milled stored in a drier.

#### 3.2.5. Differential scanning calorimetry (DSC) and Differential thermogravimetric (DTG) Analysis

TGA/DSC analyses were realised in a temperature range from 25°C to 1000°C, under air as reactive gas and with a heating rate of 5°C/min.

#### 3.2.6. X-ray diffraction (XRD)

The material phase was characterized with X-ray diffractometer (XRD). XRD of samples subjected to different calcination temperatures was performed using an X-ray diffractometer (Bruker D8 advance) with Cu K $\alpha$  radiation of wavelength 1.54 Å. The scans were recorded at 40 kV, 40 mA, 2 theta ranges between 5° to 65° and a step size of 0.02° and 0.5 seconds per step. Phase identification was carried out using the software Diffrac Eva®.

**Table 2 Precursor quantities and and thermal treatment of acetate based samples**

<b>Sample name</b>	<b>TEOS (g)</b>	<b>TEP (g)</b>	<b>Calcium acetate monohydrate (g)</b>	<b>Sodium acetate (g)</b>	<b>Drying temperature (°C)</b>	<b>Calcination (°C)</b>
<b>0Na MBG</b>						
<b>Small scale</b>	15.62	3.64	2.64	0	60	450,480
<b>Large scale</b>	78.12	18.22	13.21	0	60	380
<b>2.5Na MBG</b>						
<b>Small scale</b>	15.62	3.64	2.20	0.41	60	450,480
<b>Large scale</b>	78.12	18.22	11.01	2.05	60	380
<b>5Na MBG</b>						
<b>Small scale</b>	15.62	3.64	1.76	0.82	60	450,480
<b>Large scale</b>	78.12	18.22	8.81	4.10	60	380
<b>7.5Na MBG</b>						
<b>Small scale</b>	15.62	3.64	1.32	1.23	60	450,480
<b>Large scale</b>	78.12	18.22	6.61	6.15	60	380
<b>10Na MBG</b>						
<b>Small scale</b>	15.62	3.64	0.88	1.64	60	450,480
<b>Large scale</b>	78.12	18.22	4.40	8.20	60	380

### 3.3. Results and discussion

#### 3.3.1. Fabricating MBG using nitrate precursors

In the first trial to prepare our samples we chose to fabricate 2 batches of 10Na MBG composition in small scale. The MBGs were prepared following the protocol mentioned in **Section 3.2.2**. The dried gels of both batches, after taking out from a 60°C oven, were subjected to a thermal treatment of 600°C for 5 hours to remove the organic surfactant and the inorganic nitrates. The samples after thermal treatment were completely black and reminiscent of carbon dust. Therefore we subjected the batch 1 sample to further thermal treatment at 700°C for 4 hours. The batch 1 sample after thermal treatment is shown in **Figure 7** and, as can be seen, still retains the black colour.



**Figure 7** 10Na MBG prepared using nitrate precursors after 700°C calcination for 4 hours

We further thermal-treated samples of batch 2 after the first calcination in a gradient kiln at 600°C, 700°C, 850°C and 950°C for 6 hours. As shown in **Figure 8** only at 850°C does the sample start to turn whitish. At 950°C, the sample was white but was completely sintered to the base of the crucible.



**Figure 8** 10Na MBG prepared using nitrate precursors after 850°C and 950°C calcination in a gradient kiln

The sample calcined at 950°C was characterized by X-ray diffraction and the results showed that the sample was a glass-ceramic with the major crystalline phases being tridymite, cristobalite, tetra sodium pyrophosphate and buchwaldite (**Figure 9**).

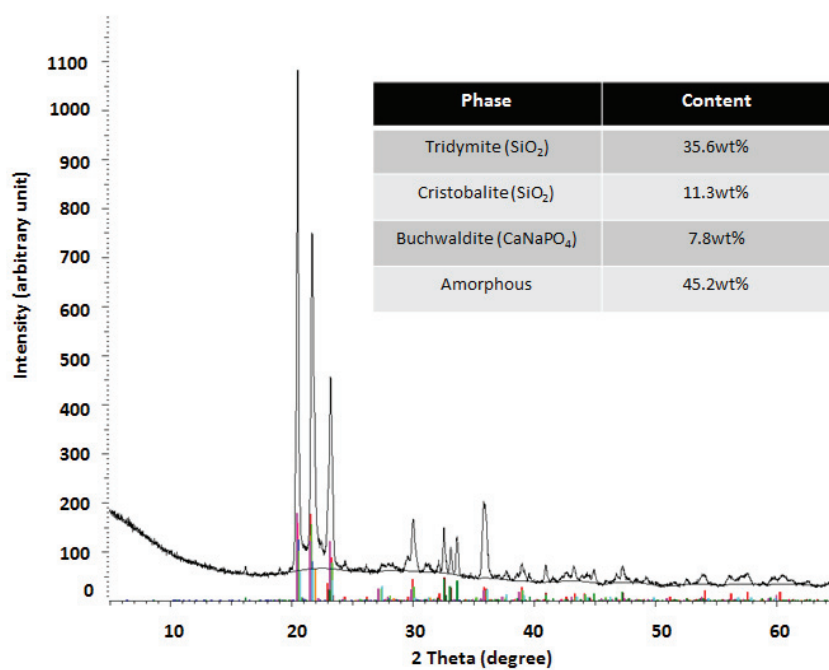


**Figure 9** XRD of 10Na MBG prepared using nitrate precursors after 950°C calcination

### 3.3.2. MBG vs BG comparison

To investigate the reason of this issue further we prepared 10Na MBG again but at a larger scale in order to have enough sample for more extensive characterization. We also prepared 10Na BG (glass without surfactant) by following the same protocol mentioned in **Section 3.2.2** but without adding the surfactant. Both samples were milled and thermal treated at 700°C for 5 hours.

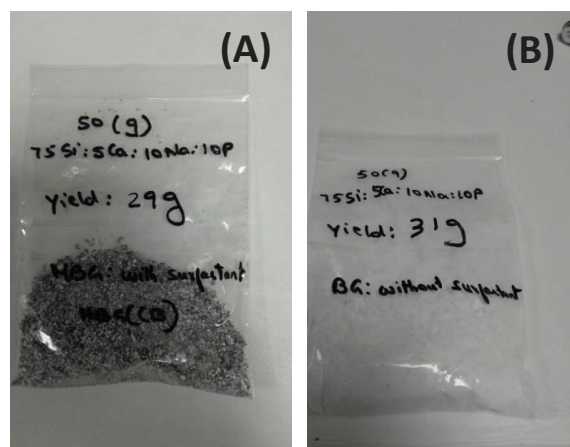


**Figure 10** Large scale samples prepared using nitrate precursors after 700°C calcination for 5 hours

It was interesting to note that the sample 10Na BG without surfactant was all white (**Figure 10B**) whereas the 10Na MBG was black as before (**Figure 10A**). The XRD results of the 10Na BG sample showed that it was also a glass-ceramic and exhibited similar crystalline phases as that of 10Na MBG after 950°C thermal treatment (**Figure 11**). The only difference between these systems is the presence of surfactant demonstrating that the surfactant was one of the main factors influencing this carbon deposit.

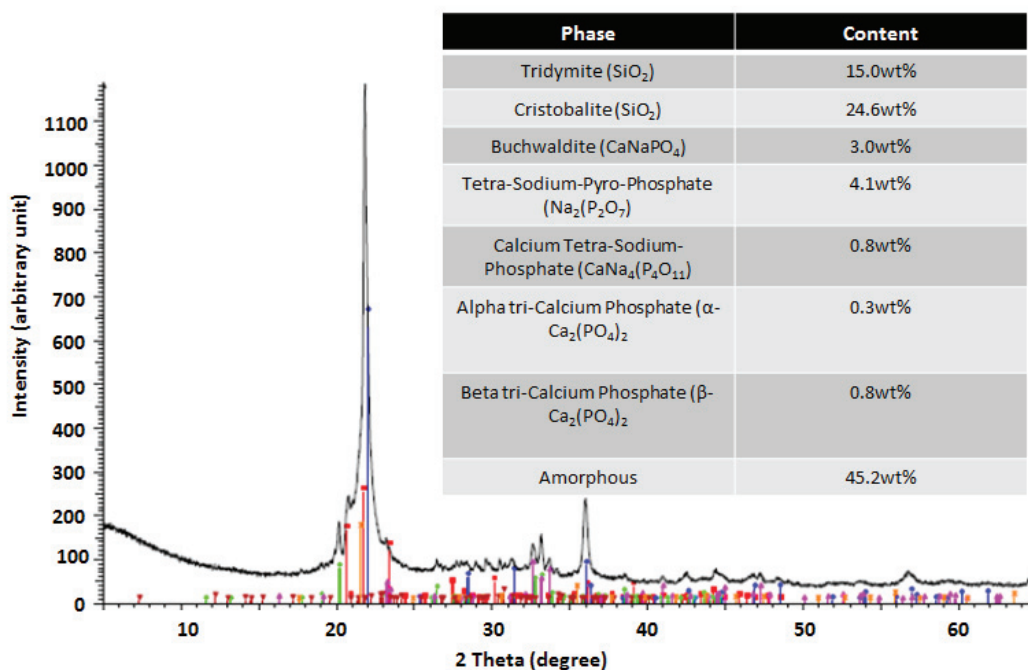


**Figure 11** XRD of 10Na BG prepared using nitrate precursors after 700°C calcination

### 3.3.3. Literature repetition

To validate if the way the surfactant is used in the elaboration process is correct we repeated a sample from the literature (Yan *et al.*, 2004) with the composition  $80\text{SiO}_2:15\text{CaO}:5\text{P}_2\text{O}_5$  and also prepared the 10Na MBG following the same method. After milling, both samples were calcined at  $700^\circ\text{C}$  for 5 hours. Interestingly, this time the literature replicated sample was white (**Figure 12A**) as it should be and the 10Na MBG had carbon deposit again (**Figure 12B**). On characterizing the literature replicate sample by X-ray diffraction we found that the sample was almost completely amorphous (**Figure 13**).

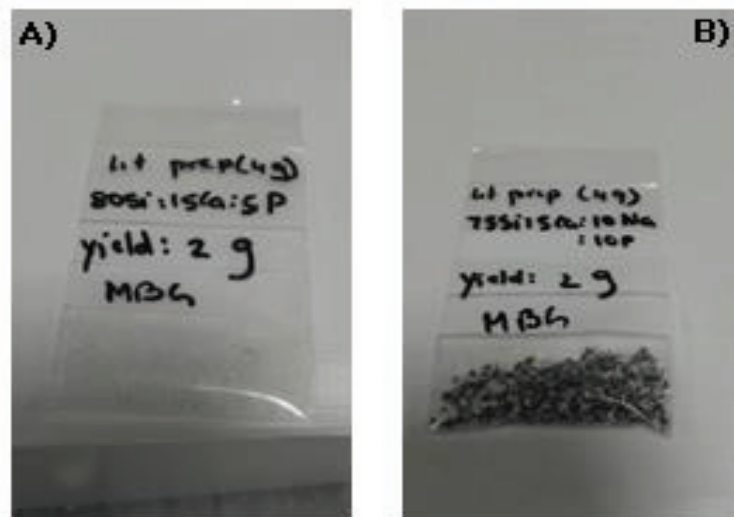


Figure 12 (A)Literature replicate sample after  $700^\circ\text{C}$  calcination (B) 10Na MBG sample after  $700^\circ\text{C}$  calcination

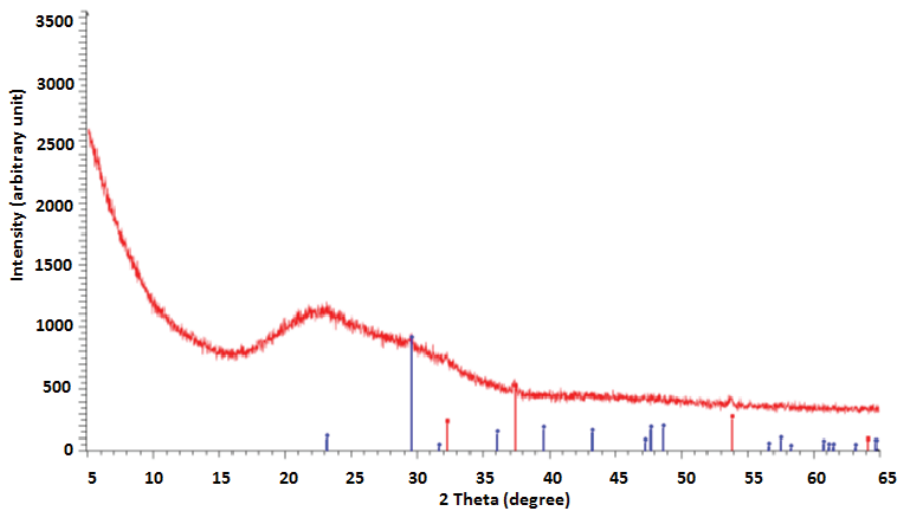


Figure 13 XRD of literature replicate sample after  $700^\circ\text{C}$  calcination

Comparing the outcomes of the trials performed (**Table 3**) it became evident that the surfactant alone is not the problem; composition also plays a part. The main difference in composition between the literature replicate and 10Na MBG is that the 10Na MBG is a quaternary system that has 10 percent sodium oxide as a network modifier besides calcium oxide whereas the literature replicate is a ternary system with only 15 percent calcium oxide as the network modifier. It seems from these outcomes that the surfactant in combination with sodium oxide in our composition has led to the carbon deposit.

It is known that in the MBG system, the surfactants form micelles around which the glass network is formed. Also, it is well known that sodium oxide is a flux which means that it reduces the melting point and glass transition temperatures in compositions, thereby tending the glass towards early crystallization and possibly a loss of porosity. The gels were ramped up to 700°C and held at that temperature for 5 hours. The decomposition of the surfactant must have occurred at lower temperatures. Ramping up directly at 700°C may have not given enough time for the decomposition of the organic micelles and the progressive melting of the gel during the temperature rise must have fused the pores or densified the network thus trapping the micelles within them. Therefore, it seemed logical that composition, crystallization and surfactant played a part in causing carbon entrapment in the final material.

**Table 3 Comparison of the outcomes after various trials using nitrate precursors**

<p><b>BG (Bioglass without surfactant)</b></p> <p><b>Composition:</b> 75SiO<sub>2</sub>-5CaO-10Na<sub>2</sub>O-10P<sub>2</sub>O<sub>5</sub></p> <p><b>Calcined:</b> 700°C for 5 hours</p>	<p><b>Colour:</b> White</p> <p><b>Phase:</b> Glass-ceramic</p>
<p><b>MBG (with sodium)</b></p> <p><b>Composition:</b> 75SiO<sub>2</sub>-5CaO-10Na<sub>2</sub>O-10P<sub>2</sub>O<sub>5</sub></p> <p><b>Calcined:</b> 700°C for 5 hours</p> <p><b>Calcined:</b> 950°C for 6 hours</p>	<p><b>Colour:</b> Black</p> <p><b>Colour:</b> White</p> <p><b>Phase:</b> Glass-ceramic</p>
<p><b>MBG (without sodium)</b></p> <p><b>Composition:</b> 80SiO<sub>2</sub>-15CaO-5P<sub>2</sub>O<sub>5</sub></p> <p><b>Calcined:</b> 700°C for 5 hours</p>	<p><b>Colour:</b> White</p> <p><b>Phase:</b> Amorphous</p>

To deal with these parameters, we opted for a system which requires even lower temperatures for network stabilization. Hence, we chose to synthesize glass with acetate precursors which unlike the nitrates need not to be thermal treated up to 700°C for stabilization of the glass network. Furthermore acetates are non-toxic and organic which makes them a safe choice for making bioactive glasses.

#### 3.3.4. Acetate system:

We thus prepared MBGs of increasing sodium oxide content (0Na, 2.5Na, 5Na, 7.5Na and 10Na) in an acetic acid-assisted, acetate-based sol-gel system. This was performed at a small and large scale. As experienced from previous trials it was decided not to directly thermal treat these samples but to first subject them to Differential Scanning Calorimetry (DSC)/Thermo-Gravimetric Analysis (TGA) as a means of determining the temperature of surfactant decomposition and crystallization. The aim was to identify a thermal treatment protocol featuring a peak temperature that is higher than the temperature for surfactant decomposition but below that for crystallization. This way it is proposed that the decomposition of organic micelles is not hindered.

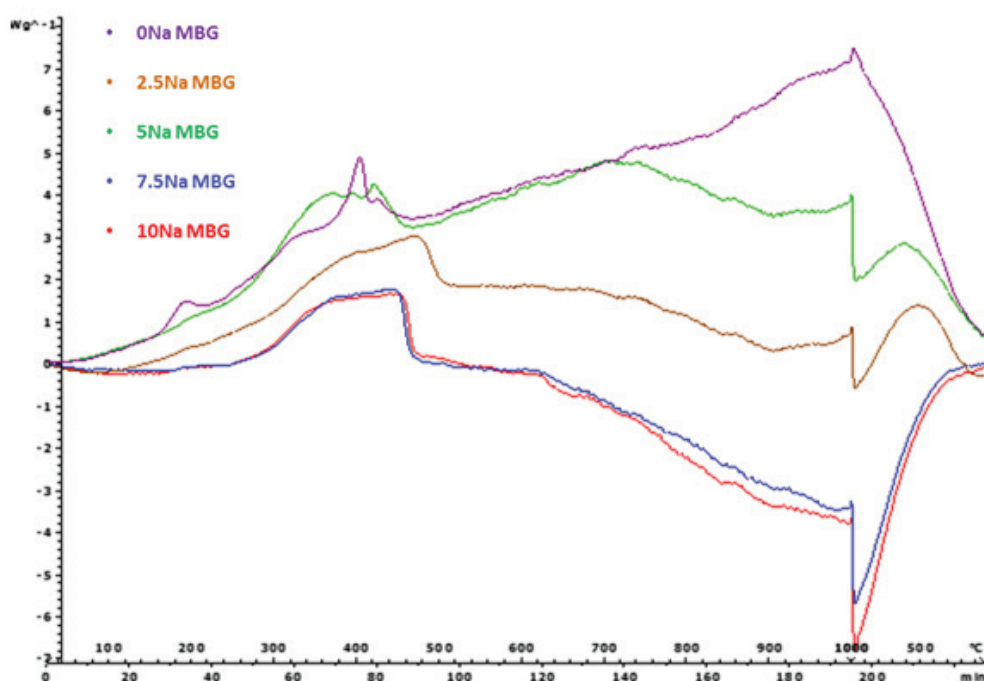


**Figure 14** DSC curves of small scale samples of various compositions prepared using acetate precursors

The DSC and DTG curves of the small scale samples of varying compositions are shown in **Figure 14** and **Figure 15** respectively. An exothermic peak between 300°C to 500°C can be seen in the DSC curves of the small scale samples. At a closer look, we can find a double exothermic peak specifically in

the 0Na and 5Na MBGs. Examination of DTG curves also shows a double peak phenomena in that temperature range which is more evident in the 0Na MBG and becomes less distinct with increasing  $\text{Na}_2\text{O}$ . Similarly, the DSC curves of the large-scale samples (**Figure 18**) also exhibits sharp double exothermic peaks in the same temperature range. However, in the DTG curves there is a temperature gap between the weight loss associated with the two peaks (**Figure 19**). We supposed that the double exothermic peaks were a result of polymer decomposition and crystallization occurring at a close temperature range. The two phenomena overlap each other in the small-scale samples but a small temperature gap between them exists in the large scale samples. The weight loss at temperature below  $250^\circ\text{C}$  in the small and large scale samples was assigned to solvent decomposition. It should be mentioned here that the weight loss associated with the crystallization in the DTG curves is not due to glass crystallization but due to the decomposition of the calcium precursors which is discussed in detail in Chapter 5.

Based on these results we chose to thermal treat the small-scale samples at  $450^\circ\text{C}$  as the DTG showed that it was close to the end of polymer decomposition.

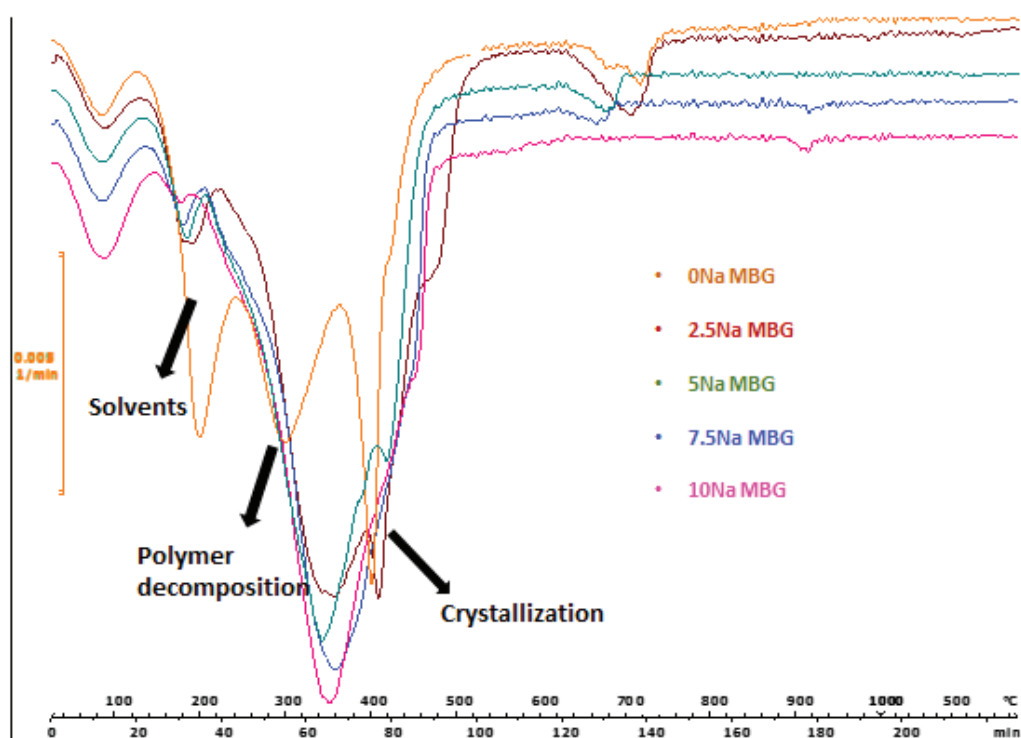


**Figure 15** DTG curves of small scale samples of various compositions prepared using acetate precursors

The samples were calcined at 450°C for 5 hours at 5°C per min. After calcination we once again observed a deposition of black carbon soot on the samples whose intensity increased with increasing sodium oxide in the composition as seen in **Figure 16**.



**Figure 16** Small scale samples prepared using acetate precursors calcined at 450°C for 5 hours

For the next attempt we increased the peak temperature from 450°C to 480°C and ramped up at a very slow rate of 1°C per minute before holding at 480°C for 5 hours. Ramp-down to room temperature was achieved in 8 hours.



**Figure 17** Small scale samples prepared using acetate precursors calcined at 480°C for 5 hours; (A) 10Na MBG (B) 7.5Na MBG (C) 5Na MBG

As can be seen from **Figure 17** the carbon soot deposit was not found in any of the samples. These results suggest that slow ramp up and holding at the temperature range of polymer decomposition followed by slow ramp down would give sufficient time for the polymer to decompose away.

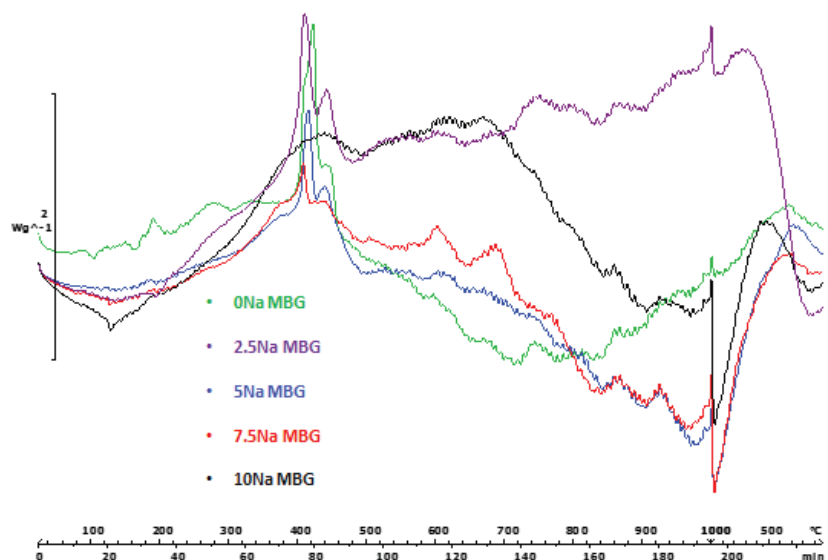


Figure 18 DSC curves of large scale samples of various compositions prepared using acetate precursors

As already mentioned, for the large-scale samples there was a temperature gap between polymer decomposition ( $\sim 250^\circ\text{C}$ ) and crystallization ( $400^\circ\text{C}$ ). Therefore, samples were individually calcined at  $380^\circ\text{C}$  for 5 hours with  $1^\circ\text{C}$  per minute ramp up and cooled to room temperature in 8 hours.

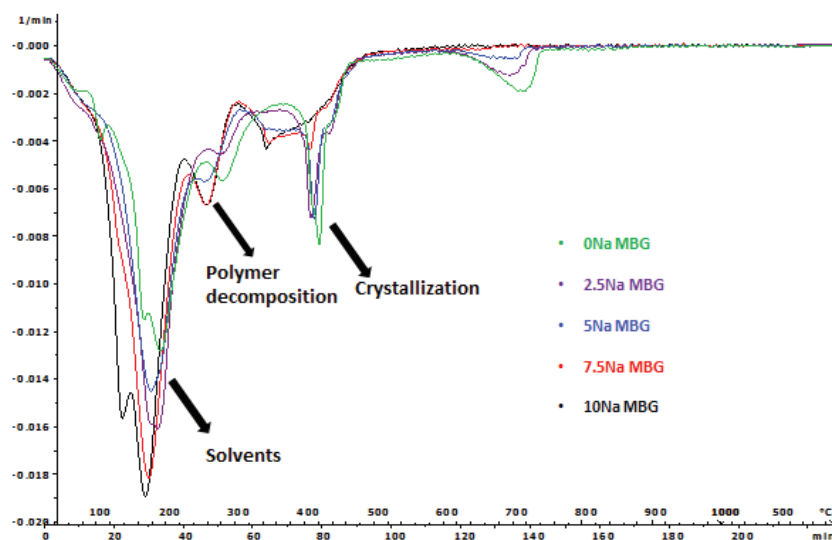


Figure 19 DTG curves of small scale samples of various compositions prepared using acetate precursors



Figure 20 Large scale samples prepared using acetate precursors calcined at  $380^\circ\text{C}$  for 5 hours; (A) 10Na MBG (B) 7.5Na MBG (C) 5Na MBG

The samples appeared clean without any carbon deposit and whiter than the small scale samples after thermal treatment (**Figure 20**).

### **3.4. Conclusion**

Novel compositions of MBGs for elaboration were determined, based on a short literature research. Initial preparation of MBGs was attempted using nitrate precursors for the network modifiers. The samples after thermal treatment were full of carbon deposit and further investigation revealed that (a) early crystallization due to high sodium content in the composition and (b) associated surfactant entrapment were the reasons for the obtained results. The MBGs were re-prepared using acetate precursors to minimise the temperature required for stabilization. The DSC/DTG analysis showed that the polymer decomposition and crystallization were occurring within a close temperature range. Calcination of samples using a very slow ramp rate and a “hold” at a temperature close to the surfactant decomposition temperature followed by a slow ramp down resulted in clean carbon free samples.

## 4. Influence of scale on the surface characteristics of MBGs

### 4.1. Introduction

In the previous chapter we discussed the process that led us to the elaboration of small and large scale samples using acetate precursors. In this chapter we study the influence of preparation scale on the surface characteristics of these MBGs. While performing our literature review for elaborating these MBGs we noticed that most studies reporting MBGs with high surface area featured samples prepared in very small quantities, typically less than 4 grams [89,90,92,93,97–104]. One of the main advantages of the melt quench system over sol-gel is that large quantities of samples can be prepared because it is a non-wet chemical synthesis route involving much fewer synthesis parameters in comparison to sol-gel. That is the reason why melt-quenched bioactive glasses are favoured by industries and are more prevalent in the market today. On the downside, the intricate surface characteristics such as surface area and porosity of the sol-gel glasses is absent in the melt-quenched glasses [105–107]. Therefore, improving the production scale of sol-gel glasses is imperative to materialise the use of these textured particles in a product. Since the quantities of MBGs reported in the literature are very minimal, there is a need to make multiple batches to even characterize these samples completely in order to study their physico-chemical and bioactive properties. Such an approach runs the risk of batch-to-batch variations that makes the identification of trends more difficult. As this is not a very pragmatic approach we decided to elaborate samples in “small scale” (10g) and “large scale” (50g) to see the effect scaling up has on the surface characteristics of these particles. Though the quantity we have mentioned is also not comparable to an industrial scale we believed that it represents a good starting point.

### 4.2. Materials and Methods

#### 4.2.1. Materials and Sample preparation

The materials and preparation details of the small and large scale samples are detailed in **Sections 3.2.1 and 3.2.4.**

#### 4.2.2. X-ray diffraction

The material phase was characterized with X-ray diffractometer (XRD). XRD of samples after calcination was performed using an X-ray diffractometer (XRD, X'Pert Philips, Netherlands) with Cu K $\alpha$  radiation of wavelength 1.54 Å. The scans were recorded at 30 kV, 30 mA, 2 theta ranges between

5° to 60° and a step size of 0.02° and 90.17 seconds per step. Phase identification was carried out using the software X'Pert Highscore®.

#### 4.2.3. BET/BJH

The surface area and pore volume parameters were determined by nitrogen adsorption/desorption isotherms at 77 K in a Surface area analyzer (Gemini 2385). The samples were degassed at 200°C for 4 hours prior to measurement. The Brunauer-Emmett-Teller (BET) equation was used for the specific surface area and pore volume quantification while Barret-Joyner-Halenda (BJH) was used for average pore diameter determination.

### 4.3. Results and discussion

**Figure 21(A)** shows the phase composition of the small scale samples with varying Na<sub>2</sub>O/CaO content. It appeared that, aside from 10Na MBG, all the other samples exhibit crystallinity with calcite as the only crystalline phase.

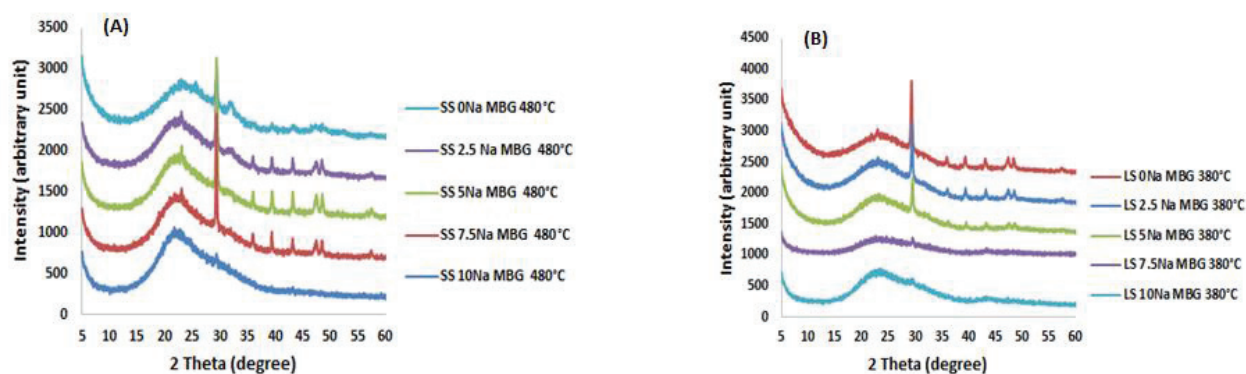


**Figure 21** XRD of samples after thermal treatment (A) Small scale samples calcined at 480°C (SS) (B) Large scale sample calcined at 380°C (LS)

In the large scale samples (**Figure 21B**) the 10Na and 7.5Na MBGs are amorphous whilst the remaining samples exhibit the same calcite phase. The crystallization seems to be increased with increasing CaO in the composition.

The textural characteristics of the samples assessed using BET/BJH revealed that, regardless of the scale, the surface area and pore volume increased with increasing CaO content in the composition (**Figure 22**). Furthermore the average pore size decreased with increasing CaO in the composition. These trends signify that the porosity is driven by CaO in the MBG composition. The reason for the

calcite phase occurring in these samples and CaO driving the porosity have been discussed in detail in Chapter 5 and hence will not be detailed here.

The BET/BJH data also suggests that the large scale samples have much higher surface area, pore volume and lower mean pore size than the small scale samples. In general terms, the large scale samples have increased porosity compared with the small scale samples.

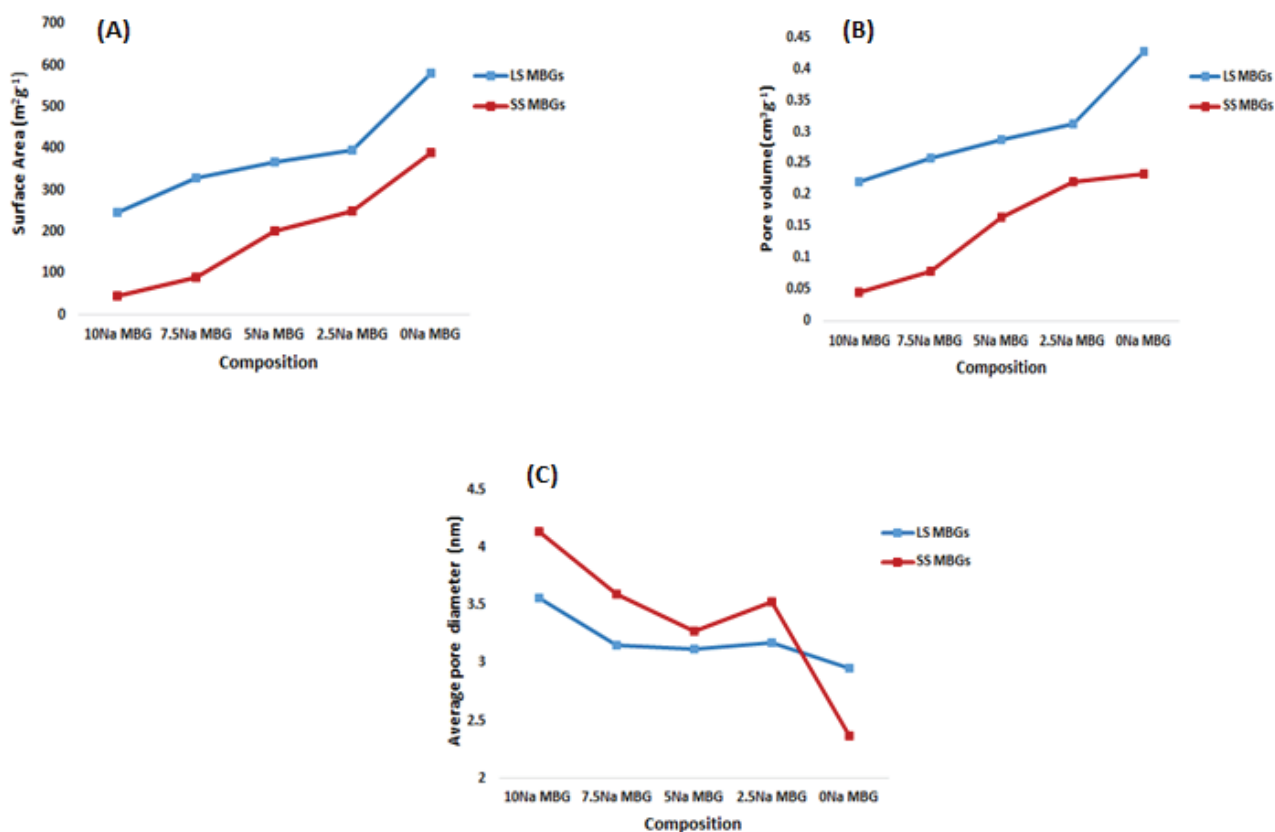
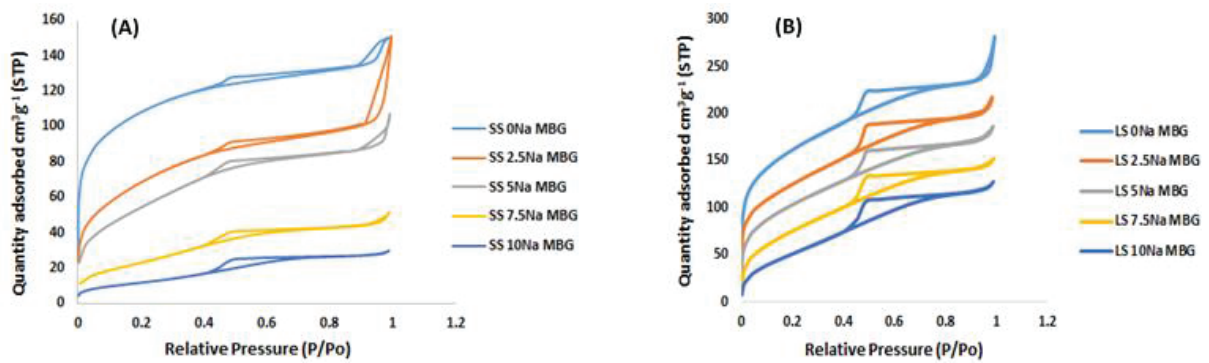


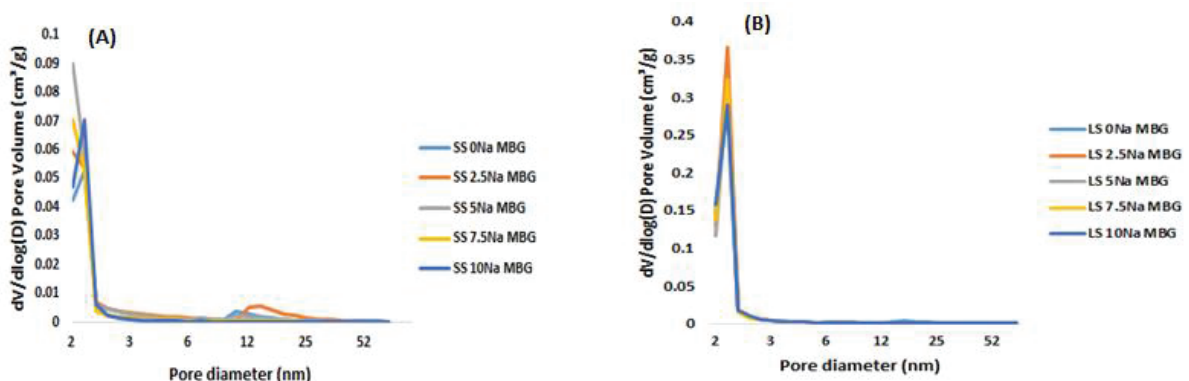
Figure 22 BET/BJH analysis of small scale samples (SS MBGs) and large scale samples (LS MBGs). (A) Surface area (B) Pore volume (C) Pore size

Figure 23 shows the adsorption desorption isotherms of the small and large-scale samples. In general, samples in both scales fall under type IV isotherm which is typical for mesoporous materials. However, there is a subtle difference in the hysteresis loops of the small and large scale MBGs. While both small and large scale MBGs possess H2 type hysteresis loops the 0Na, 2.5Na and 5Na MBG versions of small-scale samples express a combination of H2 and H4 type loops (Figure 23A). The H2 loops are an indication of samples with ink-bottled shape pores and the H4 loops are seen in samples that have a mixture of micropores and mesopores.



**Figure 23** Adsorption and desorption isotherms of small scale samples (SS MBGs, A) and large scale samples (LS MBGs, B)

The pore size distribution of the small-scale samples confirms that although all samples exhibit some microporosity, the majority of the pores are mesoporous between 2-3nm range. Furthermore, the 0Na and 2.5Na MBGs also express some population of bigger sized pores between 12-25nm (**Figure 24A**). The narrow loop in the adsorption-desorption isotherm in the high P/Po range for the 0Na to 5Na MBG small scale samples could be a result of these bigger sized pores. All large-scale samples exhibit mesoporosity in the 2-3nm range (**Figure 24B**). The only difference between the small scale and large scale samples is the quantity of oxide precursors used for their elaboration. Since, the quantity of solvents and surfactant were fixed in both cases it naturally makes the small-scale samples have a higher concentration of surfactant than the large scale samples. The bigger sized pores of 12-25 nm in the 0-5Na MBGs of small scale MBGs could therefore be a result of the pores created by some well formed micelles which is absent in the large scale MBGs. The higher concentration of surfactant in the small-scale samples could also explain the reason for them requiring relatively higher temperatures compared with large-scale samples for full carbon removal.



**Figure 24** Pore size distribution of small scale samples (SS MBGs, A) and large scale samples (LS MBGs, B)

The increased thermal treatment in the small-scale samples and the associated melting and densification of the network could be the possible reason for the reduction in their porosity compared to the large scale samples.

#### **4.4. Conclusion**

Though scale-up did not drastically alter the surface characteristics, the thermal treatment associated with the large-scale samples delivered an increased porosity compared to the small scale samples. Therefore, we decided to carry forward the large-scale samples for further investigations as it presented more advantages in terms of color, quantity and texture.

## 5. Influence of network modifiers on the surface characteristics of MBGs

### 5.1. Introduction

In bioactive glasses the network modifiers are an important aspect as they not only alter the glass surface characteristics, but also, the release of these ions is crucial to initiate their bioactivity.

In this chapter we outline the influence the varying networking modifiers (CaO: Na<sub>2</sub>O) have on the surface characteristics of the large scale MBGs prepared in an acetate based sol-gel bioactive glass system. In the previous chapter we mentioned the formation of calcite phase in these glasses and also the porosity being driven by CaO content of the glass composition. These trends have been assessed using characterizations such as XRF, XRD, BET/BJH, FTIR, ICP, SEM and TEM and the possible reason behind these findings are presented as an article published in the *Journal of Microporous and Mesoporous materials*.



## Influence of network modifiers in an acetate based sol-gel bioactive glass system



Delihtha Fernando <sup>a</sup>, Nina Attik <sup>a, b, \*</sup>, Mark Cresswell <sup>d</sup>, Ilham Mokbel <sup>a</sup>,  
Nelly Pradelle-Plasse <sup>a, e, f</sup>, Phil Jackson <sup>d</sup>, Brigitte Grosogeat <sup>a, b, c</sup>, Pierre Colon <sup>a, e, f</sup>

<sup>g</sup> Laboratoire des Multimateriaux et Interface, Universite de Lyon, Universite Claude Bernard Lyon 1, Lyon, France

<sup>h</sup> Faculte d'Odontologie, Universite de Lyon, Universite Claude Bernard Lyon 1, Lyon, France

<sup>i</sup> Service d'Odontologie, Hospices Civils de Lyon, Lyon, France

<sup>j</sup> Lucideon Inc., Penkhull, Stoke-On-Trent ST4 7LQ, UK

<sup>k</sup> Faculte d'Odontologie, Universite Paris Diderot, Paris, France

<sup>l</sup> APHP, Hopital<sup>^</sup> Rothschild, Service d'Odontologie, Paris, France

## article info

## Article history:

Received 28 June 2017

Received in revised form

4 August 2017

Accepted 16 August 2017

Available online 18 August 2017

## Keywords:

Bioactive glass

Mesoporous

Acetate

Sol-gel

Network modifier

## abstract

The aim of this study was to assess the influence of CaO/Na<sub>2</sub>O ratio on the structural and textural properties of mesoporous bioactive glasses generated from an acetic acid catalysed acetate based sol-gel system. The glass network formers (SiO<sub>2</sub> and P<sub>2</sub>O<sub>5</sub>) were fixed and the network modifiers were varied [75SiO<sub>2</sub>:XCaO:(15-X)Na<sub>2</sub>O:10P<sub>2</sub>O<sub>5</sub> where X = 5, 10, 15, in mole percent] such that increasing alkaline earth oxide is compensated by decreasing alkali oxide. The glass properties were assessed using techniques such as XRF, XRD, FTIR, BET/BJH, SEM, TEM and ICP. The rapid gelling of the sol resulted in the deposition of the calcium and sodium acetate precursors on the particle surface which required thermal treatment to facilitate their entry into the glass network. The results of our study demonstrated that the porosity was clearly driven by CaO in the composition possibly due to its inferior fluxing effect in comparison to Na<sub>2</sub>O. The sample with highest CaO content reached a high surface area and pore volume (535 m<sup>2</sup> g<sup>-1</sup> and 0.33 cm<sup>3</sup> g<sup>-1</sup>) even in a non-surfactant based preparation suggesting that acetic acid catalysed acetate system favours improved textural properties. In vitro SBF tests confirmed the potential of the sample with highest CaO for earlier apatite formation.

© 2017 Elsevier Inc. All rights reserved.

## 1. Introduction

Bioactive glasses are extensively used for bone regeneration and continue to be explored in the field of bone tissue engineering and dentistry due to their ion mediated antibacterial [1], angiogenic [2], osteogenic [3,4], odontogenic [5] and remineralizing effects [6,7]. Ever since the introduction of bioactive glass by Professor Larry Hench in 1969 [8] the evolution of these bioactive particles has been diverse. Initially, bioactive glasses were prepared by the melt quench technique [9] which is a top down approach of making glass involving melting the oxide precursors at very high temperatures and quickly quenching them to avoid crystallization.

Corresponding author. Equipe Biomateriaux et Interfaces Biologiques, Laboratoire Multimateriaux et Interfaces (UMR CNRS 5615), Faculte d'Odontologie, Universite Claude Bernard Lyon1. 11, Rue Guillaume Paradin, 69372 Lyon Cedex 08, France.

E-mail address: [nina.attik@univ-lyon1.fr](mailto:nina.attik@univ-lyon1.fr) (N. Attik).

<http://dx.doi.org/10.1016/j.micromeso.2017.08.029> 1387-1811/© 2017 Elsevier Inc. All rights reserved.

In 1991, an alternate route of producing these particles was introduced by Lie et al., [10] termed as sol-gel bioactive glasses. The sol-gel method is a bottom up wet chemical approach of making glass which involves hydrolysis and condensation reactions of glass precursors. In contrast to the melt quench, sol-gel bioactive glasses are innately porous [11] and are synthesized at low temperatures [12]. It is well known that the percentage of silica should not exceed 60% in bioactive glasses prepared by melt quench route as they lose their bioactivity due to low dissolution of the glass network [13]. However, bioactive glasses up to 90% silica have been fabricated by sol-gel route and their bioactivity has been demonstrated [14] highlighting that bioactivity of sol-gel glass is not solely composition dependent but that the surface area features of these glasses play a vital part in driving the outcome.

Inspired by these findings, a further advancement in sol-gel bioactive glass synthesis was made in 2004 by Yan et al., [15] who prepared the first mesoporous bioactive glasses (MBG's) by introducing block co-polymers as structure directing agents in sol-

gel bioactive glass synthesis. The surfactants form micelles around which the glass network is formed with the micelles subsequently removed by thermal treatment or a washing step. The removal of micelles creates ordered pores in the places where they previously remained thus allowing for a marked increase in glass porosity and surface area. This further complements the bioactivity of these glasses and are reported to form apatite within hours of immersion in simulated body fluid [16]. Besides the surfactant or target composition, the process parameters of the sol-gel technique (e.g. oxide precursor chemistry, synthesis temperature, catalyst, drying and calcination temperature) can be altered to tailor the final glass properties.

Despite these advantages of sol-gel technique one of the problems that has been reported is the inhomogeneity of the glass composition due to improper incorporation of the salt precursors. Most studies so far have used nitrates as the precursors for network modifying oxides [17,18], tetraethyl orthosilicate (TEOS) for silica and triethyl phosphate (TEP) for phosphate along with nitric acid or hydrochloric acid as a catalyst. The struggle to incorporate the modifying precursors especially calcium nitrate and the resulting inhomogeneity has lead studies to explore other possible pre-cursors such as citrates and methoxyethoxides. Yu et al., [19] evaluated three calcium precursors (calcium chloride, calcium nitrate and calcium methoxyethoxide) and found methoxyethoxide to be favourable in attaining homogeneity. Similarly, Catteaux et al., also obtained a perfectly amorphous matrix at low temperature by using dimethoxy calcium as calcium precursor. Even though thermal treatment removes the "methoxyethoxide" or "meth-oxide" component the toxicity of these precursors would make it less favourable considering Registration, Evaluation, Authorisation and Restriction of Chemicals (REACH) and Food and Drug Administration (FDA) regulations for industrial manufacturing.

We therefore aimed to explore the use of acetate precursors for incorporating network modifiers as a more viable, safer system for medical application. The present study mainly investigates the influence of network modifiers (CaO/Na<sub>2</sub>O) on the structural and textural properties of acetate based sol-gel bioactive glass system. This understanding is crucial to tailor bioactive glasses with desired properties during a targeted synthesis of these materials.

### (3) Materials and methods

#### 2.1. Materials

Tetraethyl orthosilicate (TEOS, 98%), triethyl phosphate (TEP, 99%), calcium acetate monohydrate (Ca (CH<sub>3</sub>COO)<sub>2</sub>·H<sub>2</sub>O, 99%), sodium acetate anhydrous (CH<sub>3</sub>COONa), ethyl alcohol (EtOH, 99.7%), triblock copolymer EO<sub>20</sub>PO<sub>70</sub>EO<sub>20</sub> (P123, Mw=5650) and glacial acetic acid (CH<sub>3</sub>COOH) were used from Sigma Aldrich.

#### 2.2. Sample preparation

The MBG's with 1.8 wt% surfactant of composition 75SiO<sub>2</sub>:XCaO:(15-X)Na<sub>2</sub>O:10P<sub>2</sub>O<sub>5</sub> where X=5,10,15 have been synthesized by an acid catalysed sol-gel method assisted by evaporation induced self-assembly (EISA) process. The composition, precursor quantities, temperature of drying and calcinations are detailed in Table 1. Each step was performed in 1 h intervals. Step 1 involved dissolving 2 g of P123 surfactant in 30 g ethanol. In step 2, 37.5 ml of de-ionised water and 214.5 ml of glacial acetic acid were added to the ethanol surfactant mixture. Each glass precursor was added to the ongoing reaction in 1 h intervals (step 3) in the order TEOS, TEP, calcium acetate monohydrate and sodium acetate. The solution gelled in about 1 h after adding the last precursor and was allowed to undergo EISA at room temperature (RT) for 4 days, followed by drying at 60°C for 2 days.

The dried gel was milled down and calcined at different temperatures (Table 1) at a ramp rate of 1°C per minute to reach the set temperature, held for 5 h at the set temperature and finally cooled to RT in 8 h. Conventional bioactive glasses (BG) of the compositions 0Na BG and 10Na BG were also prepared following the same protocol but excluding the addition of surfactant (Table 1).

#### 2.3. Sample characterization

##### 2.3.1. XRF

The glass composition of 0Na MBG and 10Na MBG after 380°C thermal treatment was determined by semi-quantitative X-ray fluorescence (XRF) method. A small quantity of material was smeared onto a filter paper and presented to the XRF spectrometer (Panalytical Axios) and run on the preinstalled semi quantitative XRF package.

##### 2.3.2. XRD

The glass phase was characterized with X-ray diffractometer (XRD). XRD of samples in the uncalcined state and after different calcination temperatures (310°C, 340°C, 380°C) was performed using an X-ray diffractometer (XRD, X'Pert Philips, Netherlands) with Cu K $\alpha$  radiation of wavelength 1.54 Å. The scans were recorded at 30 kV, 30 mA, 2 theta ranges between 5 and 60 and a step size of 0.02 and 90.17 s per step. Phase identification was carried out using the software X'Pert Highscore.

##### 2.3.3. BET/BJH

The surface area and pore volume parameters were determined by nitrogen adsorption/desorption isotherms at 77 K in a Surface area analyzer (Gemini 2385). The samples were degassed at 200°C for 4 h prior to measurement. The Brunauer-Emmett-Teller (BET) equation was used for the specific surface area and pore volume quantification while Barret-Joyner-Halenda (BJH) was used for average pore diameter determination.

##### 2.3.4. FTIR

The glass network was studied using Fourier transform infra-red spectroscopy (FTIR) on a Safas Monaco spectrometer. The spectra was collected in a wavelength range of 340-4000 cm<sup>-1</sup> at a spectral resolution of 4 cm<sup>-1</sup>.

##### 2.3.5. SEM

The morphology of the copper coated 0Na MBG and 10Na MBG samples after 310°C thermal treatment was examined by scanning electron microscopy (FEI-Quanta 250, Thermo Fisher Scientific, France) at a magnification of 1000.

##### 2.3.6. TEM

The textural properties of 0Na MBG and 10Na MBG after 310°C and 380°C treatment was imaged using transmission electron microscopy (TEM, Jeol 2100F) at 200 kV.

##### 2.3.7. ICP

The ion dissolution from the particles was studied on 0Na MBG, 5Na MBG, 10Na MBG samples after 310°C and 380°C heat treatment. Dissolution was performed in de-ionised water with samples analysed after 1, 3 and 7 days. The pH was measured using a Hannah pH meter, the particles were passed through a 0.2 mm filter and the dissolution extracts were collected and analysed with inductive coupled plasma spectrometry (ICP, VistaeMPX, CCD simultaneous ICP-OES instrument and ICP expert software).

Table 1  
Composition, precursor quantities, temperature of drying and calcinations.

Sample name	Composition	TEOS (g)	TEP (g)	Calcium acetate monohydrate (g)	Sodium acetate (g)	Drying temperature ( C)	Calcination ( C)
0Na MBG	75SiO <sub>2</sub> -15CaO-0Na <sub>2</sub> O-10P <sub>2</sub> O <sub>5</sub>	78.12	18.22	13.21	0	60	310, 340 and 380
5Na MBG	75SiO <sub>2</sub> -10CaO-5Na <sub>2</sub> O-10P <sub>2</sub> O <sub>5</sub>	78.12	18.22	8.81	4.10	60	310, 340 and 380
10Na MBG	75SiO <sub>2</sub> -5CaO-10Na <sub>2</sub> O-10P <sub>2</sub> O <sub>5</sub>	78.12	18.22	4.40	8.20	60	310, 340 and 380
0Na BG	75SiO <sub>2</sub> -15CaO-0 Na <sub>2</sub> O-10P <sub>2</sub> O <sub>5</sub>	78.12	18.22	13.21	0	60	340 and 380
10Na BG	75SiO <sub>2</sub> -5CaO-10 Na <sub>2</sub> O-10P <sub>2</sub> O <sub>5</sub>	78.12	18.22	4.40	8.20	60	340 and 380

The text in bold signifies the variable parts in the composition of the bioactive glass particles.

#### 2.4. In vitro bioactive test

To test the bioactivity, 0Na MBG and 10Na MBG samples subjected to a 310° C heat treatment were each immersed in SBF at 37°C for 1,3 and 7 days at a concentration of 1.5 mg/ml. At each time point, the samples were collected, left to air dry, copper coated (10 nm) and analysed using SEM imaging (FEI-Quanta 250, Thermo Fisher Scientific, France).

### 3. Results

#### 3.1. XRF

The XRF semi-quantitative results of 0Na MBG and 10Na MBG calcined at 380 C are shown in Tables 2 and 3 as mole percent. Both samples have attained the expected content of SiO<sub>2</sub>, CaO and Na<sub>2</sub>O but not P<sub>2</sub>O<sub>5</sub>. The 0Na MBG sample contains relatively higher P<sub>2</sub>O<sub>5</sub> levels than the 10Na MBG sample. However, the expected difference between CaO and Na<sub>2</sub>O has been achieved in both compositions.

#### 3.2. XRD

The uncalcined 0Na MBG and 10Na MBG samples show heavy crystallinity identified as calcium acetate acetic hydrate for 0Na MBG and sodium hydrogen acetate for 10Na MBG (Fig. 1A). These phases correspond to the calcium and sodium precursors in combination with the solvent used for preparing these MBGs. Following a 310°C thermal treatment 10Na MBG is completely amorphous whereas the 5Na MBG and 0Na MBG still show some crystalline peaks corresponding to calcium acetate acetic hydrate (Fig. 1B). After a 340°C heat treatment 5Na and 10Na MBGs are completely amorphous whilst peaks corresponding to calcium acetate acetic hydrate remain in 0Na MBG (Fig. 1C); however the peaks are less prominent than the peaks observed in the same sample following a 310°C heat treatment. Finally, after a 380°C thermal treatment the samples exhibit calcite phase (calcium carbonate) and the level of calcite increases with increasing CaO content in the glass composition (Fig. 1D).

Table 2  
XRF result of 0Na MBG after 380°C thermal treatment.

0Na MBG	SiO <sub>2</sub>	CaO	Na <sub>2</sub> O	P <sub>2</sub> O <sub>5</sub>
Expected	75	15	0	10
Reached	79.74	14.82	0	5.43

Table 3  
XRF result of 10Na MBG after 380°C thermal treatment.

10Na MBG	SiO <sub>2</sub>	CaO	Na <sub>2</sub> O	P <sub>2</sub> O <sub>5</sub>
Expected	75	5	10	10
Reached	79.29	5.65	11.3	3.74

Fig. 1E represents the phases present in 0Na BG and 10Na BG after a 340°C thermal treatment. As seen, both compositions are amorphous with complete disappearance of precursors after 340°C in the non-surfactant system. The summary of the XRD results is indicated in Table 4.

#### 3.3. FTIR

The FTIR spectra for 0Na MBG and 10Na MBG after 310°C and 380°C are shown below (Fig. 2A and B). In the 0Na MBG at 310°C we have identified the peak at 3440 cm<sup>-1</sup> as the OH from the surface silanols in the glass [21,22] and the peak at 1610 cm<sup>-1</sup> as being due to OH from the adsorbed water [21]. The Si-O-Si asymmetric stretch can be seen at 1078 cm<sup>-1</sup>[16,23,24], Si-O-Si symmetric bending at 796 cm<sup>-1</sup> [21,23-26] and Si-O-Si rocking mode at 462 cm<sup>-1</sup> [21,25,26]. The P-O bond was evident at 564 cm<sup>-1</sup> [16,23-26] and the peak at 954 cm<sup>-1</sup>[21,22,27] corresponds to Si-O-NBO (where NBO = non-bridging oxygen). The peaks at 1420 cm<sup>-1</sup> and 1552 cm<sup>-1</sup>[21] correspond to COO<sup>-</sup> present in the salts. On comparing the 0Na MBG and 10Na MBG samples at 310°C we find the same peaks present but with the peaks corresponding to COO<sup>-</sup> of the salts being much smaller in the 10Na MBG sample.

At 380°C, we can see a peak corresponding to the C-O of the carbonate (1430 cm<sup>-1</sup>) in the 0Na MBG sample. This is believed to be associated with the calcite phase revealed by XRD. We do not see this peak in the 10Na MBG sample because XRD shows it to be amorphous at 380°C.

#### 3.4. BET/BJH

The surface area, pore volume and average pore diameter of 0Na, 5Na and 10Na MBGs after a 340°C heat treatment are shown in Fig. 3(A-C). The surface area and pore volume increases with increasing CaO in the composition and there is a reduction in average pore diameter of the 0Na and 5Na MBG samples compared to 10Na MBG.

Fig. 4(A-C) shows a comparison of the surface area, pore volume and average pore diameter for 0Na MBG and 10Na MBG at 310°C, 340°C and 380°C thermal treatments. First, it can be seen that for all 3 thermal treatments the surface area and pore volume for 0Na MBG is higher and the average pore diameter is lower than 10Na MBG. Next we observe that in the 10Na MBG sample there is a decrease in the surface area and pore volume from 310°C to 380°C. This is accompanied by a pronounced increase in average pore diameter during the 310°C-340°C treatment followed by a mild decrease in average pore diameter from the 340°C-380°C treatment. However, in the 0Na MBG there is a marked increase in surface area, pore volume and average pore diameter during 310°C-340°C heat treatment followed by a mild decrease in all three parameters at 380°C.

Table 5 contains the surface area characteristics of 0Na BG and 10Na BG after 340°C thermal treatment. The results demonstrate that BGs follow the same trend as MBGs i.e. an increase in surface area, pore volume and a decrease in average pore diameter with increasing CaO in the composition.

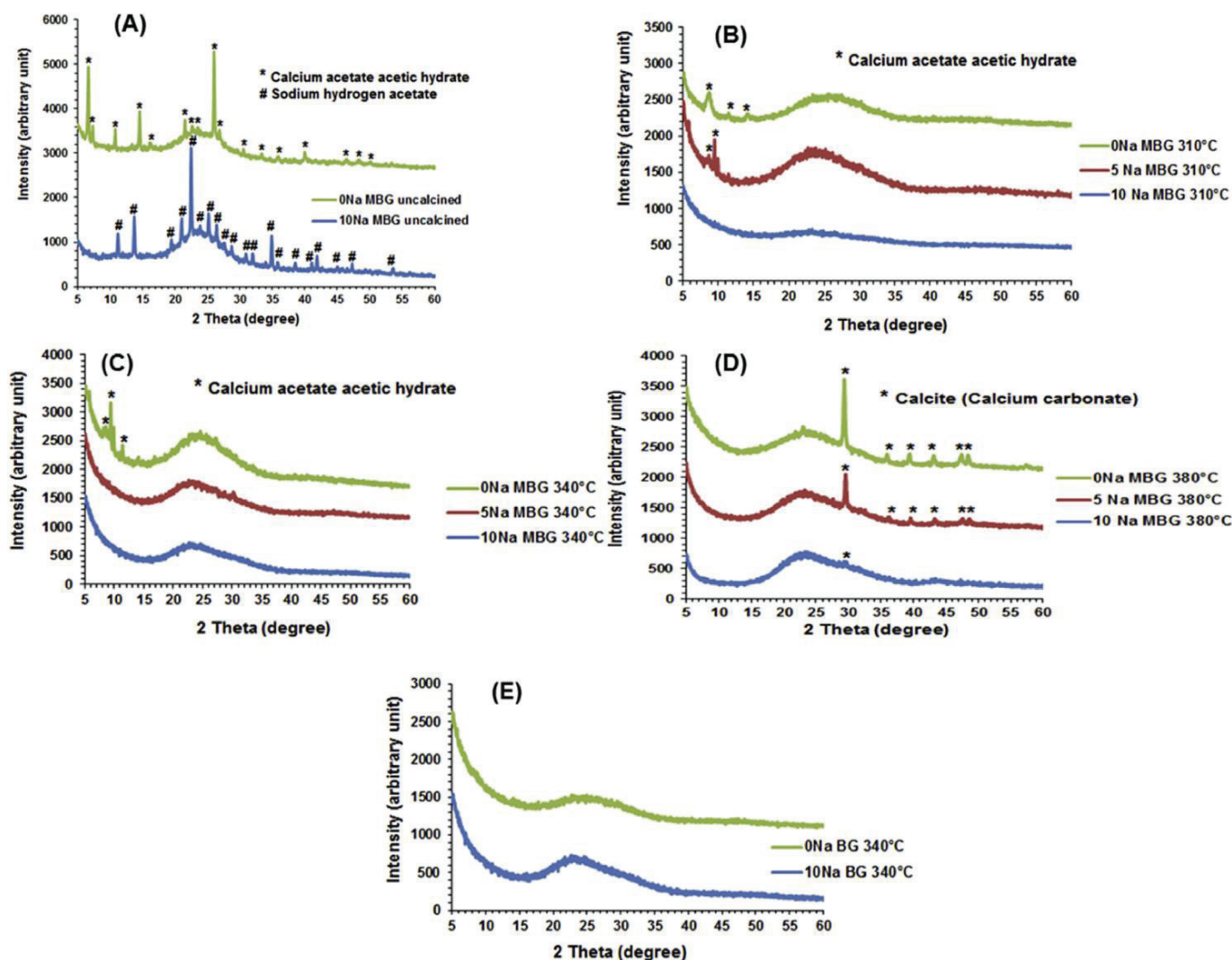


Fig. 1. XRD of samples without and after different thermal treatments (A) XRD of uncalcined 0Na MBG and 10Na MBG; (B) XRD of 0Na MBG, 5Na MBG and 10Na MBG after 310°C; (C) XRD of 0Na MBG, 5Na MBG and 10Na MBG after 340°C; (D) XRD of 0Na MBG, 5Na MBG and 10Na MBG after 380°C; (E) XRD of 0Na BG and 10Na BG after 340°C.

Table 4  
Summary of XRD results.

Composition	Heat treatment	XRD phase	Significance
0Na MBG	No heat treatment	Calcium acetate acetic hydrate	Calcium precursor deposition
	310°C	Calcium acetate acetic hydrate	Entry of sodium precursor and remnant calcium precursor
	340°C	Calcium acetate acetic hydrate	Remnant calcium precursor
5Na MBG	310°C	Calcium acetate acetic hydrate	Decomposition of acetate from the precursor or entry of calcium ions
	340°C	Amorphous	Entry of sodium precursor and remnant calcium precursor
	380°C	Calcite (Calcium carbonate)	Entry of calcium precursor
10Na MBG	310°C	Calcite (Calcium carbonate)	Decomposition of acetate from the precursor or entry of calcium ions
	No heat treatment	Sodium hydrogen acetate	Sodium precursor deposition
	340°C	Amorphous	Entry of sodium and calcium precursor
0Na BG	340°C	Amorphous	Stabilization
	380°C	Beginning of calcite	Decomposition of acetate from precursor or entry of calcium ions
10Na BG	340°C	Amorphous	Entry of sodium and calcium precursor
	340°C	Amorphous	Entry of sodium and calcium precursor

Interestingly, the BGs have reached higher values of surface area and pore volume compared to the corresponding MBGs but with lower average pore diameter.

The adsorption-desorption isotherms and pore size distribution of 0Na, 10Na BGs and MBGs at 340°C have been shown in Appendix 1.(A-C). The 0Na BG, 0Na MBG and 10Na BG display type 4 isotherm with H2 hysteresis

loops which is indicative of ink bottle shaped pores and the 10Na MBG displays H5 type loop which indicates a mixture of open and closed pores (Appendix 1.A). The pore size distribution confirms that the samples are mesoporous yet the 0Na BG and MBG retains some microporosity (Appendix 1.B) which is absent in the 10Na BG and MBG samples (Appendix 1.C).

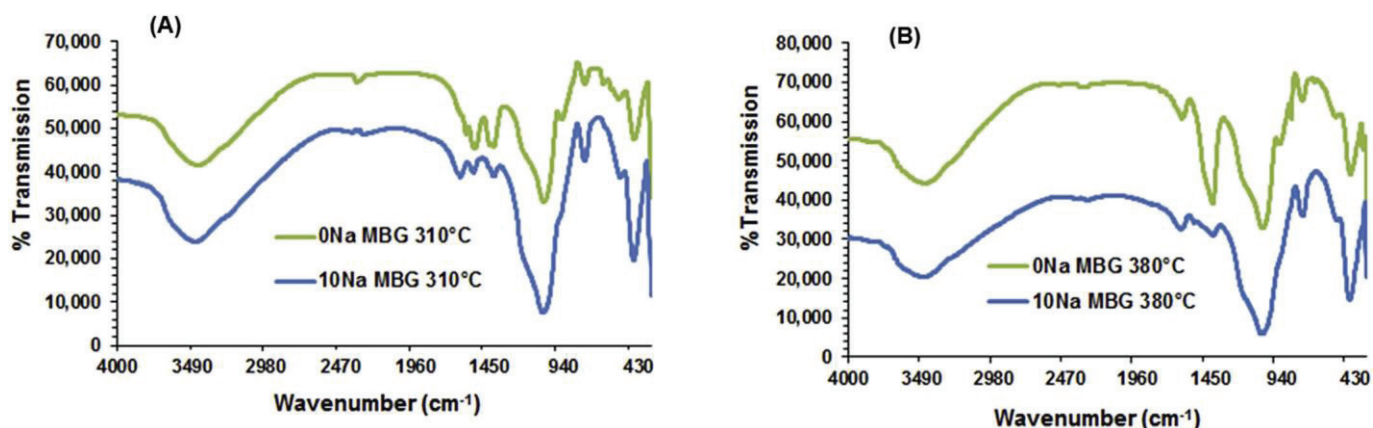


Fig. 2. FTIR analysis of samples after thermal treatments (A) FTIR of 0Na MBG and 10Na MBG after 310°C; (B) FTIR of 0Na MBG and 10Na MBG after 380°C.

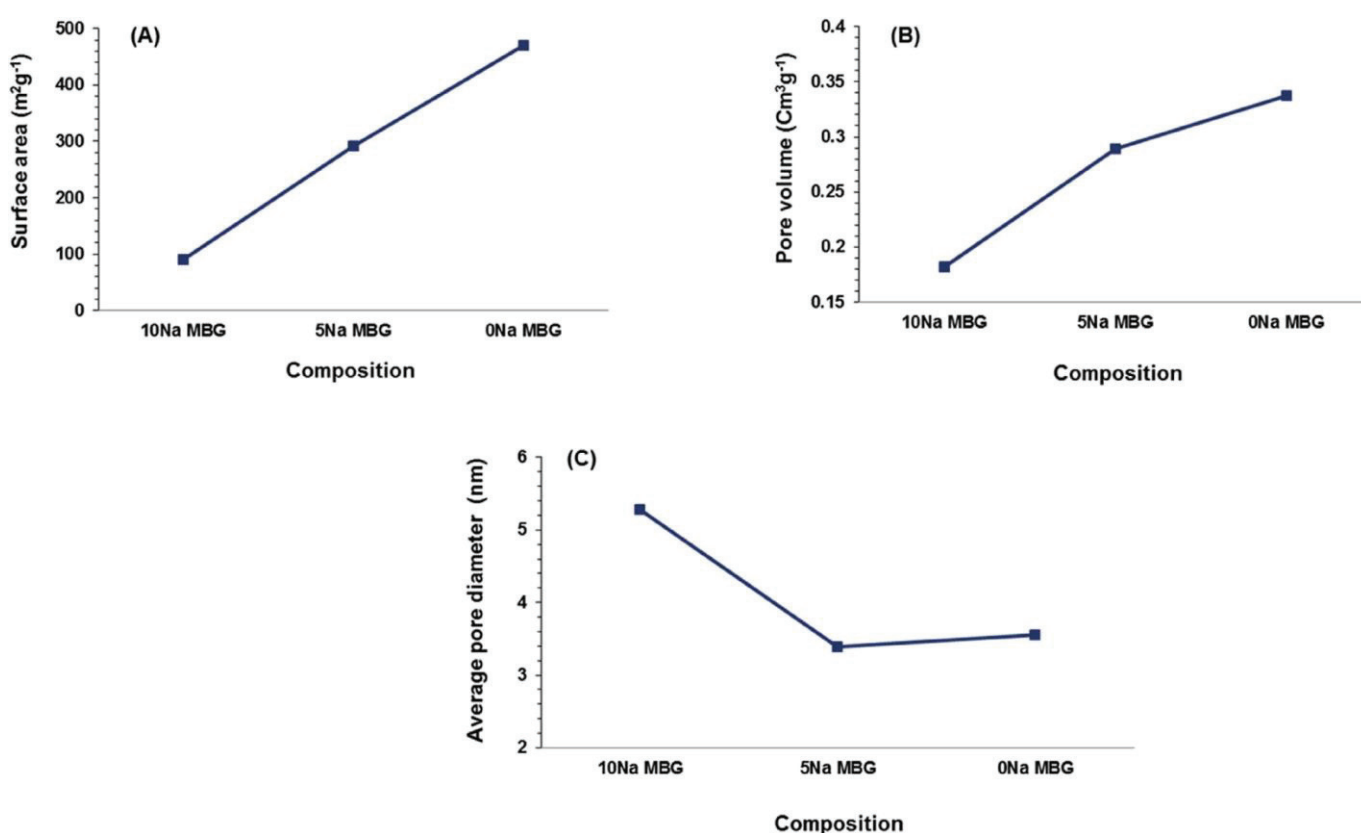


Fig. 3. Influence of composition on textural properties (A) Surface area of 0Na, 5Na and 10Na MBG after 340°C; (B) Pore volume of 0Na, 5Na and 10Na MBG after 340°C; (C) Average pore diameter of 0Na, 5Na and 10Na MBG after 340°C.

Furthermore, on comparing the BGs and MBGs it is seen that the MBGs host a population of bigger sized pores in comparison to BGs which seems to be concentrated between 5 and 10 nm for 10Na MBG and 15–45 nm for 0Na MBG.

### 3.5. ICP and pH measurement

The  $\text{Ca}^{2+}$  and  $\text{Na}^{+}$  release trends are in agreement with the composition of these glasses as the highest  $\text{Ca}^{2+}$  release is achieved in 0Na MBG and decreases with increase in  $\text{Na}_2\text{O}$ . The reverse trend is observed with  $\text{Na}^{+}$  release (Fig. 5C and D). The trend also shows an increase in  $(\text{SiO}_4)^{4-}$  release with increasing  $\text{Na}_2\text{O}$  in the composition (Fig. 5A) and interestingly,

$(\text{PO}_4)^{3-}$  release is lower in the 5Na MBG compared to 0Na MBG and 10Na MBG samples (Fig. 5B). Furthermore, the concentration of ions released from the glasses at 310°C thermal treatment is comparatively higher than 380°C thermal treatment.

Fig. 6A and B demonstrates  $\text{Na}^{+}$  release profiles of 10Na MBG and  $\text{Ca}^{2+}$  release profiles of 0Na MBG in de-ionised water up to 7 days. These figures also compare the trends for MBGs that have been thermally treated at both 310°C and 380°C. There is a gradual increase in the concentration of ions released from the 0Na and 10Na MBGs with time after both thermal treatments. There is reduction in concentration of ions released from the

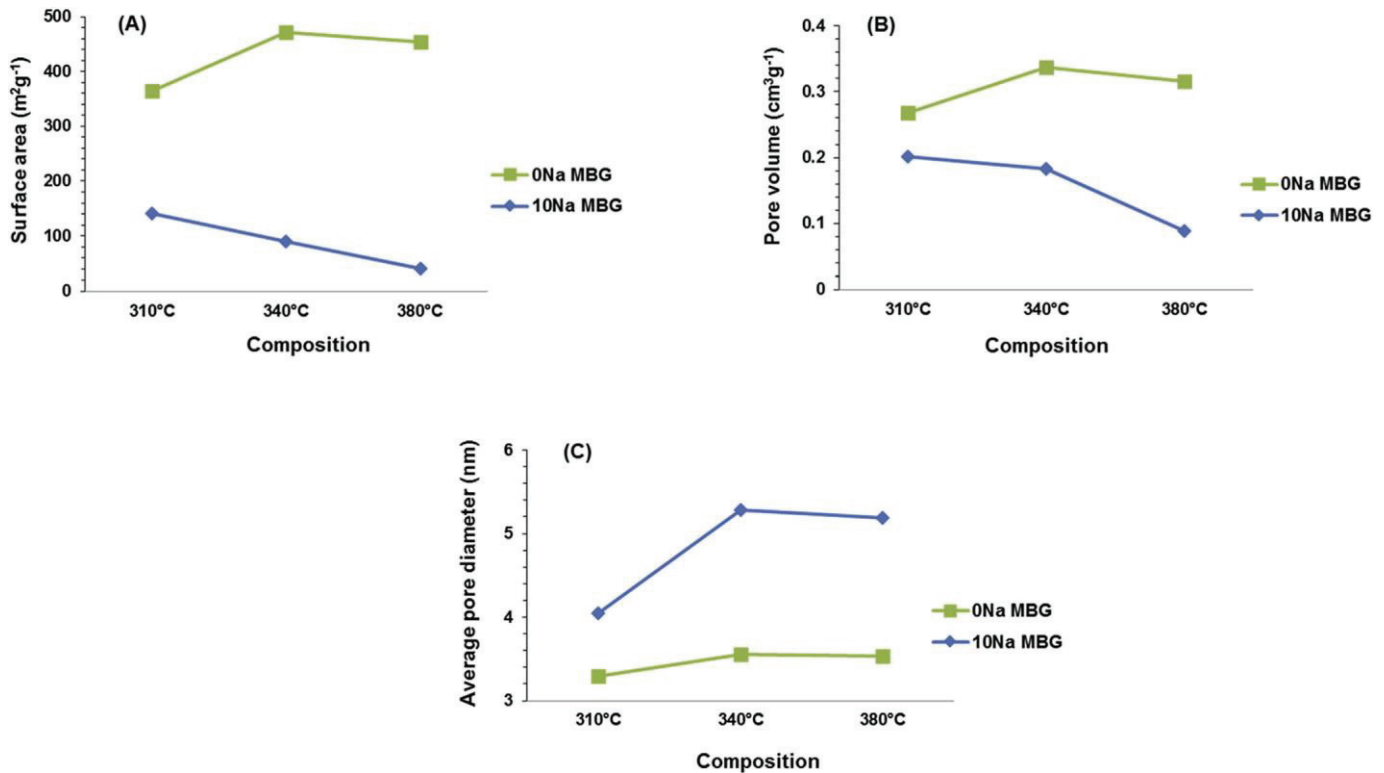


Fig. 4. Influence of changing thermal treatment on textural properties: (A) Surface area of 0Na and 10Na MBG after 310 C, 340 C and 380 C; (B) Pore volume of 0Na and 10Na MBG after 310 C, 340 C and 380 C; (C) Average pore diameter of 0Na and 10Na MBG after 310 C, 340 C and 380 C.

Table 5

Surface area, pore volume and average pore diameter of 0Na BG and 10Na BG glasses after 340 C.

Composition	Surface area (m <sup>2</sup> g <sup>-1</sup> )	Pore volume (cm <sup>3</sup> g <sup>-1</sup> )	Average pore diameter (nm)
0Na BG 340°C	535.08	0.3389	2.97
10Na BG 340°C	174.75	0.2194	3.87

samples treated at 380°C compared to 310°C. Noticeably, the reduction in Ca<sup>2+</sup> ions is more distinct in comparison to Na<sup>+</sup> ions in samples treated at 380°C.

The initial pH rise with time increases with increasing Na<sub>2</sub>O in the composition (5Na and 10Na MBGs reach an alkaline pH of 8.1 and 9.3 respectively at day 1). Beyond day 1 the pH stabilizes somewhat (Fig. 7). However, in the 0Na MBG there is a slight decrease in pH from 7.2 to 6.9 at day 1 after which they remain stabilized till day 7.

### 3.6. SEM analysis

Fig. 8 illustrates the surface morphology of 0Na MBG and 10Na MBG after 310°C calcination. Both samples have a similar morphology and inhomogeneous particle size distribution with a few larger-sized particles and a large amount of fine particles.

### 3.7. TEM

TEM analysis was performed on 0Na MBG and 10Na MBG after 310°C and 380°C calcinations. The high porosity of 0Na MBG in comparison with 10Na MBG is evident after both the 310°C and 380°C thermal treatments (Fig. 9). Furthermore, after the 380°C thermal treatment both samples display compressed pore size.

### 3.8. Bioactivity assay

SEM images of 0Na MBG after bioactivity testing (defined in section 2.4) shows apatite-like globules with tiny protruding needles. This is evident after 3 days but becomes more prominent after 7 days (Fig. 10). The 10Na MBG has the same structure as it had at day 0 after 3 days in SBF with apatite-like globules developing by day 7. It should be noted that there is not needle structure in 10Na MBG.

## 4. Discussion

The influence of CaO/Na<sub>2</sub>O network modifier ratio on the structural and textural properties of bioactive glass in an acetate based sol-gel system has been characterized and reported for the first time to the best of our knowledge. The XRF result of the 0Na and 10Na MBGs shows that the target composition has been closely reached (especially the difference in the ratio of network modifiers) except for the P<sub>2</sub>O<sub>5</sub> content (Tables 2 and 3). This is not uncommon because it is already known that the unreacted phosphate precursors are quite volatile and are easily removed during thermal treatment [28,29]. Therefore, the decrease in P<sub>2</sub>O<sub>5</sub> content is observed as a relative increase in SiO<sub>2</sub> content in both compositions compared to the expected concentration.

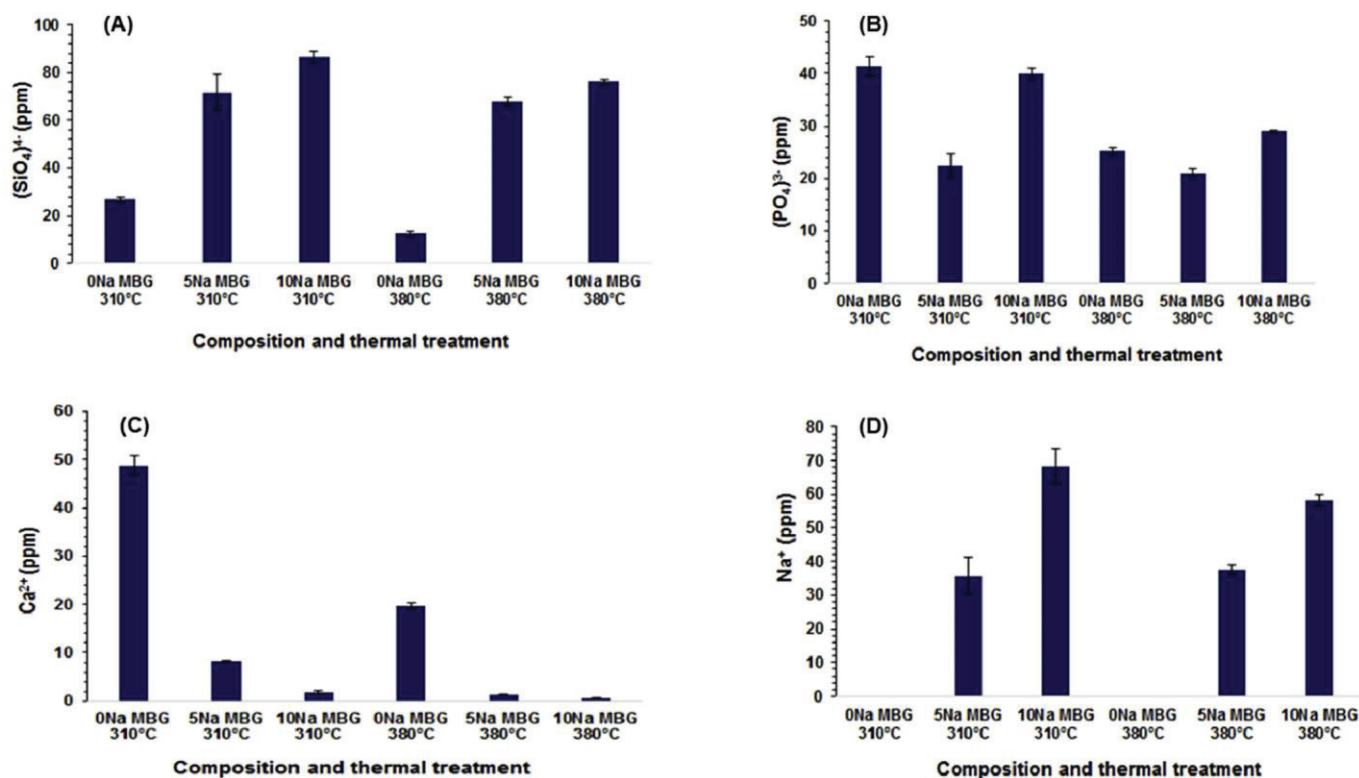


Fig. 5. Ions release after 24 h from samples of varying compositions and thermal treatments: (A)  $(SiO_4)^{4-}$  release from 0Na, 5Na and 10Na MBGs after 310°C and 380°C; (B)  $(PO_4)^{3-}$  release from 0Na, 5Na and 10Na MBGs after 310°C and 380°C; (C)  $Ca^{2+}$  release from 0Na, 5Na and 10Na MBGs after 310°C and 380°C; (D)  $Na^+$  release from 0Na, 5Na and 10Na MBGs after 310°C and 380°C; (n = 2 for all samples).

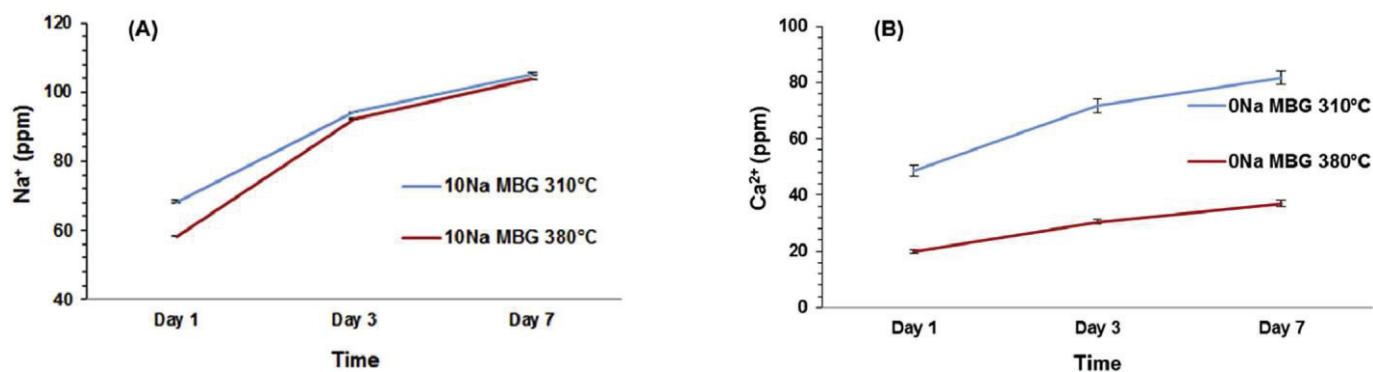


Fig. 6. Ions release upto 7 days from 0Na MBG and 10Na MBG after varying thermal treatments: (A)  $Na^+$  release over 7 days from 10Na MBG after 310°C and 380°C; (B)  $Ca^{2+}$  release over 7 days from 0Na MBG after 310°C and 380°C; (n = 2 for all samples).

The identification of calcium and sodium precursor as the crystalline phase in the uncalcined 0Na MBG and 10Na MBG samples (Fig. 1A) demonstrates that some or most of the calcium and sodium precursors have deposited on the surface of the particles after the sol-gel reaction. The necessity of thermal treatment for the complete entry of the modifying precursor ions into the glass network is demonstrated by the XRD patterns of 0Na, 5Na and 10Na MBG after 310°C–380°C (Fig. 1B, C and 1D). The calcium precursor phase in 0Na MBG and 5Na MBG samples at 310°C seen in XRD data (Fig. 1B) along with the corresponding  $COO^-$  peak in FTIR spectra of the 0Na MBG (Fig. 2A) confirms the presence of remnant calcium precursor that hasn't yet entered into the glass mixture of these samples. However, the 10Na MBG sample (with least calcium) is completely amorphous at 310°C (Fig. 1B) whilst the very small peak corresponding to  $COO^-$  seen in the FTIR spectra (Fig. 2A)

suggests that sodium's entry into the network is easier and requires lower temperatures than calcium. This is also supported by the finding of Catteaux et al., [20] who used sodium acetate as sodium precursor and found that there was complete entry of precursors in their system at low temperatures.

The XRD patterns after various thermal treatments also indicates that the temperature required for the complete entry of calcium precursor is dependent on the concentration of sodium: For example there is complete entry of the calcium precursor in the 10Na MBG at 310°C (Fig. 1B) whilst for 5Na MBG it requires 340°C (Fig. 1C). In contrast the remnant precursor still exists in the 0Na MBG (highest calcium) sample at 340°C (Fig. 1D). This could be explained by the superior network disruptive ability of  $Na_2O$  in

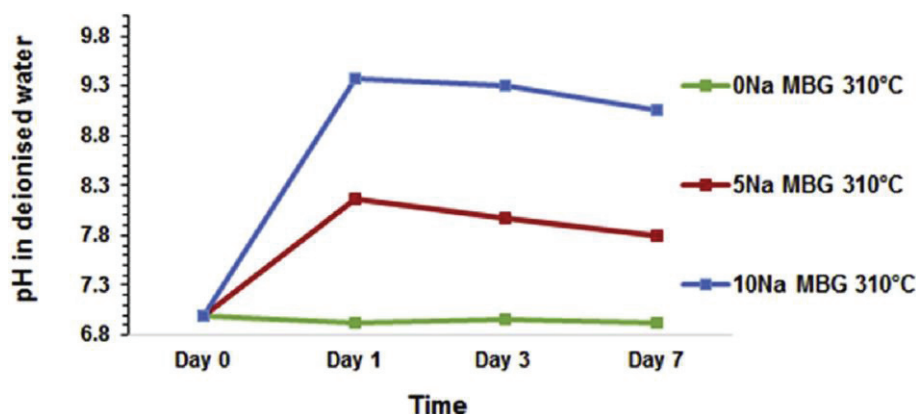


Fig. 7. pH variation of 0Na, 5Na and 10Na MBGs after 310°C in de-ionised water over 7 days.

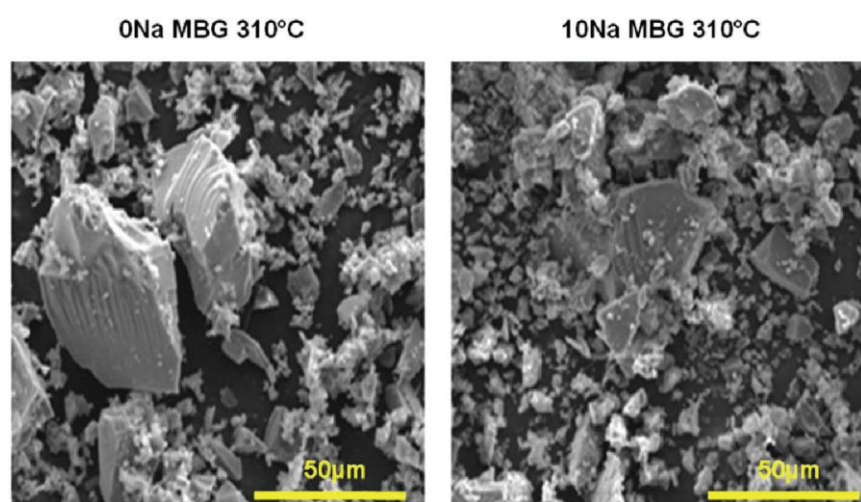


Fig. 8. Surface morphology of 0Na MBG and 10Na MBG after 310°C; Scale bar 50 µm.

comparison to CaO which lowers the glass transition temperature and promotes the entry of calcium into the network. The absence of Na<sub>2</sub>O in the 0Na MBG thus imposes struggle for the complete entry of calcium precursor at 340°C. Further heat treatment for stabilization results in the decomposition of the acetates from calcium precursor into carbonate as represented by the C-O peaks in FTIR spectra (Fig. 2B) and the calcite phase of the XRD pattern at 380°C (Fig. 1D).

Lin et al., [30] performed a study to understand the mechanism of nanoparticle formation and the calcium incorporation in a simple silica-calcium network prepared by sol-gel wherein calcium nitrate was the calcium precursor. They also reported that there was complete deposition of calcium nitrate on the surface of the glass particles after the sol-gel reaction with the nitrates only decomposing around 400°C after which the disruptive effect of calcium ions in the network materialised. Hence, Lin et al., [30] concluded that calcium nitrate may not be a good precursor choice when aiming to incorporate calcium in the network at lower temperatures. The BET/BJH results of our samples show that the surface area and pore volume increases with increasing CaO in the composition even at 310°C and 340°C (Figs. 3 and 4) which in our system is before the decomposition of acetates of the calcium precursor. Furthermore, while the 10Na MBG undergoes a rapid network densification seen by the gradual decrease in pore volume during elevated heat treatments (310°C-380°C), the 0Na MBG contrastingly shows an

increase in pore volume during 310°C-340°C (Fig. 4). This confirms that as the remnant calcium precursor that existed in this sample at 310°C (Fig. 1B) becomes accepted a Ca<sup>2+</sup> into the glass structure during 340°C treatment (Fig. 1C) there is a further disruption to the network seen as an increase in pore volume. Continuing the heat treatment from 340°C to 380°C shows only a small decrease in pore volume compared to the 10Na MBG (Fig. 4) because the continued gradual entry of calcium ions during the decomposition of acetate creates more disruption of the network thus lessening the reduction in pore volume during densification. This phenomenon is also supported by the pronounced reduction in the level Ca<sup>2+</sup> ions released into an aqueous phase from the 380°C treated 0Na MBG in comparison the 310°C treated equivalent sample (Fig. 6B). This is indicative of more calcium entering into the network and being retained by two oxygen bonds to silicon or phosphorous.

These findings processed together imply that either a part of the calcium disrupts the network during the sol-gel reaction in itself and there is progressive disruption during the thermal treatment or there is complete deposition of the precursors on the glass surface after the sol-gel reaction and the network disruption commences and continues only during thermal treatment. Nevertheless, when compared to calcium nitrates, we find that acetate-based systems deliver earlier incorporation of a part of the calcium into the network as a modifier even before the complete decomposition of the acetate from the calcium source.

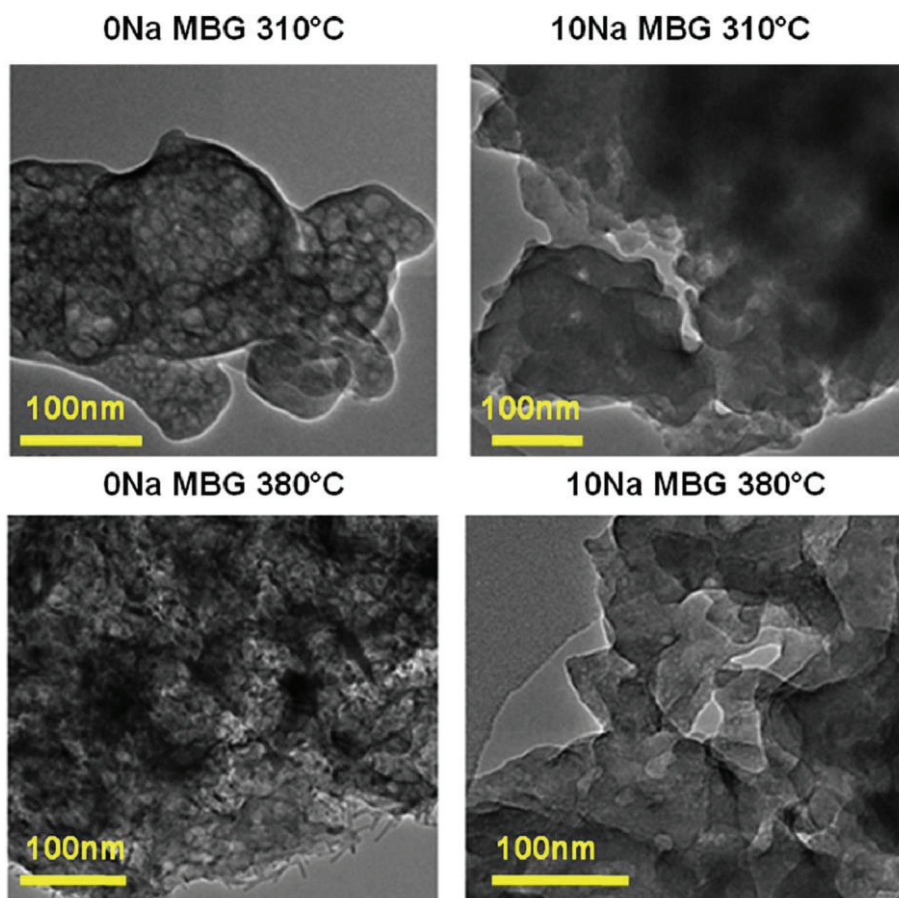


Fig. 9. Textural morphology of 0Na MBG and 10Na MBG after 310°C and 380°C thermal treatments; Scale bar 100 nm.

TEM results (Fig. 9) also confirm that in our system the porosity is driven by calcium oxide as opposed to sodium oxide which is interesting because sodium is a strong network disrupter compared to calcium. The reason for the reduction in porosity with increasing sodium oxide could be attributed to its equally enhanced fluxing effect that may have increased the viscous flow during thermal treatment and fused the pores. However, this point needs further investigation. Notably, the sample with highest calcium oxide has reached a very high surface area ( $535 \text{ m}^2 \text{ g}^{-1}$ ) and pore volume ( $0.33 \text{ cm}^3 \text{ g}^{-1}$ ) even in a non-surfactant system (Table 5). Lei et al., [31] reported that bioactive glass prepared by using acetic acid instead of hydrochloric acid leads to increased surface area. They achieved an increase in specific surface area from  $92 \text{ m}^2 \text{ g}^{-1}$  in hydrochloric acid catalysed system to  $189 \text{ m}^2 \text{ g}^{-1}$  in acetic acid system while using a nitrate precursor for calcium. Similarly in our acetic acid catalysed system, 0Na BG has reached a remarkably high surface area of  $535 \text{ m}^2 \text{ g}^{-1}$  and 10Na BG has also reached a high surface area of  $175 \text{ m}^2 \text{ g}^{-1}$  that contained acetate precursors for calcium and sodium. This suggests that acetic acid catalysed systems in general facilitate high surface area and the additional network disruption by the modifying ions further increases the surface area by increasing the pore volume of the system.

Two notable differences exist between the surfactant and non-surfactant system of the same composition. First, in the 0Na BG there is complete entry of calcium precursor in the network even at  $340^\circ\text{C}$  in comparison to the 0Na MBG where there are still some remaining precursors as shown by XRD (Fig. 1E and C). Next, we find that the surface area and pore volume of the MBGs

are lower than the BGs but with a higher average pore diameter (Fig. 3 and Table 5). This suggests that presence of surfactants imposes a struggle for the calcium's entry in to the network as the removal of surfactant by thermal treatment is necessary for the precursor's entry. The reduction in surface area and pore volume of the MBGs in comparison to BGs could be due to the very low concentration of surfactant used that may have not been favourable for forming well-defined micelle structures. Thus, the dominant increase in porosity through concentrated micelle formation may have not been realised thus explaining the increased average pore diameter without increase in porosity.

The exchange of ions from the glass with the surrounding fluids is a key trigger for bioactivity. The ions released in de-ionised water revealed that increase in  $(\text{SiO}_4)^+$  is correlated to  $\text{Na}^+$  from the samples (Fig. 5A and D). As  $\text{Na}^+$  readily exchanges with  $\text{H}^+$  ions in comparison to  $\text{Ca}^{2+}$ , the faster early release of  $\text{Na}^+$  from Si-O- $\text{Na}^+$  bond leads to the subsequent release of the silicate ( $\text{SiO}_4^+$  ions). This explains the greater initial increase in pH with increasing  $\text{Na}_2\text{O}$  in the composition (Fig. 7). However, despite the increased alkalinity of the 10Na MBG our bioactivity test indicates its apatite forming ability is slower than the 0Na MBG (Fig. 10). This confirms that increased surface area and calcium concentration favour apatite formation more than alkaline conditions.

## 5. Conclusion

High calcium oxide content bioactive glasses exhibiting improved surface area have been obtained by an acetic acid

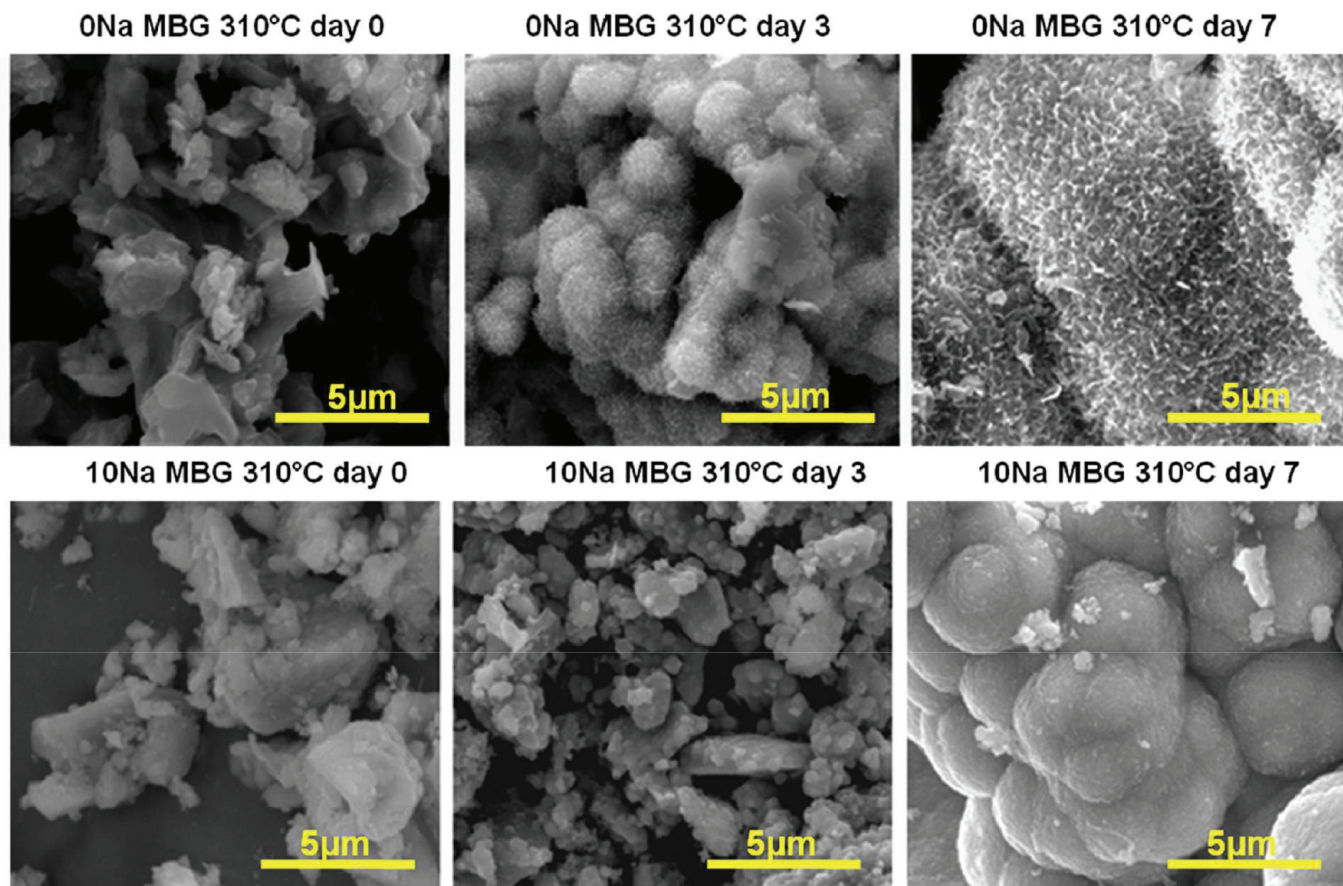


Fig. 10. Morphology of 0Na MBG and 10Na MBG at day 0, day 3 and day 7 in SBF; Scale bar 5  $\mu\text{m}$ .

catalysed acetate based sol-gel synthesis. The fast gelling of acetate system seems to hamper the complete entry of the network modifying precursors into the glass network during the sol-gel reaction. The heat treatment for stabilization triggers entry of network modifiers into the system with sodium incorporation being facile and requiring lower temperatures compared to calcium. However, the enhanced fluxing in compositions with high sodium impacts the textural features by reducing the porosity due to fusion of pores. Therefore, the porosity increases with increasing calcium oxide as opposed to sodium oxide. In our novel acetate based sol-gel system a part of the calcium gains entry into the network during early thermal treatment (310°C-340°C) in comparison to nitrate precursors that requires more than 400°C to initiate their entry. Moreover, a very high surface area has been reached in the composition with highest calcium oxide which also exhibits enhanced apatite forming ability in vitro. These bioactive glasses prepared by using acetate precursors are not only safe for industrial use but also offer valuable structural and textural advantages in comparison to existing sol-gel systems. Future investigation will focus on using these highly porous bioactive glasses as fillers in dental adhesives to achieve dentin remineralization. Furthermore, the cytocompatibility of these bioactive glasses will also be evaluated to expand their medical applications towards bone and dentin regeneration.

#### Conflict of interest

The authors declare that there is no conflict of interest, financial or otherwise regarding the publication of this paper.

#### Acknowledgements

The research work leading to this manuscript has received funding from the European Union Seventh Framework Program (FP7/2007-2013) under grant agreement n 608197. We would like to extend our sincere thanks to Dr. Catherine Jourmet for the TEM analysis and Mr. Vincenzo Farano for contributing to the discussion of results.

#### Appendix A. Supplementary data

Supplementary data related to this article can be found at <http://dx.doi.org/10.1016/j.micromeso.2017.08.029>.

#### References

- [1] S. Hu, J. Chang, M. Liu, C. Ning, *J. Mater. Sci. Mater. Med.* 20 (2009) 281–286.
- [2] R.M. Day, *Tissue Eng.* 11 (2005) 768–777.
- [3] X. Mo, Y. Wei, X. Zhang, Q. Cai, Y. Shen, X. Dai, S. Meng, X. Liu, Y. Liu, Z. Hu, X. Deng, *J. Nanomater.* 2016 (2016) e5613980.
- [4] M. Ojansivu, S. Vanhatupa, L. Björkvik, H. Häkkinen, M. Kellomäki, R. Autio, J.A. Ihalainen, L. Hupa, S. Miettinen, *Acta Biomater.* 21 (2015) 190–203.
- [5] S. Wang, X. Gao, W. Gong, Z. Zhang, X. Chen, Y. Dong, *Acta Biomater.* 10 (2014) 2792–2803.
- [6] D. Fernando, N. Attik, N. Pradelle-Plasse, P. Jackson, B. Grosgeat, P. Colon, *Mater. Sci. Eng. C* 76 (2017) 1369–1377.
- [7] Z. Wang, Y. Shen, M. Haapasalo, J. Wang, T. Jiang, Y. Wang, T.F. Watson, S. Sauro, *J. Biomater. Sci. Polym. Ed.* 25 (2014) 679–697.
- [8] L.L. Hench, *J. Mater. Sci. Mater. Med.* 17 (2006) 967–978.
- [9] G. Kaur, G. Pickrell, N. Sriranganathan, V. Kumar, D. Homa, *J. Biomed. Mater. Res. B Appl. Biomater.* 104 (2016) 1248–1275.
- [10] R. Li, A.E. Clark, L.L. Hench, *J. Appl. Biomater.* 2 (1991) 231–239.
- [11] W.C. Lepry, S.N. Nazhat, *Chem. Mater.* 27 (2015) 4821–4831.
- [12] P. Sepulveda, J.R. Jones, L.L. Hench, *J. Biomed. Mater. Res.* 58 (2001) 734–740.

- [13] R.A. Martin, S. Yue, J.V. Hanna, P.D. Lee, R.J. Newport, M.E. Smith, J.R. Jones, *Philos. Trans. R. Soc. Math. Phys. Eng. Sci.* 370 (2012) 1422–1443.
- [14] C. Turdean-Ionescu, B. Stevansson, J. Grins, I. Izquierdo-Barba, A. García, D. Arcos, M. Vallet-Regí, M. Edén, *RSC Adv* 5 (2015) 86061–86071.
- [15] X. Yan, C. Yu, X. Zhou, J. Tang, D. Zhao, *Angew. Chem. Int. Ed.* 43 (2004) 5980–5984.
- [16] C.-C. Shih, C.-S. Chien, J.-C. Kung, J.-C. Chen, S.-S. Chang, P.-S. Lu, C.-J. Shih, *Appl. Surf. Sci.* 264 (2013) 105–110.
- [17] F.-Y. Hsu, R.-C. Weng, H.-M. Lin, Y.-H. Lin, M.-R. Lu, J.-L. Yu, H.-W. Hsu, *Microporous Mesoporous Mater.* 212 (2015) 56–65.
- [18] C. Vaid, S. Murugavel, C. Das, S. Asokan, *Microporous Mesoporous Mater.* 186 (2014) 46–56.
- [19] B. Yu, C.A. Turdean-Ionescu, R.A. Martin, R.J. Newport, J.V. Hanna, M.E. Smith, J.R. Jones, *Langmuir* 28 (2012) 17465–17476.
- [20] R. Catteaux, I. Grattepanche-Lebecq, F. Désanglois, F. Chai, J.-C. Hornez, S. Hampshire, C. Follet-Houttemane, *Chem. Eng. Res. Des.* 91 (2013) 2420–2426.
- [21] J. Ma, C.Z. Chen, D.G. Wang, J.Z. Shi, *Mater. Sci. Eng. C* 30 (2010) 886–890.
- [22] A.T. Shah, Q. Ain, A.A. Chaudhry, A.F. Khan, B. Iqbal, S. Ahmad, S.A. Siddiqi, I. ur Rehman, *J. Mater. Sci.* 50 (2015) 1794–1804.
- [23] Z. Hong, R.L. Reis, J.F. Mano, *J. Biomed. Mater. Res. A* 88A (2009) 304–313.
- [24] A.J. Salinas, A.I. Martín, M. Vallet-Regí, *J. Biomed. Mater. Res. A* 61 (2002) 524–532.
- [25] A. López-Noriega, D. Arcos, I. Izquierdo-Barba, Y. Sakamoto, O. Terasaki, M. Vallet-Regí, *Chem. Mater.* 18 (2006) 3137–3144.
- [26] W.-C. Chen, J.-C. Kung, C.-H. Chen, Y.-C. Hsiao, C.-J. Shih, C.-S. Chien, *Appl. Surf. Sci.* 283 (2013) 833–842.
- [27] I. Cacciotti, M. Lombardi, A. Bianco, A. Ravaglioli, L. Montanaro, *J. Mater. Sci. Mater. Med.* 23 (2012) 1849–1866.
- [28] Z. Zhou, J. Ruan, J. Zou, Z. Zhou, X. Shen, *J. Cent. South Univ. Technol.* 14 (2007) 301–304.
- [29] A. Kiani, N.J. Lakhkar, V. Salih, M.E. Smith, J.V. Hanna, R.J. Newport, D.M. Pickup, J.C. Knowles, *Philos. Trans. R. Soc. Lond. Math. Phys. Eng. Sci.* 370 (2012) 1352–1375.
- [30] S. Lin, C. Ionescu, K.J. Pike, M.E. Smith, J.R. Jones, *J. Mater. Chem.* 19 (2009) 1276–1282.
- [31] B. Lei, X. Chen, Y. Wang, N. Zhao, C. Du, L. Zhang, *J. Non-Cryst. Solids* 355 (2009) 2583–258

## **6. The influence of precursor addition order on the porosity of sol-gel bioactive glasses**

### **6.1. Introduction**

In the previous chapter, the influence of network modifiers on the surface characteristics of these novel mesoporous bioactive glasses has been discussed. Interestingly, the results confirmed that the porosity in the glasses was driven by calcium oxide content in the composition as opposed to sodium oxide. Theoretically, sodium oxide is a strong depolymeriser of the glass network and hence should have a strong impact on the glass porosity. As the results in our study contradict this, we reasoned that the fluxing effect of sodium and the associated melting of the glass must have fused away the pores in the samples with increasing sodium oxide content. In order to verify if this is the case we have to strike out the other possible reasons that may have caused this trend.

To explain further, in the acetate based sol-gel system we noticed that there was rapid gelling soon after the last precursor was added. The precursors have always been added in the order of TEOS, TEP, calcium acetate monohydrate and sodium acetate anhydrous with one hour interval between each precursor addition. As the sol turned into a gel in less than an hour after the sodium was added we questioned if this may have affected the way in which the precursors altered the network connectivity/ microstructure/ morphology? Precisely, since calcium entered the system first when the sol was less viscous, did it get more chance/ mobility to disrupt the network as opposed to sodium which came in later when the sol was more viscous and tending towards a gel? To clarify if this is a possibility we decided to choose the composition with highest sodium (10Na MBG) and prepare it by switching the order of network modifying precursors addition ie, sodium before calcium, calcium before sodium, mixing both sodium and calcium and also by preparing a complete sodium system (15Na MBG/0Ca MBG) as this would help us in understanding the order of precursors addition vs the composition effect on controlling the porosity of these glasses.

***This work has been submitted as a manuscript in Journal of Dental Materials and is currently under revision.***

# The influence of precursor addition order on the porosity of sol-gel bioactive glasses

Delihita Fernando<sup>1</sup>, Nina Attik<sup>1,2</sup>, Mark Cresswell<sup>3</sup>, Catherine Journet<sup>1</sup>, Nelly Pradelle-Plasse<sup>1,5,6</sup>, Phil Jackson<sup>3</sup>, Brigitte Grosgeat<sup>1,2,4</sup>, Pierre Colon<sup>1,5,6</sup>

<sup>1</sup>Université Lyon, Université Claude Bernard Lyon 1, CNRS, Laboratoire des Multimatériaux et Interfaces, Villeurbanne, France

<sup>2</sup>Faculté d'Odontologie, Université Claude Bernard Lyon 1, Lyon, France

<sup>3</sup>Lucideon Inc., Penkhull, Stoke-On-Trent ST4 7LQ, UK

<sup>4</sup>Service d'Odontologie, Hospices Civils de Lyon, Lyon, France

<sup>5</sup>APHP, Hôpital Rothschild, Service d'Odontologie, Paris, France

<sup>6</sup>Faculté d'Odontologie, Université Paris Diderot, Paris, France

## Abstract

### Objective

The superior textural properties of sol-gel derived bioactive glasses compared to conventional melt quench glasses accounts for their accelerated bioactivity *In vitro*. Several studies have explored ways to improve the surface properties of sol-gel glasses in order to maximise their efficiency for bone and tooth regeneration. In this study, we investigated the order of network modifying precursor additions effect on the textural properties of sol-gel derived bioactive glasses.

### Methods

The effect of precursor addition order on the glass characteristics was assessed by switching the order of network modifying precursor (calcium acetate monohydrate and sodium acetate anhydrous) addition for a fixed composition of bioactive glass (75SiO<sub>2</sub>: 5CaO: 10Na<sub>2</sub>O:10P<sub>2</sub>O<sub>5</sub>).

### Results

The results of this study showed that the order of precursor addition does influence the porosity of these glasses. For the glasses of a fixed composition and preparation conditions we achieved a doubling of surface area, a 1.5 times increase in pore volume and a 1.2 times decrease in pore size just by mixing the network modifying precursors and adding them together in the sol-gel preparation.

### Significance

This simple and straightforward route adaptation to the preparation of bioactive glasses would allow us to enhance the textural properties of existing and novel composition of bioactive glasses and thus accelerate their bioactivity.

## Key words

Bioactive glass, Sol-gel, porosity, surface area, mesoporous, network modifiers, precursors order.

## 1 Introduction

Bioactive glasses are well known materials researched for their application in bone and dental restoration / regeneration [88,102,108–110]. Thanks to the addition of dopants such as copper, zinc, strontium and magnesium to bioactive glasses, their potential for angiogenesis [111], enhanced antibacterial effects [112] and improved bioactivity [113–116] has been unveiled. Due to their impressive bioactivity and bone bonding ability bioactive glasses are used in clinical applications as bone graft, implant coating [117,118] and recently in dentifrices such as Sensodyne® and BioMin™ to treat dentin hypersensitivity and induce remineralization of dental tissues .

The conventional synthesis of bioactive glasses (melt-quench) involves melting oxide precursors at very high temperatures followed by rapid quenching in order to obtain an amorphous matrix [119]. The other dominant synthesis technique is sol-gel which represents a bottom up approach to making these glasses involving hydrolysis and condensation reactions of glass precursors to form a 3-dimensional polymeric glass network [120]. In contrast to the melt quench technique, sol-gel synthesis encompasses various process parameters that could be modulated to change the final glass characteristics. As such, sol-gel is a relatively more complex yet versatile route of making glasses. Furthermore, sol-gel bioactive glasses have earned significant interest due to their inherent porosity and improved surface area which allows for faster ion exchange translating into heightened bioactivity in comparison to traditional melt quenched glasses [121] . Besides bioactivity associated with apatite formation and cytocompatibility, porous bioactive glasses have the potential advantage of hosting drug molecules and growth factors thereby elevating the application of these glasses for therapeutic purposes [102,122,123] .

Therefore, different optimization strategies of sol-gel process have been reported in an attempt to improve the structural and textural properties of these glasses such as varying the composition [124], type of precursors [125–127], ageing temperature [23, 24][20, 23] catalyst [89], pH [130], surfactants type [97,101,131] and concentration [30, 31]. However, to the best of our knowledge, the influence of order of network modifying precursor addition influence on the textural properties of sol-gel glasses has never been assessed. Therefore, this study aimed to evaluate if the porosity of a given composition of sol-gel bioactive glasses can be improved by modulating the sequence of the network modifying precursor addition during the sol-gel process. The effect of precursor addition order on the glass characteristics was assessed by switching the order of network modifying precursor addition for a fixed composition of bioactive glass. This understanding could contribute to a simple and effective way of improving the textural characteristics of such glasses.

## 2 Materials and Methods

### 2.1 Materials

Tetraethyl orthosilicate (TEOS, 98%), triethyl phosphate (TEP, 99%), calcium acetate monohydrate (Ca (CH<sub>3</sub>COO)<sub>2</sub>•H<sub>2</sub>O, 99%), sodium acetate anhydrous (CH<sub>3</sub>COONa), ethyl alcohol (EtOH, 99.7%), triblock copolymer EO<sub>20</sub>PO<sub>70</sub>EO<sub>20</sub> (P123, Mw= 5650) and glacial acetic acid (CH<sub>3</sub>COOH) were used as supplied from Sigma Aldrich.

## 2.2 Sample preparation

The Mesoporous Bioactive Glasses (MBG's) with 1.8 wt% surfactant in the composition  $75\text{SiO}_2: 5\text{CaO}: 10\text{Na}_2\text{O}: 10\text{P}_2\text{O}_5$  have been synthesized by an acid catalysed sol-gel method assisted by evaporation induced self-assembly (EISA) process. Different glasses were created based purely on varying the order of network modifying precursor (Ca or Na) addition. Each step was performed at one hour intervals. Step 1 involved dissolving 2g of P123 surfactant in 30g ethanol. In step 2, 37.5mL of de-ionised water and 214.5mL of glacial acetic acid were added to the ethanol surfactant mixture. Each glass precursor was then added to the ongoing reaction in one hour intervals (step 3) in the order (a) TEOS, TEP, calcium acetate monohydrate followed by sodium acetate for **Ca before Na sample**, (b) TEOS, TEP, sodium acetate followed by calcium acetate monohydrate for **Na before Ca sample** and (c) TEOS, TEP followed by mixtures of sodium acetate and calcium acetate monohydrate for **mixed precursor sample**. Complete calcium (**15Ca/0Na MBG**) and sodium samples (**15Na/0Ca MBG**) were also prepared to provide reference compositions. The solution gelled in about one hour after adding the last precursor and was allowed to undergo EISA at room temperature (RT) for 4 days, followed by drying at 60°C for 2 days. The dried gels were milled down and calcined at 340°C at a ramp rate of 1°C per minute to reach the set temperature, held for 5 hours at 340°C and finally cooled to RT in 8 hours.

## 2.3 Sample characterization

### 2.3.1. XRD

The glass phase was characterized with X-ray diffractometer (XRD). XRD of samples after 340°C calcination was performed using an X-ray diffractometer (XRD, X'Pert Philips, Netherlands) with Cu K $\alpha$  radiation of wavelength 1.54Å. The scans were recorded at 30 kV, 30 mA, 2 theta ranges between 5° to 60° and a step size of 0.02° and 90.17 seconds per step.

### 2.3.2. ATR-FTIR

The glass network was studied using Attenuated Total Reflection Fourier Transform Infra-Red spectroscopy (ATR-FTIR) on a Safas Monaco spectrometer. The spectra were collected in a wavelength range of 340-2000  $\text{cm}^{-1}$  at a spectral resolution of 4  $\text{cm}^{-1}$ .

### 2.3.3 BET/BJH

The surface area and pore volume parameters were determined by nitrogen adsorption/desorption isotherms at 77 K in a Surface Area analyzer (Gemini 2385). The samples were degassed at 200°C for 4 hours prior to measurement. The Brunauer-Emmett-Teller (BET) equation was used for the specific surface area and pore volume quantification while the Barret-Joyner-Halenda (BJH) equation was used for average pore diameter determination. The results for **0Na and 10Na BGs** (samples without surfactant) were used as baseline data from a study previously published [134] to help understand the results of this study.

### 2.3.4 TEM

The textural properties of the "**Ca before Na**", "**Na before Ca**" and "**mixed precursor**" samples after 340°C thermal treatment were imaged using transmission electron microscopy (TEM, Jeol 2100F) at 200 kV.

## 3 Results

Fig. 1 depicts the XRD patterns of Ca before Na, Na before Ca and mixed precursor samples after 340°C thermal treatment. As can be seen, all samples display a broad halo in the 2 theta range 18 to 33 degree indicating that they are all amorphous.

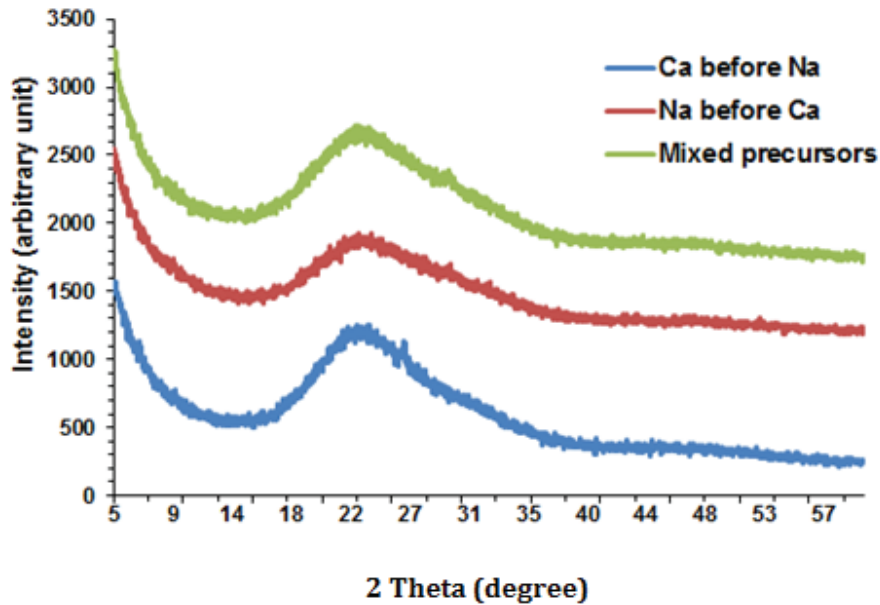


Fig. 1 XRD of Ca before Na, Na before Ca and mix precursor samples after 340°C thermal treatment.

The ATR-FTIR patterns of the glass samples are shown in Fig. 2. All samples exhibit the Si-O-Si asymmetric stretch seen at  $1078\text{ cm}^{-1}$ , Si-O-Si symmetric bending at  $796\text{ cm}^{-1}$  and Si-O-Si rocking mode at  $462\text{ cm}^{-1}$ . The P-O bond was evident at  $564\text{ cm}^{-1}$  and the peak at  $954\text{ cm}^{-1}$  corresponds to Si-O-NBO (where NBO = non-bridging oxygen). The peaks at  $1420\text{ cm}^{-1}$  and  $1552\text{ cm}^{-1}$  correspond to  $\text{COO}^-$  present in the salts. Notably, the  $\text{COO}^-$  peak in the **mixed precursor** and **Na before Ca** samples is less intense than in the **Ca before Na** sample indicating better incorporation of modifying ions in the glass network.

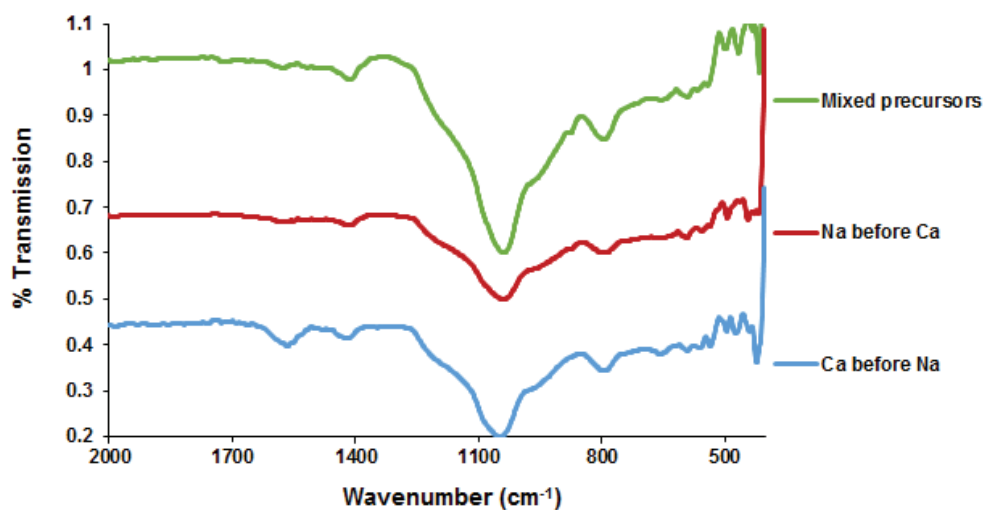


Fig. 2 FTIR analysis of Ca before Na, Na before Ca and mix precursor samples after 340°C thermal treatment.

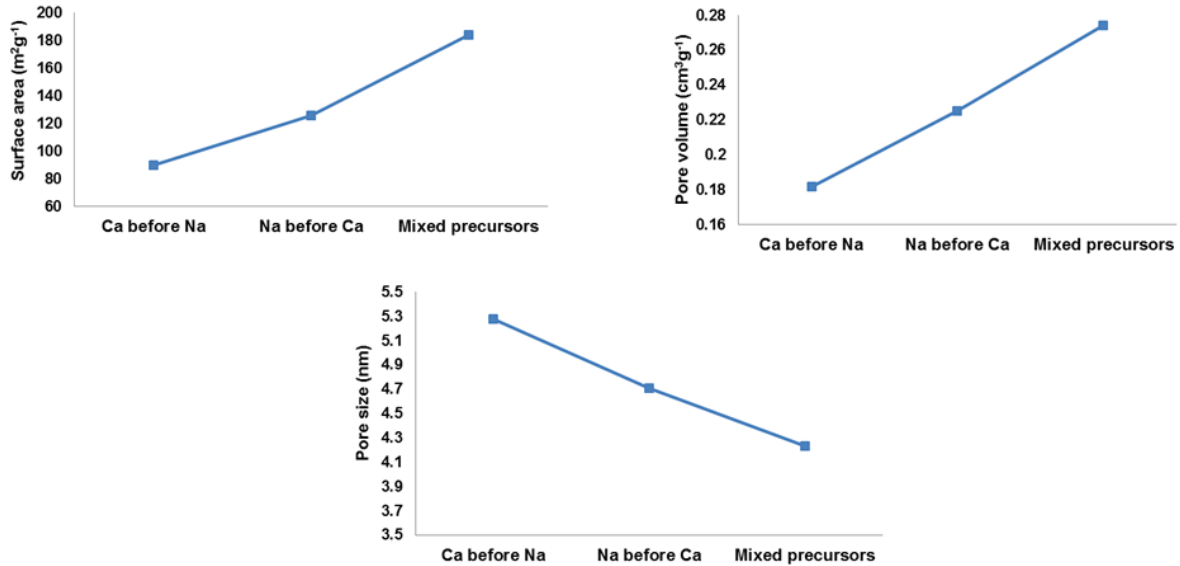


Fig. 3 Surface area, pore volume and pore size analysis of Ca before Na, Na before Ca and mix precursor samples after 340°C thermal treatment.

The textural properties of these glasses assessed by BET/BJH methods (Fig. 3) shows that for the same composition adding sodium acetate before calcium acetate monohydrate has resulted in an increase in surface area from 89.7m<sup>2</sup>g<sup>-1</sup> to 125.9 m<sup>2</sup>g<sup>-1</sup>. Further increases in surface area to 183.8 m<sup>2</sup>g<sup>-1</sup> is achieved by mixing both precursors and adding them together. The **mixed precursor** system has almost twice higher surface area, 1.5 times increase in pore volume and 1.2 times decrease in pore size compared to the **Ca before Na** sample. This increase in surface area, pore volume accompanied by decreasing mean-pore size means an increased porosity of the sample. The TEM images of the **Ca before Na**, **Na before Ca** and **mixed precursor** samples can be seen in Fig. 4. All samples contain a mixture of bigger sized and smaller sized pores. However, the increase in porosity revealed by BET data is not very distinctly seen in the TEM images except for the comparatively bigger pore size present in the **Ca before Na** samples.

Table 1 shows the surface characteristics of complete sodium and complete calcium compositions. We can see that **0Na/15Ca MBG** sample has much higher surface area, pore volume and lower pore size than the **15Na /0Ca MBG**.

Table 1 Surface area, pore volume and pore size analysis of 15Na MBG and 15Ca MBG after 340°C thermal treatment

Composition	Surface area (m <sup>2</sup> g <sup>-1</sup> )	Pore volume (Cm <sup>3</sup> g <sup>-1</sup> )	Pore size (nm)
15Na MBG	72.90	0.188	5.59
15Ca MBG	471.47	0.337	3.56

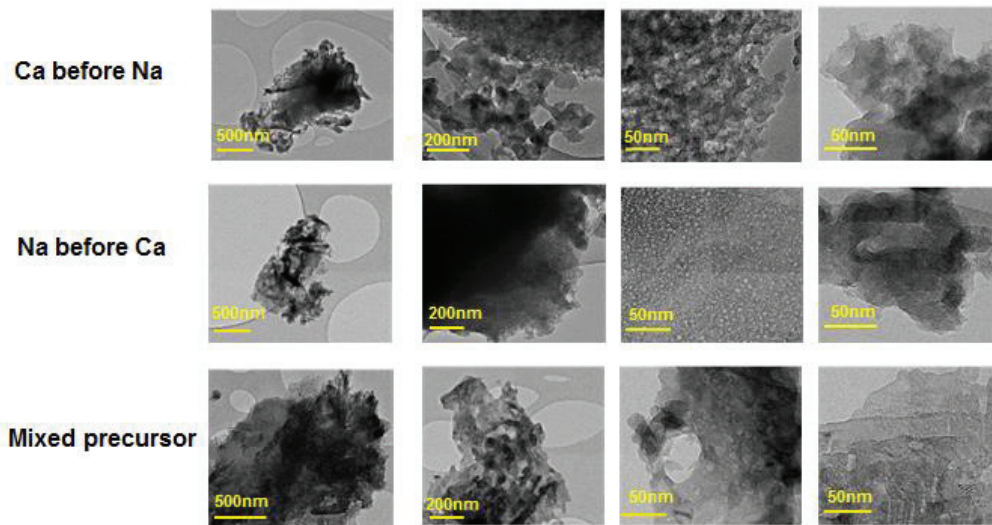


**Fig. 4** TEM images of Ca before Na, Na before Ca and mix precursor samples after 340°C thermal treatment.

In the pore size distribution of the **Ca before Na** sample (**Fig. 5A**) there are 3 size population of pores in the ranges 2-4 nm, 4-10nm and 10-60nm. In the **Na before Ca** sample there are 2 size distribution of pores at 2-4nm and 4-10nm but there is a shift in the population of 4-10nm pores towards the lower sized pores (**Fig. 5B**). This is seen as an increase in the volume of 2-4nm pores from 0.6 ( $\text{cm}^3\text{g}^{-1}$ ) $\cdot\text{\AA}$  in the **Ca before Na** to 1.1 ( $\text{cm}^3\text{g}^{-1}$ ) $\cdot\text{\AA}$  in the **Na before Ca** samples. There is also a mild increase in the volume of 4-10 nm pores from 0.27 ( $\text{cm}^3\text{g}^{-1}$ ) $\cdot\text{\AA}$  in **Ca before Na** sample to 0.52 ( $\text{cm}^3\text{g}^{-1}$ ) $\cdot\text{\AA}$  in the **Na before Ca** sample. In the **mixed precursor** MBG we can see that there is a further increase in the volume of 2-4nm pores to 1.6 ( $\text{cm}^3\text{g}^{-1}$ ) $\cdot\text{\AA}$  and also an increase in the volume of 4-10 nm pore population to 0.8 ( $\text{cm}^3\text{g}^{-1}$ ) $\cdot\text{\AA}$  which seems to be more or less the added values of the **Ca before Na** and **Na before Ca** pore distribution volume (**Fig. 5C**). Furthermore, the mixed precursor sample also displays a much more homogeneous pore size distribution.

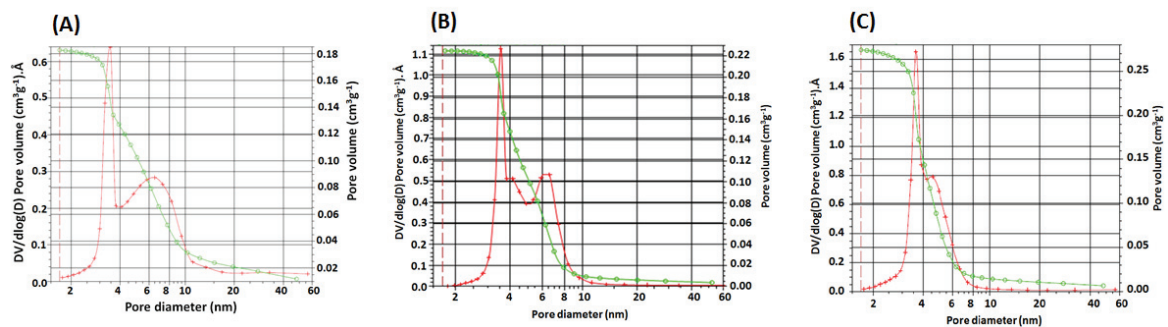


**Fig. 5** Pore size distribution of (A) Ca before Na sample (B) Na before Ca sample and (C) Mix precursor sample.

**Fig. 6** is a comparison of the pore size distribution of **0Na BG** and **0Na MBG** samples. No drastic difference can be seen expect that the addition of surfactant leads to a mild increase in the volume of 20-40nm sized pores in the **0Na MBG**. However, the comparative pore size distribution of the **10Na BG** and **MBG** samples reveals that there is a significant increase in 4-10 nm sized pore population due to the addition of surfactant in the **10Na MBG** (**Fig. 7**). This is more evident in the complete sodium system (**15Na MBG**) where there is a much higher

population of 4-10nm sized pore as opposed to the high population of 2-4nm sized pores found in **0Na MBG** (**Fig. 8**).

**Fig. 9** shows the pH study of the **Ca before Na**, **Na before Ca** and **mixed precursor** sample in de-ionised water. The maximum pH is reached within first 15 minutes for all the samples. The **Ca before Na** sample retains the highest pH value of 9.6 followed by the **mixed precursor** sample with pH of about 9.2 after 30mins and **Na before Ca** sample maintains the lowest pH of 8.9 among the compared samples.

#### 4 Discussion

In this study we investigated the order of network modifying precursor effect on the surface characteristics of sol-gel bioactive glasses. The BET/BJH results of our study confirm that the porosity of a given composition of bioactive glasses can be increased by just modulating the order of precursor addition during the sol-gel bioactive glass synthesis (**Fig. 3**). However, the increase in porosity indicated by the BET/BJH results is not distinctly evident in the TEM images of these samples (**Fig. 4**). This could be because the 1.2-fold increase in pore volume between the samples is not sufficient to find distinguishable differences in porosity by TEM.

On comparing the pore size distribution of the **Ca before Na**, **Na before Ca** and **mixed precursor** samples we find that the order of network of modifying precursor addition significantly influences the pore size distribution of these particles. In order to gain an in depth understating on this, we compared the pore size distribution of **0Na BG**, **10Na BG**, **0Na MBG**, **10Na MBG** and **15Na MBG** to delineate the effect of composition and surfactant influence on the pore size distribution. With regards to surfactant, the results suggest that there is a better interaction of the surfactant with sodium compared to calcium ions as there is remarkable increase in 4-10nm sized pore population in the 10Na MBG and 15Na MBG compared to 10Na BG after adding surfactant (**Fig. 7** and **Fig. 8**).

In terms of composition, the results suggest that calcium favours micro porosities and smaller sized mesopores while sodium in general drives the system towards mesoporosity (**Fig. 6**, **Fig. 7** and **Fig. 8**). Therefore, in the high sodium composition (**10Na MBG**) where we modified the order of precursor addition it is natural to expect mainly mesopores which is what we find in **Fig. 5**.

However by switching the order of precursor addition it seems that in the **Ca before Na** sample calcium must have reacted first and at least part of the sodium must have deposited on the surface of the gel (As seen in our previous study [134]). The entry of the remnant sodium during thermal treatment must have preferably increased the population of 4-10nm sized pores (**Fig. 5A**). On the contrary, in the **Na before Ca** sample since sodium entered first it must have favoured the population of 4-10nm pores that is why there is an increase in this pore population ( $0.52 \text{ (cm}^3\text{g}^{-1})\text{.Å}$ ) as compared to the **Ca before Na** sample. The entry of remnant calcium during thermal treatment in this case should have increased the concentration of smaller sized pores and that is why we see a shift toward smaller pores in **Fig. 5B** which reflects as an increase in the volume of 2-4 nm pores in this sample.

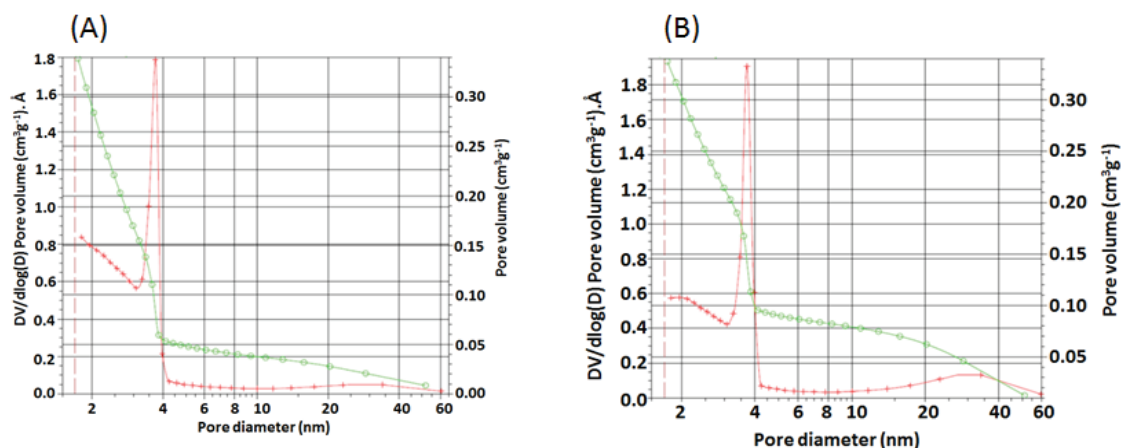


Fig. 6 Pore size distribution of (A) 0Na/ 15Ca BG (B) 0Na/15Ca MBG.

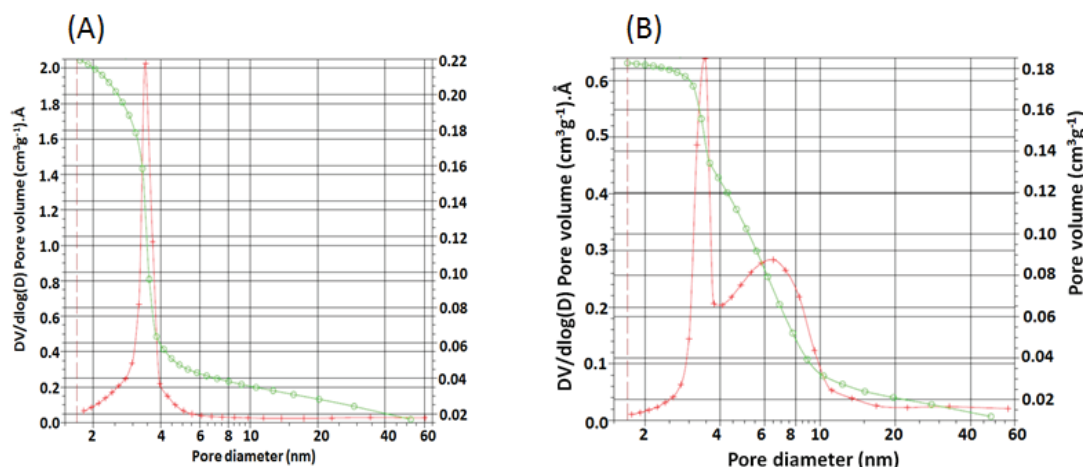


Fig. 7 Pore size distribution of (A) 10Na BG (B) 10Na MBG.

It is clear from these results that the faster gelling observed in the acetate system hinders the network modifying efficiency of the last precursor that is added to the on-going reaction as increased viscosity of the sol associated with gelling arrests the mobility of the ions in the network. When the deposited precursors (mostly the last one added) enter into the network during thermal treatment further disruption is realised and the size of pores thus created is determined by the type of ions that enter. When the modifying precursors are mixed and added together in the sol-gel reaction, it gives them a wider window of time to react and effectively disrupt the network before the sol progresses to a gel. Therefore, in the **mixed precursor** system since the modifying precursors are added together, both modifiers get to react equally and effectively disrupt the network which has resulted in increased porosity with relatively homogenous pore size distribution (Fig. 5C).

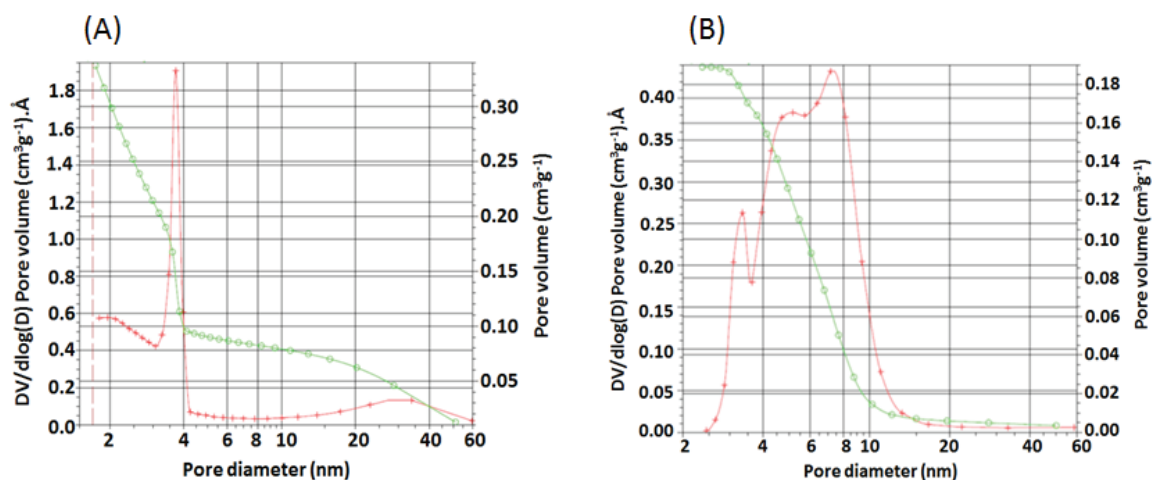


Fig. 8 Pore size distribution of (A) 15Ca/ 0Na MBG (B) 15Na/ 0Ca MBG.

The comparatively higher pH in the Ca before Na sample can be due to the increased release of more easily accessible surface sodium. In contrast, the **Na before Ca** sample where sodium went in first is likely to feature sodium ions situated more evenly throughout the 3-D network. The **mixed precursor** sample maintains a mid pH value due to the homogeneity in the composition (Fig. 9).

The surface characteristics of the 0Na MBG and 0Ca MBG confirm that the composition has a dominant effect on the porosity of these glasses (Table 1). However the BET/BJH results for the 10Na MBGs in this study confirm that for a given composition of glass the surface characteristics can be tuned or improved by modulating the order of adding the modifying precursors.

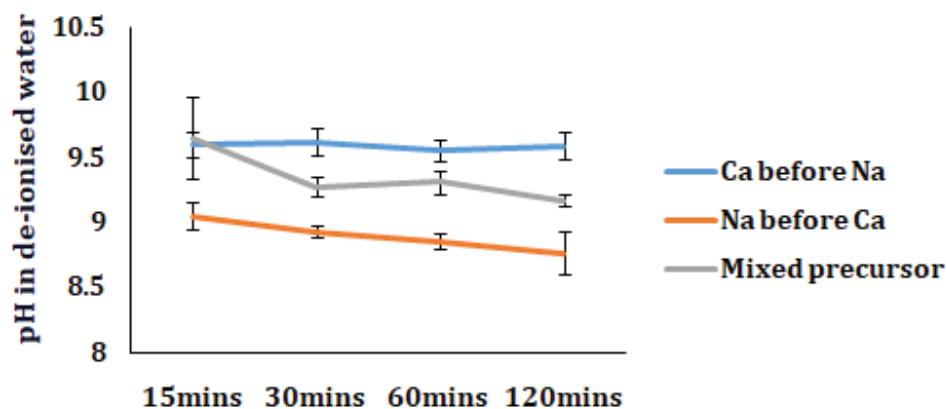


Fig. 9 pH variations of Ca before Na, Na before Ca and mix precursor samples in de-ionised water.

In summary, the present study reports a simple and effective way to improve the textural properties of a given composition of sol-gel derived bioactive glass. Maintaining constant the composition, precursor type and preparation conditions, we varied only the sequence of network modifying precursor addition during the sol-gel synthesis. The mixed precursor system wherein the calcium and sodium precursors were mixed and added together resulted in enhanced porosity with homogeneous pore size distribution compared to the other sequences. This is attributed to the equal and effective disruption of the silicate / phosphate network by both

of the modifiers before the gelling of the reaction. Though composition has a dominant effect on the porosity of these glasses, this method, which enables the textural properties to be tailored by keeping the composition unaltered, would be beneficial not only in accelerating the apatite forming ability of bioactive glass compositions but also to functionalise their porosity and pore size for drug delivery in medical and dental applications. Our objective of introducing such mesoporous BG particles in a dental adhesive could be achieved with respect of a convenient size of particles.

## Acknowledgements

The research work leading to this manuscript has received funding from the European Union Seventh Framework Program (FP7/2007-2013) under grant agreement n°608197.

## References

- [1] Khvostenko D, Hilton TJ, Ferracane JL, Mitchell JC, Kruzic JJ. Bioactive glass fillers reduce bacterial penetration into marginal gaps for composite restorations. *Dent Mater* 2016;32:73–81. doi:10.1016/j.dental.2015.10.007.
- [2] Jones JR, Lin S, Yue S, Lee PD, Hanna JV, Smith ME, et al. Bioactive glass scaffolds for bone regeneration and their hierarchical characterisation. *Proc Inst Mech Eng [H]* 2010;224:1373–87. doi:10.1243/09544119JEM836.
- [3] Fernando D, Attik N, Pradelle-Plasse N, Jackson P, Grosogeat B, Colon P. Bioactive glass for dentin remineralization: A systematic review. *Mater Sci Eng C Mater Biol Appl* 2017;76:1369–77. doi:10.1016/j.msec.2017.03.083.
- [4] Taha AA, Patel MP, Hill RG, Fleming PS. The effect of bioactive glasses on enamel remineralization: A systematic review. *J Dent* 2017. doi:10.1016/j.jdent.2017.09.007.
- [5] Zhang X, Zeng D, Li N, Wen J, Jiang X, Liu C, et al. Functionalized mesoporous bioactive glass scaffolds for enhanced bone tissue regeneration. *Sci Rep* 2016;6:srep19361. doi:10.1038/srep19361.
- [6] Wu C, Zhou Y, Xu M, Han P, Chen L, Chang J, et al. Copper-containing mesoporous bioactive glass scaffolds with multifunctional properties of angiogenesis capacity, osteostimulation and antibacterial activity. *Biomaterials* 2013;34:422–33. doi:10.1016/j.biomaterials.2012.09.066.
- [7] Gargiulo N, Cusano AM, Causa F, Caputo D, Netti PA. Silver-containing mesoporous bioactive glass with improved antibacterial properties. *J Mater Sci Mater Med* 2013;24:2129–35. doi:10.1007/s10856-013-4968-4.
- [8] Diba M, Tapia F, Boccaccini AR, Strobel LA. Magnesium-Containing Bioactive Glasses for Biomedical Applications. *Int J Appl Glass Sci* 2012;3:221–53. doi:10.1111/j.2041-1294.2012.00095.x.
- [9] Bejarano J, Detsch R, Boccaccini AR, Palza H. PDLLA scaffolds with Cu- and Zn-doped bioactive glasses having multifunctional properties for bone regeneration. *J Biomed Mater Res A* 2017;105:746–56. doi:10.1002/jbm.a.35952.

- [10] Wu C, Zhou Y, Lin C, Chang J, Xiao Y. Strontium-containing mesoporous bioactive glass scaffolds with improved osteogenic/cementogenic differentiation of periodontal ligament cells for periodontal tissue engineering. *Acta Biomater* 2012;8:3805–15. doi:10.1016/j.actbio.2012.06.023.
- [11] Hoppe A, Mouriño V, R. Boccaccini A. Therapeutic inorganic ions in bioactive glasses to enhance bone formation and beyond. *Biomater Sci* 2013;1:254–6. doi:10.1039/C2BM00116K.
- [12] Montazerian M, Dutra Zanotto E. History and trends of bioactive glass-ceramics. *J Biomed Mater Res A* 2016;104:1231–49. doi:10.1002/jbm.a.35639.
- [13] Nandi SK, Kundu B, Datta S. Development and Applications of Varieties of Bioactive Glass Compositions in Dental Surgery, Third Generation Tissue Engineering, Orthopaedic Surgery and as Drug Delivery System 2011. doi:10.5772/24942.
- [14] Kaur G, Pickrell G, Sriranganathan N, Kumar V, Homa D. Review and the state of the art: Sol-gel and melt quenched bioactive glasses for tissue engineering. *J Biomed Mater Res B Appl Biomater* 2016;104:1248–75. doi:10.1002/jbm.b.33443.
- [15] Zheng K, Boccaccini AR. Sol-gel processing of bioactive glass nanoparticles: A review. *Adv Colloid Interface Sci* 2017. doi:10.1016/j.cis.2017.03.008.
- [16] Sepulveda P, Jones JR, Hench LL. Characterization of melt-derived 45S5 and sol-gel-derived 58S bioactive glasses. *J Biomed Mater Res A* 2001;58:734–740.
- [17] Li Y, Liu Y-Z, Long T, Yu X-B, Tang T-T, Dai K-R, et al. Mesoporous bioactive glass as a drug delivery system: fabrication, bactericidal properties and biocompatibility. *J Mater Sci Mater Med* 2013;24:1951–61. doi:10.1007/s10856-013-4960-z.
- [18] Wu C, Chang J, Xiao Y. Mesoporous bioactive glasses as drug delivery and bone tissue regeneration platforms. *Ther Deliv* 2011;2:1189–98. doi:10.4155/tde.11.84.
- [19] Pérez-Pariente J, Balas F, Román J, Salinas A, Vallet-Regí M. Influence of Composition and Surface Characteristics on the in Vitro Bioactivity of SiO<sub>2</sub>-CaO-P<sub>2</sub>O<sub>5</sub>-MgO sol-Gel Glasses. *J Biomed Mater Res* 1999;47:170–5. doi:10.1002/(SICI)1097-4636(199911)47:2<170::AID-JBM6>3.0.CO;2-J.
- [20] Shah AT, Ain Q, Chaudhry AA, Khan AF, Iqbal B, Ahmad S, et al. A study of the effect of precursors on physical and biological properties of mesoporous bioactive glass. *J Mater Sci* 2015;50:1794–804. doi:10.1007/s10853-014-8742-x.
- [21] Yu B, Turdean-Ionescu CA, Martin RA, Newport RJ, Hanna JV, Smith ME, et al. Effect of Calcium Source on Structure and Properties of Sol-Gel Derived Bioactive Glasses. *Langmuir* 2012;28:17465–76. doi:10.1021/la303768b.
- [22] Ren H, Tian Y, Li A, Martin RA, Qiu D. The influence of phosphorus precursor on the structure and properties of SiO<sub>2</sub>-P<sub>2</sub>O<sub>5</sub>-CaO bioactive glass. *Biomed Phys Eng Express* 2017;3:045017. doi:10.1088/2057-1976/aa7daa.

- [23] Zheng K, Solodovnyk A, Li W, Goudouri O-M, Stähli C, Nazhat SN, et al. Aging Time and Temperature Effects on the Structure and Bioactivity of Gel-Derived 45S5 Glass-Ceramics. *J Am Ceram Soc* 2015;98:30–8. doi:10.1111/jace.13258.
- [24] Letaief N, Lucas-Girot A, Oudadesse H, Meleard P, Pott T, Jelassi J, et al. Effect of aging temperature on the structure, pore morphology and bioactivity of new sol-gel synthesized bioglass. *J Non-Cryst Solids* 2014;Complete:194–9. doi:10.1016/j.jnoncrysol.2014.06.005.
- [25] Zhang Y, Hong Z, Ren Y, Wang D, Yokogawa Y. Highly ordered mesoporous bioactive glass with high surface areas using H<sub>3</sub>PO<sub>4</sub> as the catalyst. *J Non-Cryst Solids* 2014;402:149–52. doi:10.1016/j.jnoncrysol.2014.05.030.
- [26] Valliant EM, Turdean-Ionescu CA, Hanna JV, Smith ME, Jones JR. Role of pH and temperature on silica network formation and calcium incorporation into sol-gel derived bioactive glasses. *J Mater Chem* 2011;22:1613–9. doi:10.1039/C1JM13225C.
- [27] Gómez-Cerezo N, Izquierdo-Barba I, Arcos D, Vallet-Regí M. Tailoring the biological response of mesoporous bioactive materials. *J Mater Chem B* 2015;3:3810–9. doi:10.1039/C5TB00268K.
- [28] Letaief N, Lucas-Girot A, Oudadesse H, Dorbez-Sridi R. Influence of Synthesis Parameters on the Structure, Pore Morphology and Bioactivity of a New Mesoporous Glass. *J Biosci Med* 2014;02:57. doi:10.4236/jbm.2014.22009.
- [29] Letaief N, Lucas-Girot A, Oudadesse H, Dorbez-Sridi R, Boullay P. Investigation of the surfactant type effect on characteristics and bioactivity of new mesoporous bioactive glass in the ternary system SiO<sub>2</sub>-CaO-P<sub>2</sub>O<sub>5</sub>: Structural, textural and reactivity studies. *Microporous Mesoporous Mater* 2014;195:102–11. doi:10.1016/j.micromeso.2014.03.035.
- [30] Shih C-C, Chien C-S, Kung J-C, Chen J-C, Chang S-S, Lu P-S, et al. Effect of surfactant concentration on characteristics of mesoporous bioactive glass prepared by evaporation induced self-assembly process. *Appl Surf Sci* 2013;264:105–10. doi:10.1016/j.apsusc.2012.09.134.
- [31] Shih S-J, Lin Y-C, Valentino Posma Panjaitan L, Rahayu Meyla Sari D. The Correlation of Surfactant Concentrations on the Properties of Mesoporous Bioactive Glass. *Mater Basel Switz* 2016;9. doi:10.3390/ma9010058.
- [32] Fernando D, Attik N, Cresswell M, Mokbel I, Pradelle-Plasse N, Jackson P, et al. Influence of network modifiers in an acetate based sol-gel bioactive glass system. *Microporous Mesoporous Mater* 2018;257:99–109. doi:10.1016/j.micromeso.2017.08.029.

## **7. The influence of increasing surfactant concentration on the microstructure of MBGs**

### **7.1. Introduction**

In the previous chapters the elaboration of novel MBGs, influence of scale, network modifiers and order of network modifying precursor addition on the surface characteristics of these glasses were studied. Though a very high surface area and porosity as normally expected of a mesoporous bioactive glass has been reached, and ways to improve these features has also been discussed, one target remained unattained. That is, the ordered arrangement of pores. The hysteresis loop of the BET/BJH data in addition to the TEM images of the samples so far (Chapter 5 and 6) have confirmed that the pores were randomly arranged and were of varying size ranges. This brings into question the role of surfactant in the system. As mentioned in the introduction, surfactants typically form micelles around which the glass network is formed. Therefore, burning out the pore-forming agents during thermal treatment should induce pore formation in the places they existed. Furthermore, since the micelles take on a consistent shape and arrangement, the pores induced by them are also expected to decorate the network with a pattern of ordered and uniform porosity.

One of the reasons for not achieving the aforementioned ordered porosity could be because the previous samples had only 1.8 weight percent surfactant with respect to the glass precursors. This could have been too low to realise any significant impact on the porosity even if the surfactant played its expected role by forming micelles. Therefore, it was decided to increase the surfactant concentration of 0Na MBG to 4, 8 and 16 weight percent and assess the impact on thermal treated MBG microstructure. 0Na MBG was selected as this composition had consistently shown the highest porosity. We also increased the surfactant concentration of 10Na MBG to 4 weight percent to use as valuable comparison to understand the results.

### **7.2. Materials and Methods**

#### **7.2.1. Materials**

Tetraethyl orthosilicate (TEOS, 98%), triethyl phosphate (TEP, 99%), calcium acetate monohydrate ( $\text{Ca}(\text{CH}_3\text{COO})_2 \cdot \text{H}_2\text{O}$ , 99%), sodium acetate anhydrous ( $\text{CH}_3\text{COONa}$ ), ethyl alcohol (EtOH, 99.7%), triblock copolymer  $\text{EO}_{20}\text{PO}_{70}\text{EO}_{20}$  (P123, Mw= 5650) and glacial acetic acid ( $\text{CH}_3\text{COOH}$ ) were used as supplied from Sigma Aldrich.

### 7.2.2. Sample preparation

The 0Na MBG composition (75SiO<sub>2</sub>: 15CaO:10P<sub>2</sub>O<sub>5</sub>) was fabricated with 1.8 wt%, 4 wt%, 8 wt% and 16 wt% surfactant concentration. 10Na MBG (75SiO<sub>2</sub>: 5CaO: 10Na<sub>2</sub>O: 10P<sub>2</sub>O<sub>5</sub>) was made using 1.8 and 4 wt% surfactant concentration. In all cases an acid catalysed sol-gel method assisted by evaporation induced self-assembly (EISA) process was used. Each step was performed in one hour intervals. Step 1 involved dissolving respective quantities of P123 surfactant in 30g ethanol (**Table 4**). In step 2, 37.5ml of de-ionised water and 214.5ml of glacial acetic acid were added to the ethanol surfactant mixture. Each glass precursor was added to the ongoing reactions at one hour intervals (step 3) in the order TEOS, TEP and calcium acetate monohydrate followed by sodium acetate anhydrous. The solution gelled in about one hour after adding the last precursor and was allowed to undergo EISA at room temperature (RT) for 4 days, followed by drying at 60°C for 2 days. The dried gel was milled down and initially calcined at 380°C using a ramp rate of 1°C per minute to reach the peak temperature, followed by a hold for 5 hours at 380°C and finally cooling to RT in 8 hours.

#### 7.2.2.1. Ethanol ultrasonication:

5g of uncalcined sample was ultrasonicated in 500ml of ethanol for 25 minutes followed by vacuum filtering and drying at 60°C for 3 hours. The dried samples were subjected to calcination at 380°C and 340°C.

### 7.2.3. Sample characterization

#### 7.2.3.1. XRD

The material phase was characterized by X-ray diffractometer (XRD). XRD analysis of samples after 340°C calcination was performed using an X-ray diffractometer (XRD, X'Pert Philips, Netherlands) with Cu K $\alpha$  radiation of wavelength 1.54 Å. The scans were recorded at 30 kV, 30 mA, 2 theta ranges between 5° to 60° and a step size of 0.02° and 90.17 seconds per step.

#### 7.2.3.2. BET/BJH

The surface area and pore volume parameters were determined by nitrogen adsorption/desorption isotherms at 77 K in a surface area analyzer (Gemini 2385). The samples were degassed at 200°C for 4 hours prior to measurement. The Brunauer-Emmett-Teller (BET) equation was used for the specific surface area and pore volume quantification while Barret-Joyner-Halenda (BJH) was used for average pore diameter determination.

**Table 4 Surfactant, solvent, catalyst and precursor quantities**

Sample	P123 Surfactant (g)	Ethanol (g)	De-ionised water (ml)	Acetic acid glacial (ml)	TEOS (g)	TEP (g)	Calcium acetate monohydrate (g)	Sodium acetate anhydrous (g)
1.8wt% 0Na MBG	2	30	37.5	214.5	78.12	18.22	13.21	-
4wt% 0Na MBG	4.5	30	37.5	214.5	78.12	18.22	13.21	-
8wt% 0Na MBG	9.5	30	37.5	214.5	78.12	18.22	13.21	-
16wt% 0Na MBG	20.8	30	37.5	214.5	78.12	18.22	13.21	-
1.8wt% 10Na MBG	2	30	37.5	214.5	78.12	18.22	4.40	8.20
4wt% 10Na MBG	4.5	30	37.5	214.5	78.12	18.22	4.40	8.20

### 7.3. Results and Discussion

The images of 0Na MBG samples featuring 4, 8 and 16 weight percent surfactant after 380°C calcination are shown in **Figure 25**. It could be seen that there is a mild carbon deposit on the 8 wt% 0Na MBG which intensifies in the 16 wt% 0Na MBG.

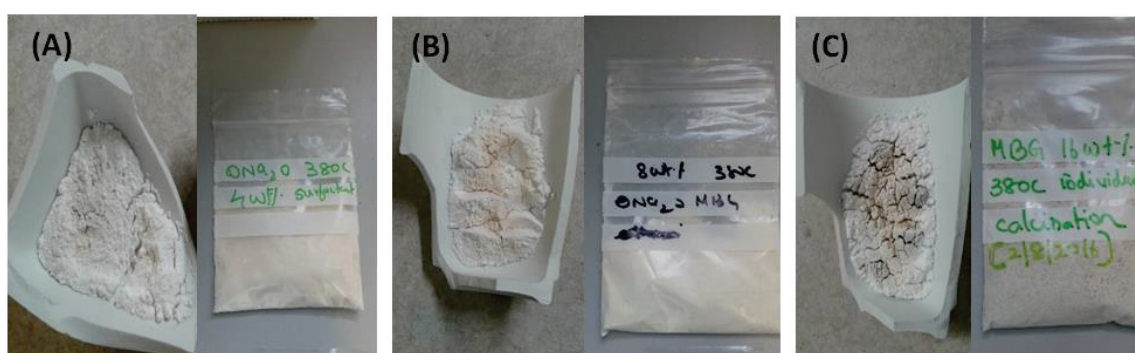


**Figure 25 (A) 4wt% 0Na MBG, (B) 8wt% 0Na MBG and (C) 16wt% 0Na MBG after direct calcination at 380°C**

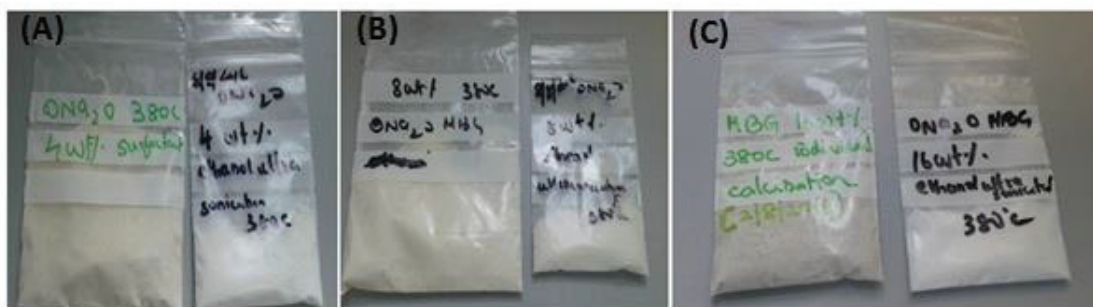


Figure 26 (A) 4wt% 0Na MBG, (B) 8wt% 0Na MBG and (C) 16wt% 0Na MBG after ethanol ultrasonication and calcination at 380°C

To resolve the carbon entrapment problem, a protocol was employed (Section 7.2.2.1) which involved ultrasonating the uncalcined sample in ethanol followed by drying in the oven at 60°C for 3hrs and then subjecting samples to calcination at 380°C. As can be seen from Figure 26 the washing step seemed to have a positive effect on removing the surfactant as the samples were white without any carbon entrapment.

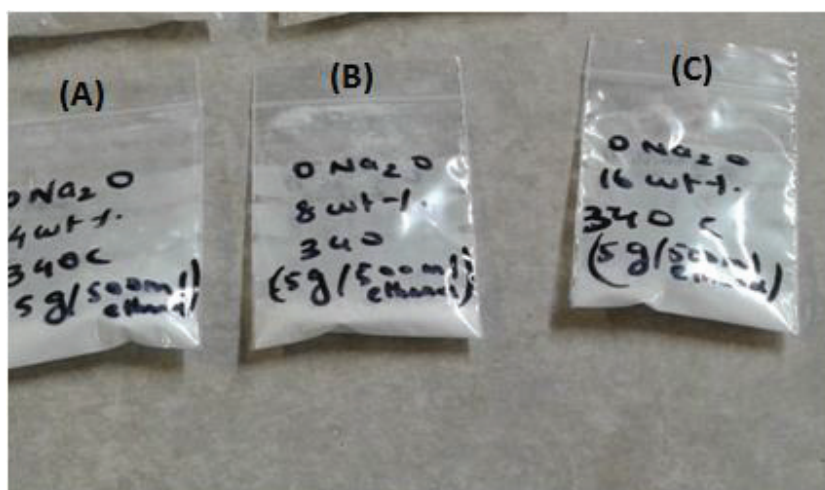
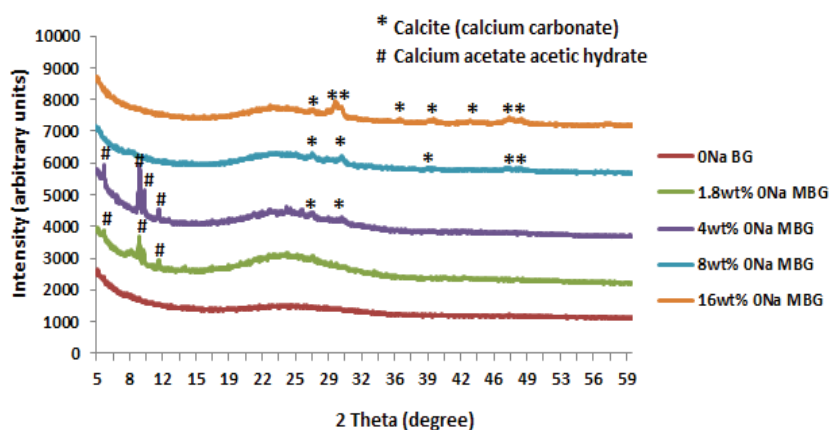


Figure 27 (A) 4wt% 0Na MBG, (B) 8wt% 0Na MBG and (C) 16wt% 0Na MBG after ethanol ultrasonication and calcination at 340°C

Finally, we followed the aforementioned protocol but calcined the samples at 340°C (**Figure 27**) in order to allow comparisons to be drawn with the previous samples which showed optimal surface characteristics at this temperature.

**Figure 28** shows the phase composition of **0Na BG** and **MBGs** of varying surfactant concentration after 340°C thermal treatment. As can be seen, similar to the 1.8wt% 0Na MBG the 4wt% 0Na MBG also has remnant calcium precursor (calcium acetate) that has yet to enter the network. However at 8wt% and 16wt% surfactant concentration there is complete entry of calcium precursor, as can be inferred by the removal of any latent calcium acetate phase. Interestingly, the 0Na MBG with 4wt% surfactant concentration shows the start of calcite occurrence at 340°C whose intensity increases with increasing surfactant concentration. This means that there is early entry and as a result earlier decomposition of the calcium precursor with increasing surfactant concentrations. Similarly for the 4wt% 10Na MBG we find the same calcite phase emerging already at 340°C (**Figure 29**). In drug delivery applications using surfactants it is known that when the concentration of surfactant molecules goes above the critical micelle concentration (the concentration above which the surfactants start to form micelles) there is a rapid increase in the solubilisation of a poorly soluble drug which linearly increases with increasing surfactant concentration. This is because the drug molecules are adsorbed “on/in between” the hydrophilic heads of the micelles or in the hydrophobic tails depending on the nature of the drug molecule [135]. The early entry of calcium precursor with increasing concentration of the surfactant therefore should be due to the enhanced solubilisation of this precursor induced by micelles formation.



**Figure 28** Phase composition of 0Na BG, 1.8Wt%, 4wt%, 8wt% and 16wt% 0Na MBGs

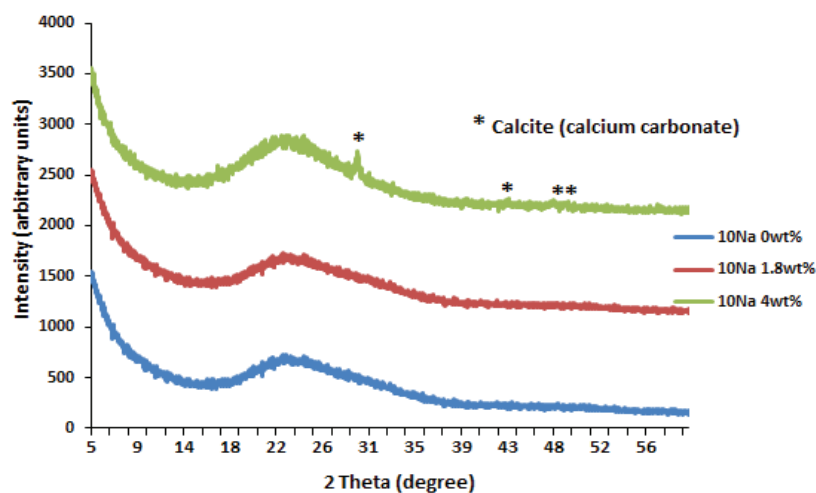


**Figure 29** Phase composition of 10Na BG, 1.8wt% and 4wt% 10Na MBGs

**Figure 30** shows the changes in the surface area, pore volume and pore size of the 0Na BG and MBG samples with increasing surfactant concentrations after 340°C heat treatment. The fluctuating trend in these figures needs careful interpretation. The surface area and pore volume results show that with the initial addition of surfactant (1.8wt %) there is a mild reduction in pore volume which reflects as a prominent decrease in surface area. Increasing the surfactant concentration to 4wt% leads to a strong increase in pore volume from 0.3 cm<sup>3</sup>g<sup>-1</sup> in 1.8wt% 0Na MBG to 0.6 cm<sup>3</sup>g<sup>-1</sup> in 4wt% 0Na MBG. Interestingly, further increases in surfactant concentration to 8wt% leads to a reduction in pore volume once again similar to the pore volume of 1.8wt% 0Na MBG. Continued increase of surfactant concentration to 16wt% leads to an increase in pore volume and surface area. It could be seen that with the addition of surfactant mean pore size gradually increased from 2.9 nm in 0Na BG (non-surfactant) up to 4.1 nm in the 4wt% 0Na MBG. This increase in mean pore size with the addition of surfactant indicates the pores induced by surfactant aggregation and micelle formation. Similar to the pore volume and surface area trend the mean pore size also decreases at 8wt% and later increases at 16wt% of surfactant concentration.

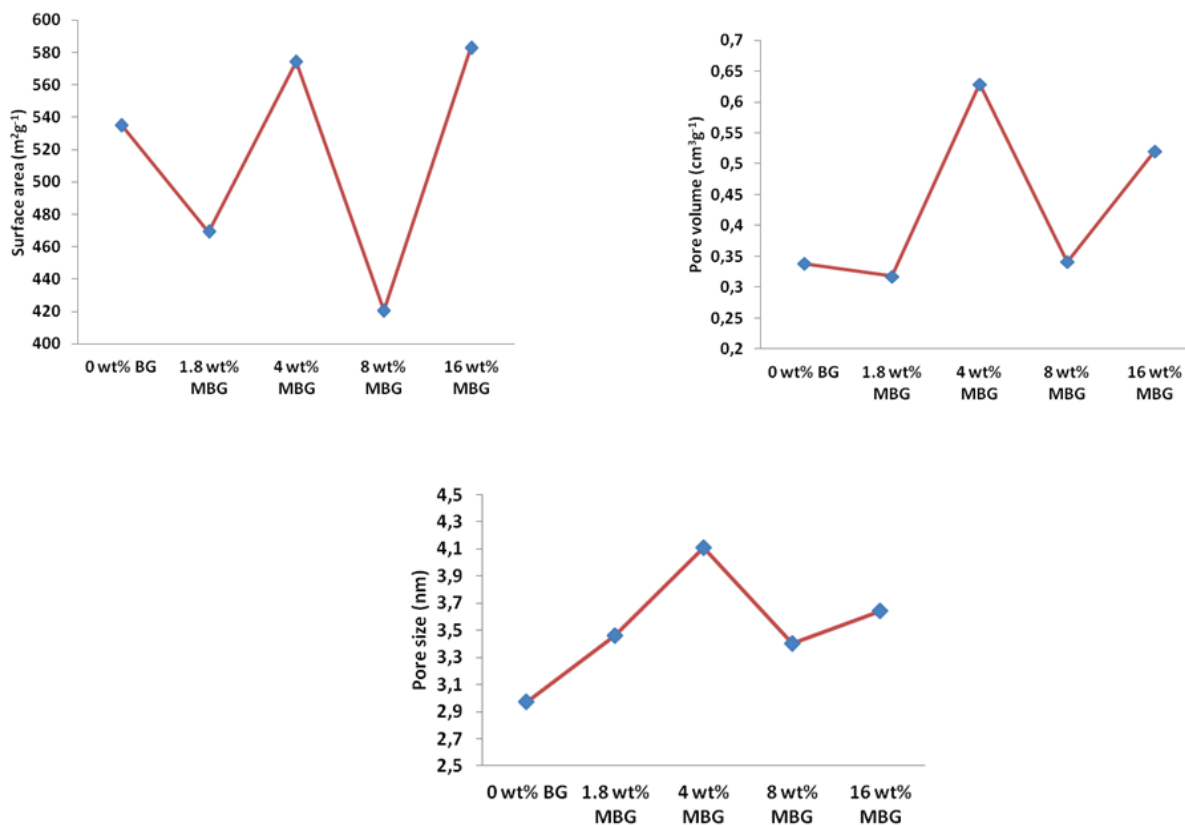


**Figure 30** Surface area, pore volume and pore size results of 0Na BG, 1.8Wt%, 4wt%, 8wt% and 16wt% 0Na MBGs

Considering the MBGs alone, we find that the mean pore size, pore volume and surface area share the same trend. That is with increase in mean pore size there is an increase in pore volume and surface area and vice versa. This means that more than the pore density (number of pores per unit area) the pore size contributes to the changes in pore volume and surface area.

The surface area, pore volume and mean pore size results of the 10Na BG and MBGs (**Figure 31**) also demonstrate the same trend similar to 0Na BG and MBGs up to the 4wt% surfactant concentration that has been investigated. However, we can see that at 4wt% surfactant concentration the 10Na MBG has reached very high pore size and increased pore volume compared to the 0Na MBG but with a lower surface area. This once again shows that the 0Na MBG has higher pore density than the 10Na MBG.

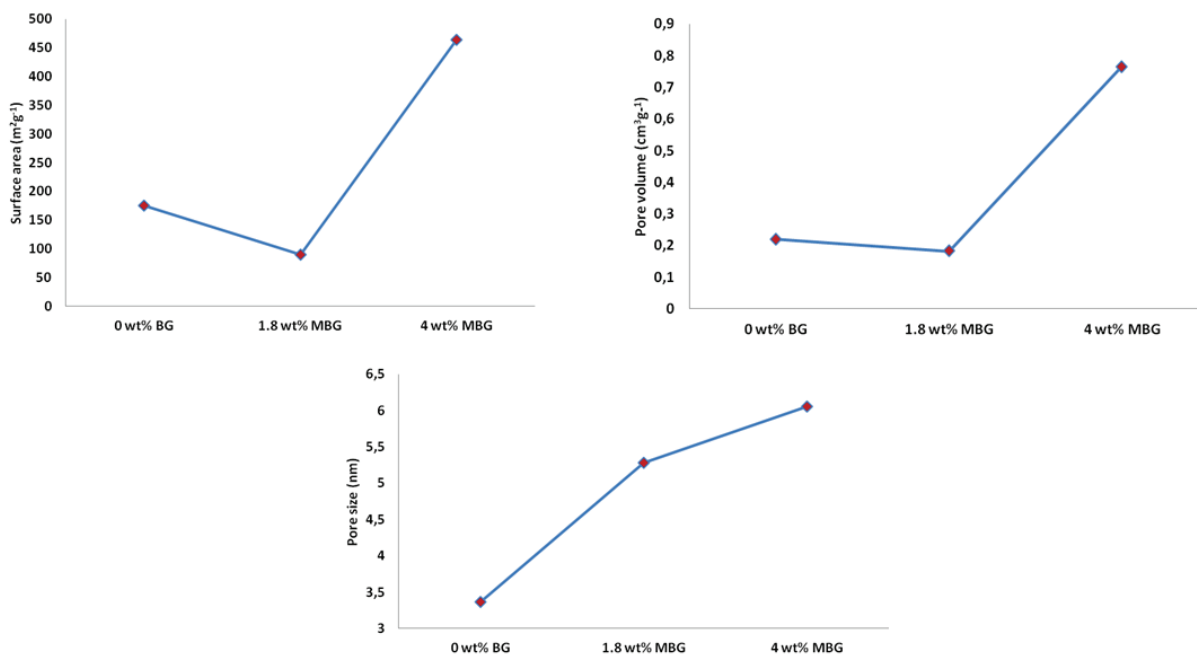


**Figure 31** Surface area, pore volume and pore size results of 10Na BG with 0 wt% (BG) 1.8Wt% and 4wt% (MBG) surfactant

On examining the hysteresis loops of the 0Na BG and MBGs (**Figure 32**) we find that the quantity of gas adsorbed at the capillary condensation relative pressure corresponds to the pore volume trends of these samples. At 4wt% and 16wt% we can see that there is increased adsorption of gas in the capillary condensation region of the hysteresis loops. However all samples exhibit type IV isotherms with H2 type hysteresis loops which is typical of mesoporous materials with bottle neck shaped interconnected pores.

The hysteresis loops of the 10Na BG and MBGs (**Figure 33**) are rather interesting as with increasing surfactant concentration we find that the type IV isotherms of the samples changes from H2 type hysteresis loop in 10Na BG to H5 type loop (open and closed pores) at 1.8wt% surfactant concentration and H4 type loop at 4wt% surfactant concentration (slit like micro and mesopores). These changes in the hysteresis loop type with increasing surfactant concentration indicates that there is a dynamic change in the pore morphology of the 10Na MBGs in comparison to 0Na MBGs.

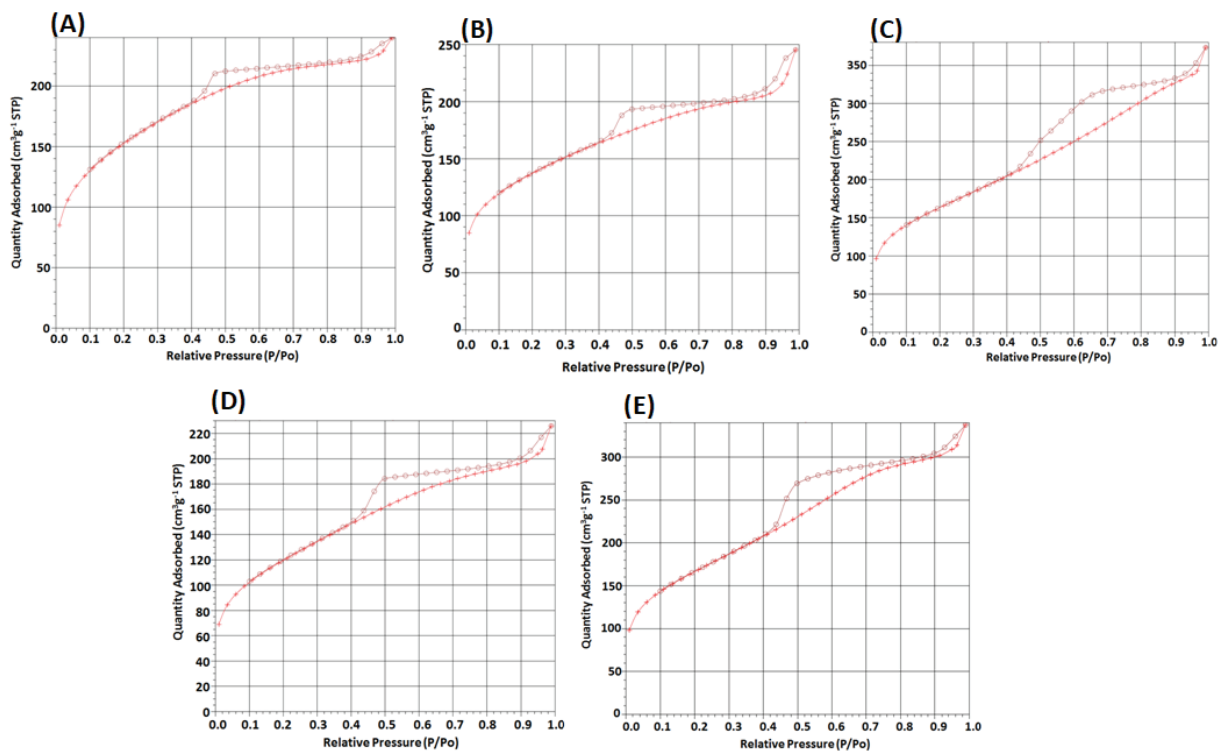


Figure 32 Hysteresis loops of (A) 0Na BG, (B) 1.8wt% 0Na MBG, (C) 4wt% 0Na MBG, (D) 8wt% 0Na MBG and (E) 1.6wt% 0Na MBG

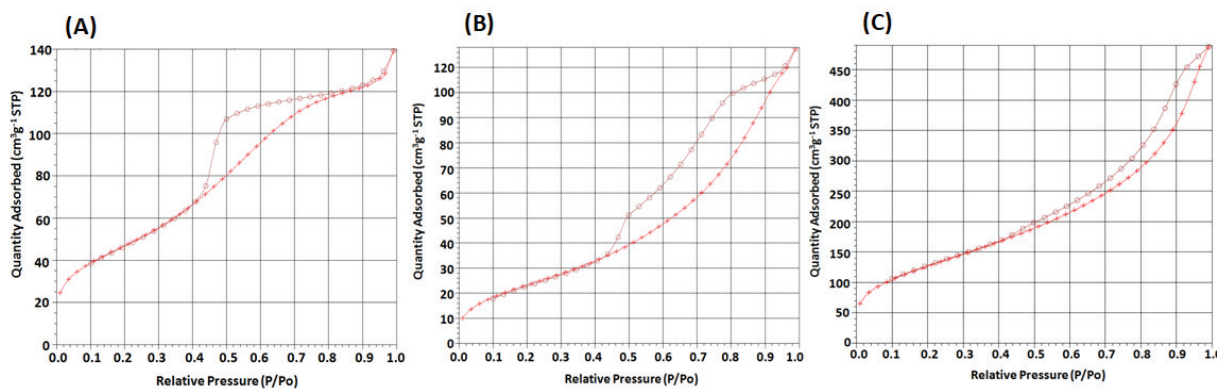


Figure 33 Hysteresis loops of (A) 10Na BG, (B) 1.8wt% 10Na MBG and (C) 4wt% 10Na MBG

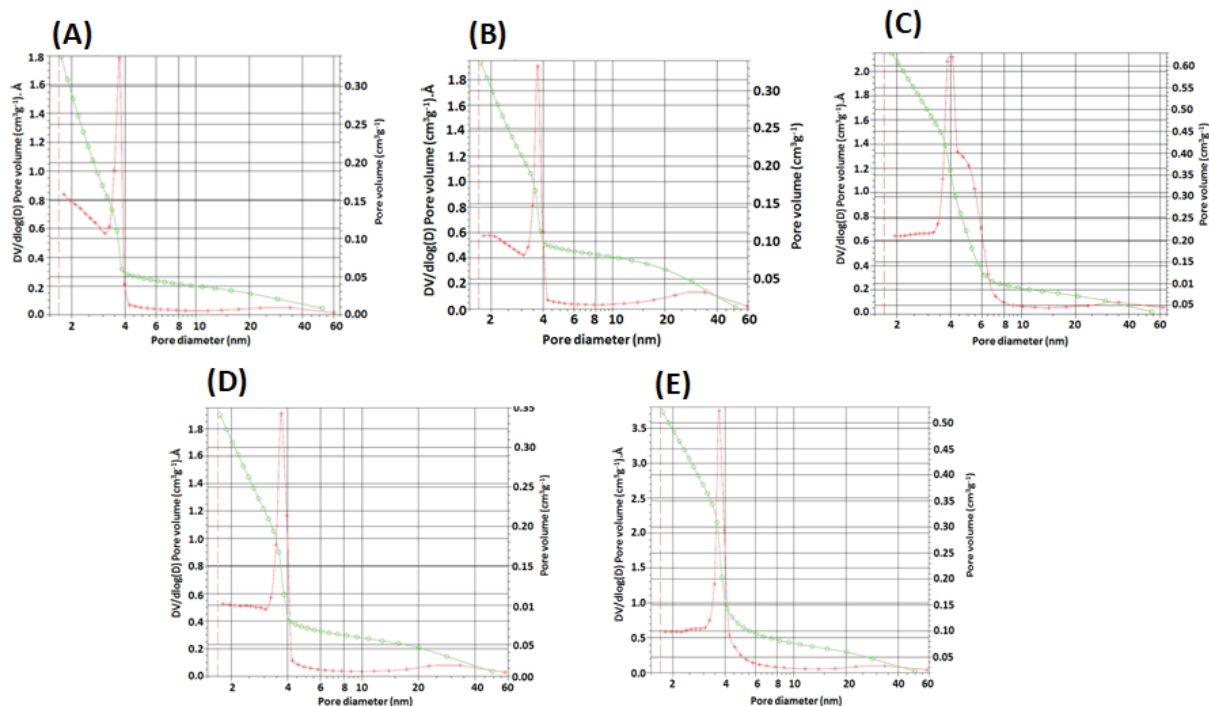


Figure 34 Pore size distributions of A) 0Na BG, (B) 1.8wt% 0Na MBG, (C) 4wt% 0Na MBG, (D) 8wt% 0Na MBG and (E) 1.6wt% 0Na MBG

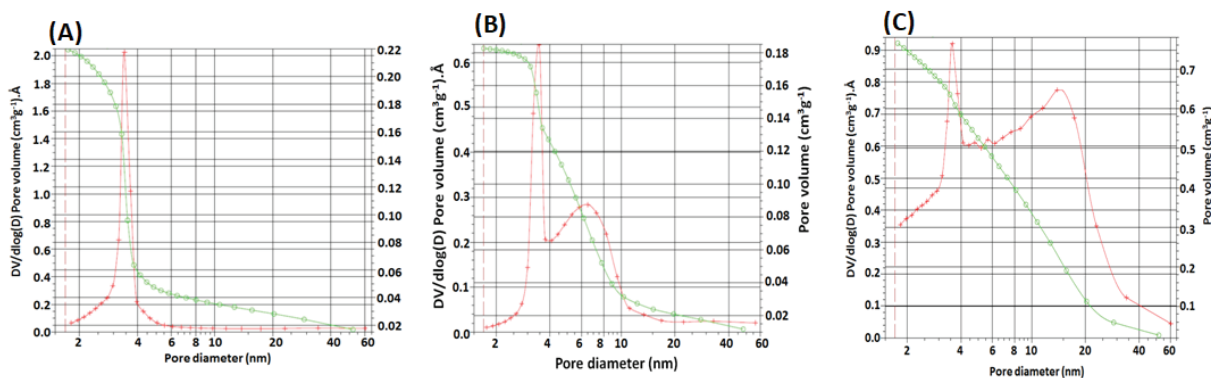


Figure 35 Pore size distributions of (A) 10Na BG, (B) 1.8wt% 10Na MBG and (C) 4wt% 10Na MBG

**Figure 34** shows the pore size distribution of 0Na MBGs with increasing surfactant concentration. As discussed in the previous chapter the 0Na BG and 1.8wt% 0Na MBG displays mainly a population of micropores (less than 2nm), smaller sized mesopores (2-4nm) and also a population of bigger sized mesopores (20-50nm). By increasing the surfactant concentration to 1.8wt% there is only a slight increase in the volume of 20-50nm sized pores (as discussed in the previous chapter). However

at 4wt% surfactant concentration we find that a population of 4-10nm sized pores emerges which was typical for 1.8wt% 10Na MBGs. In addition, the differential volume of 2-4 nm sized pores also slightly increases to  $2.1 \text{ (cm}^3\text{g}^{-1})\text{\AA}$  in the 4wt% 0Na MBG. This suggests that the increase in pore volume could be a result of well-formed micelles. However, at 8wt% surfactant concentration the pore size distribution goes back to being similar to that of 1.8wt% surfactant concentration. There is clearly a reduction in pore size and hence the pore volume and surface area. Further at 16wt% surfactant concentration the pore size distribution trend remains similar to 8wt% 0Na MBG but there is a marked increase in the differential pore volume of 2-4nm sized pores to  $3.5 \text{ (cm}^3\text{g}^{-1})\text{\AA}$ , even higher than 4wt% 0Na MBG.

The pore size distribution and hysteresis loop trends when considered together with the surface area, pore volume and pore size results for 0Na BG and MBG samples suggest that there is a transition stage at intermittent surfactant concentrations that affects the way in which the micelles are formed. To elaborate, at 1.8wt% surfactant concentration there is a decrease in pore volume despite the increase in pore size induced by the micelles. This means that at this surfactant concentration the micelles aren't well formed in the sense that they may have not taken any matured shape and remained as aggregates. Therefore this intermediate state must have had an impact on the pore density of the 1.8wt% 0Na MBG by reducing the microporosities innately present in the 0Na BG. At 4wt% the increased emergence of 4-10nm pores (reflected as an increased mean pore size) and thereby the increase in pore volume and surface area is a reflection of well-formed micelles (that is, the surfactant molecules may have combined to take up a defined shape). At this stage it is clear that the increase in surface area and pore volume is mainly due to increase in the size of the existing pores and not due to increase in pore density. At 8wt% surfactant concentration there must be another micelle shape transition similar to that experienced at 1.8wt% and hence there is a drop in mean pore size thus bringing down the pore volume and surface area. Further increase in surfactant concentration to 16wt% increases the mean pore size again signifying that the micelles are starting to take another shape. It should be noted that the mean pore size and pore volume of 16wt% 0Na MBG is lower than the 4wt% 0Na MBG however they both share almost similar surface area. This means that at 16wt% additions there must be an actual increase of pore density in these samples.

The pore size distribution of 10Na BG and MBGs (**Figure 35**) shows that in comparison to BG the 1.8wt% MBG hosts a population of 4-10nm sized pores. This aspect was previously discussed in

Chapter 5. However unlike the 0Na MBG, by increasing the surfactant concentration to 4wt% there is a dramatic increase in the bigger sized pores spanning 4-60nm. This clearly indicates that there is an enhanced effect of surfactant mediated increase in pore size realised in the 10Na MBG compared to 0Na MBGs.

Very few studies in the literature have investigated the effect of increasing surfactant concentration of the surface bulk microstructure of MBGs.

**Table 5 Surfactant to ethanol concentration impact on pore order from literature**

<b>Surfactant to Ethanol concentration (Weight percent)</b>	<b>Results</b>	<b>Reference</b>
2.1	Not ordered	[96]
2.34	Ordered	[133]
5.4	Ordered	[96]
6.21	Ordered	[133]
6.25	Ordered	[136]
6.25	Ordered	[98]
6.25	Ordered	[92]
6.25	Ordered	[103,104]
6.25	Ordered	[89]
9.1	Ordered	[96]
10.38	Moderate	[133]
10.44	Moderate	[100]
12.5	Not ordered	[96]
14.25	Collapsed	[133]

**Table 6 Surfactant to glass precursor concentration impact on pore order from literature**

<b>Surfactant to glass precursors concentration (Weight percent)</b>	<b>Results</b>	<b>Reference</b>
12.74	Not ordered	[96]
14	Ordered	[133]
29.8	Ordered	[96]
30.6	Ordered	[92]
31	Ordered	[133]
31.2	Ordered	[103,104]
32.2	Ordered	[89]
35.18	Ordered	[136]
36.93	Ordered	[98]
40	Ordered	[96]
44	Moderate	[133]
44	Moderate	[100]
49.25	Not ordered	[96]
53	Collapsed	[133]

**Table 7 Surfactant concentration with respect to ethanol and glass precursors of samples investigated in this study.**

<b>Surfactant to Ethanol concentration (Weight percent)</b>	<b>Surfactant to glass precursors concentration (Weight percent)</b>
6.25	1.8
13.19	4
24.10	8
41.03	16

Most studies opt for the golden standard of dissolving 4g surfactant in 60g ethanol for about 6g-7g of glass precursors. This would make the surfactant concentration with respect to ethanol as 6.25wt% and that of glass precursors to be 30-36wt%. Similarly, comparing the results of studies from the

literature that have varied the concentration of surfactant in a bid to achieve ordered porosity as indicated by TEM (**Table 5 and Table 6**) it seems that 5.4-9.1 weight percent of surfactant concentration with respect to ethanol and 30-40 weight percent of surfactant with respect to glass precursors is needed to achieve ordered porosity. In our system (**Table 7**) we have increased the surfactant concentration only from 1.8 to 16wt% with respect to the glass precursors which seems way below the 30-40 percent limit to realise ordered porosity induced by micelles. Similarly, the concentration of surfactant with respect to ethanol varied from 6.25 to 41wt%. At 6.25wt% level, which seems ideal for ethanol, the concentration of surfactant with respect to glass precursors in our studies was only 1.8wt%. By increasing the concentration of surfactant to 4wt% with respect to glass precursors (and recognising that we kept the amount of ethanol constant) the weight percent of surfactant with respect to ethanol increased to 13wt% which is above the 6-9 percent range. Therefore, in this case we may have pushed the system above the ideal surfactant to ethanol concentration range and so the micelles may have either formed as tubes or sheets instead of uniform spherical /cylindrical structures or collapsed. This may be a possible explanation both to the fluctuating trends and as to why we have not achieved ordered porosity in our system despite the increase in surfactant concentration with respect to the glass precursors. Future work in this area should try to prepare this MBG by using 47g surfactant to 671g ethanol with the same amount of glass precursors mentioned in **Section 7.2.2**. This would make the surfactant to ethanol concentration as 6.5wt% and to that of glass precursors as 30wt%.

Nevertheless, we find that within the system investigated, a dramatic increase in pore size and hence the pore volume in the high sodium system can be achieved by increasing the surfactant concentration. In the high calcium composition there is increase in pore density at 16wt% but the pore size distribution is more uniform than high sodium composition. This instigates that the network modifiers Ca and Na also highly influencing the structure induced by micelles. In general, in the non-surfactant system we find that the high sodium composition gives bigger pore size than high calcium composition. This must be because sodium is a strong network depolymeriser and it freely disrupts the network and creates bigger holes. An alternative viewpoint is to recognise that sodium is expanding the network by adding porosity. In contrast calcium ions require 2 oxides to attain charge balance and this leads to a relative contraction of the sol-gel network. In the case of MBGs where the silica and phosphate network is formed around the micelles, the overall glass network will again be

comparatively expanded compared with the non-surfactant BGs. Therefore, the entry of the modifiers and their disruptive effect seems to magnify the very nature of their interactions. To summarise, in high sodium sol-gel systems increased disorderliness in pore characteristics (size, shape and arrangement) whilst in high calcium compositions ensure more uniformity is maintained. As studies so far have not investigated the network modifiers interaction with the surfactant these results demand that more studies should focus in this area in future.

#### **7.4. Conclusion**

Influence of surfactant concentration on the surface characteristics of MBGs has been studied. Increased concentration of surfactant molecules facilitates early incorporation of calcium precursor into the glass network. MBGs with high sodium content display drastic increase in pore size and changes in pore shape compared to MBGs with high calcium content with increasing surfactant concentration. Ordered porosity has not been achieved in any of the samples and the possible reasons have been speculated.

## **8. Evaluation of “apatite forming ability” and “cytocompatibility” of MBGs on Human Gingival Fibroblasts.**

### **8.1. Introduction**

In the preceding chapters the synthesis, characterization, options for improvement and factors influencing the surface characteristics and microstructure of MBGs have been detailed. This chapter focuses on bioactivity-related evaluations such as “apatite-forming ability” and “cytocompatibility” for selected MBGs.

As stated in the introduction these MBGs have been targeted for application as fillers in dental adhesives to encourage remineralization at the adhesive-dentin interface. Therefore evaluating the apatite forming ability of these particles is crucial to assess their potential for the targeted application.

In recent years bioactive glasses have also been assessed for their ability to induce dentin mineralization by stimulating the odontoblasts at the pulp dentin interface[137–148]. One of the prerequisites for such an application is to ensure that they are cytocompatible. Therefore the MBG particles have been evaluated for cytocompatibility on primary human gingival fibroblasts (HGF) cells. The reason for choosing HGFs is because they are found in significant concentrations in the proximity of the restoration and are quite representative of oral cells. Therefore initial evaluation of the cytocompatibility on these cells seemed a good starting point.

Cytocompatibility can be evaluated by direct or indirect contact. In the direct contact, as the name implies, the cells are directly interfaced with the samples[149–157]. In the indirect contact the samples are immersed in culture media for different time points and the ions extracts are collected and contacted with cells to evaluate the cytocompatibility [158–174]. Most studies in the literature have performed indirect contact; however we chose a direct contact for the cytocompatibility evaluation for two reasons:

First, direct contact is a crude evaluation because the cells are directly in contact with samples and any potential cytotoxicity can be easily determined. Second, for remineralizing dentin researches using bioactive glasses two protocols are widely employed in research articles. In the one of them the particles are mixed with the resin or cement and the filled material is then interfaced with dentin

[175–180] (indirect application). The other method consists of applying a paste of particles directly on the etched dentin followed by resin application and curing (bonding application). Alternatively, the etched dentin covered with particles is immersed in remineralizing solutions[181–188] (tooth paste or air abrasion applications) in which case the particles are in direct contact with dentin. In these studies we chose direct contact as it could be both a robust evaluation for cytotoxicity and also because it would be relevant to the clinical scenario (application of bioactive glass) for dentin remineralization depending on the chosen restorative approach.

## **8.2. Materials and methods**

### **8.2.1. Materials**

Sodium chloride (99.5%), sodium bicarbonate (99.5%), potassium chloride (99.5%), potassium hydrogen phosphate trihydrate (99.0%), magnesium chloride hexahydrate (98.0%), Hydrochloric acid (35.4%), calcium chloride (95.0%), sodium sulphate (99.0%), tris buffer (99.9%) , acetone were purchased from Alfa aser.

Dubelcco's Modified Eagle's Medium (DMEM) with phenol red, trypsin, Phosphate Buffer Saline (PBS), Foetal Bovine Serum (FBS), Penicillin/Streptomycin, Amphotericin  $\beta$ , Calcein AM, Ethidium homodimer-1, Alamar blue were purchased from Thermo Fischer Scientific.

### **8.2.2. Simulated Body Fluid (SBF) preparation**

The ingredients for SBF preparation are listed in **Table 8**. 750ml of ultra pure water was added to a 1000mL beaker. The water was stirred and maintained at 37°C with a heater. Each chemical upto and including #8 in table 1 was weighed and added into the water one by one the order shown until each ingredient was completely dissolved. Ingredient #9 was added in parts to avoid a local increase of pH. After this step a pH electrode was placed in the solution and the pH at 37°C recorded as 7.5. The pH was then adjusted to 7.4 at 37°C using a 1M HCl solution. Finally, ultrapure water was added and the total volume was adjusted to 1000mL.

**Table 8 Reagents for preparation of SBF**

Order	Reagent	Quantity
#1	NaCl	7.996 g
#2	NaHCO <sub>3</sub>	0.350 g
#3	KCl	0.224 g
#4	K <sub>2</sub> HPO <sub>4</sub> ·3H <sub>2</sub> O	0.228 g
#5	MgCl <sub>2</sub> ·6H <sub>2</sub> O	0.305 g
#6	1M HCl	40 mL
#7	CaCl <sub>2</sub>	0.278 g
#8	Na <sub>2</sub> SO <sub>4</sub>	0.071 g
#9	(CH <sub>2</sub> OH) <sub>5</sub> CNH <sub>2</sub>	6.057 g
#10	1M HCl	Appropriate amount for adjusting pH

### 8.2.3. Apatite forming ability in vitro (SBF test)

The apatite forming ability test was performed initially with **short time points (trial 1)**-day 1, day 3, day 7 and later with **long time points (trial 2)**-day 1, day 3, day 7, day 14 and day 21. The samples were immersed in SBF at a concentration of 1.5mg/ml for both trials. At each time point in trial 1, the pH of the SBF solution containing the samples were measured at room temperature. Samples were then collected, washed with acetone and left to air dry. The samples were subjected to XRD, FTIR and SEM characterizations. For trail 2 the samples were collected, washed with acetone, air dried and subjected to XRD and FTIR analysis.

#### 8.2.3.1. X-Ray Diffraction (XRD)

XRD analysis of samples before and after immersion in SBF was performed using an X-ray diffractometer (XRD, X'Pert Philips, Netherlands) with Cu K $\alpha$  radiation of wavelength 1.54Å. The scans were recorded at 30 kV, 30 mA, 2 theta ranges between 5° to 60° and a step size of 0.02° and 90.17 seconds per step.

#### 8.2.3.2. Fourier transform infra-red spectroscopy (FTIR)

The glass network of the samples before and after immersion in SBF was studied using (FTIR) on a Safas Monaco spectrometer. The spectra were collected in a wavelength range of 340-4000 cm<sup>-1</sup> at a spectral resolution of 4 cm<sup>-1</sup>.

### **8.2.3.3. SEM-EDX**

The morphology of the copper coated (10nm) samples before and after immersion in SBF was examined by scanning electron microscopy (FEI-Quanta 250, Thermo Fisher Scientific, France) coupled with EDX at a magnification of 1000X.

## **8.2.4. Cytocompatibility evaluation on Human gingival fibroblasts**

### **8.2.4.1. Growth and maintenance of HGF cell cultures**

Human gingival fibroblasts were isolated from healthy gingival tissue biopsies of patients taken during routine orthodontic extractions (in compliance with French legislation (informed consent and was conducted with local ethical committee approval). Obtained cells were cultured in Dulbecco's modified Eagle medium (DMEM) in the presence of 10% fetal bovine serum (FBS), 2% Penicillin/Streptomycin and 1% Amphotericin B. Cells were maintained at 37°C under a humidified atmosphere of 5% CO<sub>2</sub> in air. The medium was changed every 3 days, and the cells were passaged every 5 days. After reaching confluence, the cells were trypsinized and resuspended in the culture medium. The cells were centrifuged at 1200 rpm/min for 5 min and counted with a Scepter handheld automated cell counter (Millipore, USA).

### **8.2.4.2. HGFs contact with MBGs**

50mL of 10% FBS, 5ml of 1% Penicillin/Streptomycin and 1ml of Amphotericin  $\beta$  were added to 500mL of DMEM and used as a culture media. HGFs were seeded on 24 well culture plates at a concentration of 10<sup>4</sup>cells/mL and left overnight for attachment. The following day, the samples were sterilized under UV for 30 minutes after which they were suspended in the culture media at a concentration of 800 $\mu$ g/ml. The media containing the samples were directly contacted with attached Human gingival fibroblasts (1mL/well). The controls cells were contacted with normal media. At day 1 and day 3 cells growth was observed using optical microscopy. Live / dead staining was performed on day 3 and the metabolic activity of cells was quantified at day 2 and day 6.

### **8.2.4.3. Live dead staining**

The Live/Dead<sup>®</sup> cell cytotoxicity for mammalian stain was used according to the manufacturer's instructions (Invitrogen European Headquarters, UK). The kit provides a two-color fluorescence assay of cell viability relying on membrane integrity: viable cells are stained by Calcein and fluorescence green, while damaged cells are stained by Ethidium homodimer-1 (EthD-1) and fluoresce red. The determination of cell viability depends on these physical and biochemical

properties of cells. A working solution of a final concentration containing 2  $\mu\text{M}$  of Calcein AM and 4  $\mu\text{M}$  EthD-1 (prepared by combining the two stain reagents), was found to be suitable for fibroblasts. The stain was then added to the control cells and to the cells contacted with MBGs. This short staining protocol allowed direct observation of the original cell structure under fluorescence microscopy. No centrifugation or fixation steps were needed. Microscopic observations started 15 minutes after staining. Excitation/emission maxima for Calcein and EthD-1 are 495/515 and 525/635 nm, respectively.

#### **8.2.4.4. Alamar blue assay**

Cell mitochondrial activity was measured using the Alamar Blue assay, the Alamar Blue solution, which is blue-colored in its oxidized state, becomes pink colored when reduced to the Resorufin by the metabolic activity of cells. At day 2 and day 6, 100  $\mu\text{L}$  of Alamar blue solution was added to each well (10%, v/v) and incubated at 37°C for 6 hours without shaking. The amount of formed Resorufin was determined by measuring fluorescence intensity using a fluorescent plate reader (Infinite®F200, Tecan group LTD. France) for excitation at 530 nm and emission at 580 nm. For each point, three wells were analyzed. The statistical analysis was performed using Student t-test.

### **8.3. Results and discussion**

#### **8.3.1. Apatite forming ability**

**Figure 36** shows the pH changes of the 0Na, 5Na and 10Na MBGs thermal treated at 310°C in de-ionised water and SBF. As can be seen, the pH increment is correlated to the sodium content in the glass composition in both cases. This is because, compared to  $\text{Ca}^{2+}$  ions,  $\text{Na}^{+}$  ions in the glass more rapidly exchanges with  $\text{H}^{+}$  ions in the de-ionised water. This loss of  $\text{H}^{+}$  ions (or increase in  $\text{OH}^{-}$  ions) increases the pH. Thus the composition with highest  $\text{Na}_2\text{O}$  content (10NaMBG) attained the greatest increase: pH 9.3 in de-ionised water (**Figure 36A**) and pH 7.7 in SBF (**Figure 36B**). As SBF is a buffered solution the increase in pH is lower compared to de-ionised water.

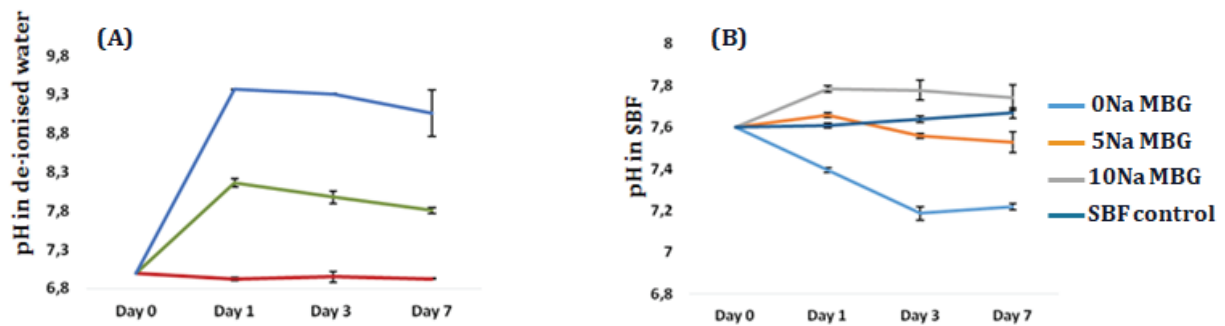


Figure 36 pH of 0Na, 5Na and 10Na MBG thermal treated at 310°C; (A) in De-ionised water (B) in SBF

Interestingly, we find that in both de-ionised water and SBF containing 0Na MBG there is a reduction of pH. This is also seen in the solutions containing 5Na MBG at later time points (after day 3). High release of phosphate ions from bioactive glass is known to reduce the pH of the solution. Even though 5Na and 10Na MBGs have phosphate contents similar to the 0Na MBG sample, the release of sodium strongly dominates the initial ion exchange and increases the pH. However, in the 0Na MBG the lack of sodium could have unmasked the pH changes due to the release of phosphate and as a result pH reduction is more evident. Likewise in the 5Na MBG the decreased level of sodium in comparison to 10Na MBG must have led to this effect (pH reduction) at later time points.

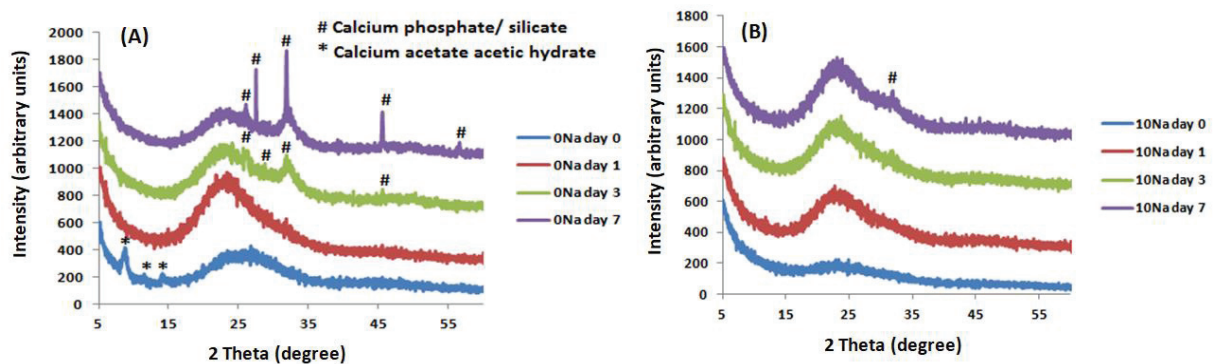
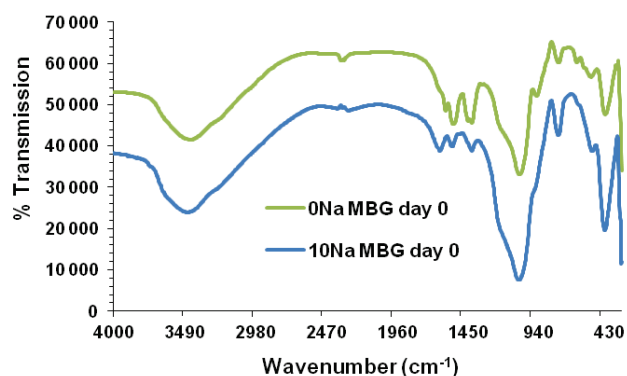


Figure 37 XRD of MBGs before and after immersion in SBF; (A) 0Na MBG (B) 10Na MBG for up to a week (short time points)

The phase changes in the 0Na and 10Na MBG samples after immersion in SBF up to a week is shown in **Figure 37**. In the 0Na MBG at day 0 (before immersion in SBF) the remnant calcium precursor that is yet to enter the network or free surface calcium could be seen (**Figure 37A**). After 24 hours of immersion in SBF (0Na MBG day 1) we find that the peaks corresponding to the calcium precursor

has disappeared and a completely amorphous sample remains. This means that the free surface calcium has dissolved in the SBF. At day 3 we find new crystalline peaks emerging in the 0Na MBG whose phase matches to both calcium phosphate and calcium silicate. The crystallinity of the 0Na MBG increased at day 7 indicated by multiple peaks in the XRD pattern which again matched with both calcium phosphate and silicate phases. In the 10Na MBG there was no difference in phase until day 3 as the sample was amorphous (**Figure 37B**). However, at day 7 a very small peak emerged. This single peak is insufficient to be assessed for phase matching using the XRD software.



**Figure 38 FTIR of 0Na and 10Na MBG before immersion in SBF**

The FTIR characterization on the samples indicating the glass structure at a molecular level before immersion in SBF is shown in **Figure 38**. In the 0Na MBG at day 0 (before immersion in SBF) the peak at  $3440\text{ cm}^{-1}$  has been identified as the OH from the surface silanols in the glass and the peak at  $1610\text{ cm}^{-1}$  as being due to OH from the adsorbed water. The Si-O-Si asymmetric stretch can be seen at  $1078\text{ cm}^{-1}$ , Si-O-Si symmetric bending at  $796\text{ cm}^{-1}$  and Si-O-Si rocking mode at  $462\text{ cm}^{-1}$ . The P-O bond was evident at  $564\text{ cm}^{-1}$  and the peak at  $954\text{ cm}^{-1}$  corresponds to Si-O-NBO (where NBO = non-bridging oxygen). The peaks at  $1420\text{ cm}^{-1}$  and  $1552\text{ cm}^{-1}$  correspond to  $\text{COO}^-$  present in the salts. On comparing the 0Na and 10Na MBG samples at day 0 we find the same peaks present but with the peaks corresponding to  $\text{COO}^-$  of the salts being much smaller in the 10Na MBG sample. This ties in nicely with the day 0 XRD observations in **Figure 37**. The FTIR pattern of these samples after SBF testing also confirms the previous observations in XRD analysis.

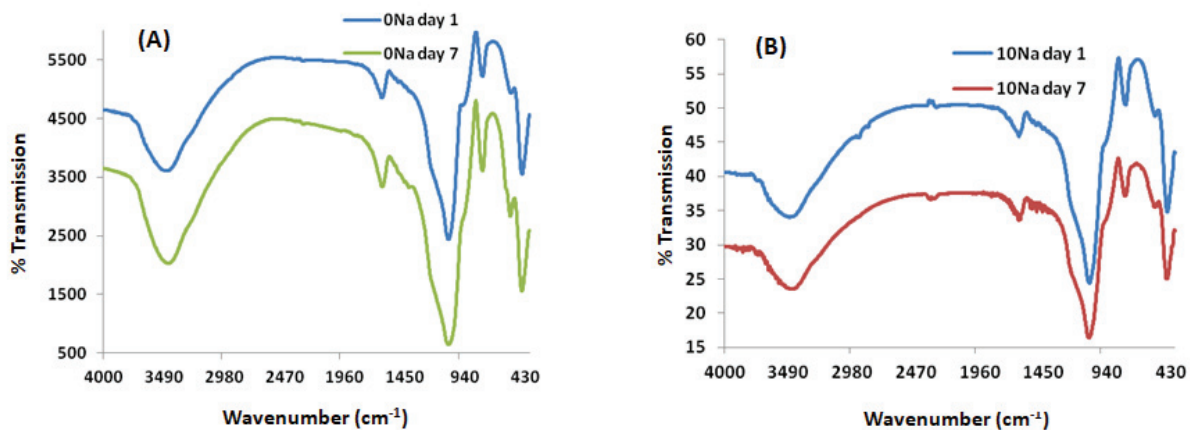


**Figure 39** FTIR of MBGs after immersion in SBF (A) 0Na MBG (B) 10Na MBG for up to a week (short time points)

The FTIR characterization on the samples to assess the changes in the glass structure at a molecular level as a result of immersion in SBF is shown in **Figure 39**. In the 0Na MBG sample (**Figure 39A**) we can find that at day 1 that there is disappearance of the  $\text{COO}^-$  peaks corresponding to the salt and also a reduction of the Si-NBO bond which indicates that the ionic exchange has begun. At day 7, we see the development of a C-O peak and also increase in of the P-O bond intensity at  $564\text{ cm}^{-1}$ . However, we do not find the splitting of the P-O bond which is specific to crystalline phosphate and is one of main indicators of apatite formation. This is in agreement with the XRD data at day 7 that suggested we only have either calcium silicate or calcium phosphate phase and the reaction is still progressing. In the 10NaMBG sample we find the disappearance of the  $\text{COO}^-$  peaks at day 1 but we do not find any significant difference in the other bonds between day 1 and day 7 (**Figure 39B**).

The SEM images of the samples show that in the 0Na MBG spherical globules develop at day 3 which progresses into needle-like structures at day 7 (**Figure 42**). In the 10Na MBG we find the spherical globule-like structure appears only at day 7 in line with the XRD results which showed a small peak emerging at this time point. The EDX analysis of the 0Na MBG confirms that at day 3 and day 7 there is an increase in the calcium and phosphate levels compared to day 0; in contrast the 10Na MBG shows an increase only seen at day 7.

Overall, the XRD, FTIR and SEM results show that despite the impressive increase of pH (one of the main factors supporting apatite formation) in the 10Na MBG sample, the formation of calcium phosphate precipitate and subsequent potential to form apatite is much lower compared to 0Na MBG.

However, both samples did not specifically show hydroxyapatite formation within the tested time period.

Therefore it was decided to repeat the apatite-forming ability test with longer time points (Trial 2). **Figure 40** shows the XRD results of the 0Na and 10Na MBGs immersed in SBF for up to 3 weeks. Similar to the first evaluation we find that the peaks corresponding to the calcium precursor disappears at day 1 in the 0Na MBG followed by the emergence of calcium silicate/phosphate phase at day 3 (**Figure 40A**). However, until day 21 we find the same calcium silicate/ phosphate phase retained in 0Na MBG. In contrast, in 10Na MBG no difference in phase occurred over the period of 3 weeks (**Figure 40B**).

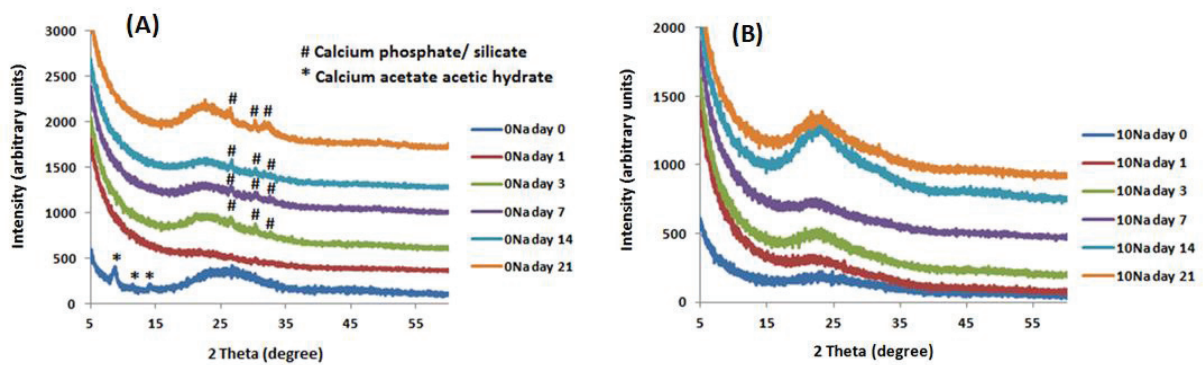


**Figure 40** XRD of MBGs before and after immersion in SBF; (A) 0Na MBG (B) 10Na MBG for up to 3 weeks (long time points)

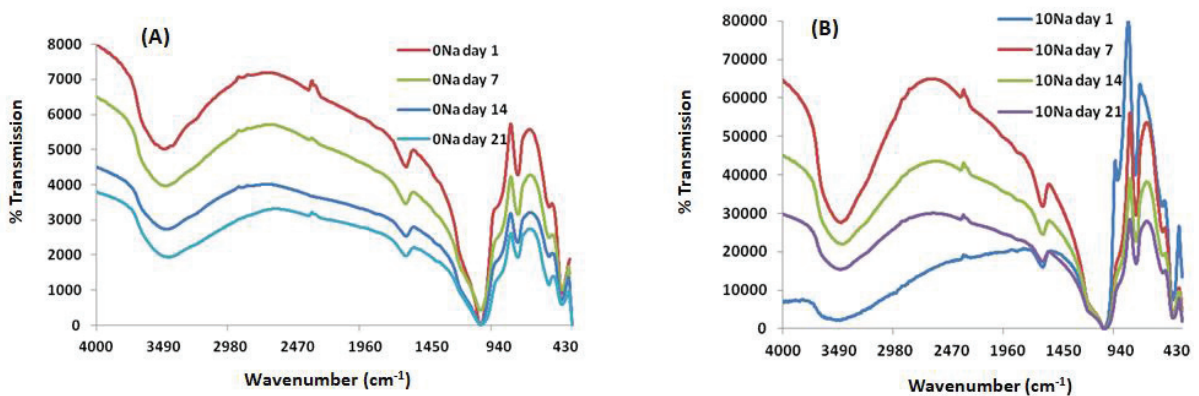


**Figure 41** FTIR of MBGs after immersion in SBF (A) 0Na MBG (B) 10Na MBG for up to 3 weeks (long time points)

The FTIR results of the 0Na MBG sample immersed in SBF for long time points (**Figure 41A**) also followed similar trends as seen in trail 1 up to day 7 (**Figure 39A**) with the disappearance COO<sup>-</sup> peaks

corresponding to the calcium precursor. However, the increase in the peak corresponding to the P-O bond was evident only at day 21. Furthermore, no indication of crystalline phosphate was observed up to day 21 confirming that the apatite formation was not realised in these samples. Likewise the 10Na MBG sample showed no change in the structure up to day 21 except for the disappearance of COO<sup>-</sup> peaks at day 1 (**Figure 41B**).

The apatite forming ability of 0Na and 10Na MBG was assessed for short and extended periods of time using XRD, FTIR and SEM (Short time period). In both trials we observed that in comparison to 10Na MBG, the 0Na MBG has better reactivity in SBF. However, at the long time points (trial 2) the intensity of the newly formed crystalline phase at day 3 and day 7 in the 0Na MBG (**Figure 40A**) was much lower than what was observed in trial 1 (**Figure 37A**, short time point). Furthermore, the increase of P-O peak intensity in FTIR observed at day 7 in the first trial (**Figure 39A**) was observed only at day 21 in the second trial (**Figure 41A**). This shows that the same reaction was very much slowed down in the long time points test. Although it is unclear why, the only difference between both tests is the quantity of samples (mass) in SBF. That is, in both tests the concentration of samples in SBF was the same (1.5mg/mL) but in the long time point trial the SBF volume was 10mL instead of the 25mL that was used in the short time point trial. Therefore, in the short time point trial there was 37.5mg of samples exposed to the total volume of SBF whereas in the long time point trial only 15mg of samples was exposed. Our results suggest that alongside the concentration, the quantity of sample exposed to SBF could also affect reaction kinetics and in turn the crystallinity and size of the newly formed crystals. If not, the other possible experimental factor causing this change may have been the uncontrolled particle size of the samples used in these trials.

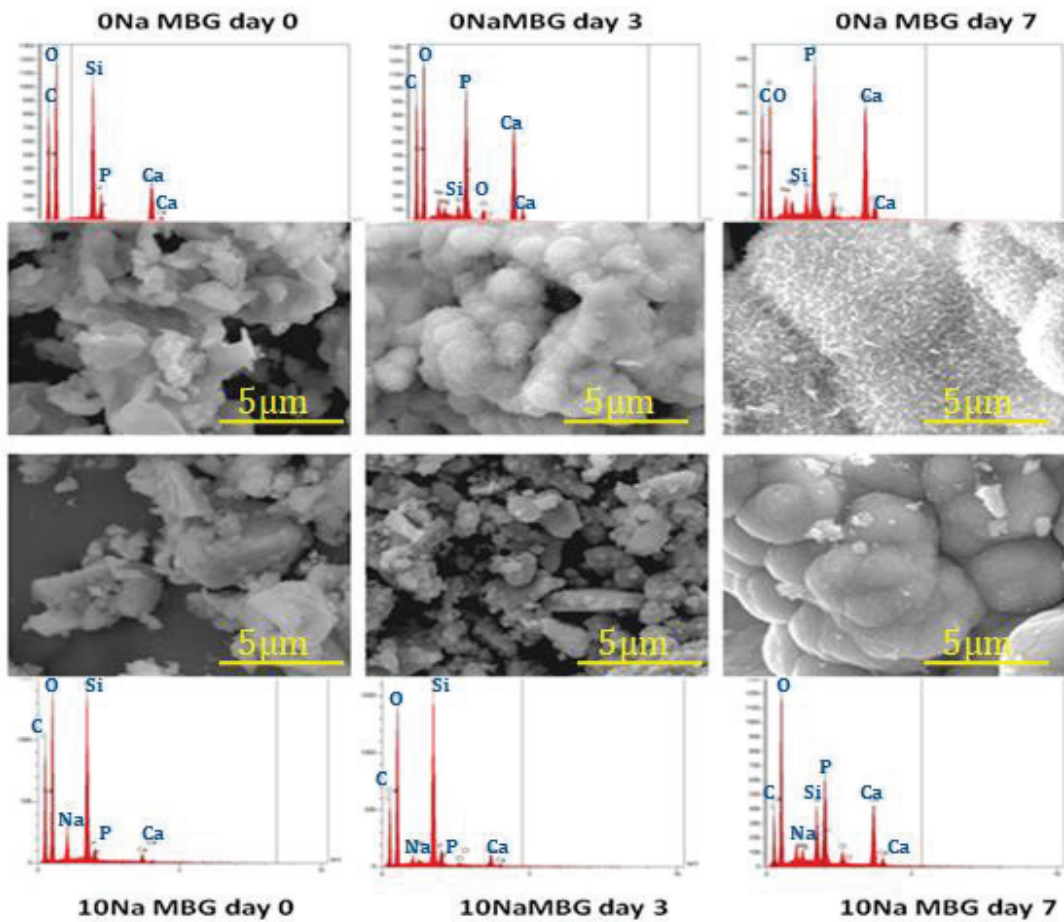


Figure 42 Morphology of 0Na MBG and 10Na MBG at day 0, day 3 and day 7 in SBF; Scale bar 5μm

The new crystalline phase seen in the 0Na MBG (XRD) after immersion in SBF matches with both calcium silicate as well as calcium phosphate. Although the FTIR characterization does not show the splitting of P-O bond at  $564\text{cm}^{-1}$  which is an indicator of crystalline phosphate, it does show the increase of the P-O bond with time suggesting the growth of phosphate. Furthermore the SEM-EDX analysis on the short time points sample clearly confirms the increase in calcium and phosphate level after immersion in SBF. Therefore the observed crystalline phase in XRD of 0Na MBG at and after day 3 could be calcium phosphate, possibly existing as low levels of a calcium rich crystalline phase in combination with an amorphous or poorly crystalline calcium phosphate.

In both trials apatite formation was clearly not achieved under the tested conditions. According to Hench's mechanism for apatite formation associated with bioactive glass immersion in SBF, initially there is rapid exchange of  $\text{Na}^+$  and  $\text{Ca}^{2+}$  ions from the glass with  $\text{H}^+$  ions in the physiological fluid. This

exchange, in addition to the breakdown of Si-O-Si to form silicic acid ( $\text{Si}(\text{OH})_4$ ), leads to the formation of surface silanols. These surface silanols undergo condensation and repolymerization to form a  $\text{SiO}_2$  rich layer which provides nucleation sites for apatite formation. The super saturation of the fluid with calcium and phosphate ions causes the deposition of  $\text{Ca}^{2+}$  and  $\text{PO}_4^{3-}$  on the silica rich layer as amorphous calcium phosphate. In time this amorphous calcium phosphate layer evolves into a crystalline hydroxyapatite. In our studies the formation of a calcium-rich layer and the growth of phosphate indicate that either the deposited  $\text{Ca}^{2+}$  and  $\text{PO}_4^{3-}$  ions form less stable phases than hydroxyapatite or the reaction needs more time for the calcium rich phase to evolve into hydroxyapatite. It is proposed that the high calcium content and increased surface area in the 0Na MBG accounts for its enhanced reactivity in SBF compared to 10Na MBG.

However, in comparison to other studies in literature that have shown apatite formation on MBG samples with high surface area and ordered pore structure in less than a week the 0Na MBG in this study shows no apatite formation despite its high surface area and calcium rich composition. This indicates that there could be other factors that are needed alongside the high surface area and calcium rich compositions to realize apatite formation such as controlled particle size[189], optimal pore size[190], pore shape, pH of the media, and increased concentration and mass of samples in SBF. Future work should first optimise the experimental set up by investigating variables such as increased concentration of MBGs in SBF, pH of the SBF, particle size of MBGs etc and evaluating the associated apatite forming ability of the 0Na MBG samples. If the results are still not favourable then systematic optimisation of particle size and pore characteristics such size and shape would be needed in order to realise apatite formation. Nevertheless, the 0Na MBG shows a good potential to for apatite formation in comparison to 10Na MBGs.

### **8.3.2. Cytocompatibility**

A cytocompatibility evaluation was performed on samples with varying Na/Ca ratio. 0Na, 5Na and 10Na MBGs were treated at  $310^\circ\text{C}$  in order to evaluate the effect of composition on cell behaviour. In addition, 0Na MBG samples thermal treated at  $340^\circ\text{C}$  and  $380^\circ\text{C}$  were also included to study the effect of increased thermal treatment on cell behaviour.

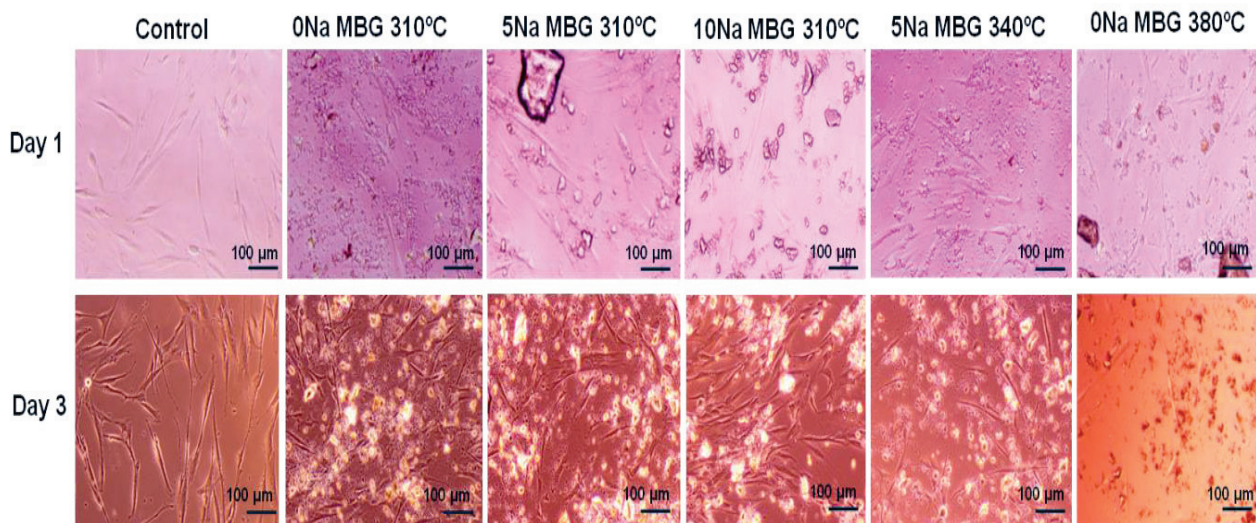


**Figure 43** Optical microscopic images of MBGs interfaced with Human gingival fibroblasts at day 1 and day 3

The optical microscopy images of the control cells and cells treated with samples at a concentration of 800ug/ml is shown in **Figure 43**. At day 1 the cells interfaced with samples show similar response to the control cells. Positively at day 3 a significant increase in cell growth is observed in 0Na MBG 310°C, 5Na MBG 310°C and 10Na MBG 310°C comparable to the control cells. However, a slight reduction in cells growth is observed in 0Na MBG treated at 340°C and a profound reduction in cells growth is observed in the 0Na MBG treated at 380°C.

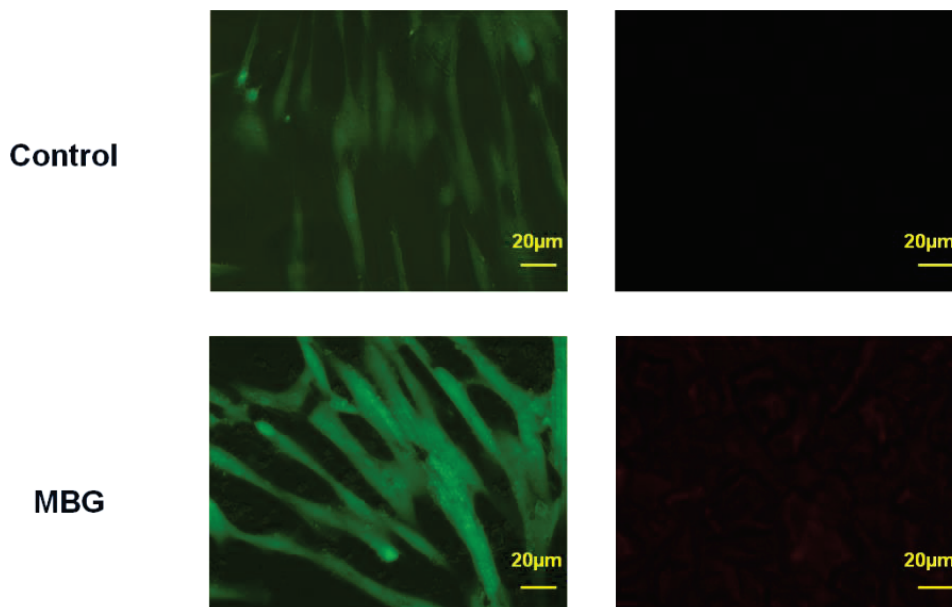


**Figure 44** Live dead images of MBGs interfaced with human gingival fibroblasts at day 3

The live dead staining was performed on all samples at day 3 (**Figure 44**). Since the results of cells treated with all MBGs were similar, the images for cells treated with 0Na MBG 310°C is shown as representative of all stained cells interfaced with MBGs. It can be seen from **Figure 44** that both control cells and cells treated with sample emitted strong green fluorescence. The Calcein-AM is a dye that is highly lyphophilic and cell membrane permeable; the dye is converted into Calcein by esterase in the cells. The calcein in the cell emits strong green fluorescence which is an indicator of viable cells. Alternatively, the Ethidium homodimer dye that stains the nucleus cannot penetrate live cells with an intact membrane as it needs damaged cell membrane to enter the cell and intercalate with the nucleus to emit red fluorescence. All cells emitting strong green fluorescence and the absence of cells emitting red fluorescence confirms that the samples are non-cytotoxic.

The metabolic activity of cells was quantified by performing Alamar blue assay (**Figure 45**). At early time points (day2), the metabolic activity of cells treated with samples were similar to the control cells.

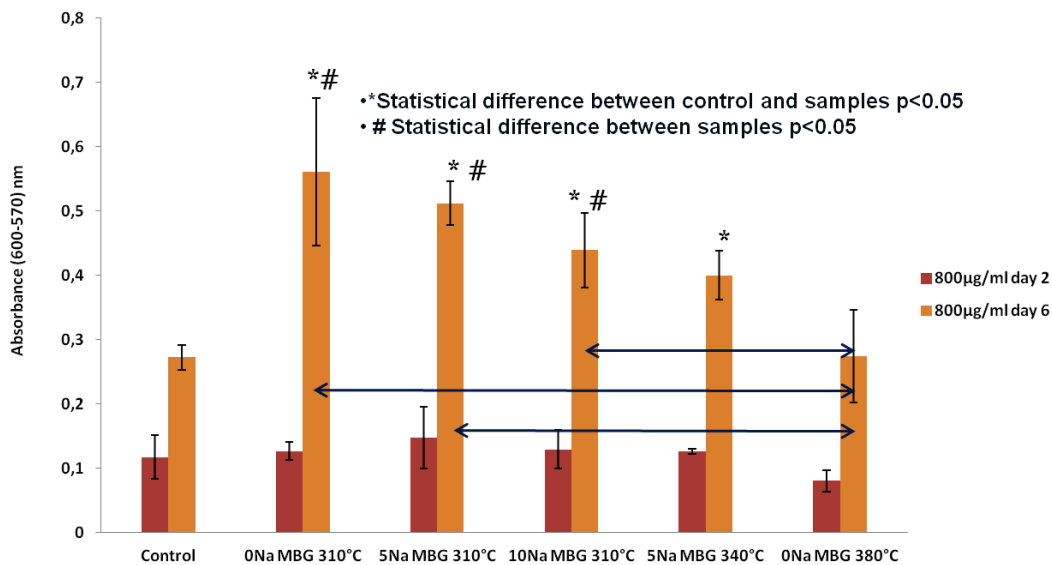


**Figure 45 Metabolic activity of human gingival fibroblasts interfaced with MBGs at day 2 and day 6**

Interestingly at day 6, cells treated with 0Na MBG 310°C, 5Na MBG 310°C, 10Na MBG 310°C expressed significantly higher metabolic activity than the control cells suggesting that these samples stimulate cell metabolic activity. Furthermore, the metabolic activity of cells treated with 0Na, 5Na and 10Na MBG thermal treated at 310°C was significantly higher than 0Na MBG 340°C and 0Na MBG

380°C. This suggests that rather than the difference in chemical composition, the thermal treatment has a profound influence of cells response. The reason for the reduction in cells growth and metabolic activity in the samples that underwent increased thermal treatment could be due to the reduction in level of calcium released from the sample as seen by ICP (**Chapter 5, Figure 6**). Nevertheless, the metabolic activity of the cells contacted 0Na MBG 380°C was not inhibited and still comparable to that of the control cells.

#### **8.4. Conclusion**

High surface area and calcium content in 0Na MBG seems to enhance calcium rich crystalline phase precipitation on the glass surface. However, apatite formation was not realised in the samples under the tested conditions. Optimization in the experimental methods and surface characteristics is suggested.

In terms of cytocompatibility, all samples were non-cytotoxic and furthermore samples treated at low temperature enhanced the metabolic activity of HGFs.

## **9. MBGs in adhesives-Particle size reduction, viscosity and apatite forming ability**

### **9.1. Introduction**

Blending the MBGs with adhesives and examining the viscosity and apatite forming ability of the material are two of the preliminary tests needed to assess if MBGs could be used as effective fillers in dentin adhesives to improve the longevity of the adhesive-dentin interface. The 0Na MBG thermally treated at 310°C has been chosen for this purpose as this sample possesses enhanced porosity, increased surface area, high calcium content and has also shown positive response both with cells (HGFs) and in forming calcium phosphate precipitate when immersed in SBF in vitro. As the adhesives or bonding resins used in a composite restoration are in general flowable resins with low viscosity, it is important to have fillers with a particle size at least less than 10µm so that the viscosity is not negatively affected. Since the MBGs studied so far (in previous chapters) had inhomogeneous size distributions ranging from less than 10 to 1000µm it was crucial to first reduce the size of the particles to less than 10µm before they are blended with the adhesive resins. As a consequence of reducing particle size by milling, the surface characteristics of the particles could change and hence it was decided to perform re-characterisation and analysis. Therefore, in this chapter we will discuss the process of reducing the particle size of the 0Na MBG, the influence of the said process on the surface characteristics of MBGs, the viscosity of the adhesives filled with MBGs and the apatite forming potential of adhesive resin pellets containing different weight percent 0Na MBG as fillers in vitro.

### **9.2. Materials and Methods**

#### **9.2.1. 0Na MBG preparation**

0Na MBG was synthesized following the exact protocol mentioned in Chapter 5, up to and including sol-gel synthesis and drying step. However, after drying at 60°C the sample was directly subjected to a 310°C thermal treatment without prior disc milling (TEMA).

#### **9.2.2. Ball milling**

Ball milling was performed on the 0Na MBG sample thermally treated at 310°C with the aim to reduce the primary particle size to less than 10µm. 72.5g of 5mm zirconia beads was added to each jar of the ball milling machine (Fritsch Pulverisette 7 premium line planetary ball mill) along with 5g of sample. Two cycles of dry milling was performed at 750rpm for 5minutes with 10 minutes pause

between each cycle to minimize temperature build-up. The milled samples were passed through a 355 micron sieve in order to separate the milled sample from the zirconia beads. Next, 100g of 1mm zirconia beads was added to each jar of the ball milling machine along with the 5 grams of previously milled sample. Milling was carried out for 2 cycles using the same speed and pause settings. Finally, 15g of ethanol was added to each jar containing the milled sample with 1mm zirconia beads and the milling was continued for 2 more cycles with the same settings (wet milling). The milled sample-ethanol slurry along with the 1mm beads was passed through a 355 micron sieve by simultaneous rinsing with ethanol to separate the zirconia beads from the slurry. The slurry was left to dry at room temperature in a fume hood for 3 days to evaporate the solvent. Finally the agglomerates were broken by a brief milling with mortar and pestle.

#### **9.2.3. Particle size measurement**

A particle size distribution analysis was performed using a Malvern laser diffraction particle size analyser on the unmilled, dry milled and wet milled samples immediately after milling. After the Master Sizer cleaning protocol had been followed, sample was added in a beaker containing 500mL of deionized water. The particle size distribution was measured and the data were collected.

#### **9.2.4. BET/BJH**

The surface area and pore volume parameters were determined by nitrogen adsorption/desorption isotherms at 77 K in a Surface area analyzer (Gemini 2385). The samples were degassed at 200°C for 4 hours prior to measurement. The Brunauer-Emmett-Teller (BET) equation was used for the specific surface area and pore volume quantification while Barret-Joyner-Halenda (BJH) was used for average pore diameter determination.

#### **9.2.5. Adhesive with MBG-Viscosity and pellet preparation**

The unfilled adhesive (Trendy bond) was obtained from Saremco, Switzerland. All preparation involving the adhesive resin was performed in a dark room as the adhesive resin is light sensitive. The adhesive was filled with 3%, 10%, 20% and 30% (weight percent) of milled 0Na MBG by manual mixing with a spatula until a homogenous mixture was obtained. The unfilled resin (0% filled) served as a control. The uncured samples (0%, 3%, 10%, 20% and 30% filled) were subjected to viscosity measurements in a Rheometer (TA, Discovery HR-2 instrument) using a parallel-plate (20mm) geometry and gap width of 500 $\mu$ m. The space between the plates was filled with material

and excess was removed. A flow sweep test was performed with shear rates ranging from 0.1 to 100s<sup>-1</sup>.

Disc-shaped adhesive pellets were prepared by adding the uncured samples to a Teflon mold (6mm in diameter and 2mm in height)sealed in between 2 glass plates and light cured with a LED curing unit (20 seconds exposure on each side of the pellet).

#### 9.2.6. Apatite forming ability

The apatite forming ability of 0% filled, 10% filled and 30% filled adhesives in SBF was assessed at 7, 14 and 21 days. SBF was prepared following the protocol mentioned in **Chapter 8, Section 8.2.2**. Each adhesive pellet was immersed in 10mL of SBF and placed in a shaker at 37°C. Triplicates were used for each material type. At respective time points the samples were taken out of the SBF rinsed with 70% acetone in water solution and dried at room temperature. The dried samples were examined using SEM imaging.

#### 9.2.7. SEM

Back Scattered Electron Imaging has been carried out on carbon coated samples using a JEOL JSM-6490LV Scanning Electron Microscope (SEM). The conditions in the SEM chambers during imaging and analysis were; High Vacuum, 10KV, working distance of 10mm.

### 9.3. Results and discussion

The particle size distribution of 0Na MBG after the sol-gel synthesis and thermal treatment is represented by **Figure 46A**. As seen in the figure the initial sample consists of a broad size distribution spanning 2-1000 microns. However, the D90 value indicates that 90 percent of the particles are less than 623µm and the D50 indicates that 50 percent is less than 177µm (**Table 9**). The dry milling of particles with 5mm and 1mm zirconia beads has considerably reduced the particle size as indicated by aD90 of 113µm and a D50 of 34µm (**Figure 46B**). Further reduction in particle size to less than 10 microns is achieved by wet milling and the target D90 of 2.97µm was achieved, indicating that 90 percent of the primary particles are less than 3 microns in the wet milled slurry (**Figure 46C**).

**Table 9 D10, D50 and D90 values 0Na MBG sample before and after milling**

<b>Samples</b>	<b>D10 (μm)</b>	<b>D50(μm)</b>	<b>D90(μm)</b>
Unmilled 0Na MBG	18	177	623
Dry ball milled 0Na MBG	7	34	113
Wet milled 0Na MBG	0.003	0.157	2.970

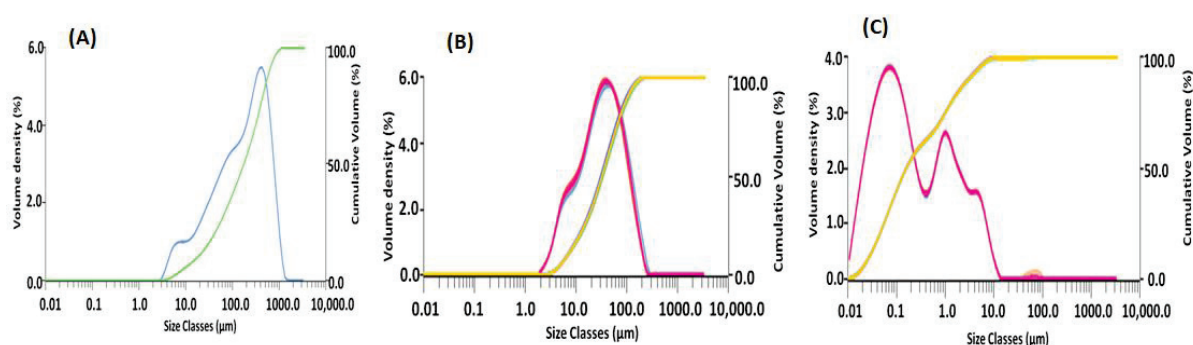


**Figure 46 Particle size distribution of 0Na MBG thermally treated at 310°C; (A) unmilled, (B) dry ball milled and (C) wet ball milled**

**Table 10 Surface area, pore volume and pore size of 0Na MBG before and after milling**

<b>Sample</b>	<b>Surface area (m<sup>2</sup>g<sup>-1</sup>)</b>	<b>Pore volume (cm<sup>3</sup>g<sup>-1</sup>)</b>	<b>Pore size (nm)</b>
0Na MBG unmilled	422	0.421	3.6
0Na MBG tema milled	365	0.268	3.3
0Na MBG dry milled	73	0.097	10.9
0Na MBG dry +wet milled	171	0.120	9.4

The changes in the surface area, pore volume and pore diameter of 0Na MBG as a result of particle size reduction are summarized in **Table 10**. Before comparing the changes in surface characteristics observed between the unmilled and ball milled samples (dry and wet) it is important to clarify the difference between the surface area characteristics of unmilled 0Na MBG and the 0Na MBG used in

previous Chapter 5, 7, 8. As seen in **Table 10** the surface area, pore volume and pore size of the 0Na MBG mentioned in previous chapters (indicated here as “TEMA milled”) is lower than the unmilled 0Na MBG sample. This is because previously the 0Na MBG was subjected to brief disc milling (TEMA) before thermal treatment. However, since the aim of this part of the thesis was to reduce the particle size before interfacing them with resin it was decided to skip the disc milling process and go ahead entirely with ball milling to reduce the particle size after thermal treatment. The reduction in pore volume and surface area between unmilled and disc milled sample (TEMA) indicates that there is a loss of porosity due to milling. This becomes more evident when the unmilled samples are subjected to coarse dry ball milling with 5mm and 1mm zirconia beads. The surface area reduces from  $422\text{m}^2\text{g}^{-1}$  to  $72.86\text{m}^2\text{g}^{-1}$  and similarly the pore volume reduces from  $0.421\text{cm}^3\text{g}^{-1}$  to  $0.097\text{cm}^3\text{g}^{-1}$ . Contrastingly, the pore size increases from  $3.6\text{nm}$  to  $10.9\text{nm}$ . Further wet milling slightly increases the surface area to  $171\text{m}^2\text{g}^{-1}$  and pore volume to  $0.12\text{cm}^3\text{g}^{-1}$  while decreasing the pore size to  $9.4\text{nm}$ .

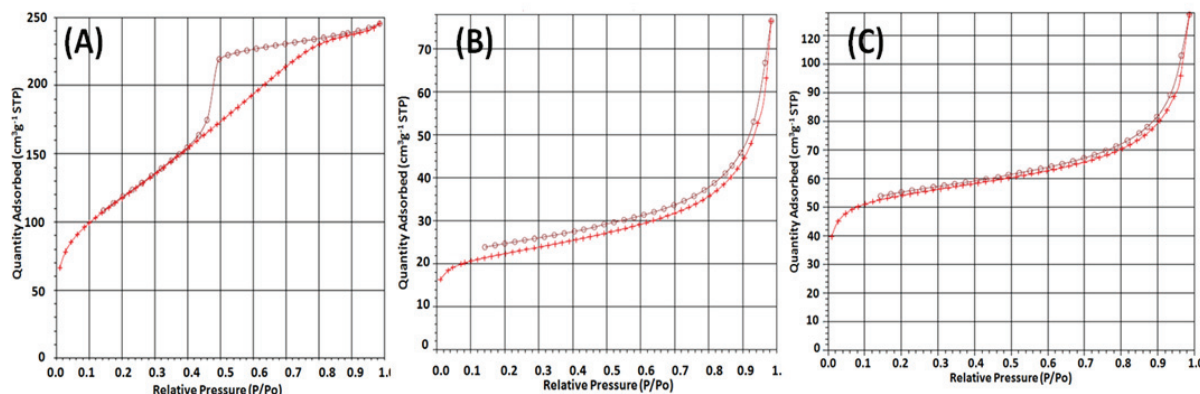


**Figure 47** Hysteresis loops of 0Na MBG thermal treated at 310°C; (A) unmilled, (B) dry ball milled and (C) wet ball milled

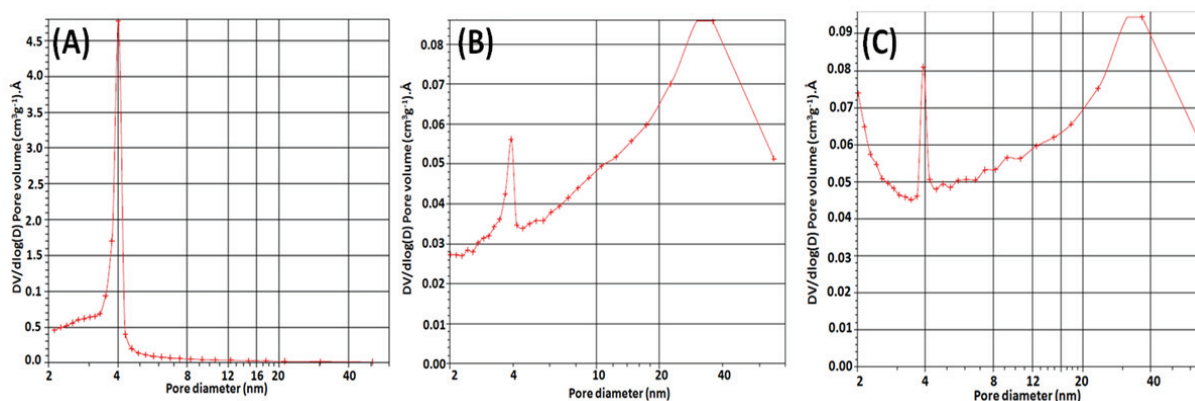


**Figure 48 Pore size distribution of 0Na MBG thermal treated at 310°C; (A) unmilled, (B) dry ball milled and (C) wet ball milled**

Examining the hysteresis loop changes of 0Na MBGs (**Figure 47**) reveals that the unmilled 0Na MBG has ink bottle and irregular shaped pores of varying size distributions (type IV isotherm, H2 hysteresis loop, **Figure 47A**). Upon ball milling the hysteresis loop changes from H2 to H5 indicating that the material mainly hosts slit shaped pores (**Figure 47B and Figure 47C**). Further analysis on the pore size distribution shows that unmilled 0Na MBG displays a tight population of 3-4nm sized pores whose differential volume is  $4.5\text{cm}^3\text{g}^{-1}\text{\AA}$  (**Figure 48A**). Interestingly, dry milling the sample drastically reduces the differential volume of 3-4nm sized pores to  $0.055\text{cm}^3\text{g}^{-1}\text{\AA}$  and induces a new population of bigger sized pores spanning from 10-40nm. Wet milling slightly increases the volume of 3-4nm sized pores to  $0.08\text{cm}^3\text{g}^{-1}\text{\AA}$  and also has a similar population of bigger sized pores.

The combined results of the surface area, pore volume, pore size, hysteresis loops and pore size distribution confirms that there is a reduction in particle porosity due to the milling process. The  $4.5\text{cm}^3\text{g}^{-1}\text{\AA}$  volume of 3-4 nm sized pores in the unmilled 0Na MBG represents the innate porosity of 0Na MBG particle. After dry and wet milling only 1.7 percent of the particle porosity seems to remain. The possible theory is that by milling the particle structure is broken down and hence the pores in the particles are opened as a result (**Figure 49**). This explains both the loss of particle porosity as well as the change of pores type from irregular/ ink bottle shape to slit shaped. As the particle size reduces it is normal that they start to agglomerate in order to reduce the surface energy which is explained by the 10-40 nm sized pores in the dry milled and wet milled samples. When compared to dry milling, wet milling with a solvent must have broken down some of the agglomerates which should explain the mild increase in pore volume, surface area and decrease in pore size after wet milling.

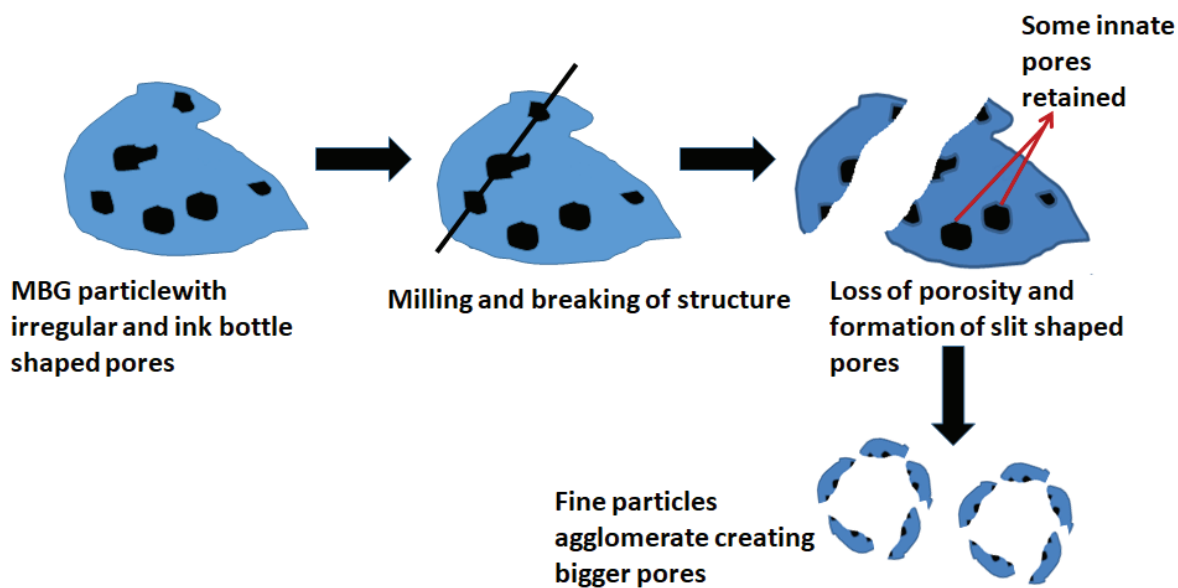


**Figure 49** Impact of milling on loss of particle porosity, change of pore structure and size.

Initially porosity, high surface area and calcium content promoting better reactivity (calcium phosphate precipitate in SBF) were the attractive attributes of 0Na MBG to be used as fillers in dentin adhesive resins. Moreover, porous fillers are also advantageous because the pores could be functionalised with antibacterial drugs or growth factors to combat secondary caries / promote cell-mediated mineralization. Reduction of particle size was mandatory in order to ensure that viscosity of the adhesive resin is still in the acceptable range with the fillers inside. But, this heightened loss of porosity as a result of milling is quite a drawback for these particles as it seems that by achieving the fine particle size we lose a majority of the pores.

Future work should focus on alternative processing to reduce the particle size of such glasses whilst preserving the original porosity. Alternatively, may be spray pyrolysis processing as achieved by Shih *et al.*, [191] could be employed. It is perhaps also possible that particles can still be used in composite resins in the unmilled form (highly porous) to remineralize the underlying tissue as composite resins tend to be a more viscous paste. Nevertheless, these particles even after milling still retain some of their innate porosity. Even though it is only 1.7 percent compared to the porosity of the same unmilled particle we still do not know the significance of this level of porosity compared to other porous bioactive glasses with controlled particle size in literature. This aspect also needs to be studied in future work.

The viscosity of the adhesive resin filled with milled 0Na MBG at varying weight fractions is indicated in **Figure 50**. We observe that viscosity of the resin with 3 weight percent of fillers is similar to the unfilled control and at 10 weight percent there is a slight increase in viscosity that still, nevertheless, offers a flowable consistency appropriate for an adhesive resin. Increasing the filler content to 20 percent generates a steep increase in viscosity and the material turns into a paste, the same holds true for 30 percent filled resins.

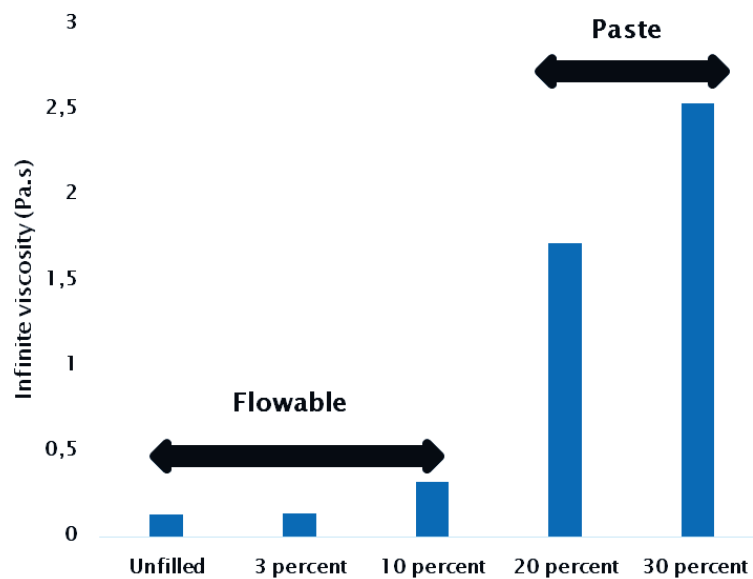


**Figure 50** Viscosity of unfilled commercial resin with varying weight percent of 0Na MBG

The shear rate vs viscosity data of the filled and unfilled samples in general shows that the viscosity decreases with increasing shear rate. This is normal as shearing breaks down agglomerates and enhances the dispersity of the particles in the resin. Tauback *et al.*, [192] performed a similar study by incorporating nanosized bioactive glasses in adhesive resin at 10 and 20 weight percent concentration and compared the viscosity with commercial adhesive and composite resins with similar shear rates. Comparing our data with their results we can see that at high shear rates ( $10s^{-1}$  and  $100s^{-1}$ ) the viscosity of the 30 percent filled sample (**Table 11**) in this study is much lower than their 10 and 20 percent filled samples. Moreover, it was also about 5 times lower than Filtex supreme XTE flowable restorative (commercial composite resin). Furthermore the 10 percent filled samples viscosity value (**Table 11**) from this study is also lower than Heliobond commercial adhesive resins based on their data. Although the absolute values cannot be compared as they vary

based on the measurement setting (gap width, rotation rate etc.), these results are quite encouraging as the viscosity range of 10 percent filled resin with 0Na MBG seems comparable to the commercial adhesives.

**Table 11** viscosity vs shear rate of unfilled commercial resin with varying weight percent of 0Na MBG

Shear rate (s <sup>-1</sup> )	Viscosity (Pa.s) (0 percent)	Viscosity (Pa.s) (3 percent)	Viscosity (Pa.s) (10 percent)	Viscosity (Pa.s) (20 percent)	Viscosity (Pa.s) (30 percent)
0.01	0.943	0.362	414	1049	3192
0.1	0.171	0.234	91.180	149.430	315.290
1	0.142	0.200	6.558	31.140	57.4000
10	0.128	0.147	0.597	4.831	8.721
100	0.129	0.145	0.301	2.145	3.131

Finally, the outcome of an apatite-forming ability test performed on 0 percent, 10 percent and 30 percent filled adhesive resin pellets dispersed in SBF is shown in **Figure 51**. At day 0, before immersing the samples in SBF, the visual difference in samples due to filler content among the samples is very evident. Unexpectedly, after immersing in SBF up to 21 days there was no calcium phosphate precipitate or apatite layer observed on any of the samples. Only a few specs of salt precipitation were observed in the SEM images of these samples. At first the results seemed disappointing but after taking a step back and verifying the methodology of this part we noticed that there was an evident problem with the sample concentration (surface area of the sample to SBF volume ratio).

In general there is no ISO standard test defined for apatite-forming ability in dental adhesives. In this test we immersed each sample pellet (6mm in diameter and 2mm in height) in 10mL of SBF which closely matches with the surface area to volume ratio specifications mentioned in ISO 23317. ISO 23317 is a general standard for in vitro apatite forming ability of implant materials. It specifies that the  $V=100S_a$ , which means the volume of SBF (mm<sup>3</sup>) should be 100 times the surface area (mm<sup>2</sup>) of the specimen. However, it is very general and does not differentiate between specimens made completely out of supposed bioactive material (bioactive glass pellet) and specimens containing bioactive material entrapped in a matrix (bioactive glasses in degradable material, resin based composites or adhesives) which greatly changes the bioavailability of the ions and in turn the

potential bioactive response. For instance if the entire specimen is made out of bioactive glass it is obvious that a high concentration of ions will be released from the specimen to saturate the SBF in comparison to a composite or adhesive specimen containing only 20 or 30 percent of bioactive glass. Besides the lower concentration of the bioactive material in the specimen it should also be noted that they will be entrapped in a highly hydrophobic matrix which not only makes their contact with SBF an indirect one but also impacts the ion release kinetics. Moreover, we know that restorative composites are in general 70 percent filled with filler such as silica, barium, strontium glass including bioactive particles which means that the particles are bound by only 30 percent of resin matrix. It is not the same for dental adhesives which are mostly unfilled or have less than 20 percent of fillers. Therefore the particles are bound by 80 percent of resin matrix in the specimen. This highly reduces the level of ions releasable from a bioactive glass-filled adhesive specimen in comparison to bioactive glass-filled restorative composites even if they have the same bioactive glass concentration present.

Therefore using the ISO standard 23317 for all scenarios does not seem logical. In our adhesive samples the low wt% MBG content is likely to mean an insufficient concentration of ions were released to supersaturate the SBF and to realise a calcium phosphate precipitate or apatite formation. Other articles in the literature that have tested the apatite forming ability of bioactive material (bioactive glass or amorphous calcium phosphate) in an adhesive resin or composite have not followed ISO 23317 and used a range of specimen dimensions, type of solution (SBF, PBS, artificial saliva) and concentration. For instance Tauback *et al.*, used specimen dimension (6mm diameter, 2mm height) similar to our study but immersed 1 pellet in 1mL of PBS. Whereas Chatzistavrou *et al.*, immersed 3 specimens of bigger dimension (10mm diameter, 2mm height and hence increased surface area per specimen by 2.3 times) in 30ml of SBF. Overall it is clear that in the previous studies (**Table 12**) where ion release or calcium phosphate/apatite formation has been demonstrated when investigating resin-based materials containing bioactive particles, either each pellet is immersed in 1 or 2mL of media or 3 pellets (increased dimension) are immersed in 30-50mL of media. This indicates that the 1 pellet in 10mL used in this study is not sufficient to supersaturate the contact media to realise any precipitate. Therefore the apatite forming ability test of adhesive resin containing 10 and 30 percent filler content should be repeated by immersing each pellet in 1mL of SBF to comment on the apatite forming ability of these samples.

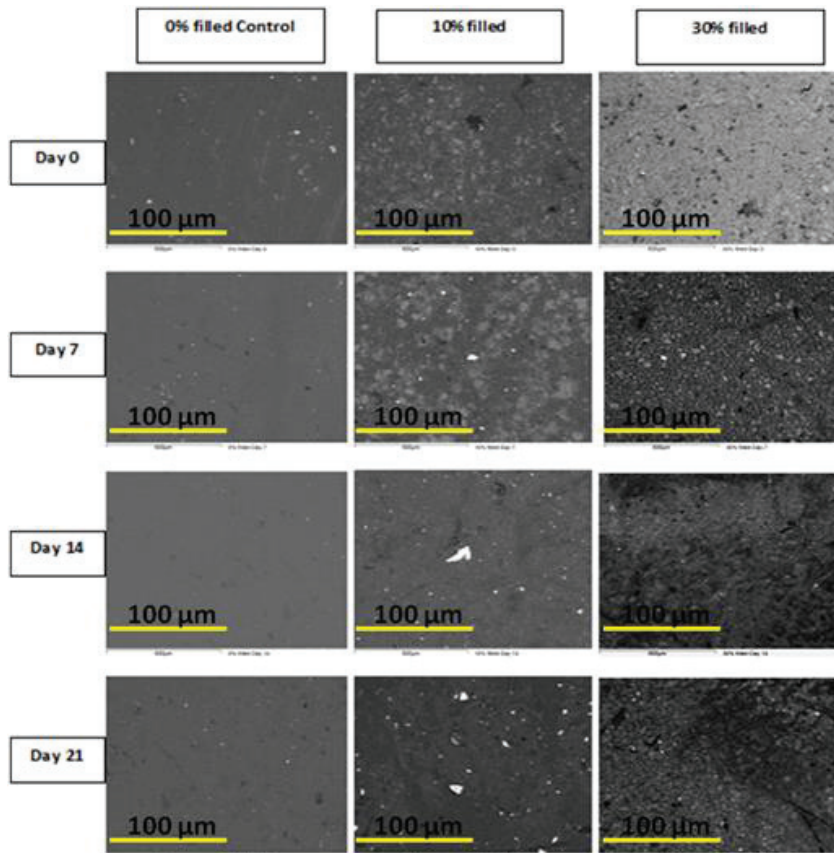


Figure 51 SEM images of 0%, 10% and 30% filled adhesive resin immersed in SBF upto 21 days

Table 12 Filler type, characteristics, media and concentration of bioactive particles containing resins in literature

Articles	Filler type	Particle size	Specimen dimension and filler content	Media	Concentration
Carneiro <i>et al.</i> , 2017[193]	Melt quench Niobium bioactive glass	<20 microns	Disc 5mm diameter 1mm height 30% filled	PBS 28 days	Not mentioned
Rizk <i>et al.</i> , 2017[194]	45S5 bioactive glass with bismuth  POSS particle	Nano sized BG  POSS particles	1 wt% BG And 10wt% POSS adhesive 6mm in diameter and 2mm height	Artificial saliva or deionised water	3 pellets in 15 ml
Xiao <i>et al.</i> ,	ACP	116nm	2x2x25mm	Artificial	1 specimen in

2017[195]			mold 30% ACP filled composite	saliva , Lactic acid	1ml
Chatzistavrou <i>et al.</i> , 2015[196]	Sol gel Bioactive glass	25microns	10mm diameter, 2mm height  5, 10 and 15% filled	SBF	3 specimens in 30ml
Taubock <i>et al.</i> , 2014[192]	Flame spray Bioactive glass	30-50nm	6mm diameter, 2mm height 10, 20% filled	PBS	1sample in 1ml
Xie <i>et al.</i> , 2017[197]	ACP	116nm	8mm diameter, 0.5mm height	Mc Bain artificial saliva growth medium	1 sample in 1.5ml

#### 9.4. Conclusion

Preparation of primary powder particle sizes of less than 3microns suitable for use as a filler in adhesive has been achieved by ball milling the 0Na MBG sample using dry and then wet conditions. However, reduction of particle size in turn drastically reduces the innate porosity which in turn affects their surface characteristics. The viscosity of 10 percent filled 0Na MBG resin seems comparable with commercial adhesive resin. Optimisation of surface area of specimen to SBF volume ratio is needed to evaluate the apatite forming ability of adhesives containing 0Na MBG.

## 10. Conclusion

The goal of this research work was to fabricate novel mesoporous bioactive glasses and explore their physico-chemical characteristics and biological behaviour in order to evaluate their potential to be used as fillers in dental adhesives. Most MBGs reported in the literature are prepared in very small quantities (less than 4g) which seems insufficient even for complete material characterization from the same batch. We aimed to prepare MBGs with varying network modifier (CaO: Na<sub>2</sub>O) content at a small (10g) and large scale (50g) in order to study the effect of scale up on the surface characteristics. The main filler characteristics and initial target outcomes were:

- To obtain MBGs with high porosity, ordered pore structure and increased surface area.
- To achieve the above characteristics in compositions with sufficient calcium oxide content to enhance their biological behaviour.
- To create fillers that are capable of forming apatite as well as being non-cytotoxic to oral cells in vitro.
- To optimise the particle size of MBGs to be used as fillers in adhesives and identify the optimal concentration of fillers in adhesive resins that is sufficient to induce an appropriate biological response without adversely affecting the viscosity of the dental adhesive.
- To realise apatite formation on the adhesive containing MBGs when immersed in SBF.

These objectives were individually studied and the results have been discussed in the Chapters 3 to 9. In this chapter the main findings from each chapter are brought together to draw overall conclusions.

In chapter 3 the preparation of novel MBGs by a sol-gel process using various precursors has been detailed. Initial experiments to prepare MBGs with nitrate precursors led to carbon entrapment problems after thermal treatment. The possible reasons identified were the combination of composition, improper decomposition of surfactant, glass crystallization and the high temperature needed for stabilization. Acetate-based precursors seemed most suitable for synthesis of MBGs at low temperatures and therefore, with the aid of DSC/TGA appropriate thermal treatment temperatures were identified and MBGs were thus prepared in small (10g) and large scale (50g). Large scale samples appeared whiter than small scale samples without any carbon entrapment.

In chapter 4 the influence of preparation scale on the surface characteristics of MBGs with varying network modifiers ratio (CaO: Na<sub>2</sub>O) was examined. Thermal treatment led to the formation of calcite

phase and the level of crystallization was higher in small scale samples compared to large scale. The large scale samples also had increased porosity versus small scale samples. However as the small scale samples experienced increased thermal treatment compared to large scale sample (based on DSC/TGA) the increase in crystallinity and decrease in porosity seems to be an effect of thermal treatment and not the scale. Nevertheless, the large scale preparation is more advantageous in terms of quantity, colour and surface characteristics in comparison to small scale samples.

In chapter 5 the influence of varying network modifiers (CaO: Na<sub>2</sub>O) on the surface characteristics of large scale MBGs prepared in an acetate based sol-gel system was examined. In all cases the target composition was reached as confirmed by XRF characterization. Fast gelling of acetate based sol-gel system lead to deposition of network modifying precursors on the sample surface which needed subsequent thermal treatment for their entry into the sol-gel glass structure. The level of calcite phase after thermal treatment, surface area and pore volume increased with increasing CaO content in the composition. The calcite phase was a result of decomposition of the calcium precursor. Increased thermal treatment lead to a decrease in ions released from the samples. Nevertheless MBG samples with high porosity, enhanced surface area coupled with high CaO content were obtained. However, ordered porosity was not achieved in any of the MBGs.

In chapter 6 the reason for increase in porosity with increasing CaO as opposed to Na<sub>2</sub>O content was explored in more depth. As the acetate system creates fast gelling and so deposition of network modifying precursors on the sample surface, we questioned if the order of precursor addition in an acetate based sol-gel system can influence the porosity of the glasses. We had already observed that the composition plays a dominant role in influencing the porosity however, for a fixed composition we also found that the porosity can be affected by modulating the order of precursor addition during sol-gel synthesis. Pre-mixing the network modifying precursors and adding them together enhances the porosity and homogeneity of the MBGs.

In chapter 7 efforts taken to achieve ordered porosity in MBGs by increasing the surfactant concentration and exploring it's effect on the surface characteristics were discussed. Increasing the surfactant concentration seemed to enhance the solubility of calcium precursor during the sol-gel process and hence there was an increase in the rate of entry and decomposition of the calcium precursor. Ordered porosity could not be achieved in this system even with an increase in surfactant

concentration of up to 16 weight percent of glass precursors. Interestingly, MBGs with high sodium content display a drastic increase in pore size and changes in pore shape in comparison to MBGs with high calcium content suggesting that the network modifiers influence the surfactants interaction in a sol-gel system.

In chapter 8 the in vitro apatite forming ability of the MBGs in SBF and the cytocompatibility of MBGs on human gingival fibroblasts were studied. MBG with high calcium content that had increased surface area and porosity demonstrated enhanced calcium phosphate phase formation in SBF as opposed to high sodium MBG where crystalline calcium phosphate phase could not be determined. Interestingly, the level of calcium phosphate crystallinity and crystal size for the same sample type seemed to vary based on the bulk sample quantity in the SBF though the concentration was the same. However, neither MBG showed hydroxyapatite formation in SBF under the tested conditions. On the other hand all samples were non-cytotoxic and samples thermally treated at lower temperatures enhanced the metabolic activity of human gingival fibroblasts.

In chapter 9 the primary particle size of the MBG sample with high calcium content was reduced to less than 3 microns to make it suitable to be used as fillers in adhesive resin. The reduction of particle size of this sample by planetary ball milling led to a huge decrease in the porosity compared to its unmilled form, due to the breaking of the particle structure. However 1.7 percent of particle porosity remained and its significance compared to other existing porous particles in the literature with controlled particle size needs to be verified. Adhesive resins filled with 10 percent of milled MBG displayed optimal viscosity suitable for the purpose. ISO standard 23317 did not seem appropriate to evaluate the apatite forming ability of MBG filled adhesive pellets and repetition of this evaluation with optimisation of the surface area of specimen to volume ratio of SBF has been suggested.

The results obtained have been graded based on the outcomes expected at the commencement of this research. “A” means fully achieved, “B” means partially achieved and “C” denotes not achieved.

<b>Expected</b>	<b>Achievement grade</b>	<b>Comments</b>
High porosity	A	Achieved in 0Na MBG
Increased surface area	A	Achieved in 0Na MBG

Ordered pore structure	C	Not achieved in any of the MBGs
High porosity + increased surface area + ordered pore structure + high calcium content	B	MBG with increased surface area, high porosity and calcium content has been obtained but not with ordered pore structure.
Fillers with apatite forming ability	B	0Na MBG demonstrated enhanced calcium phosphate phase with a seeming potential for apatite under altered conditions.
Fillers that are non-cytotoxic and enhance cell response	A	All fillers were non-cytotoxic and fillers treated at low temperatures enhanced the metabolic activity of HGFs.
MBGs with optimised particle size to be used as fillers in adhesive resins	B	0Na MBG particle size has been reduced to less than 3 microns but it has an adverse impact on the porosity
Optimal concentration of fillers in adhesive resin without affecting the viscosity	A	Adhesive filled with 10 weight percent of milled 0Na MBG possessed optimal viscosity.
Apatite forming ability of adhesive pellets filled with MBGs	-	Needs to be verified with optimised test conditions.

Most of the outcomes aimed for have been achieved completely or partially except for the ordered porosity. Nevertheless, MBGs with high surface area, calcium content, porosity, and fine particle size have been obtained. Furthermore the MBG filler leads to enhanced calcium phosphate phase formation when immersed in SBF in vitro and also promoted the metabolic activity of Human gingival fibroblasts. The viscosity of the dental adhesive prepared with milled MBG filler was maintained at suitable levels for application by a dentist with up to 10 percent of filler content. Overall, the MBG fillers possess interesting characteristics for use as fillers in adhesive resins. Further research is needed to evaluate their potential to protect and enhance the adhesive-dentin interface by sealing the dentin tubules to prevent water penetration and also through remineralization.

### 10.1. Future perspectives

Though the research work for this thesis ends here, the research opportunities continue....

The ONa MBG will be subjected for further evaluation to assess their potential to improve the longevity of the adhesive-dentin interface.

- First, the apatite forming ability test for the adhesives filled with ONa MBGs at concentrations of 10 and 30 weight percent will be re-evaluated with optimised surface area to SBF volume.
- Next, the MBG fillers will be interfaced with acid etched bovine dentine by direct contact (MBG particles mixed in de-ionised water as a paste and applied on acid etched dentine followed by the application of an adhesive resin) and indirect contact (resin filled with 10 percent MBG will be applied on the acid etched dentine). SEM images will be taken. The aim here is to evaluate and choose the right contact method for further evaluation. The advantage of direct contact is that the fillers form a layer on the etched dentin (replacing water molecules) which could protect the collagen from degradation. Furthermore, the layer could also seal the dentinal tubules and minimise water penetration which in turn will reduce the water up take (water trees) by the resin tags. Direct contact should also favour the fillers to rapidly form calcium phosphate precipitate/ apatite formation at the interface by interacting with the dentinal fluids in comparison to MBG as fillers in adhesives (indirect contact) as the MBGs contact with the fluid to facilitate ion exchange will be minimised. However, it is crucial to evaluate by SEM imaging if in the direct contact the resin is still able to penetrate the dentinal tubules to form resin tags or if the particles are too large to occlude the tubules and obstruct the resin penetration. If the resin penetration is impeded by the particles this would severely affect the mechanical properties such as the bond strength of the resin to the dentin. Therefore in this case indirect contact should be the pragmatic approach to perform further evaluations.
- Once the contact method is decided, based on the outcomes of the SEM analysis, then the sealing of the tubules from water penetration and remineralizing ability of the MBG fillers at the resin dentin interface will be evaluated.
- Furthermore, the MBG filler will be subjected to cell tests with cementoblasts and pulp stem cells to evaluate their potential to induce cell-mediated mineralization.

- Besides the targeted application, the developed MBG can also be subjected for evaluation in other applications such as ion releasing material in dentrifices and implant coatings.

## 11. References

- [1] Takahashi N, Nyvad B. Caries ecology revisited: microbial dynamics and the caries process. *Caries Res* 2008;42:409–18. doi:10.1159/000159604.
- [2] González-Cabezas C. The Chemistry of Caries: Remineralization and Demineralization Events with Direct Clinical Relevance. *Dent Clin* 2010;54:469–78. doi:10.1016/j.cden.2010.03.004.
- [3] Axelsson P. Diagnosis and risk prediction of dental caries. vol. 2. Chicago : Quintessence Pub. Co., United States c2000;2:207
- [4] Gugnani N, Pandit IK, Gupta M, Josan R. Caries infiltration of noncavitated white spot lesions: A novel approach for immediate esthetic improvement. *Contemp Clin Dent* 2012;3:S199–202. doi:10.4103/0976-237X.101092.
- [5] Cunha-Cruz J, Stout JR, Heaton LJ, Wataha JC. Dentin Hypersensitivity and Oxalates. *J Dent Res* 2011;90:304–10. doi:10.1177/0022034510389179.
- [6] Davari A, Ataei E, Assarzadeh H. Dentin Hypersensitivity: Etiology, Diagnosis and Treatment; A Literature Review. *J Dent* 2013;14:136–45.
- [7] García AH, Lozano MAM, Vila JC, Escribano AB, Galve PF. Composite resins. A review of the materials and clinical indications. *Med Oral Patol Oral Cir Bucal* 2006;11:E215–220.
- [8] Miyazaki M, Tsujimoto A, Tsubota K, Takamizawa T, Kurokawa H, Platt JA. Important compositional characteristics in the clinical use of adhesive systems. *J Oral Sci* 2014;56:1–9.
- [9] Eick JD, Cobb CM, Chappell RP, Spencer P, Robinson SJ. The dentinal surface: its influence on dentinal adhesion. Part I. *Quintessence Int Berl Ger* 1985 1991;22:967–77.
- [10] Erickson RL. Surface interactions of dentin adhesive materials. *Oper Dent* 1992;Suppl 5:81–94.

- [11] Spencer P, Jonggu Park QY, Misra A, Bohaty BS, Singh V, Parthasarathy R, et al. Durable bonds at the adhesive/dentin interface: an impossible mission or simply a moving target? *Braz Dent Sci* 2012;15:4–18.
- [12] Nakabayashi N, Ashizawa M, Nakamura M. Identification of a resin-dentin hybrid layer in vital human dentin created in vivo: durable bonding to vital dentin. *Quintessence Int Berl Ger* 1985 1992;23:135–41.
- [13] Reis A, Carrilho M, Breschi L, Loguercio AD. Overview of clinical alternatives to minimize the degradation of the resin-dentin bonds. *Oper Dent* 2013;38:E1–25. doi:10.2341/12-258-LIT.
- [14] Habib E, Wang R, Wang Y, Zhu M, Zhu XX. Inorganic Fillers for Dental Resin Composites: Present and Future. *ACS Biomater Sci Eng* 2016;2:1–11. doi:10.1021/acsbomaterials.5b00401.
- [15] Mousavinasab SM. Effects of Filler Content on Mechanical and Optical Properties of Dental Composite Resin. *Met Ceram Polym Compos Var Uses* 2011. doi:10.5772/21405.
- [16] Mjör IA, Dahl JE, Moorhead JE. Age of restorations at replacement in permanent teeth in general dental practice. *Acta Odontol Scand* 2000;58:97–101.
- [17] Opdam NJM, Bronkhorst EM, Roeters JM, Loomans BAC. A retrospective clinical study on longevity of posterior composite and amalgam restorations. *Dent Mater Off Publ Acad Dent Mater* 2007;23:2–8. doi:10.1016/j.dental.2005.11.036.
- [18] Ito S, Hashimoto M, Wadgaonkar B, Svizero N, Carvalho RM, Yiu C, et al. Effects of resin hydrophilicity on water sorption and changes in modulus of elasticity. *Biomaterials* 2005;26:6449–59. doi:10.1016/j.biomaterials.2005.04.052.
- [19] Yoshida E, Uno S, Nodasaka Y, Kaga M, Hirano S. Relationship between water status in dentin and interfacial morphology in all-in-one adhesives. *Dent Mater Off Publ Acad Dent Mater* 2007;23:556–60. doi:10.1016/j.dental.2006.03.014.

- [20] Tay FR, Pashley DH. Have dentin adhesives become too hydrophilic? *J Can Dent Assoc* 2003;69:726–31.
- [21] Feitosa VP, Leme AA, Sauro S, Correr-Sobrinho L, Watson TF, Sinhoreti MA, et al. Hydrolytic degradation of the resin–dentine interface induced by the simulated pulpal pressure, direct and indirect water ageing. *J Dent* 2012;40:1134–43. doi:10.1016/j.jdent.2012.09.011.
- [22] Tay FR, Hashimoto M, Pashley DH, Peters MC, Lai SCN, Yiu CKY, et al. Aging affects two modes of nanoleakage expression in bonded dentin. *J Dent Res* 2003;82:537–41. doi:10.1177/154405910308200710.
- [23] Breschi L, Mazzoni A, Ruggeri A, Cadenaro M, Di Lenarda R, De Stefano Dorigo E. Dental adhesion review: aging and stability of the bonded interface. *Dent Mater Off Publ Acad Dent Mater* 2008;24:90–101. doi:10.1016/j.dental.2007.02.009.
- [24] Jacobsen T, Söderholm KJ. Some effects of water on dentin bonding. *Dent Mater Off Publ Acad Dent Mater* 1995;11:132–6. doi:10.1016/0109-5641(95)80048-4.
- [25] Ferracane JL. Hygroscopic and hydrolytic effects in dental polymer networks. *Dent Mater Off Publ Acad Dent Mater* 2006;22:211–22. doi:10.1016/j.dental.2005.05.005.
- [26] Santerre JP, Shajii L, Leung BW. Relation of dental composite formulations to their degradation and the release of hydrolyzed polymeric-resin-derived products. *Crit Rev Oral Biol Med Off Publ Am Assoc Oral Biol* 2001;12:136–51.
- [27] Soares CJ, Faria-E-Silva AL, Rodrigues M de P, Vilela ABF, Pfeifer CS, Tantbirojn D, et al. Polymerization shrinkage stress of composite resins and resin cements - What do we need to know? *Braz Oral Res* 2017;31:e62. doi:10.1590/1807-3107BOR-2017.vol31.0062.
- [28] Malhotra N, Kundabala M, Shashirashmi A. Strategies to overcome polymerization shrinkage--materials and techniques. A review. *Dent Update* 2010;37:115–8, 120–2, 124–5.

- [29] Ito S, Tay FR, Hashimoto M, Yoshiyama M, Saito T, Brackett WW, et al. Effects of multiple coatings of two all-in-one adhesives on dentin bonding. *J Adhes Dent* 2005;7:133–41.
- [30] Pashley EL, Agee KA, Pashley DH, Tay FR. Effects of one versus two applications of an unfilled, all-in-one adhesive on dentine bonding. *J Dent* 2002;30:83–90.
- [31] Hashimoto M, Sano H, Yoshida E, Hori M, Kaga M, Oguchi H, et al. Effects of multiple adhesive coatings on dentin bonding. *Oper Dent* 2004;29:416–23.
- [32] Brackett WW, Ito S, Tay FR, Haisch LD, Pashley DH. Microtensile dentin bond strength of self-etching resins: effect of a hydrophobic layer. *Oper Dent* 2005;30:733–8.
- [33] Pashley DH, Tay FR, Yiu C, Hashimoto M, Breschi L, Carvalho RM, et al. Collagen degradation by host-derived enzymes during aging. *J Dent Res* 2004;83:216–21. doi:10.1177/154405910408300306.
- [34] Scaffa PMC, Vidal CMP, Barros N, Gesteira TF, Carmona AK, Breschi L, et al. Chlorhexidine inhibits the activity of dental cysteine cathepsins. *J Dent Res* 2012;91:420–5. doi:10.1177/0022034511435329.
- [35] Thompson JM, Agee K, Sidow SJ, McNally K, Lindsey K, Borke J, et al. Inhibition of endogenous dentin matrix metalloproteinases by ethylenediaminetetraacetic acid. *J Endod* 2012;38:62–5. doi:10.1016/j.joen.2011.09.005.
- [36] Golub LM, Ramamurthy NS, McNamara TF, Greenwald RA, Rifkin BR. Tetracyclines inhibit connective tissue breakdown: new therapeutic implications for an old family of drugs. *Crit Rev Oral Biol Med Off Publ Am Assoc Oral Biol* 1991;2:297–321.
- [37] Acharya MR, Venitz J, Figg WD, Sparreboom A. Chemically modified tetracyclines as inhibitors of matrix metalloproteinases. *Drug Resist Updat Rev Comment Antimicrob Anticancer Chemother* 2004;7:195–208. doi:10.1016/j.drug.2004.04.002.

- [38] Hao JL, Nagano T, Nakamura M, Kumagai N, Mishima H, Nishida T. Galardin inhibits collagen degradation by rabbit keratocytes by inhibiting the activation of pro-matrix metalloproteinases. *Exp Eye Res* 1999;68:565–72. doi:10.1006/exer.1998.0637.
- [39] Han B, Jaurequi J, Tang BW, Nimni ME. Proanthocyanidin: a natural crosslinking reagent for stabilizing collagen matrices. *J Biomed Mater Res A* 2003;65:118–24. doi:10.1002/jbm.a.10460.
- [40] Niu L, Zhang W, Pashley DH, Breschi L, Mao J, Chen J, et al. Biomimetic remineralization of dentin. *Dent Mater Off Publ Acad Dent Mater* 2014;30. doi:10.1016/j.dental.2013.07.013.
- [41] Sauro S, Pashley DH. Strategies to stabilise dentine-bonded interfaces through remineralising operative approaches-State of The Art. *Int J Adhes Adhes* 2016. doi:10.1016/j.ijadhadh.2016.03.014.
- [42] Jones JR. Review of bioactive glass: From Hench to hybrids. *Acta Biomater* 2013;9:4457–86. doi:10.1016/j.actbio.2012.08.023.
- [43] Hench LL. Chronology of Bioactive Glass Development and Clinical Applications. *New J Glass Ceram* 2013;03:67. doi:10.4236/njgc.2013.32011.
- [44] Combes C, Rey C. Amorphous calcium phosphates: Synthesis, properties and uses in biomaterials. *Acta Biomater* 2010;6:3362–78. doi:10.1016/j.actbio.2010.02.017.
- [45] Gurunathan D, Somasundaram S, Kumar S. Casein phosphopeptide-amorphous calcium phosphate: a remineralizing agent of enamel. *Aust Dent J* 2012;57:404–8. doi:10.1111/adj.12006.
- [46] Zhao J, Liu Y, Sun W, Yang X. First detection, characterization, and application of amorphous calcium phosphate in dentistry. *J Dent Sci* 2012;7:316–23. doi:10.1016/j.jds.2012.09.001.
- [47] Rivera-Muñoz EM. Hydroxyapatite-Based Materials: Synthesis and Characterization. *Biomed Eng - Front Chall* 2011. doi:10.5772/19123.

- [48] Abdel-Fattah WI, Reicha FM, Elkhooly TA. Nano-beta-tricalcium phosphates synthesis and biodegradation: 1. Effect of microwave and  $\text{SO}_4^{2-}$  ions on  $\beta$ -TCP synthesis and its characterization. *Biomed Mater* 2008;3:034121. doi:10.1088/1748-6041/3/3/034121.
- [49] Hench LL, Splinter RJ, Allen WC, Greenlee TK. Bonding mechanisms at the interface of ceramic prosthetic materials. *J Biomed Mater Res* 1971;5:117–41. doi:10.1002/jbm.820050611.
- [50] Vichery C, Nedelec J-M. Bioactive Glass Nanoparticles: From Synthesis to Materials Design for Biomedical Applications. *Materials* 2016;9:288. doi:10.3390/ma9040288.
- [51] Kaur G, Pickrell G, Sriranganathan N, Kumar V, Homa D. Review and the state of the art: Sol-gel and melt quenched bioactive glasses for tissue engineering. *J Biomed Mater Res B Appl Biomater* 2016;104:1248–75. doi:10.1002/jbm.b.33443.
- [52] Abbasi Z, Bahrololoom M, Shariat MH, Bagheri R. Bioactive Glasses in Dentistry: A Review. *J Dent Biomater* 2015;2:1–9.
- [53] Zhong J, Greenspan DC. Processing and properties of sol-gel bioactive glasses. *J Biomed Mater Res* 2000;53:694–701.
- [54] Zheng K, Boccaccini AR. Sol-gel processing of bioactive glass nanoparticles: A review. *Adv Colloid Interface Sci* 2017;249:363–73. doi:10.1016/j.cis.2017.03.008.
- [55] School of Dentistry, 1011 North University, Ann Arbor, MI, 48109, USA, Wang Y-Y, Chatzistavrou X, Faulk D, Badylak S, Zheng L, et al. Biological and bactericidal properties of Ag-doped bioactive glass in a natural extracellular matrix hydrogel with potential application in dentistry. *Eur Cell Mater* 2015;29:342–55. doi:10.22203/eCM.v029a26.
- [56] Bühner G, Rottensteiner U, Hoppe A, Detsch R, Dafinova D, Fey T, et al. Evaluation of in vivo angiogenic effects of copper doped bioactive glass scaffolds in the AV loop model. *Biomed Glas* 2016;2. doi:10.1515/bglass-2016-0013.

- [57] Bejarano J, Detsch R, Boccaccini AR, Palza H. PDLLA scaffolds with Cu- and Zn-doped bioactive glasses having multifunctional properties for bone regeneration. *J Biomed Mater Res A* 2017;105:746–56. doi:10.1002/jbm.a.35952.
- [58] Bejarano J, Caviedes P, Palza H. Sol-gel synthesis and in vitro bioactivity of copper and zinc-doped silicate bioactive glasses and glass-ceramics. *Biomed Mater Bristol Engl* 2015;10:025001. doi:10.1088/1748-6041/10/2/025001.
- [59] Vernè E, Nunzio SD, Bosetti M, Appendino P, Vitale Brovarone C, Maina G, et al. Surface characterization of silver-doped bioactive glass. *Biomaterials* 2005;26:5111–9. doi:10.1016/j.biomaterials.2005.01.038.
- [60] Brauer DS, Karpukhina N, O'Donnell MD, Law RV, Hill RG. Fluoride-containing bioactive glasses: Effect of glass design and structure on degradation, pH and apatite formation in simulated body fluid. *Acta Biomater* 2010;6:3275–82. doi:10.1016/j.actbio.2010.01.043.
- [61] Shah FA. Fluoride-containing bioactive glasses: Glass design, structure, bioactivity, cellular interactions, and recent developments. *Mater Sci Eng C* 2016;58:1279–89. doi:10.1016/j.msec.2015.08.064.
- [62] Nandi SK, Mahato A, Kundu B, Mukherjee P. Doped Bioactive Glass Materials in Bone Regeneration. *Adv Tech Bone Regen* 2016. doi:10.5772/63266.
- [63] Isaac J, Nohra J, Lao J, Jallot E, Nedelec JM, Berdal A, et al. Effects of strontium-doped bioactive glass on the differentiation of cultured osteogenic cells. *Eur Cell Mater* 2011;21:130–43.
- [64] Strobel LA, Hild N, Mohn D, Stark WJ, Hoppe A, Gbureck U, et al. Novel strontium-doped bioactive glass nanoparticles enhance proliferation and osteogenic differentiation of human bone marrow stromal cells. *J Nanoparticle Res* 2013;15:1780. doi:10.1007/s11051-013-1780-5.

- [65] Gorustovich AA, Steimetz T, Cabrini RL, Porto López JM. Osteoconductivity of strontium-doped bioactive glass particles: a histomorphometric study in rats. *J Biomed Mater Res A* 2010;92:232–7. doi:10.1002/jbm.a.32355.
- [66] Palaniswamy UK, Prashar N, Kaushik M, Lakkam SR, Arya S, Pebbeti S. A comparative evaluation of remineralizing ability of bioactive glass and amorphous calcium phosphate casein phosphopeptide on early enamel lesion. *Dent Res J* 2016;13:297. doi:10.4103/1735-3327.187872.
- [67] Mehta AB, Kumari V, Jose R, Izadikhah V. Remineralization potential of bioactive glass and casein phosphopeptide-amorphous calcium phosphate on initial carious lesion: An in-vitro pH-cycling study. *J Conserv Dent JCD* 2014;17:3–7. doi:10.4103/0972-0707.124085.
- [68] Taha AA, Patel MP, Hill RG, Fleming PS. The effect of bioactive glasses on enamel remineralization: A systematic review. *J Dent* 2017;67:9–17. doi:10.1016/j.jdent.2017.09.007.
- [69] Graumann SJ, Sensat ML, Stoltenberg JL. Air Polishing: A Review of Current Literature. *Am Dent Hyg Assoc* 2013;87:173–80.
- [70] Banerjee A, Hajatdoost-Sani M, Farrell S, Thompson I. A clinical evaluation and comparison of bioactive glass and sodium bicarbonate air-polishing powders. *J Dent* 2010;38:475–9. doi:10.1016/j.jdent.2010.03.001.
- [71] Tauböck TT, Zehnder M, Schweizer T, Stark WJ, Attin T, Mohn D. Functionalizing a dentin bonding resin to become bioactive. *Dent Mater Off Publ Acad Dent Mater* 2014;30:868–75. doi:10.1016/j.dental.2014.05.029.
- [72] Khvostenko D, Hilton TJ, Ferracane JL, Mitchell JC, Kruzic JJ. Bioactive glass fillers reduce bacterial penetration into marginal gaps for composite restorations. *Dent Mater Off Publ Acad Dent Mater* 2016;32:73–81. doi:10.1016/j.dental.2015.10.007.
- [73] AlOthman Z. A Review: Fundamental Aspects of Silicate Mesoporous Materials. *Materials* 2012;5:2874–902. doi:10.3390/ma5122874.

- [74] Wu C, Chang J. Mesoporous bioactive glasses: structure characteristics, drug/growth factor delivery and bone regeneration application. *Interface Focus* 2012;2:292–306. doi:10.1098/rsfs.2011.0121.
- [75] Akinjokun AI, Ojumu TV, Ogunfowokan AO. Biomass, Abundant Resources for Synthesis of Mesoporous Silica Material. *Microporous Mesoporous Mater* 2016. doi:10.5772/63463.
- [76] Arcos D, Vila M, López-Noriega A, Rossignol F, Champion E, Oliveira FJ, et al. Mesoporous bioactive glasses: Mechanical reinforcement by means of a biomimetic process. *Acta Biomater* 2011;7:2952–9. doi:10.1016/j.actbio.2011.02.012.
- [77] Zhao L, Yan X, Zhou X, Zhou L, Wang H, Tang J, et al. Mesoporous bioactive glasses for controlled drug release. *Microporous Mesoporous Mater* 2008;109:210–5. doi:10.1016/j.micromeso.2007.04.041.
- [78] Wu C, Chang J, Xiao Y. Mesoporous bioactive glasses as drug delivery and bone tissue regeneration platforms. *Ther Deliv* 2011;2:1189–98. doi:10.4155/tde.11.84.
- [79] Yan X, Yu C, Zhou X, Tang J, Zhao D. Highly Ordered Mesoporous Bioactive Glasses with Superior In Vitro Bone-Forming Bioactivities. *Angew Chem Int Ed* 2004;43:5980–4. doi:10.1002/anie.200460598.
- [80] López-Noriega A, Arcos D, Izquierdo-Barba I, Sakamoto Y, Terasaki O, Vallet-Regí M. Ordered Mesoporous Bioactive Glasses for Bone Tissue Regeneration. *Chem Mater* 2006;18:3137–44. doi:10.1021/cm060488o.
- [81] Xia W, Chang J. Well-ordered mesoporous bioactive glasses (MBG): A promising bioactive drug delivery system. *J Controlled Release* 2006;110:522–30. doi:10.1016/j.jconrel.2005.11.002.
- [82] Kaya S, Cresswell M, Boccaccini AR. Mesoporous silica-based bioactive glasses for antibiotic-free antibacterial applications. *Mater Sci Eng C* 2018;83:99–107. doi:10.1016/j.msec.2017.11.003.

- [83] Chen W-C, Kung J-C, Chen C-H, Hsiao Y-C, Shih C-J, Chien C-S. Effects of bioactive glass with and without mesoporous structures on desensitization in dentinal tubule occlusion. *Appl Surf Sci* 2013;283:833–42. doi:10.1016/j.apsusc.2013.07.027.
- [84] Chen W-C, Chen C-H, Kung J-C, Hsiao Y-C, Shih C-J, Chien C-S. Phosphorus Effects of Mesoporous Bioactive Glass on Occlude Exposed Dentin. *Materials* 2013;6:5335–51. doi:10.3390/ma6115335.
- [85] Lee J-H, Kang M-S, Mahapatra C, Kim H-W. Effect of Aminated Mesoporous Bioactive Glass Nanoparticles on the Differentiation of Dental Pulp Stem Cells. *PLOS ONE* 2016;11:e0150727. doi:10.1371/journal.pone.0150727.
- [86] Kim G-H, Park Y-D, Lee S-Y, El-Fiqi A, Kim J-J, Lee E-J, et al. Odontogenic stimulation of human dental pulp cells with bioactive nanocomposite fiber. *J Biomater Appl* 2015;29:854–66. doi:10.1177/0885328214546884.
- [87] Lee J-H, Mandakhbayar N, El-Fiqi A, Kim H-W. Intracellular co-delivery of Sr ion and phenamil drug through mesoporous bioglass nanocarriers synergizes BMP signaling and tissue mineralization. *Acta Biomater* 2017;60:93–108. doi:10.1016/j.actbio.2017.07.021.
- [88] Fernando D, Attik N, Pradelle-Plasse N, Jackson P, Grosgeat B, Colon P. Bioactive glass for dentin remineralization: A systematic review. *Mater Sci Eng C Mater Biol Appl* 2017;76:1369–77. doi:10.1016/j.msec.2017.03.083.
- [89] Zhang Y, Hong Z, Ren Y, Wang D, Yokogawa Y. Highly ordered mesoporous bioactive glass with high surface areas using H<sub>3</sub>PO<sub>4</sub> as the catalyst. *J Non-Cryst Solids* 2014;402:149–52. doi:10.1016/j.jnoncrysol.2014.05.030.
- [90] Arcos D, Vila M, López-Noriega A, Rossignol F, Champion E, Oliveira FJ, et al. Mesoporous bioactive glasses: mechanical reinforcement by means of a biomimetic process. *Acta Biomater* 2011;7:2952–9. doi:10.1016/j.actbio.2011.02.012.
- [91] Yan X, Yu C, Zhou X, Tang J, Zhao D. Highly Ordered Mesoporous Bioactive Glasses with Superior In Vitro Bone-Forming Bioactivities. *Angew Chem Int Ed Engl* 2004;43:5980–4. doi:10.1002/anie.200460598.

- [92] López-Noriega A, Arcos D, Izquierdo-Barba I, Sakamoto Y, Terasaki O, Vallet-Regí M. Ordered Mesoporous Bioactive Glasses for Bone Tissue Regeneration. *Chem Mater* 2006;18:3137–44. doi:10.1021/cm060488o.
- [93] Xia W, Chang J. Well-ordered mesoporous bioactive glasses (MBG): A promising bioactive drug delivery system. *J Controlled Release* 2006;110:522–30. doi:10.1016/j.jconrel.2005.11.002.
- [94] Vaid C, Murugavel S. Alkali oxide containing mesoporous bioactive glasses: Synthesis, characterization and in vitro bioactivity. *Mater Sci Eng C* 2013;33:959–68. doi:10.1016/j.msec.2012.11.028.
- [95] Vaid C, Murugavel S, Das C, Asokan S. Mesoporous bioactive glass and glass-ceramics: Influence of the local structure on in vitro bioactivity. *Microporous Mesoporous Mater* 2014;186:46–56. doi:10.1016/j.micromeso.2013.11.027.
- [96] Shih C-C, Chien C-S, Kung J-C, Chen JC, Chang S-S, Lu P-S, et al. Effect of surfactant concentration on characteristics of mesoporous bioactive glass prepared by evaporation induced self-assembly process. *Appl Surf Sci* 2013;264:105–110. doi:10.1016/j.apsusc.2012.09.134.
- [97] Gómez-Cerezo N, Izquierdo-Barba I, Arcos D, Vallet-Regí M. Tailoring the biological response of mesoporous bioactive materials. *J Mater Chem B* 2015;3:3810–9. doi:10.1039/C5TB00268K.
- [98] Zhao S, Li Y, Li D. Synthesis of CaO-SiO<sub>2</sub>-P<sub>2</sub>O<sub>5</sub> mesoporous bioactive glasses with high P<sub>2</sub>O<sub>5</sub> content by evaporation induced self assembly process. *J Mater Sci Mater Med* 2011;22:201–8. doi:10.1007/s10856-010-4200-8.
- [99] Yan XX, Deng HX, Huang XH, Lu GQ, Qiao SZ, Zhao DY, et al. Mesoporous bioactive glasses. I. Synthesis and structural characterization. *J Non-Cryst Solids* 2005;351:3209–17. doi:10.1016/j.jnoncrysol.2005.08.024.

- [100] Chen W-C, Kung J-C, Chen C-H, Hsiao Y-C, Shih C-J, Chien C-S. Effects of bioactive glass with and without mesoporous structures on desensitization in dentinal tubule occlusion. *Appl Surf Sci* 2013;283:833–42. doi:10.1016/j.apsusc.2013.07.027.
- [101] Letaief N, Lucas-Girot A, Oudadesse H, Dorbez-Sridi R. Influence of Synthesis Parameters on the Structure, Pore Morphology and Bioactivity of a New Mesoporous Glass. *J Biosci Med* 2014;02:57. doi:10.4236/jbm.2014.22009.
- [102] Zhang X, Zeng D, Li N, Wen J, Jiang X, Liu C, et al. Functionalized mesoporous bioactive glass scaffolds for enhanced bone tissue regeneration. *Sci Rep* 2016;6:srep19361. doi:10.1038/srep19361.
- [103] Sun J, Li Y, Li L, Zhao W, Li L, Gao J, et al. Functionalization and bioactivity in vitro of mesoporous bioactive glasses. *J Non-Cryst Solids* 2008;354:3799–805. doi:10.1016/j.jnoncrysol.2008.05.001.
- [104] Yan X, Yu C, Zhou X, Tang J, Zhao D. Highly Ordered Mesoporous Bioactive Glasses with Superior In Vitro Bone-Forming Bioactivities. *Angew Chem Int Ed Engl* 2004;43:5980–4. doi:10.1002/anie.200460598.
- [105] Li R, Clark AE, Hench LL. An investigation of bioactive glass powders by sol-gel processing. *J Appl Biomater* 1991;2:231–9. doi:10.1002/jab.770020403.
- [106] Sepulveda P, Jones JR, Hench LL. Characterization of melt-derived 45S5 and sol-gel-derived 58S bioactive glasses. *J Biomed Mater Res* 2001;58:734–40.
- [107] Polini A, Bai H, Tomsia AP. Dental applications of nanostructured bioactive glass and its composites. *Wiley Interdiscip Rev Nanomed Nanobiotechnol* 2013;5:399–410. doi:10.1002/wnan.1224.
- [108] Khvostenko D, Hilton TJ, Ferracane JL, Mitchell JC, Kruzic JJ. Bioactive glass fillers reduce bacterial penetration into marginal gaps for composite restorations. *Dent Mater* 2016;32:73–81. doi:10.1016/j.dental.2015.10.007.

- [109] Jones JR, Lin S, Yue S, Lee PD, Hanna JV, Smith ME, et al. Bioactive glass scaffolds for bone regeneration and their hierarchical characterisation. *Proc Inst Mech Eng [H]* 2010;224:1373–87. doi:10.1243/09544119JEIM836.
- [110] Taha AA, Patel MP, Hill RG, Fleming PS. The effect of bioactive glasses on enamel remineralization: A systematic review. *J Dent* 2017. doi:10.1016/j.jdent.2017.09.007.
- [111] Wu C, Zhou Y, Xu M, Han P, Chen L, Chang J, et al. Copper-containing mesoporous bioactive glass scaffolds with multifunctional properties of angiogenesis capacity, osteostimulation and antibacterial activity. *Biomaterials* 2013;34:422–33. doi:10.1016/j.biomaterials.2012.09.066.
- [112] Gargiulo N, Cusano AM, Causa F, Caputo D, Netti PA. Silver-containing mesoporous bioactive glass with improved antibacterial properties. *J Mater Sci Mater Med* 2013;24:2129–35. doi:10.1007/s10856-013-4968-4.
- [113] Diba M, Tapia F, Boccaccini AR, Strobel LA. Magnesium-Containing Bioactive Glasses for Biomedical Applications. *Int J Appl Glass Sci* 2012;3:221–53. doi:10.1111/j.2041-1294.2012.00095.x.
- [114] Bejarano J, Detsch R, Boccaccini AR, Palza H. PDLLA scaffolds with Cu- and Zn-doped bioactive glasses having multifunctional properties for bone regeneration. *J Biomed Mater Res A* 2017;105:746–56. doi:10.1002/jbm.a.35952.
- [115] Wu C, Zhou Y, Lin C, Chang J, Xiao Y. Strontium-containing mesoporous bioactive glass scaffolds with improved osteogenic/cementogenic differentiation of periodontal ligament cells for periodontal tissue engineering. *Acta Biomater* 2012;8:3805–15. doi:10.1016/j.actbio.2012.06.023.
- [116] Hoppe A, Mouriño V, R. Boccaccini A. Therapeutic inorganic ions in bioactive glasses to enhance bone formation and beyond. *Biomater Sci* 2013;1:254–6. doi:10.1039/C2BM00116K.
- [117] Montazerian M, Dutra Zanotto E. History and trends of bioactive glass-ceramics. *J Biomed Mater Res A* 2016;104:1231–49. doi:10.1002/jbm.a.35639.

- [118] Nandi SK, Kundu B, Datta S. Development and Applications of Varieties of Bioactive Glass Compositions in Dental Surgery, Third Generation Tissue Engineering, Orthopaedic Surgery and as Drug Delivery System 2011. doi:10.5772/24942.
- [119] Kaur G, Pickrell G, Sriranganathan N, Kumar V, Homa D. Review and the state of the art: Sol-gel and melt quenched bioactive glasses for tissue engineering. *J Biomed Mater Res B Appl Biomater* 2016;104:1248–75. doi:10.1002/jbm.b.33443.
- [120] Zheng K, Boccaccini AR. Sol-gel processing of bioactive glass nanoparticles: A review. *Adv Colloid Interface Sci* 2017. doi:10.1016/j.cis.2017.03.008.
- [121] Sepulveda P, Jones JR, Hench LL. Characterization of melt-derived 45S5 and sol-gel-derived 58S bioactive glasses. *J Biomed Mater Res A* 2001;58:734–740.
- [122] Li Y, Liu Y-Z, Long T, Yu X-B, Tang T-T, Dai K-R, et al. Mesoporous bioactive glass as a drug delivery system: fabrication, bactericidal properties and biocompatibility. *J Mater Sci Mater Med* 2013;24:1951–61. doi:10.1007/s10856-013-4960-z.
- [123] Wu C, Chang J, Xiao Y. Mesoporous bioactive glasses as drug delivery and bone tissue regeneration platforms. *Ther Deliv* 2011;2:1189–98. doi:10.4155/tde.11.84.
- [124] Pérez-Pariente J, Balas F, Román J, Salinas A, Vallet-Regí M. Influence of Composition and Surface Characteristics on the in Vitro Bioactivity of SiO<sub>2</sub>-CaO-P<sub>2</sub>O<sub>5</sub>-MgO sol-Gel Glasses. *J Biomed Mater Res* 1999;47:170–5. doi:10.1002/(SICI)1097-4636(199911)47:2<170::AID-JBM6>3.0.CO;2-J.
- [125] Shah AT, Ain Q, Chaudhry AA, Khan AF, Iqbal B, Ahmad S, et al. A study of the effect of precursors on physical and biological properties of mesoporous bioactive glass. *J Mater Sci* 2015;50:1794–804. doi:10.1007/s10853-014-8742-x.
- [126] Yu B, Turdean-Ionescu CA, Martin RA, Newport RJ, Hanna JV, Smith ME, et al. Effect of Calcium Source on Structure and Properties of Sol-Gel Derived Bioactive Glasses. *Langmuir* 2012;28:17465–76. doi:10.1021/la303768b.

- [127] Ren H, Tian Y, Li A, Martin RA, Qiu D. The influence of phosphorus precursor on the structure and properties of  $\text{SiO}_2$ - $\text{P}_2\text{O}_5$ -CaO bioactive glass. *Biomed Phys Eng Express* 2017;3:045017. doi:10.1088/2057-1976/aa7daa.
- [128] Zheng K, Solodovnyk A, Li W, Goudouri O-M, Stähli C, Nazhat SN, et al. Aging Time and Temperature Effects on the Structure and Bioactivity of Gel-Derived 45S5 Glass-Ceramics. *J Am Ceram Soc* 2015;98:30–8. doi:10.1111/jace.13258.
- [129] Letaief N, Lucas-Girot A, Oudadesse H, Meleard P, Pott T, Jelassi J, et al. Effect of aging temperature on the structure, pore morphology and bioactivity of new sol-gel synthesized bioglass. *J Non-Cryst Solids* 2014;Complete:194–9. doi:10.1016/j.jnoncrysol.2014.06.005.
- [130] Valliant EM, Turdean-Ionescu CA, Hanna JV, Smith ME, Jones JR. Role of pH and temperature on silica network formation and calcium incorporation into sol-gel derived bioactive glasses. *J Mater Chem* 2011;22:1613–9. doi:10.1039/C1JM13225C.
- [131] Letaïef N, Lucas-Girot A, Oudadesse H, Dorbez-Sridi R, Boullay P. Investigation of the surfactant type effect on characteristics and bioactivity of new mesoporous bioactive glass in the ternary system  $\text{SiO}_2$ -CaO-P $_2\text{O}_5$ : Structural, textural and reactivity studies. *Microporous Mesoporous Mater* 2014;195:102–11. doi:10.1016/j.micromeso.2014.03.035.
- [132] Shih C-C, Chien C-S, Kung J-C, Chen J-C, Chang S-S, Lu P-S, et al. Effect of surfactant concentration on characteristics of mesoporous bioactive glass prepared by evaporation induced self-assembly process. *Appl Surf Sci* 2013;264:105–10. doi:10.1016/j.apsusc.2012.09.134.
- [133] Shih S-J, Lin Y-C, Valentino Posma Panjaitan L, Rahayu Meyla Sari D. The Correlation of Surfactant Concentrations on the Properties of Mesoporous Bioactive Glass. *Mater Basel Switz* 2016;9. doi:10.3390/ma9010058.
- [134] Fernando D, Attik N, Cresswell M, Mokbel I, Pradelle-Plasse N, Jackson P, et al. Influence of network modifiers in an acetate based sol-gel bioactive glass system. *Microporous Mesoporous Mater* 2018;257:99–109. doi:10.1016/j.micromeso.2017.08.029.

- [135] Rangel-Yagui CO, Pessoa Jr A, Tavares LC. Micellar solubilization of drugs. *J Pharm Pharm Sci* 2005;8:147–163.
- [136] Wu C, Fan W, Gelinsky M, Xiao Y, Simon P, Schulze R, et al. Bioactive SrO–SiO<sub>2</sub> glass with well-ordered mesopores: Characterization, physiochemistry and biological properties. *Acta Biomater* 2011;7:1797–806. doi:10.1016/j.actbio.2010.12.018.
- [137] Huang M, Hill RG, Rawlinson SCF. Zinc bioglasses regulate mineralization in human dental pulp stem cells. *Dent Mater* 2017;33:543–52. doi:10.1016/j.dental.2017.03.011.
- [138] Goudouri OM, Theodosoglou E, Kontonasaki E, Will J, Chrissafis K, Koidis P, et al. Development of highly porous scaffolds based on bioactive silicates for dental tissue engineering. *Mater Res Bull* 2014;49:399–404. doi:10.1016/j.materresbull.2013.09.027.
- [139] Lee J-H, Kang M-S, Mahapatra C, Kim H-W. Effect of Aminated Mesoporous Bioactive Glass Nanoparticles on the Differentiation of Dental Pulp Stem Cells. *Plos One* 2016;11:e0150727. doi:10.1371/journal.pone.0150727.
- [140] Houreh AB, Labbaf S, Ting H-K, Ejeian F, Jones JR, Esfahani M-HN. Influence of calcium and phosphorus release from bioactive glasses on viability and differentiation of dental pulp stem cells. *J Mater Sci* 2017;52:8928–41. doi:10.1007/s10853-017-0946-4.
- [141] Lee J-H, Mandakhbayar N, El-Fiqi A, Kim H-W. Intracellular co-delivery of Sr ion and phenamil drug through mesoporous bioglass nanocarriers synergizes BMP signaling and tissue mineralization. *Acta Biomater* 2017;60:93–108. doi:10.1016/j.actbio.2017.07.021.
- [142] Gong W, Huang Z, Dong Y, Gan Y, Li S, Gao X, et al. Ionic Extraction of a Novel Nano-sized Bioactive Glass Enhances Differentiation and Mineralization of Human Dental Pulp Cells. *J Endod* 2014;40:83–8. doi:10.1016/j.joen.2013.08.018.
- [143] Qu T, Liu X. Nano-structured gelatin/bioactive glass hybrid scaffolds for the enhancement of odontogenic differentiation of human dental pulp stem cells. *J Mater Chem B* 2013;1:4764–72. doi:10.1039/c3tb21002b.

- [144] Wang S, Gao X, Gong W, Zhang Z, Chen X, Dong Y. Odontogenic differentiation and dentin formation of dental pulp cells under nanobioactive glass induction. *Acta Biomater* 2014;10:2792–803. doi:10.1016/j.actbio.2014.02.013.
- [145] Bae W-J, Min K-S, Kim J-J, Kim J-J, Kim H-W, Kim E-C. Odontogenic responses of human dental pulp cells to collagen/nanobioactive glass nanocomposites. *Dent Mater* 2012;28:1271–9. doi:10.1016/j.dental.2012.09.011.
- [146] El-Gendy R, Yang XB, Newby PJ, Boccaccini AR, Kirkham J. Osteogenic Differentiation of Human Dental Pulp Stromal Cells on 45S5 Bioglass (R) Based Scaffolds In Vitro and In Vivo. *Tissue Eng Part A* 2013;19:707–15. doi:10.1089/ten.tea.2012.0112.
- [147] Lee S-I, Lee E-S, El-Fiqi A, Lee S-Y, Kim E-C, Kim H-W. Stimulation of Odontogenesis and Angiogenesis via Bioactive Nanocomposite Calcium Phosphate Cements Through Integrin and VEGF Signaling Pathways. *J Biomed Nanotechnol* 2016;12:1048–62. doi:10.1166/jbn.2016.2209.
- [148] Huang M, Hill RG, Rawlinson SCF. Strontium (Sr) elicits odontogenic differentiation of human dental pulp stem cells (hDPSCs): A therapeutic role for Sr in dentine repair? *Acta Biomater* 2016;38:201–11. doi:10.1016/j.actbio.2016.04.037.
- [149] Chiang Y-C, Lin H-P, Chang H-H, Cheng Y-W, Tang H-Y, Yen W-C, et al. A Mesoporous Silica Biomaterial for Dental Biomimetic Crystallization. *ACS Nano* 2014;8:12502–13. doi:10.1021/nn5053487.
- [150] De Caluwé T, Vercruyse CWJ, Declercq HA, Schaubroeck D, Verbeeck RMH, Martens LC. Bioactivity and biocompatibility of two fluoride containing bioactive glasses for dental applications. *Dent Mater* 2016;32:1414–28. doi:10.1016/j.dental.2016.09.014.
- [151] Montazerian M, Yekta BE, Marghussian VK, Bellani CF, Siqueira RL, Zanotto ED. Bioactivity and cell proliferation in radiopaque gel-derived CaO–P2O5–SiO2–ZrO2 glass and glass–ceramic powders. *Mater Sci Eng C* 2015;55:436–47. doi:10.1016/j.msec.2015.05.065.

- [152] Kansal I, Goel A, Tulyaganov DU, Pascual MJ, Lee H-Y, Kim H-W, et al. Diopside (CaO•MgO•2SiO<sub>2</sub>)–fluorapatite (9CaO•3P<sub>2</sub>O<sub>5</sub>•CaF<sub>2</sub>) glass-ceramics: potential materials for bone tissue engineering. *J Mater Chem* 2011;21:16247. doi:10.1039/c1jm11876e.
- [153] Lee J-H, Kang M-S, Mahapatra C, Kim H-W. Effect of Aminated Mesoporous Bioactive Glass Nanoparticles on the Differentiation of Dental Pulp Stem Cells. *PLOS ONE* 2016;11:e0150727. doi:10.1371/journal.pone.0150727.
- [154] Alcaide M, Portolés P, López-Noriega A, Arcos D, Vallet-Regí M, Portolés MT. Interaction of an ordered mesoporous bioactive glass with osteoblasts, fibroblasts and lymphocytes, demonstrating its biocompatibility as a potential bone graft material. *Acta Biomater* 2010;6:892–9. doi:10.1016/j.actbio.2009.09.008.
- [155] Wang S, Gao X, Gong W, Zhang Z, Chen X, Dong Y. Odontogenic differentiation and dentin formation of dental pulp cells under nanobioactive glass induction. *Acta Biomater* 2014;10:2792–803. doi:10.1016/j.actbio.2014.02.013.
- [156] Liu S, Gong W, Dong Y, Hu Q, Chen X, Gao X. The effect of submicron bioactive glass particles on in vitro osteogenesis. *RSC Adv* 2015;5:38830–6. doi:10.1039/C5RA03786G.
- [157] Massera J, Kokkari A, Närhi T, Hupa L. The influence of SrO and CaO in silicate and phosphate bioactive glasses on human gingival fibroblasts. *J Mater Sci Mater Med* 2015;26. doi:10.1007/s10856-015-5528-x.
- [158] Ojansivu M, Vanhatupa S, Björkvik L, Häkkänen H, Kellomäki M, Autio R, et al. Bioactive glass ions as strong enhancers of osteogenic differentiation in human adipose stem cells. *Acta Biomater* 2015;21:190–203. doi:10.1016/j.actbio.2015.04.017.
- [159] Wu C, Chang J, Fan W. Bioactive mesoporous calcium–silicate nanoparticles with excellent mineralization ability, osteostimulation, drug-delivery and antibacterial properties for filling apex roots of teeth. *J Mater Chem* 2012;22:16801. doi:10.1039/c2jm33387b.
- [160] Carvalho SM, Oliveira AAR, Jardim CA, Melo CBS, Gomes DA, de Fátima Leite M, et al. Characterization and induction of cementoblast cell proliferation by bioactive glass

nanoparticles: Induction of cementoblast proliferation. *J Tissue Eng Regen Med* 2012;6:813–21. doi:10.1002/term.488.

[161] Saffarian Tousi N, Velten MF, Bishop TJ, Leong KK, Barkhordar NS, Marshall GW, et al. Combinatorial effect of Si<sup>4+</sup>, Ca<sup>2+</sup>, and Mg<sup>2+</sup> released from bioactive glasses on osteoblast osteocalcin expression and biomineralization. *Mater Sci Eng C* 2013;33:2757–65. doi:10.1016/j.msec.2013.02.044.

[162] Carvalho S, Oliveira A, Andrade V, de Fatima Leite M, Goes A, Pereira M. Comparative Effect of the Ionic Products from Bioactive Glass Dissolution on the Behavior of Cementoblasts, Osteoblasts, and Fibroblasts. *Key Eng Mater* 2009;396–398:55–9. doi:10.4028/www.scientific.net/KEM.396-398.55.

[163] Ajita J, Saravanan S, Selvamurugan N. Effect of size of bioactive glass nanoparticles on mesenchymal stem cell proliferation for dental and orthopedic applications. *Mater Sci Eng C* 2015;53:142–9. doi:10.1016/j.msec.2015.04.041.

[164] Li HC, Wang DG, Meng XG, Chen CZ. Effect of ZrO<sub>2</sub> additions on the crystallization, mechanical and biological properties of MgO–CaO–SiO<sub>2</sub>–P<sub>2</sub>O<sub>5</sub>–CaF<sub>2</sub> bioactive glass-ceramics. *Colloids Surf B Biointerfaces* 2014;118:226–33. doi:10.1016/j.colsurfb.2014.03.055.

[165] Varanasi VG, Odatsu T, Bishop T, Chang J, Owyong J, Loomer PM. Enhanced osteoprogenitor elongated collagen fiber matrix formation by bioactive glass ionic silicon dependent on Sp7 (osterix) transcription: Si IONS ENHANCE OSTEOGENITOR ELONGATED COLLAGEN FIBER FORMATION. *J Biomed Mater Res A* 2016;104:2604–15. doi:10.1002/jbm.a.35795.

[166] Liu J, Rawlinson SCF, Hill RG, Fortune F. Fluoride incorporation in high phosphate containing bioactive glasses and in vitro osteogenic, angiogenic and antibacterial effects. *Dent Mater* 2016;32:e221–37. doi:10.1016/j.dental.2016.07.003.

- [167] Rismanchian M, Khodaeian N, Bahramian L, Fathi M, Sadeghi-Aliabadi H. In-vitro comparison of cytotoxicity of two bioactive glasses in micropowder and nanopowder forms. *Iran J Pharm Res IJPR* 2013;12:437.
- [168] Catauro M, Bollino F, Papale F, Gallicchio M, Pacifico S. Influence of the polymer amount on bioactivity and biocompatibility of SiO<sub>2</sub>/PEG hybrid materials synthesized by sol-gel technique. *Mater Sci Eng C* 2015;48:548–55. doi:10.1016/j.msec.2014.12.035.
- [169] Catauro M, Renella RA, Papale F, Vecchio Cipriotti S. Investigation of bioactivity, biocompatibility and thermal behavior of sol-gel silica glass containing a high PEG percentage. *Mater Sci Eng C* 2016;61:51–5. doi:10.1016/j.msec.2015.11.077.
- [170] Gong W, Huang Z, Dong Y, Gan Y, Li S, Gao X, et al. Ionic Extraction of a Novel Nano-sized Bioactive Glass Enhances Differentiation and Mineralization of Human Dental Pulp Cells. *J Endod* 2014;40:83–8. doi:10.1016/j.joen.2013.08.018.
- [171] Huang M, Hill RG, Rawlinson SCF. Strontium (Sr) elicits odontogenic differentiation of human dental pulp stem cells (hDPSCs): A therapeutic role for Sr in dentine repair? *Acta Biomater* 2016;38:201–11. doi:10.1016/j.actbio.2016.04.037.
- [172] Liu J, Rawlinson SCF, Hill RG, Fortune F. Strontium-substituted bioactive glasses in vitro osteogenic and antibacterial effects. *Dent Mater* 2016;32:412–22. doi:10.1016/j.dental.2015.12.013.
- [173] Gentleman E, Stevens MM, Hill RG, Brauer DS. Surface properties and ion release from fluoride-containing bioactive glasses promote osteoblast differentiation and mineralization in vitro. *Acta Biomater* 2013;9:5771–9. doi:10.1016/j.actbio.2012.10.043.
- [174] Varanasi VG, Owyong JB, Saiz E, Marshall SJ, Marshall GW, Loomer PM. The ionic products of bioactive glass particle dissolution enhance periodontal ligament fibroblast osteocalcin expression and enhance early mineralized tissue development. *J Biomed Mater Res A* 2011;98A:177–84. doi:10.1002/jbm.a.33102.

- [175] Osorio E, Fagundes T, Navarro MF, Zanotto ED, Peitl O, Osorio R, et al. A novel bioactive agent improves adhesion of resin-modified glass-ionomer to dentin. *J Adhes Sci Technol* 2015;29:1543–52. doi:10.1080/01694243.2015.1030897.
- [176] Xie D, Zhao J, Weng Y, Park J-G, Jiang H, Platt JA. Bioactive glass-ionomer cement with potential therapeutic function to dentin capping mineralization. *Eur J Oral Sci* 2008;116:479–487.
- [177] Osorio R, Yamauti M, Sauro S, Watson TF, Toledano M. Experimental Resin Cements Containing Bioactive Fillers Reduce Matrix Metalloproteinase-mediated Dentin Collagen Degradation. *J Endod* 2012;38:1227–32. doi:10.1016/j.joen.2012.05.011.
- [178] Wang Z, Shen Y, Haapasalo M, Wang J, Jiang T, Wang Y, et al. Polycarboxylated microfillers incorporated into light-curable resin-based dental adhesives evoke remineralization at the mineral-depleted dentin. *J Biomater Sci Polym Ed* 2014;25:679–97. doi:10.1080/09205063.2014.891926.
- [179] Profeta AC. Preparation and properties of calcium-silicate filled resins for dental restoration. Part II: Micro-mechanical behaviour to primed mineral-depleted dentine. *Acta Odontol Scand* 2014;72:607–17. doi:10.3109/00016357.2014.880188.
- [180] Sauro S, Osorio R, Watson TF, Toledano M. Therapeutic effects of novel resin bonding systems containing bioactive glasses on mineral-depleted areas within the bonded-dentine interface. *J Mater Sci Mater Med* 2012;23:1521–32. doi:10.1007/s10856-012-4606-6.
- [181] Bakry AS, Takahashi H, Otsuki M, Sadr A, Yamashita K, Tagami J. CO<sub>2</sub> Laser Improves 45S5 Bioglass Interaction with Dentin. *J Dent Res* 2011;90:246–50. doi:10.1177/0022034510387793.
- [182] Wang Z, Jiang T, Sauro S, Wang Y, Thompson I, Watson TF, et al. Dentine remineralization induced by two bioactive glasses developed for air abrasion purposes. *J Dent* 2011;39:746–56. doi:10.1016/j.jdent.2011.08.006.

- [183] Chen W-C, Kung J-C, Chen C-H, Hsiao Y-C, Shih C-J, Chien C-S. Effects of bioactive glass with and without mesoporous structures on desensitization in dentinal tubule occlusion. *Appl Surf Sci* 2013;283:833–42. doi:10.1016/j.apsusc.2013.07.027.
- [184] Lynch E, Brauer DS, Karpukhina N, Gillam DG, Hill RG. Multi-component bioactive glasses of varying fluoride content for treating dentin hypersensitivity. *Dent Mater* 2012;28:168–78. doi:10.1016/j.dental.2011.11.021.
- [185] Sauro S, Watson TF, Thompson I, Banerjee A. One-bottle self-etching adhesives applied to dentine air-abraded using bioactive glasses containing polyacrylic acid: An in vitro microtensile bond strength and confocal microscopy study. *J Dent* 2012;40:896–905. doi:10.1016/j.jdent.2012.07.004.
- [186] Vollenweider M, Brunner TJ, Knecht S, Grass RN, Zehnder M, Imfeld T, et al. Remineralization of human dentin using ultrafine bioactive glass particles. *Acta Biomater* 2007;3:936–43. doi:10.1016/j.actbio.2007.04.003.
- [187] Curtis AR, West NX, Su B. Synthesis of nanobioglass and formation of apatite rods to occlude exposed dentine tubules and eliminate hypersensitivity. *Acta Biomater* 2010;6:3740–6. doi:10.1016/j.actbio.2010.02.045.
- [188] Bakry AS, Takahashi H, Otsuki M, Tagami J. The durability of phosphoric acid promoted bioglass–dentin interaction layer. *Dent Mater* 2013;29:357–64. doi:10.1016/j.dental.2012.12.002.
- [189] Tamjid E, Bagheri R, Vossoughi M, Simchi A. Effect of particle size on the in vitro bioactivity, hydrophilicity and mechanical properties of bioactive glass-reinforced polycaprolactone composites. *Mater Sci Eng C* 2011;31:1526–33. doi:10.1016/j.msec.2011.06.013.
- [190] Chou Y-J, Hong B-J, Lin Y-C, Wang C-Y, Shih S-J. The Correlation of Pore Size and Bioactivity of Spray-Pyrolyzed Mesoporous Bioactive Glasses. *Materials* 2017;10:488. doi:10.3390/ma10050488.

- [191] Shih S-J, Lin Y-C, Valentino Posma Panjaitan L, Rahayu Meyla Sari D. The Correlation of Surfactant Concentrations on the Properties of Mesoporous Bioactive Glass. *Mater Basel Switz* 2016;9. doi:10.3390/ma9010058.
- [192] Tauböck TT, Zehnder M, Schweizer T, Stark WJ, Attin T, Mohn D. Functionalizing a dentin bonding resin to become bioactive. *Dent Mater* 2014;30:868–75. doi:10.1016/j.dental.2014.05.029.
- [193] Carneiro KK, Araujo TP, Carvalho EM, Meier MM, Tanaka A, Carvalho CN, et al. Bioactivity and properties of an adhesive system functionalized with an experimental niobium-based glass. *J Mech Behav Biomed Mater* 2018;78:188–95. doi:10.1016/j.jmbbm.2017.11.016.
- [194] Rizk M, Hohlfeld L, Thanh LT, Biehl R, Lühmann N, Mohn D, et al. Bioactivity and properties of a dental adhesive functionalized with polyhedral oligomeric silsesquioxanes (POSS) and bioactive glass. *Dent Mater* 2017;33:1056–65. doi:10.1016/j.dental.2017.06.012.
- [195] Xiao S, Liang K, Weir M, Cheng L, Liu H, Zhou X, et al. Combining Bioactive Multifunctional Dental Composite with PAMAM for Root Dentin Remineralization. *Materials* 2017;10:89. doi:10.3390/ma10010089.
- [196] Chatzistavrou X, Velamakanni S, DiRenzo K, Lefkelidou A, Fenno JC, Kasuga T, et al. Designing dental composites with bioactive and bactericidal properties. *Mater Sci Eng C* 2015;52:267–72. doi:10.1016/j.msec.2015.03.062.
- [197] Xie X, Wang L, Xing D, Zhang K, Weir MD, Liu H, et al. Novel dental adhesive with triple benefits of calcium phosphate recharge, protein-repellent and antibacterial functions. *Dent Mater* 2017;33:553–63. doi:10.1016/j.dental.2017.03.002.

## 12. Abstract

Improving the stability of adhesive dentin interface is crucial to extend the longevity of composite restorations. Remineralization through use of ion releasing materials is a promising approach to protect the hybrid layer from hydrolytic and enzymatic degradation. Mesoporous bioactive glasses (MBGs) offer attractive surface features (enhanced surface area and porosity) to use them as fillers in dental adhesives to promote remineralization through ions release. Moreover, the functionalization of pores with antibacterial drugs is a good way to combat secondary caries.

The present work focused on the synthesis and evaluation of novel MBGs suitable to be used as fillers in dental adhesives. The MBGs were prepared in an acetate based sol-gel system with industrially safe and non-toxic precursors. MBGs prepared in large scale (50g) offered enhanced surface characteristics in comparison to small scale (10g) MBGs. The investigation on the influence of network modifiers (CaO:Na<sub>2</sub>O) on the surface characteristics of MBGs revealed that the porosity was driven by CaO content in the composition. Notable, very high surface area (535m<sup>2</sup>g<sup>-1</sup>) and pore volume (0.33cm<sup>3</sup>g<sup>-1</sup>) was attained in the MBG with highest CaO content.

Next, the order of precursor addition effect on the surface characteristics of MBGs has been studied. By Keeping the composition fixed and varying the order of precursor addition during sol-gel synthesis a doubling of surface area, 1.5 times increase in pore volume and 1.2 times decrease in mean pore size was obtained. The demonstrated method is a simple and straightforward route to improve the porosity and homogeneity of MBGs. Furthermore, modulation of mean pore size for a fixed composition is also useful to tailor the pores of the fillers for drug delivery application.

With regards to bioactivity, the MBG fillers with highest CaO content had increased calcium phosphate precipitate in SBF after 7 days as opposed to MBG with high Na<sub>2</sub>O content. Furthermore, all tested samples were non-cytotoxic to Human Gingival Fibroblasts (HGFs) in vitro. Positively, MBGs treated at lower temperature significantly enhanced the metabolic activity of HGFs.

Ball milling was employed to reduce the primary particle size of MBG to less than 3μm. Milling seemingly had an adverse effect on the porosity of the MBG filler. Nevertheless, some porosity remained. The commercial adhesive was mixed with 3, 10, 20 and 30 weight percentage of MBG filler. MBG filled adhesive up to 10 weight percent filler content had flowable viscosity suitable for adhesive application.

The developed MBG with high porosity and CaO content appears as a new step in the development of dental adhesives and also other bioactive dental materials.